Seasonal predictability of wintertime windstorm climate over the North Atlantic and Europe

DISSERTATION
zur Erlangung des akademischen Grades eines
Doktors der Naturwissenschaften
am Fachbereich für Geowissenschaften
der Freien Universität Berlin

vorgelegt von

Dominik Renggli

Berlin, 12. Mai 2011

1. Gutachter:	Prof. Dr. Uwe Ulbrich Institut für Meteorologie, Freie Universität Berlin
2. Gutachter:	PD Gregor C. Leckebusch Institut für Meteorologie, Freie Universität Berlin
Disputationstermin:	20.07.2011

Selbstständigkeitserklärung

Hiermit erkläre ich an Eides Statt, dass ich die vorliegende Arbeit selbstständig und ohne fremde Hilfe angefertigt, keine anderen als die angegebenen Quellen und Hilfsmittel benutzt und die den benutzten Quellen wörtlich oder inhaltlich entnommenen Stellen als solche kenntlich gemacht habe. Diese Arbeit hat in gleicher oder ähnlicher Form noch keiner Prüfungsbehörde vorgelegen.

Berlin, 12. Mai 2011

Savoir pour prévoir,
prévoir pour prévenir.

Auguste Comte

Contents

Abstract

Strong extra-tropical cyclones are a characteristic feature of mid-latitudinal weather. In extreme cases, such cyclones are accompanied by severe wind speeds. These windstorms are the natural hazard with the highest loss potential in the North Atlantic and European region. Thus, prediction of windstorm climate on seasonal time scales would be beneficial for society and economy. However, the skill of seasonal predictions of wintertime windstorm occurrence and its sources have not been extensively analyzed.

Therefore, this thesis addresses the following issues: a) How can windstorms be objectively identified? b) Which factors are related to wintertime windstorm occurrence on seasonal time scales in observational data, and may therefore be considered as potential sources of seasonal predictability? c) Do state-of-the-art dynamical seasonal prediction models successfully forecast windstorm climate? d) Which factors influence the occurrence of windstorm in such prediction models, i.e., what are the sources of predictive skill?

To this end, an impact-based, objective windstorm identification scheme is developed based on surface wind speeds exceeding the local 98th percentile in consecutive timesteps. The scheme can be applied to both reanalysis products and climate (prediction) model data. It is shown to successfully identify individual historical events. Furthermore, both the spatial and temporal climatologies of the identified events are in good agreement with observations.

Windstorms identified in reanalysis data are used to analyze their relationship to observed anomalies of hemispheric-scale factors such as North Atlantic sea surface temperature and sea ice, continental snow cover extent, and the North Atlantic Oscillation. The correlation between anomalies of these factors in summer and autumn and the windstorm occurrence in subsequent winter (i.e., with a lead time of four to six months) is statistically significant with coefficients of up to 0.43. Hence, hemispheric-scale factors explain at least 20% of the inter-annual variability of windstorm climate. A composite study reveals that an anomalous state of the North Atlantic Oscillation in summer supports the generation of specific temperature anomalies in the North Atlantic ocean in autumn, namely the North Atlantic Horseshoe pattern. These anomalies persist until winter and induce anomalous growth conditions for extra-tropical cyclones over the North Atlantic

(e.g., increased baroclinicity in areas of increased meridional temperature gradients, or increased latent heat over areas of positive sea surface temperature anomalies). Such conditions are favorable for the development of strong cyclones, and therefore potentially a higher number or stronger wintertime windstorms in the North Atlantic and European region. Such physically motivated links between anomalies in the North Atlantic Ocean, their persistence and their impacts on growth conditions of cyclones are potential sources of windstorm predictability on the seasonal time scale.

The windstorm identification scheme is also applied to data of the DEMETER and ENSEMBLES projects. These data consist of seasonal hindcasts produced by several coupled ocean-atmosphere climate models. December–February windstorm frequency in the 1980–2001 period is statistically significantly predicted by the multi-model ensembles and several single-model ensembles with a lead time of one to three months, with skill ranging between 0.10–0.40. The 1980–2001 period is shown to be generally better predictable than the 1960–1980 period. Additionally, the winters with high windstorm frequency are better predicted than winters with average storm counts.

The sources of predictive skill in these model ensembles are investigated by quantifying the relation between hemispheric-scale factors, growth factors of cyclones, and windstorm occurrence in the prediction models. The relation between hemispheric-scale factors and wintertime windstorms is weaker than in observations and insignificant on the seasonal time scale. Still, composites of hindcast runs with strong North Atlantic Horseshoe anomalies reveal similar relations to growth factors as found in observations. However, the persistence of the oceanic anomalies is very different in the individual models, and generally weaker than in observations, probably related to deficiencies in the coupling between ocean and atmosphere in the prediction models. The preservation of oceanic anomalies in the models' ocean control run from summer until the onset of the hindcasts started in November is shown to be a crucial factor for predictive skill. Models able to retain such anomalies in closer agreement with observations develop stronger anomalies in sea surface temperature, growth factors of cyclones, and windstorms, and show higher skill scores. Therefore, it is argued that the North Atlantic is one source of predictive skill for seasonal windstorm predictions, and that improvements of the ocean-atmosphere coupling in prediction models could enhance skill.

Zusammenfassung

Tiefdruckgebiete sind ein charakteristisches Merkmal des Wetters der Mittleren Breiten. Starke Tiefdruckgebiete im Winter sind oft mit extremen Windgeschwindigkeiten verbunden. Solche Winterstürme sind die schadenträchtigsten meteorologischen Extremereignisse in Europa. Diesbezügliche Vorhersagen auf der saisonalen Skala sind deshalb von gesellschaftlichem und wirtschaftlichem Interesse. Über die Vorhersagbarkeit von Wintersturmaktivität auf der saisonalen Skala und ihre Quellen ist allerdings wenig bekannt.

Deshalb beschäftigt sich diese Promotion mit den folgenden Fragen: Wie lassen sich Winterstürme objektiv definieren und identifizieren? Welche Faktoren hängen Beobachtungsdaten zufolge mit dem Auftreten von Winterstürmen auf der saisonalen Skala zusammen und kommen somit als potentielle Quellen von Vorhersagbarkeit in Frage? Wie gut sagen aktuelle saisonale Vorhersagemodelle das Wintersturmklima vorher? Welche Faktoren beeinflussen in diesen Modellen die Wintersturmaktivität, d.h. was sind die Quellen der Vorhersagegüte?

Winterstürme werden mit einer objektiven Identifikationsmethode bestimmt. Die Methode basiert auf der Identifikation von räumlich konsistenten Überschreitungen des lokalen 98. Perzentils des Bodenwindes und kann sowohl auf Reanalysen als auch auf Vorhersage- und Klimamodelle angewendet werden. Historische Winterstürme werden von der Methode erfolgreich identifiziert. Die zeitlichen und räumlichen Klimatologien der identifizierten Ereignisse stimmen gut mit Beobachtungen überein.

Das in Reanalysen identifizierte Wintersturmklima wird benutzt, um dessen Zusammenhang mit beobachteten Anomalien von hemisphärisch-skaligen Faktoren wie Meeresoberflächentemperaturen und Meereis im Nordatlantik, kontinentale Schneebedeckung und der Nordatlantischen Oszillation auf saisonalen Zeitskalen zu untersuchen. Es zeigt sich, dass die hemisphärisch-skaligen Faktoren im Sommer/Herbst (d.h. mit Vorlaufzeiten von vier bis sechs Monaten) statistisch signifikant mit der Sturmaktivität im Winter (Dezember-Februar) korrelieren. Die Korrelationskoeffizienten betragen bis zu 0.43, was einer erklärten Varianz von ungefähr 20% entspricht. Eine Kompositanalyse zeigt, dass Anomalien der Nordatlantischen Oszillation im Sommer die Entstehung des sogenannten "Horseshoe patterns", eines hufeisenförmigen Musters von Anomalien der Meeresoberflächentemperaturen im Nordatlantik, im darauffolgenden Herbst begünstigt. Diese Anoma-

lien bleiben bis zum Winter erhalten und führen zu anomalen Wachstumsbedingungen für extra-tropische Zyklonen über dem Nordatlantik (z.B. erhöhte Baroklinität in Regionen mit verstärkten meridionalen Temperaturgradienten und erhöhte Werte der latenten Wärme über positiven Anomalien der Meeresoberflächentemperatur). Solche Bedingungen fördern die Entwicklung von starken Zyklonen und deshalb möglicherweise auch von mehr oder stärkeren Winterstürmen über Europa. Physikalisch begründbare Zusammenhänge wie jene zwischen Anomalien im Nordatlantik, deren Persistenz und deren Einfluss auf Wachstumsbedingungen von Zyklonen stellen potentiellen Quellen für die saisonale Vorhersagbarkeit von Winterstürmen dar.

Winterstürme werden analog zu den Reanalysen auch in den Vorhersagedaten des DEMETER und des ENSEMBLES Projekts identifiziert. Diese saisonalen Vorhersagen wurden von verschiedenen gekoppelten Ozean-Atmosphäre-Modellen gerechnet. Die Multi-Modell-Ensembles und gewisse Einzelmodelle zeigen statistisch signifikante Güte in der Vorhersage der Wintersturmanzahl im Dezember bis Februar, mit Vorlaufzeiten von einem bis drei Monaten. Der Ranked Probability Skill Score erreicht dabei Werte von 0.10–0.40. Im Zeitraum von 1980–2001 ist die Vorhersagegüte generell besser als im Zeitraum 1960–1980. Winter mit hoher Wintersturmaktivität werden grundsätzlich besser vorhergesagt als Winter mittlerer Wintersturmaktivität.

Die Quellen der Vorhersagegüte werden anhand der von den Vorhersagemodellen simulierten Zusammenhänge zwischen hemisphärisch-skaligen Faktoren, Wachstumsbedingungen für Zyklonen und Winterstürmen untersucht. Diese Zusammenhänge sind in den Modellen grundsätzlich schwächer ausgeprägt als die beobachteten Zusammenhänge. Allerdings zeigen Modellläufe mit starken Anomalien des “Horseshoe patterns” ähnliche Relationen zu Wachstumsbedingungen von Zyklonen wie die Beobachtungen. Die Persistenz dieser Anomalien ist aber in den Modellen unterschiedlich stark ausgeprägt und im Allgemeinen schwächer als die beobachtete Persistenz. Defizite in der Kopplung zwischen der Ozean- und der Atmosphärenkomponente der Vorhersagemodelle sind mögliche Gründe für diese Unterschätzung. Ein entscheidender Faktor für die Vorhersagegüte eines Modells ist seine Fähigkeit, ozeanische Anomalien im Ozean-Kontrolllauf vom Sommer bis zum Start der Wintervorhersage zu speichern. Je stärker die Persistenz solcher Anomalien, desto stärker sind entsprechende Anomalien im Nordatlantik, der Wachstumsfaktoren von Zyklonen und dem Auftreten von Winterstürmen und desto besser ist im Allgemeinen die Vorhersagegüte. Dies lässt den Schluss zu, dass der Nordatlantik eine Quelle von saisonaler Vorhersagbarkeit von Winterstürmen ist. Verbesserungen der Kopplung zwischen Ozean und Atmosphäre in den Vorhersagemodellen würden dementsprechend auch bessere Vorhersagen erlauben.

Chapter 1

Introduction

The topic of this thesis is the predictability of wintertime windstorm climate in the North Atlantic and European region on seasonal time scales, i.e., beyond the time scales of short-to-medium range forecasts. The introduction starts with a short overview on the main subject of the thesis, namely severe windstorm events, their origin and impacts on society and economy. It continues with a short history of seasonal forecasting, the physical basis of seasonal predictions, and an overview of research on seasonal predictability in the North Atlantic region, with an emphasis of existing work on the longer-term predictability of wind and windstorm climate. As will be shown there are considerable gaps in our knowledge on the seasonal predictability of windstorms, although society and economy could potentially benefit from successful forecasts. This fact motivates the research topics of this thesis. The introduction concludes with the outlines of the thesis.

1.1 Windstorms in the North Atlantic and European region

1.1.1 Physical basis

Windstorms in the mid-latitudes often reach hurricane-force surface wind speeds of 120 km/h and more. For example, maximum gusts of more than 200 km/h were observed in mountainous regions during windstorm "Kyrill" (January 2007), and many stations across Central and Western Europe reported wind speeds in excess of 120 km/h (Fink et al., 2009). Hence, large amounts of kinetic energy are associated with such systems. The ultimate source of this kinetic energy is the transformation of potential energy in the atmosphere through sinking motion of colder, denser air, and rising of warmer, less denser air (Wallace and Hobbs, 2006, chapter 7). This lowers the atmosphere's center of mass, flattens the potential temperature surfaces, and weakens the existing horizontal

temperature gradients. These horizontal temperature gradients are especially strong in the mid-latitudes in winter between subtropical warm air in the south and sub-polar cold air in the north, owing to the increased radiative cooling of the polar regions. The associated vertical wind shear leads to an increase of wind speeds with height, culminating in the west-easterly blowing sub-polar jet stream at about 200 hPa.

A salient feature of the mid-latitudes are *baroclinic waves*, which are often related to well-defined low and high pressure systems at the surface. Under favorable conditions, a small wave disturbance in upper-tropospheric levels may amplify in response to instabilities in the large-scale flow pattern (due to horizontal and vertical wind shear). In particular, if such an upper-level disturbance is advected over regions with high baroclinicity Wallace and Hobbs (i.e., with high horizontal temperature gradients and/or low static stability; 2006), the initially small disturbance may amplify. In response to the advection of vorticity and temperature, a convergence zone at the surface is initiated ahead of the upper level trough, leading to the ascent of air, and falling of surface pressure. If the baroclinic wave intensifies sufficiently, an extra-tropical cyclone with a well-organized structure of fronts, clouds, pressure tendencies and wind speeds develops (Wallace and Hobbs, 2006; Semple, 2003; Schultz et al., 1998). The northward advection and ascent of warm air behind the warm front to the southeast of the cyclone center and the southward advection and descent of cold air behind the cold front to the southwest of the cyclone center reduce the original horizontal temperature gradient. The intensification of the disturbance leads to a lowering of the surface pressure in the cyclone center. The resulting pressure gradients are associated with high wind speeds (i.e., conversion of potential energy to kinetic energy). The highest wind speeds usually occur along the warm and the cold front of a mature cyclone. Such windstorms typically affect a single location for about 6–24 hours, and reach a width of about 150–500 km (compared to about 140 km for tropical cyclones only; Malmquist, 1999).

1.1.2 Impacts of European windstorms

Among 27 weather-related events which have led to total losses of more than 2 billion US$ in the 1983–2001 period, 7 are European windstorms (Cornford, 2002): Windstorms "**Anatol**" (affecting predominantly the Channel and the North and Baltic Sea coastal regions), "**Martin**" (southern parts of France, northern parts of Spain) and "**Lothar**" (France, Switzerland, southern Germany) in December 1999 (Ulbrich et al., 2001); windstorms "**Daria**" (similar to "Anatol", Pinto et al., 2009), "**Vivian**" (France, Benelux, Germany) and "**Wiebke**" (Germany) in January and February 1990; and a windstorm known as "'**87J**" (northern France, Channel, southern England). More recently, windstorm "**Kyrill**" hit many parts of Western, Central, and Eastern Europe in January 2007

(Fink et al., 2009), and led to total losses of 10 billion US$ (Münchener Rückversicherungs-Gesellschaft 2010, NatCatSERVICE[1]). Similarly, windstorms "**Klaus**" in January 2009 and "**Xynthia**" in February 2010 led to overall losses of more than US$ 4000 million (Münchener Rückversicherungs-Gesellschaft 2010, NatCatSERVICE). According to Münchener Rückversicherungs-Gesellschaft, windstorms in the North Atlantic and European region led to total (insured) losses of about 25.2 (12.8) billion EUR in the 1980–2006 period (i.e., about 1000 (500) million EUR per year (Münchener Rückversicherungs-Gesellschaft, 2007, Fig. 6, p. 16).

Of the documented world-wide catastrophes owing to extreme weather events between 1980 and 2007, the share of wintertime windstorms is 4% in absolute numbers, 0.5% in toll of live, 6.25% in overall losses, and 14.5% in insured losses. For comparison, the respective numbers for Germany only in the 1970–1998 period are 20% in absolute numbers, 53% in overall losses, and 64% in insured losses (Fig. 1.1, Münchener Rückversicherungs-Gesellschaft, 1999). Hence, for the European sector, wintertime windstorms are by far the most important natural hazard in terms of societal and economic losses. In respect of these losses, European windstorms rivaled Atlantic hurricanes between 1990 and 1998 and rank as the second highest cause of insured loss due to natural catastrophe, after US hurricanes (Malmquist, 1999). Thus, they are of particular interest to stakeholders in the risk management, e.g., catastrophe reinsurer (Murnane et al., 2002; Murnane, 2004).

Consequently, wintertime windstorms are in the focus of professional risk management. However, the history of scientifically based risk analysis of windstorms—and natural hazards—is relatively short. Commercial and private insurance of weather-related risks became available only after the Second World War (Berz, 2008). Increased insurance coverage lead to an increase in frequency and amounts of losses owing to windstorms and other hazards. Professional risk assessment of weather-related hazards by meteorologists came up with the US property insurers in the 1960s. The leading European reinsurance companies followed in the 1970s (Berz, 2008). Besides the risk assessment of atmospheric hazards, mainly on the basis of statistical considerations of historical losses, the development of realistic loss potential scenarios for the future are becoming increasingly important today. This includes considerations of changing loss potentials in scenarios of anthropogenic climate change (Donat et al., 2010b; Schwierz et al., 2009; Ulbrich et al., 2009; Leckebusch et al., 2008b,c; Ulbrich et al., 2008; Leckebusch et al., 2007; Leckebusch and Ulbrich, 2004). Given they provide skillful forecasts, short-term climate predictions (e.g., on the decadal or seasonal time scale) could also be used to adjust risk management practices accordingly.

[1] http://www.munichre.com/en/reinsurance/business/non-life/georisks/natcatservice/default.aspx

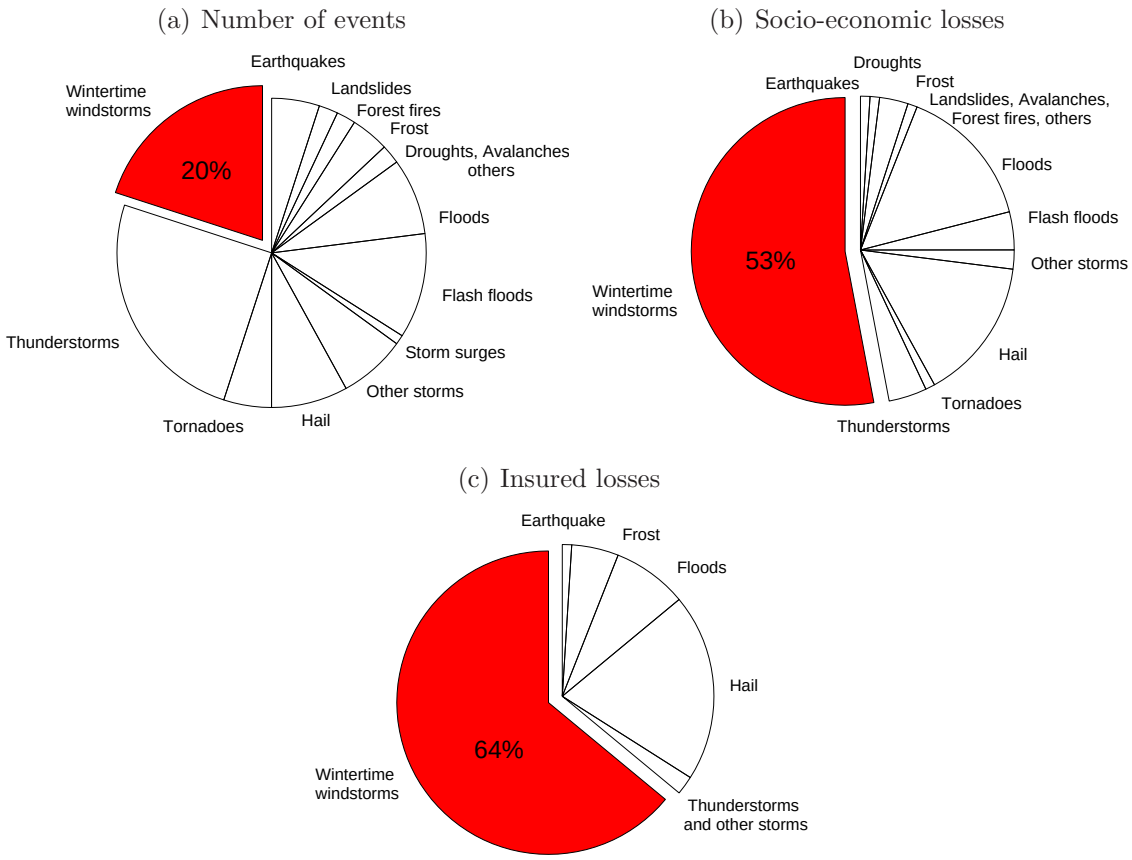

Figure 1.1: Share of wintertime windstorms (red) of the total number of natural hazard events (a), of socio-economic losses (b), and insured losses (c) in Germany in the 1970–1998 period (Münchener Rückversicherungs-Gesellschaft, 1999).

1.2 Seasonal forecasting

1.2.1 A short history of seasonal forecasting

Weather and climate have always been linked very tightly to the evolution and the history of humans (Diamond, 1998). Sudden changes in climate were among the major environmental constraints of prehistoric humans (di Lernia, 2006) and influence humanity on virtually all time scales, from millennia to days: 6000 years BP, for example, a shift towards drier climate in the Saharan region drove people into the more humid and fertile Nile valley, led to unprecedented population densities culminating in the ancient Egyptian civilization (Kuper and Kropelin, 2006). On the other end of the scale, the course of the seasons and daily variations of weather influence strongly our activities, even today. Therefore, the observation, anticipation, adaptation to and, if possible in any way, the prediction of changes in weather and climate has been a major challenge in the history of humans (Lefale, 2010; King et al., 2008). Consequently, traditional (local or regional) belief systems emerged. Such belief systems to foresee climate changes on the seasonal time scale were based on observations of the **current state of weather and climate**

(e.g., changing of winds related to movements of the Intertropical Convergence Zone to anticipate the timing of the rainy season in Uganda; Orlove et al., 2010; Speranza et al., 2010), **plant development** (e.g., timing and amount of blossom of certain trees; Green et al., 2010; King et al., 2008; Roncoli et al., 2002), or **animal behavior** (e.g., return or abundance of migration birds Lefale, 2010; King et al., 2008; Roncoli et al., 2002). **Astronomic constellations**, e.g., the visibility of the *Pleiades* constellation have been used to predict summer rainfall and autumn harvest in the Andes (Orlove et al., 2000). Changes of atmospheric moisture content associated with the El Niño phenomenon might provide some physical basis of such predictions. Given the inability of humans to interfere with the evolution of weather and climate, it is no surprise that such belief systems are in parts **spiritually influenced**. Thus, praying to deities was one way to adapt to the variability of weather (Anandaraja et al., 2008)[2]. Traditional weather lore is often an expression of superstition. Such an example is an event that takes place in Zurich, Switzerland, every year in spring: a dummy stuffed with firework resembling a snowman—the "Böögg"—is set on fire. According to the belief, the longer it takes his head to explode the longer wintery conditions will prevail into summer[3].

One particularly interesting example of historical seasonal predictions is worth mentioning since it has already included some of the most important ingredients of a modern predicting system. The farmers in Tlaxcala province, Mexico, employed a traditional method to anticipate general climate conditions for a whole year (Eakin, 1999). Basis for the prediction were the first few days of January of the beginning year. For example, 1st January is indicative of the general conditions in January, 2nd January is indicative of February, etc. The origins of this system can be traced to the times of Spanish colonizers (Eakin, 1999). Two features are unique to this method and resemble state-of-the-art approaches. First, a re-forecast is constructed on the basis of the weather in past December in a similar way as January is used to predict the coming year. Hence, the method includes a certain *model calibration*. Second, several predictions are constructed for every month of the coming year. The more the predictions for a particular month differ from each other the more the conditions are considered to be too variable and thus the predictions inconclusive. Hence, this traditional prediction method already incorporates a certain *probabilistic approach*. Obviously, the remote influence of El Niño could be a possible physical explanation.

The advent of modern seasonal forecasting methods is related to studies undertaken by the Indian Meteorological Service in the late 19th and early 20th century. The failure of the Indian monsoon in 1877/1878 led to severe droughts, food shortages and famine.

[2]For further reading refer to a Special Issue of *Climatic Change* (Volume 100, Issue 2) in 2010 entitled "Indigenous Peoples' Knowledge of Climate and Weather"

[3]This year (11 April 2011) it took 10 minutes 56 seconds, compared to the long-term average of 14 minutes...

A series of studies culminated in the identification of the "Southern Oscillation" (SO), a see-saw of atmospheric pressure between the western and eastern parts of the tropical Pacific, but also other teleconnection patterns, and their large-scale influences (Walker, 1924). Early statistical models were developed and provided encouraging results until the 1930s. It is thought that thereafter (multi-) decadal variability altered the patterns of teleconnection in a way not accounted for by such simple statistical models (Troccoli, 2010), and, as a consequence, seasonal forecasts failed. Furthermore, with the advent of early computers, more resources were devoted to Numerical Weather Prediction (NWP), i.e., the short-term prediction of the evolution of weather patterns, and seasonal prediction lost momentum.

An important hurdle towards successful seasonal forecasting, and in some way the starting signal for operational use, were studies of the mechanisms of the El Niño-Southern Oscillation (ENSO)—the coupled variability of the tropical Pacific ocean and the SO. The appreciation of the coupling between anomalies in both the tropical ocean and the atmosphere led to the recognition that sea surface temperature anomalies may have the potential to influence climate remotely on seasonal time scales (Troccoli, 2010; Harrison et al., 2008). The increasing understanding of the mechanics led to the development of first dynamical models. The strong ENSO event in 1982/1983 draw much attention in the climate community. It was a demonstration of how an oceanic pattern could influence the atmosphere and therefore climate over thousands of kilometers, with sometimes devastating impacts. The next ENSO event in 1986/1987 was successfully predicted one year in advance by Zebiak and Cane (1987).

Increasing computer power during the 1990s and the maturity of atmospheric models used in NWP led to an increasing importance of dynamical seasonal predictions (Troccoli, 2010). The first successful predictions and the recognized importance of the tropical Pacific led in 1997 to the setup of the Tropical Atmosphere Ocean (TAO) array, an observation grid of buoys to monitor the state of the tropical Pacific. The observation of the oceans was further improved by the introduction of the ARGO floats (the number of buoys increased by about 200% between 1990s and 2010, (Troccoli, 2010, his Fig. 6)). In contrast to the moored buoys of the TAO array, these floating observation buoys are transported by winds and currents around the globe. The increase in ocean data finally allowed the development of general circulation models (GCM) of the ocean. Within the European project PROVOST[4] (and a companion American project DSP[5]), a full atmospheric GCM was coupled with a full ocean GCM in order to produce seasonal predictions (Palmer and Shukla, 2000). Additionally, forecast experiments were made

[4]PRediction Of climate Variations On Seasonal to interannual Time-scales, ran from 1997 to 1999

[5]Dynamical Seasonal Prediction, informally co-ordinated research program among five US modeling groups

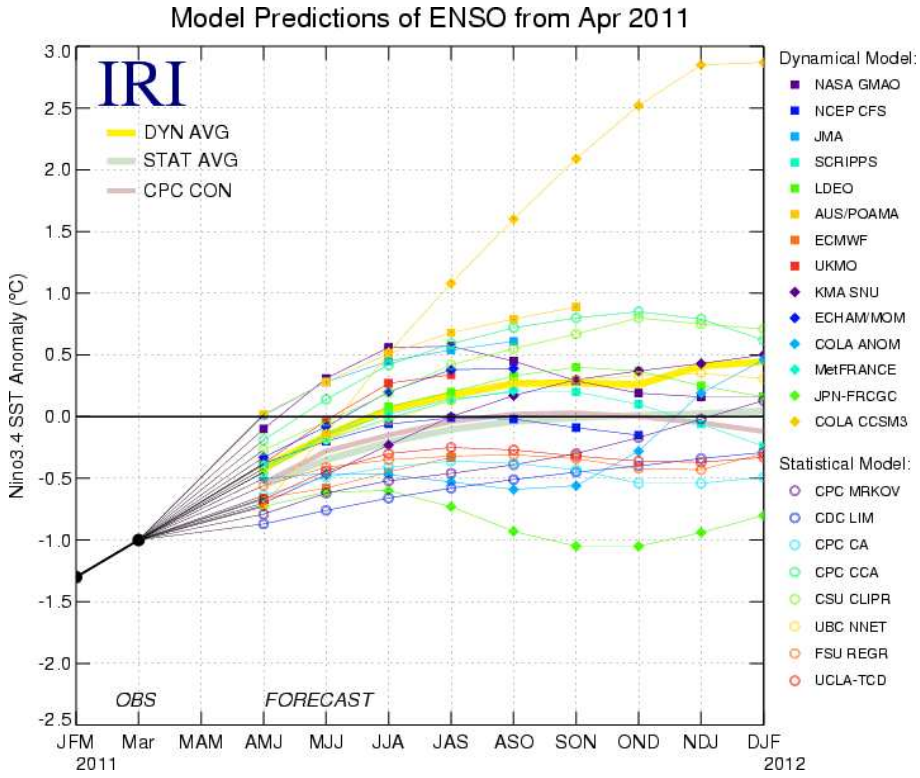

Figure 1.2: Current seasonal forecasts made by several dynamical and statistical models for SST in the Niño 3.4 region for nine overlapping 3-month periods from April–June 2011 to December–February 2011/2012. Figure courtesy of the IRI (Source: http://iri.columbia.edu/climate/ENSO/currentinfo/SST_table.gif, accessed 01-05-2011).

with uncoupled atmospheric GCMs forced by observed sea surface temperature (SST, AMIP-type experiments[6]).

Inherent uncertainty in the observations of the state of the climate system and in the prediction models limit the deterministic predictability of the evolution of the atmosphere to about 10 to 15 days (see also section 1.2.2). These uncertainties must be taken into account by probabilistic methods, e.g., ensemble prediction techniques, in order to produce meaningful predictions on longer time scales. The multi-model approach, where not only several prediction runs of a single model, but several prediction runs of more than one model are computed, was investigated within two European research projects in particularly, namely DEMETER[7] and ENSEMBLES[8]. The understanding that multi-model ensembles generally outperform single-model ensembles is a major outcome of these projects (e.g., Hagedorn et al., 2005; Doblas-Reyes et al., 2005). Today, more than 10 major centers produce operational dynamical seasonal predictions (Troccoli, 2010). Other

[6]Atmospheric Model Intercomparison Project, standard experimental protocol for global atmospheric general circulation models

[7]Development of a European Multimodel Ensemble system for seasonal to inTERannual prediction, ran from 2000 to 2003

[8]ran from 2004 to 2009

institutions use statistical methods or a combined statistical-dynamical approach. The latest seasonal forecast of ENSO summarizes the predictions currently available (Fig. 1.2). Generally, the models agree on a weakening of the current La Niña conditions over the next three to five months. The majority of the models agree on neutral conditions for the next winter, although one dynamical model predicts the onset of a strong El Niño.

1.2.2 Physical basis of seasonal forecasting

The existence of limits of deterministic forecasts have already been mentioned (section 1.2.1). Thus, neither the details of cloud coverage, the amount of precipitation, nighttime minimum temperature, nor daily average temperature will be predicted successfully beyond 15 days, whatever weather prediction model improvements may come in the future. So, why would we expect predictability of extreme events like wintertime windstorms over the North Atlantic and Europe on seasonal time scales, i.e., predictions with lead times of several months? Mainly because of two reasons (Troccoli, 2010): First, the boundaries of the atmosphere evolve more slowly than the atmosphere itself, e.g., the oceans or the land surface. Therefore, their evolution may be predicted (in the simplest case by persistence) on much longer time scales than the theoretical limits of deterministic predictability. The variability of the atmosphere is to a certain (in general regionally and seasonally varying) degree determined by its sluggishly varying boundaries (Troccoli et al., 2008; Shukla and Kinter III, 2006; Harrison, 2005; Kushnir et al., 2002; Goddard et al., 2001; Lorenz, 1979; Charney and Shukla, 1981). To the extent these boundary conditions (Fig. 1.3) can influence the atmosphere, the statistics of weather may be predictable well beyond the limits of deterministic weather predictions (Shukla and Kinter III, 2006; Harrison, 2005).

Second, the type of information of a seasonal prediction differ from the one of conventional weather forecasts. Seasonal predictions will have lower spatial and temporal resolution (e.g., the mean winter temperature for an entire country). Most importantly, however, they will be probabilistic in nature. Hence, they are not predictions of the exact evolution of weather systems but rather try to predict the (subtle) changes in the statistics of the evolution of weather systems influenced by anomalies in more slowly varying parts of the geophysical system. These changes are than expressed as probabilities that the climate system and the atmosphere will be in a certain state. In the following, these issues are addressed in more details.

Influence of the boundary conditions

The surface boundary conditions include SST (which may influence the atmosphere by convergence of moisture flux and latent and sensible heat flux), soil moisture (heat capacity

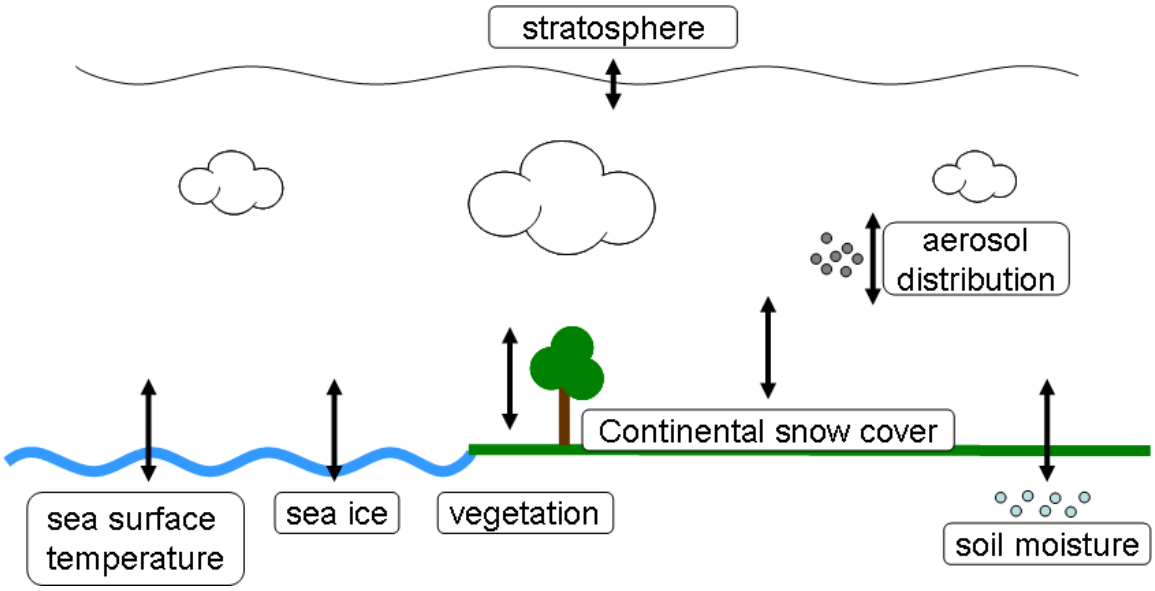

Figure 1.3: Boundary conditions and other factors with potential impacts on the variability of weather on seasonal time scales (see text for details).

of land surface, latent heat flux between continents and atmosphere), vegetation (surface temperature, latent heat flux to atmosphere), snow (surface radiative balance, latent heat flux, lag through meltdown and evaporation), and sea ice (surface radiative balance, latent heat flux from the ocean). Anomalous fluxes between the boundaries and the atmosphere can influence low-level winds and convergence through changes of, e.g., the horizontal temperature and pressure gradient. These may further develop into three-dimensional heating anomalies, which then may have impacts on the entire atmospheric circulation (see, e.g., Shukla and Kinter III, 2006; Goddard et al., 2001). Furthermore, the weather-active troposphere is capped by the overlying stratosphere (Kushnir et al., 2006; Harrison, 2005). The high static stability is the reason why the stratosphere varies on longer time scales than the troposphere. The stratosphere's influence on the troposphere is related to changes in wave propagation from and into the troposphere (Baldwin et al., 2003).

The influence of the boundary conditions is fundamentally different between tropical and extra-tropical regions. Owing to the latitudinal dependance of the Coriolis force, strong solar heating, and the convection throughout the troposphere, the large-scale seasonal atmospheric circulation and precipitation patterns are almost completely determined by the SST pattern in the tropics (Anderson, 2008; Shukla, 1998). In contrast, SSTs in the mid-latitudes are cooler than in the tropics, and the atmospheric response to anomalies in the ocean is weaker (Anderson, 2008). However, other parts of the climate systems, such as snow cover and sea ice, might affect the extra-tropical atmosphere and lead to potential seasonal predictability. Nevertheless, seasonal predictability is considerably lower in extra-tropical than in tropical regions. Kushnir et al. (2006) estimate about 10–15% of

the inter-annual variability to be possibly predicted on seasonal time scales in the North Atlantic and European region. In addition to the local effect of anomalous boundaries, the remote influence of tropical variations (both in the atmosphere and ocean) on the extra-tropics might also play a role, especially in the North Pacific and American sector.

Relevant work on the influence of boundary conditions on the atmosphere is reviewed in the following focusing on the extra-tropics and, in particular, on impacts on the large-scale circulation over the North Atlantic and Europe.

The atmosphere and the oceans are coupled through turbulent and radiative energy exchange, which depend strongly on the **sea surface temperatures** (influenced by heat transport by currents, vertical mixing and boundary layer depth) and several atmospheric parameters including wind speed, air temperature, humidity, and cloudiness (Deser et al., 2010). Oceans impart some memory to the atmosphere, at least in some parts of the globe, resulting from the fact that the ocean has a much larger heat capacity than the atmosphere and consequently is much more 'inert'. Anomalies in SST last for a few weeks or longer, depending on the spatial scale (Anderson, 2008). For most regions of the globe, the strongest signal of climate variability after the seasonal cycle is related to the ENSO phenomenon (Anderson, 2008; Troccoli et al., 2008; Shukla, 1998). The quasi-periodic occurrence of SST anomalies in the eastern tropical Pacific are related to substantial shifts in the location and strength of deep convection (cf. Shukla, 1998; McPhaden et al., 1998, and references therein for reviews on mechanisms and impacts of the ENSO phenomenon). These large-scale heating anomalies change the atmospheric circulation (e.g., the positioning of the Walker Circulation) and through the exciting of waves the signal may also be transported into other regions (Diaz et al., 2001; Alexander et al., 2002, and references therein). The knowledge of the intimate coupling of atmosphere and ocean in generating and maintaining ENSO has increased considerably over the last three decades (see section 1.2.1). This is reflected by very skillful predictions of the evolution of ENSO several months ahead. For example, current seasonal prediction models attain correlations between about 0.7 and 0.9 for lead times of six months (Jin et al., 2008; Wang et al., 2008).

The extent to which the atmospheric circulation over the North Atlantic and European region is affected by ENSO variability is still strongly under debate (Frias et al., 2010; Sutton and Hodson, 2005; Van Oldenborgh, 2005; Mathieu et al., 2004; Van Oldenborgh et al., 2000). Furthermore, the physical mechanisms associated with SST variability in the tropical Atlantic or Indian Oceans, and resulting potential predictability on the seasonal time scale, are less understood than those of ENSO (Wu et al., 2007; Schott et al., 2009; Goddard et al., 2001).

In contrast to the tropics, the dominant forcing is generally from the atmosphere to the ocean in the mid-latitudes (Kushnir et al., 2002; Frankignoul, 1985). The forcing coming

from the atmosphere is dominated by heat fluxes in lower mid-latitudes and wind-driven entrainment in high latitudes (Frankignoul, 1985). For example, Deser and Timlin (1997) found the air-sea coupling to be strongest when the atmospheric circulation leads SST by two to three weeks, twice as strong as the simultaneous co-variability and nearly four times as strong as when SST leads the atmospheric circulation by a few weeks. It is assumed that such SST anomalies only have local effects, since convection releases much smaller amounts of energy in the mid-latitudes than in the tropics and is confined to a shallow layer of the troposphere (Kushnir et al., 2002). However, Minobe et al. (2008) have recently shown that convection associated with oceanic frontal zones in the Gulfstream region may extend through the entire troposphere.

Even if the influence of mid-latitudinal SST on the atmosphere is restricted by the chaotic nature of the atmosphere-ocean system (Harrison, 2005), observational studies have reported statistically significant relations between SST and the large-scale atmospheric circulation in the North Atlantic region on seasonal time scales (Wang et al., 2004; Czaja and Frankignoul, 2002; Rodwell and Folland, 2002; Saunders and Qian, 2002; Czaja and Frankignoul, 1999). For example, Czaja and Frankignoul (1999, 2002) found specific summer North Atlantic SST anomalies resembling a horseshoe to be related to geopotential height anomalies in the following winter. Rodwell and Folland (2002) estimate the upper limit of correlation skill of seasonal predictions of the winter North Atlantic Oscillation (NAO) based on North Atlantic SST to be in the range of 0.45–0.63. These observational findings have been partly confirmed by atmospheric model runs forced by prescribed observed or reconstructed SSTs (e.g., Sutton and Hodson, 2003; Rodwell et al., 1999). Rodwell et al. (1999) found that much of the multi-annual and multi-decadal variability can be reconstructed from knowledge of the North Atlantic sea surface temperature. However, Bretherton and Battisti (2000) note that similar results may be gained from a stochastic forcing, and, hence, that useful predictability associated with mid-latitude SST anomalies may be restricted to one or two seasons. Furthermore, Lin and Derome (2003) found the response to prescribed SST to be very sensitive to the model, especially in winter. Cassou et al. (2004) found in AGCM runs with prescribed Horseshoe SST anomalies a weak but coherent early winter response projecting onto the NAO. They argue that the North Atlantic Horseshoe pattern is an oceanic response to anomalous Rossby waves propagating from the tropics into the North Atlantic region. Similarly, Peng et al. (2005) and Wu et al. (2007) state that the North Atlantic Horseshoe may be a consequence of a persistent forcing of the atmosphere by tropical SST anomalies.

Such SST anomalies are the surface expression of changes in the heat content of a well-mixed upper-ocean layer, and, therefore, are persistent on time scales of months (e-folding time scale 3–5 months, Kushnir et al., 2002). Thus, the relation between the atmosphere and the North Atlantic seems to stem from the remarkable persistence of North

Atlantic SST anomalies (Kushnir et al., 2002). Another possible mechanism involves the reemergence of spring anomalies in subsequent autumn which have been preserved below a shallow mixed layer during summer and reappear at the surface when the mixed layer deepens in autumn (Cassou et al., 2007; de Coetlogon and Frankignoul, 2003; Timlin et al., 2002; Alexander et al., 1999; Alexander and Deser, 1995).

The atmospheric response to North Atlantic SST anomalies is assumed to be smaller than the unforced variability, and therefore probably difficult to assess in coupled model runs (Kushnir et al., 2002). Indeed, studies on the potential influence of SST anomalies on the North Atlantic atmospheric circulation are ambiguous. The diversity of GCM results is potentially related to the underlying climatological state of the atmospheric model and its relationship to the SST anomaly; the baroclinic eddy (storm track) response to the forcing and its feedback on the large-scale flow; and the relationship between the SST-forced response and the model's unforced, low-frequency variability (Lin and Derome, 2003; Kushnir et al., 2002).

In conclusion, there is consensus that the mid-latitude oceans play a subtle but fundamental role stabilizing rather than directly generating atmospheric anomalies (Kushnir et al., 2006; Harrison, 2005; Kushnir et al., 2002; Blade, 1997). This might lead to improvements of the predicted probability distributions, in particular for extreme events (Harrison, 2005).

Sea ice plays another important part in the extra-tropical climate system. Nevertheless, studies on its influence on the large-scale flow are relatively rare (e.g., Deser et al., 2004). The focus of model studies so far has been more on the problem of declining sea ice in a warming climate(Budikova, 2009; Seierstad et al., 2007, and references therein) or the impact of the large-scale atmospheric flow on sea ice variability (Budikova, 2009; Holland, 2003; Marshall et al., 2001; Dickson et al., 2000; Fang and Wallace, 1994). However, a number of studies analyzed the feedback of sea ice anomalies in the North Atlantic region in general atmospheric circulation models (Kvamstø et al., 2004; Deser et al., 2004; Magnusdottir et al., 2004). They consistently report an atmospheric response to anomalous sea ice extent which projects onto the NAO pattern. In particular, they revealed a negative feedback (i.e., sea ice anomaly patterns consistent with a positive NAO forcing induce anomalies in the large-scale flow reminiscent of a negative NAO pattern). It is argued that changes in the boundary forcing induces changes in transient eddies (on time scales of weeks) which feed back onto the mean large-scale flow (on time scales of months; Deser et al., 2007). Strong et al. (2009) investigated observational data to analyze the modeled negative sea ice-NAO feedback. They indeed found that this negative feedback dampens the variability of both sea ice concentrations over the North Atlantic and NAO-driven weather and climate. Hence, the potential of sea ice to influence winter climate in the North Atlantic region is documented in both model and observational analyses.

Besides the oceans, the land surface is the second lower boundary of the atmosphere. **Continental snow cover** can influence the atmosphere, predominantly owing to its high albedo, high thermal emissivity and low thermal conductivity (Cohen, 1994; Barnett et al., 1989). Additionally, the melting of snow can provide a sink for latent heat. For example, Eurasian snow cover in spring is known to influence the Asian summer monsoon (Barnett et al., 1989, and references therein). With respect to North Atlantic/European climate statistically significant correlations have been found between summer and autumn snow cover on the northern hemisphere and the NAO in the following winter (e.g., Cohen and Entekhabi, 1999; Saito and Cohen, 2003; Saunders et al., 2003). Saito and Cohen (2003) note that snow cover in October shows the highest correlation (~ 0.55) with the subsequent winter's NAO. They also pointed out that snow cover anomalies may induce an atmospheric response by wave flux anomalies into the stratosphere and related wave-mean flow interactions. Various model studies further investigated this hypothesis (Fletcher et al., 2007; Gong et al., 2004a,b, 2003a,b). Stratospheric circulation anomalies may then propagate downwards into the troposphere (see below). However, it was also mentioned that snow cover anomalies appear not to be a necessary but modulating condition for a specific NAO pattern (Gong et al., 2002).

Soil moisture is another property with potential influence on the seasonal time scale by influencing evaporation and other surface energy fluxes (Koster et al., 2004). Its influence is argued to be most important for the prediction of the summer months (Conil et al., 2009; Douville, 2004; Douville and Chauvin, 2000), and therefore of minor importance in the context of this thesis given its focus on windstorms in winter. Nevertheless, soil moisture anomalies have been shown to precede the extreme summer heatwave in Europe in 2003 (Fischer et al., 2007; Ferranti and Viterbo, 2006). Additionally, prescribing observed soil moisture or nudging the prediction model's soil moisture to observed values improves predictive skill to forecast, e.g., surface air temperature and precipitation over Eurasia and North America (Douville, 2010), at least in specific years and regions (Conil et al., 2009). **Vegetation** has only minor impacts on seasonal predictability (Beltrán-Przekurat et al., 2008; Lu and Greatbatch, 2002) and has therefore attained only few attention.

Almost a decade ago, it was reported that **stratospheric variability** may constitute a precursor of related variability in the troposphere (Thompson et al., 2002; Baldwin and Dunkerton, 2001). Basically, strong anomalies in the stratospheric flow related to Sudden Stratospheric Warming events are transmitted downwards on time scales of weeks, finally affecting the troposphere with a signal resembling the Arctic Oscillation. Thus, knowledge of the stratospheric state and its reproduction in prediction models could finally lead to improved skill (Baldwin et al., 2003). These relations are reproduced in climate models but with a rather weak amplitude (Gerber et al., 2009).

As an additional factor, **atmospheric aerosol distribution** could lead to variability on seasonal time scales (Troccoli, 2010; Engelstaedter and Washington, 2007). However, its influence has not yet been studied systematically.

In conclusion, several (observational and model) studies suggest potential seasonal predictability of wintertime climate in the North Atlantic region. Most promising factors include the North Atlantic SST in summer, continental snow cover in summer and autumn, and Arctic sea ice. Although the internal variability of the atmosphere in the North Atlantic region is the dominant part, variability related to these factors constitute a physical basis for seasonal predictability in that region.

From deterministic to probabilistic predictions

In a series of papers in the 1960s, Edward N. Lorenz described his work on the predictability of forced dissipative non-linear dynamic systems as represented, for example, by numerical weather prediction models (Lorenz, 1963, 1965, 1969b). In such systems, initially close states evolve into completely different states over time, regardless of how small the difference between the two states was at the beginning (provided that it is not exactly zero). Ultimately, they will be indistinguishable from two randomly chosen states, i.e., there is no information left in the system from the initialization. Thus, errors on the smallest scales propagate to larger and larger scales, owing to non-linear error growth. From the rate of the error growth it is possible to estimate the temporal limits of deterministic predictability. Lorenz (1982, 1969a) estimated the error growth rate in the atmosphere from nearly-analogues in maps of observed geopotential height and reported the error doubling time to be about 2.5–8 days. Thus, the ultimate limit of deterministic (weather) predictions is about 10–15 days which is why seasonal predictions must go beyond deterministic forecasts.

Predictions with dynamical climate models are uncertain for mainly three reasons (Collins, 2007; Schwierz et al., 2006): natural variability, model uncertainty, and (though, of negligible importance for predictions on the seasonal time scale) uncertainty of the pathways of external forcing (e.g., greenhouse gas emissions) . The first reason relates to the variability of the climate system which is highly non-linear, and, therefore, predictions of such a system prone to small errors in the estimation of the initial and the boundary conditions. It is often termed "initial condition uncertainty". The second refers to the fact that the climate models used for prediction are not perfect ("model uncertainty"). It can be further divided into parameter uncertainty (referring to approximations made in the parameterization of processes not resolved by the climate model) and structural uncertainty (referring to the numerical implementation of the resolved processes), although the two are inevitably linked (Collins, 2007).

Hence, one (seasonal) climate prediction run derived from given initial conditions and a given prediction model represents only one (dynamically) possible solution of the true evolution of the climate system. If based on slightly different initial conditions or a different model, the sequence of predicted weather will be substantially different from the first prediction, but generally equally likely. Probabilistic predictions take these uncertainties into account. That means, it is not the exact evolution of the climate system which is predicted but rather the probability of the system being in a specific state or another (i.e., a Probability Density Function (PDF) of the climate state).

There are different methods of obtaining such a PDF. Statistical methods used to estimate the PDF not only exist for the mean tendency, but also for higher moments. However, given the generally very large degrees of freedom, they are difficult to adapt for operational purposes (Schwierz et al., 2006). The most successful method so far has been to compute an ensemble of predictions and to take the distribution of this ensemble as the PDF of the predicted climate state. Until recently, however, the computational costs prohibited the implementation of the ensemble approach. The earliest prediction models were developed in the 1950s (Charney et al., 1950). Such models were also the basis of Lorenz's studies on non-linear dynamical systems. The first pre-operational ensemble prediction was calculated at the UK MetOffice (Murphy and Palmer, 1986). Operational Ensemble Prediction Systems (EPS) have been established in the early 1990s at the European Center for Medium-Range Forecasting (ECMWF), the US National Center for Environmental Prediction and the Meteorological Service of Canada (Lewis, 2005).

To account for natural variability, ensemble prediction runs are often initialized by slightly different initial conditions, each assumed to be consistent with the true state of the climate system and the inevitable observation error. The error growth in a dynamical system is often dominated by only a few modes (Lorenz, 1965). If these modes can be identified, a modest ensemble size should be sufficient for a reliable estimation of the PDF. This has led to methods such as Singular Vector Decomposition (Buizza and Palmer, 1995), Ensemble Kalman Filter (Houtekamer and Mitchell, 2005), or Breeding Vectors (Toth and Kalnay, 1997). However, such sophisticated initialization techniques have not been adopted for seasonal predictions (Troccoli, 2010). To account for model uncertainty, a possibility is to combine predictions of various models into a multi-model ensemble (Collins, 2007; Schwierz et al., 2006). Operational implementations exist on both medium-range (up to 30 days, TIGGE[9]) and seasonal time scales (EUROSIP[10]). Other possibilities include stochastic physics (Palmer et al., 2005) or perturbed physics (Murphy et al., 2007) where the uncertainty of the parameterizations within an individual model is accounted for by small random perturbations to the parameterizations themselves.

[9]THORPEX Interactive Grand Global Ensemble

[10]European multi-model Seasonal to Inter-annual Prediction

An interesting, and probably somewhat neglected, issue is the dealing of forecast users with probabilities. It is well-known that people have considerable difficulty in estimating and dealing with probabilities, risk, and uncertainty (Nicholls, 1999). That is, probabilistic predictions have not only fundamentally changed our perception of the entire predictability problem, but also force forecast providers to adapt the communication and dissemination of their predictions appropriately. Furthermore, users have to develop appropriate methods to incorporate probabilistic forecasts into their daily business.

The limits of seasonal predictability

In the last two sections, it was shown that there is indeed a physical basis for seasonal predictability in the North Atlantic and European region, and that such seasonal predictions are inherently probabilistic. Another prerequisite of seasonal forecasts is, in general, the temporal and spatial aggregation. Such forecasts are and will be issued for larger domains (e.g., countries) and longer periods (e.g., 3-monthly averages) rather than single points in time and space. With the probabilistic nature in mind, seasonal forecasts will, in my opinion, never be issued as operational weather forecasts for the next few days. Hence, these forecasts will be predominantly used by specialized users (e.g., governmental administrations, or businesses related to weather and climate), and will always need special knowledge for operational decision-making.

From a scientific point of view, the most fundamental limit of seasonal predictability is the existence of mechanisms relating the evolution of the atmosphere to that of some more slowly varying components of the climate system, i.e., the existence of potential predictability inherent to the climate system. The most prominent, best-documented and understood phenomenon might be ENSO and its far-reaching teleconnections. Not surprisingly, ENSO was the starting point of all efforts on modern seasonal predictions. But even here, operational seasonal predictions do not reach its ultimate limits. Most important reasons include the model dependency of predictive skill, indicating that the physical processes are not yet sufficiently understood (Shukla and Kinter III, 2006); the limited size of ensembles employed and, related to that, the insufficient ability to catch the fastest growing modes in the ensemble predictions (Troccoli, 2010; Shukla and Kinter III, 2006); and the difficulty with coupled ocean-atmosphere-land models (Shukla and Kinter III, 2006), e.g., the coupled initialization.

Of course, these limitations are also valid for the North Atlantic and European region. However, the influence of the atmosphere's boundaries is, although present (see sections before), assumed to be smaller than compared to those of, e.g., ENSO. Or, as Kushnir et al. (2006) put it: "In all, our community would be well advised to accept that the climate of the North Atlantic, and of Europe in particular, is dominated by a mode of

climate variability that is largely unpredictable. We can, perhaps, take comfort from the fact that recognizing the fundamental unpredictability of the atmosphere was arguably the greatest scientific achievement to emerge form our field in the past century." This somewhat pessimistic view might be related to the incomplete knowledge of processes governing the North Atlantic climate. More research is needed to understand the influence of SST, sea ice, snow cover, soil moisture, vegetation and the stratosphere on the North Atlantic atmosphere (Hurrell et al., 2006). As a consequence, at least parts of the inter-annual variability (10–15%) might be predictable and be of use for certain specialized end users (Kushnir et al., 2006). According to Kushnir et al. (2006) the challenge remains to demonstrate the reliability of such forecasts.

This thesis tackles exactly that challenge by investigating the level of skill and its sources in state-of-the-art seasonal prediction models forecasting European windstorm climate, a variable of vital interest for the natural hazard risk management business.

1.3 Motivation of the thesis

1.3.1 Seasonal windstorm predictability: a review

Despite the potential importance of longer-term forecasts of windstorms for society and economy (cf. 1.1.2) there are surprisingly few studies on seasonal predictability of wintertime windstorms. A possible reason is the generally lower predictability in the mid-latitudes compared to the Tropics (Troccoli et al., 2008; Lloyd-Hughes and Saunders, 2002). In contrast to extra-tropical cyclones, seasonal predictability of tropical cyclones, as an example of extreme events relevant for risk assessment, has been studied (e.g., Vitart et al., 2007), and (empirical) seasonal predictions are issued on an operational basis[11]. Furthermore, the seasonal forecasting practices have left infancy only in recent years and the predictability studies for the European region have mainly focused on temperature and precipitation (Shongwe et al., 2007; Della-Marta et al., 2007; Graham et al., 2005; Guérémy et al., 2005; Palmer et al., 2004; Rimbu et al., 2002; Lloyd-Hughes and Saunders, 2002; Palmer et al., 2000; Brankovic and Palmer, 2000), or on specific potential user applications like hydroelectric power management (Garcia-Morales and Dubus, 2007) or crop yields (Cantelaube and Terres, 2005; Marletto et al., 2005). A number of studies have analyzed the potential of seasonal predictions of the large-scale atmospheric circulation (e.g., as described by the NAO; Müller et al., 2005; Fil and Dubus, 2005; Doblas-Reyes et al., 2003). For example, as part of the European project PROVOST, Doblas-Reyes et al. (2003) evaluated the potential predictability of the NAO in four ensembles of at-

[11]For example, by P. J. Klotzbach and W. M. Gray at the Colorado State University, http://hurricane.atmos.colostate.edu/Forecasts/

mospheric GCMs forced with observed SST in the period 1979 to 1993. They found that especially the multi-model ensemble shows statistically significant skill for different probabilistic verification measures. In particular, this skill stems from the correct simulation of the inter-annual (rather than decadal) variability. In an analogous approach Compo and Sardeshmukh (2004) studied the predictability of mid-latitudinal storm tracks (2–7-day band-passed filtered variance of vertical velocity at 500 hPa) during winter (January to March) on seasonal and decadal time scales, both over the Pacific-North American and the North Atlantic-European region. They used two different atmospheric GCMs with prescribed SST and compared these re-forecasts (so-called hindcasts) with reanalysis for the 1950–1999 period. On the seasonal scale (i.e., the inter-annual variability) they found statistically significant skill (above the 5% level) over both the Pacific and Atlantic region. In contrast, hindcasts of 5-yearly averages ("decadal" scale) are not successful over the North Atlantic region. However, these deficiencies stem from the models rather than from intrinsically low predictability, i.e., model improvements could lead to an increase of storm track predictability in the North Atlantic region. Additionally, they found a relation between ENSO and predictability of the storm tracks. Therefore, it is important to analyze not only average skill but also variability of skill. Even if skill on average is low, it might prove useful under particular conditions.

With the development of fully coupled (ocean-atmosphere) seasonal prediction models, the question of seasonal NAO predictability could be increased to harder tests. For example, Müller et al. (2005) analyzed seasonal hindcasts of the ECMWF System 2 and of the multi-model data produced by the DEMETER project. For the mean winter (DJF) NAO, they found no skill for the period 1959–2001, but surprisingly large skill of 15% (relative to a climatological reference prediction) for the period 1987–2001. Additionally, they found a weak relation between the strength of the NAO amplitude and the skill of the NAO prediction. These results were confirmed by Johansson (2007) who found that, on monthly and seasonal time scales, the level of forecast for the NAO (and also the PNA) is generally quite low, except the winter months at short lead times. However, for the target season DJF, a few models attain Anomaly Correlation Coefficients above the threshold for significant nonzero correlation. However, Johansson (2007) has not analyzed the prediction in a probabilistic sense since his work was entirely based on the ensemble mean of the different ensemble members. Furthermore, his study did not comprise multi-model ensembles.

Hence, there is indeed potential of successful seasonal predictability of the wintertime climate in the North Atlantic and European region. It is well known that the wintertime NAO (or the large-scale atmospheric circulation in the North Atlantic region in general) is closely related to the occurrence of windstorms over Western Europe (Donat et al., 2010a; Pinto et al., 2009; Hurrell et al., 2003). Therefore, the documented potential of

longer-term skill of NAO or storm track predictions could be reflected in corresponding predictability of windstorm climate. Using a *statistical* approach, Palutikof et al. (2002) presented a pilot study on the seasonal predictability of windstorms over Europe. They studied the predictability of the number of exceedances of the 90th percentile of wind speed at 153 grid points over Europe from the NCEP reanalysis. They used predictors such as regional indices of North Pacific and North Atlantic SST (derived by EOF analysis) and indices of the atmospheric circulation (namely, the NAO, Arctic Oscillation, East Atlantic/Western Russian pattern, East Atlantic pattern). In a test case for the winter 1999/2000 they found the overall error to be quite small, although exceedances are overestimated (underestimated) in regions of climatologically low (high) wind speeds. Similarly, Qian and Saunders (2003) studied the predictability of storminess in the North Atlantic region (53.75°N–61.25°N, 46.25°W–11.25°E) on the basis of anomalies in northern hemisphere summer snow cover extent. For the 1972–2000 period, correlation coefficients between the average number of days that reach strong wind speeds on the Beaufort Wind Scale[12] and July–August northern hemisphere snow extent are between −0.58 and −0.68. Cross-validated hindcasts (leave-one-out method) of the linear regression model attain correlations between 0.53 and 0.67.

In contrast to these statistical approaches, there is to the best of my knowledge no study focusing on the seasonal predictability of windstorms in *dynamical* prediction models. The only study so far at least touching this issue found little evidence of skill (Della-Marta et al., 2010). In their study, they used seasonal hindcast data of different generations of seasonal forecast systems of the ECMWF and the ECMWF contribution to the DEMETER project to improve estimates of return period of wintertime windstorms. As a prerequisite, they quantified the skill of a windstorm intensity measure (their so-called Extreme Wind Index (EWI), see also Della-Marta et al., 2009) averaged over the entire North Atlantic and European domain. Except in the first month, they found no significant skill in predictions of monthly averaged EWI from November to April. However, they introduced a slight inconsistency by using hindcast runs from different start dates (namely, 1 August and 1 November) to construct their hindcast ensemble. Whereas the predictions for November, December and January were taken from the August hindcasts, the predictions for February, March and April were taken from the November hindcasts (i.e., with lead times of 3–6 months in both cases). It is possible that using hindcasts with shorter lead times (e.g., using the November hindcasts for November, December, and January, i.e., with lead times of 0–3 months) would result in higher skill scores. Furthermore, temporal averaging is known to increase skill on the seasonal scale. Thus, it is possible that some skill on a multi-monthly basis (e.g., December to February or extended winter season) is masked when only assessing single-month averages. Therefore, it is not possible

[12]'near gale', 13.9–17.1 m/s; 'gale', 17.2–20.7 m/s; 'strong gale', 20.8–24.4 m/s; 'storm', 24.5–28.4 m/s

to conclude from Della-Marta et al. (2010, e.g., their Fig. 4) that there is no predictive skill in seasonal predictions of wintertime storminess.

In summary, although the potential of seasonal predictions of wintertime windstorms has been demonstrated with simple statistical approaches, this issue has not been systematically addressed in dynamical seasonal prediction models. Furthermore, studies of dynamical predictions of the NAO have found encouraging results.

1.3.2 Potential use of seasonal windstorm risk predictions

Seasonal predictions are nowadays operationally issued and used in a range of applications, also in the economic sector (e.g., in the energy sector; see Troccoli et al., 2008, for an overview). In contrast, seasonal predictions have not yet been used to support risk management practices with respect to European windstorms. However, skillful predictions of windstorm climate could improve risk management practices in several ways.

For example, it is not cost-effective to only respond reactively to a disaster (e.g., by insurance pay-out). Instead, more emphasis should be laid on pre-disaster approaches (Dilley, 2002). Probabilistic predictions could serve as one input for pre-disaster decision making. Given the additional information provided by seasonal forecasts, options in the (re)insurance sector include the review of risk cumul and (financial) securities to cover indemnity pay-outs, and the adaptation of provided insurance coverage (Rauch, 2005).

However, two major barriers have been identified why the use of seasonal predictions has not yet found its way into operational risk management procedures (Murnane, 2004). Firstly, the level of skill is generally assumed to be very low, especially with respect to the North Atlantic and European region and to the occurrence of extreme events. Secondly, the current forecast lead times do not conveniently match those of the business cycles (Malmquist, 1999). In order to improve the use of seasonal predictions there is therefore need of:

1. better description of the tools and discussion involved in a climate forecast (Murnane et al., 2002),

2. better understanding of physical mechanisms leading to variability of the occurrence of extreme events on different time scales (Malmquist, 1999),

3. providing users a better sense of current model skill through better documentation (Murnane et al., 2002),

4. evaluation of coupled dynamical ocean-atmosphere prediction models (Malmquist, 1999),

5. analysis of how skill in seasonal predictions of extreme events can be improved (Murnane, 2004).

This thesis deals with all these issues to a certain degree.

1.3.3 Objectives of the thesis

On the one hand, the reviews in the previous sections have shown that skillful seasonal predictions of wintertime windstorms would be valuable for socio-economic applications. On the other, there are considerable gaps regarding the scientific knowledge of potential processes leading to longer-term predictions of windstorm activity, and the quality of state-of-the-art seasonal prediction models.

Despite the reported relations between hemispheric-scale factors—such as North Atlantic SST or continental snow cover—and wintertime climate in the North Atlantic region in observational data, the impact of these slowly varying components of the climate system on windstorms on the seasonal time scale has not been analyzed extensively. In particular, physical processes relating hemispheric-scale factors and windstorm occurrence on longer time scales have been neglected. Growth factors of extra-tropical cyclones such as baroclinicity, latent heat, or upper-tropospheric divergence may be influenced by anomalies in hemispheric-scale factors, and in turn induce anomalous development of strong cyclones and windstorms. Such physically motivated links in observational or reanalysis data provide potential sources of predictability, given that current prediction models are able to reproduce them.

Indeed, it has been shown that multi-model ensembles of dynamical seasonal prediction models—e.g., those of the European projects DEMETER and ENSEMBLES—successfully forecast the large-scale atmospheric flow in the North Atlantic region. However, predictive skill to forecast wintertime windstorm activity has not been addressed systematically.

The use of such prediction model ensembles allows to analyze the reproduction of the observed relations between hemispheric-scale factors, growth factors of cyclones, and windstorm occurrence in climate model data. Hence, the sources of predictive skill can be evaluated. Differences between the individual models and with respect to the observed relations could manifest in different levels of skill, and, ultimately, point to potential model improvements.

Thus, the main topics of this thesis are:

Definition and identification of windstorms

A proper windstorm definition and identification is the basis of this thesis. Proper description of the tools used is also requested by users of seasonal forecasts (see issue 1 in section 1.3.2). With regard to the socio-economic importance of European windstorms and the use of large (multi-) model ensemble predictions, the objectives are:

- Development of an impact-orientated definition of windstorms and objective identification scheme, appropriate for application to large (multi-) model ensembles
- Application of the identification scheme to reanalysis and seasonal prediction model

Potential sources of seasonal predictability of windstorm climate

The analysis of factors influencing windstorm activity on seasonal time scales and related physical processes in **observational and reanalysis** data will help to identify potential sources of seasonal predictability of windstorm activity (in line with issue 2 in section 1.3.2). The objectives are:

- Which hemispheric-scale factors are related to windstorm activity on seasonal time scales?
- Which physical processes explain such a relation? Are hemispheric-scale factors related to growth conditions of cyclones?

Skill of dynamical seasonal prediction models

Windstorms are identified in retrospective forecasts (so-called hindcasts) of the ensembles of coupled atmosphere-ocean climate models of the European Framework Projects DEMETER and ENSEMBLES. The quality of these hindcasts is assessed with respect to the observed windstorm activity (in consistency with issues 3 and 4 in section 1.3.2). The objectives are:

- How skillful are forecasts of state-of-the-art dynamical seasonal prediction models?
- What are the characteristics of the variability of skill?

Sources of skill in dynamical seasonal prediction models

The relation between hemispheric-scale factors, growth factors of cyclones and windstorm occurrences is evaluated in the **hindcast data** and compared to relations found in observational and reanalysis data (referring to issues 4 and 5 in section 1.3.2). The objectives are:

- Are hemispheric-scale factors related to the occurrence of windstorms in seasonal prediction models?
- Which role do growth factors of extra-tropical cyclones play in these relations?
- How do these relations compare to observations and between the different models?
- Are inter-model differences related to differences in skill of seasonal windstorm predictions?

1.3.4 Outlines of the thesis

The data used in the thesis are described in chapter 2. The body of the thesis is divided into four parts, reflecting the main topics introduced in the previous section.

The windstorm definition and identification method developed during this thesis is introduced in chapter 3. The identification scheme is applied on reanalysis data and an overview of features of windstorm climate is provided. The relation of windstorm events to growth factors of cyclones is analyzed. Additionally, the sensitivity of the identification scheme on the parameter settings is discussed. The windstorm identification method has already been applied by Nissen et al. (2010) and Leckebusch et al. (2008b).

Potential sources of seasonal predictability of windstorm activity are evaluated in chapter 4. The interannual variability of windstorm climate and its relation to hemispheric-scale factors (North Atlantic SST, continental snow cover, sea ice extent, and NAO) on seasonal time scales on the basis of reanalysis and observational data is analyzed. Possible physical processes are evaluated in terms of the dependence between different hemispheric-scale factors and the impact of anomalous hemispheric-scale factors on growth factors of cyclones. The content of this chapter will be submitted to the International Journal of Climatology.

In chapter 5, the seasonal hindcasts data of the multi-model ensembles provided by the DEMETER and ENSEMBLES projects are analyzed. The windstorm identification scheme is applied to the hindcast data and the resulting windstorm climatologies compared to the climatology of the reanalysis. Predictive skill is evaluated in terms of different skill

score measures. Additionally, some aspects of the variability of skill are discussed. The content of this chapter forms parts of a publication in Monthly Weather Review[13].

The seasonal hindcast data are further analyzed in chapter 6. The relation of hemispheric-scale factors, growth factors of cyclones and windstorm occurrence in the prediction models is evaluated in analogy to chapter 4. Focusing on anomalous conditions in North Atlantic, the persistence of ocean anomalies is compared between the different models and reanalysis. Links between inter-model differences in the persistence of oceanic anomalies and predictive skill are discussed. The content of this chapter will be submitted to the International Journal of Climatology.

Finally, chapter 7 provides a summary of the main results of the thesis, followed by discussion and conclusions, including prospects of future work.

To avoid duplication of the introductionary parts and the data descriptions of the submitted manuscripts, the corresponding sections have been excluded or shortened in the chapters 4, 5, and 6. Additionally, the results of the individual chapters are discussed together in the final chapter.

[13]Renggli, Dominik, Gregor C. Leckebusch, Uwe Ulbrich, Stephanie N. Gleixner, Eberhard Faust, 2011: The Skill of Seasonal Ensemble Prediction Systems to Forecast Wintertime Windstorm Frequency over the North Atlantic and Europe. *Mon. Wea. Rev.*, **139**, 3052–3068. doi: 10.1175/2011MWR3518.1

Chapter 2

Data

2.1 Reanalysis data

Gridded data sets of observations contain artificial discontinuities owing to the change of observation instruments, changes of the availability of different kinds of observations, changes in quality control, and the evolution of numerical models used to assimilate the observations (Wallace and Hobbs, 2006). Reanalysis products are generated to reduce these inhomogeneities. Basically, a reanalysis incorporates the blending of archived global observations of, for example, temperature, humidity and pressure, with a first-guess of the current atmospheric state from a numerical weather prediction model, i.e, the model is pulled towards the observed state. The use of one and the same model and quality control procedure reduces the aforementioned discontinuities. Different methods exist to perform such an assimilation. At the ECMWF, a sophisticated four-dimensional assimilation scheme is used (4D-Var, Rabier et al., 2000; Mahfouf and Rabier, 2000; Klinker et al., 2000). 4D-Var optimizes the current state of the atmosphere in the model both in the temporal and spatial dimensions. The result of such a reanalysis is a quasi-observational, consistent, gridded data set with an best-estimate of the state of the atmosphere. The quality of such reanalysis products differ between different variables. Generally, the planetary-to-synoptic-scale flow is in very good agreement with observations (e.g., geopotential or surface pressure, which are assimilated from observations). On the other hand, diagnostic variables such as precipitation rely to a large degree on the parameterization of the model physics, and are prone to model errors.

Data of the **ERA-40 reanalysis** (Uppala et al., 2005) produced by the ECMWF are used in this thesis. It covers the 1957–2002 period and is provided on a uniform 2.5 degree grid[1]. Six-hourly surface (10 m) winds are used to identify windstorms. Furthermore, surface temperature (SST over the oceans, upper-most soil level temperature

[1]Data freely available at http://data.ecmwf.int/data

over land) and mean sea level pressure are used to characterize hemispheric-scale factors. Additionally, temperature, specific humidity and wind data on different pressure level are used to calculate specific growth factors of extra-tropical cyclones (see section 2.4).

Surface winds of the **ERA-interim reanalysis** (Berrisford et al., 2009) data set on a uniform 0.7°grid are employed in the sensitivity analysis of the windstorm identification scheme. This data set is used to be consistent with other studies on extreme wind event identification at the Institute of Meteorology.

Furthermore, ocean heat content (vertically averaged potential temperature of the upper 300 m) of the ECMWF **Ocean Reanalysis** (ORA; Balmaseda et al., 2008) has been obtained on a regular grid with 1 degree resolution. This data set can be regarded as a historical ocean re-analysis. Based on the synthesis of surface and subsurface ocean observations and surface fluxes from atmospheric (re-) analyses with a general circulation ocean model, it constitutes an important source for climate variability studies (Balmaseda et al., 2008).

2.2 Observational data

Monthly station-based **NAO** Index data is provided by the Climate Analysis Section, NCAR, Boulder, USA, for the period 1959–2001. (Hurrell, 1995). This index is based on the difference of normalized sea level pressure observations between Ponta Delgada, Azores and Stykkisholmur/Reykjavik, Iceland.

Monthly data of **snow cover extent** (in km^2) on the Eurasian and North American continent and the entire northern hemisphere has been obtained from the Rutgers University Global Snow Lab for the period 1972–2002 (Robinson et al., 1993). These data have been compiled from digital National Oceanic and Atmospheric Administration-National Environmental Satellite, Data, and Information Service (NOAA-NESDIS) weekly northern hemisphere snow charts. The original NOAA-NESDIS snow charts are derived from manual interpretation of AVHRR, GOES, and other visible-band satellite data. In addition to these scalar monthly snow-covered area data, the gridded weekly snow cover extent Version 3 product provided by the National Snow and Ice Data Center (NSIDC; Armstrong and Brodzik, 2005 (updated 2007) has been used to study anomalies in the spatial distribution of snow cover. To this end, the binary weekly maps (1 in the case an individual pixel is snow-covered, 0 otherwise) have been converted into monthly mean snow concentration for every pixel.

After 1978, the NSIDC data also include **sea ice extent** derived from sea ice concentrations from NIMBUS-7 SMMR and DMSP SSM/I Passive Microwave Data. As for snow cover, scalar data of sea ice extent (in km^2) are available for the entire northern hemisphere, the North Atlantic and North Pacific sector. Monthly maps of sea ice con-

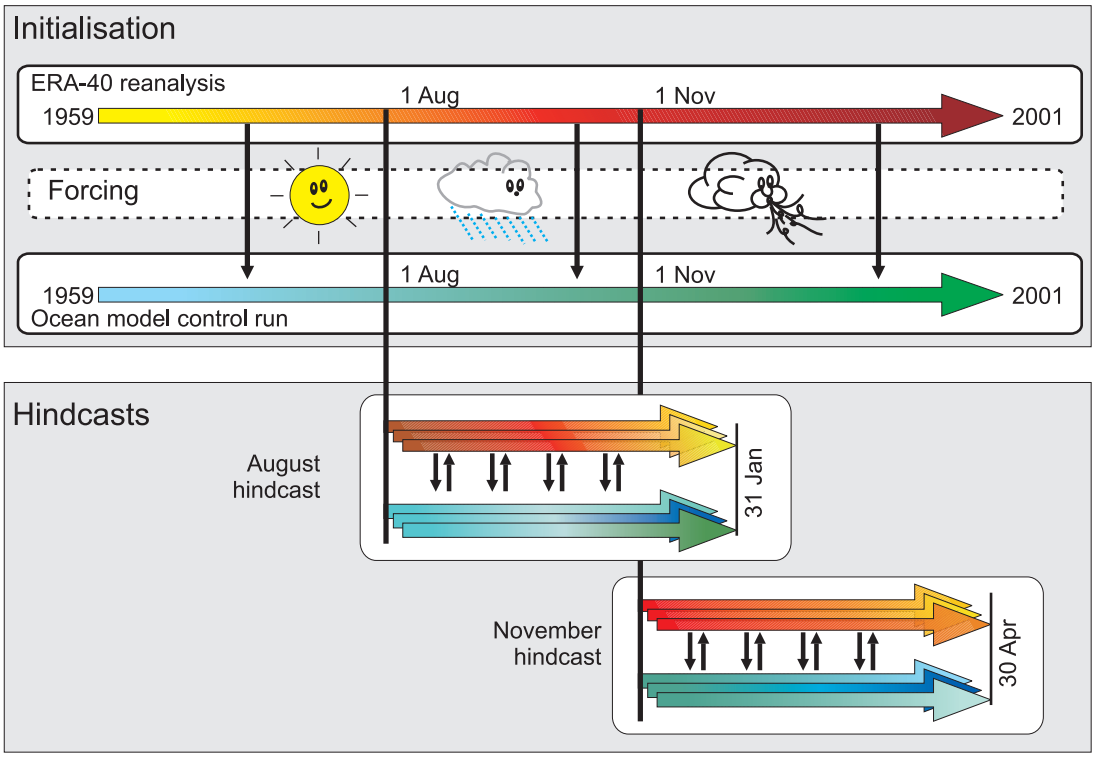

Figure 2.1: Illustration of the initialization and hindcast scheme used in the DEMETER and ENSEMBLES project (see text for details).

centration have been calculated from the weekly sea ice coverage maps in analogy to snow cover.

Both the weekly sea ice and snow coverage maps are available on the NSIDC EASE grid (721×712 pixels covering the entire northern hemisphere). However, note that since the original snow cover maps were digitized on a 89×89 cell Cartesian grid laid over a polar stereographic projection of the northern hemisphere, cell resolution of the snow data ranges from 16 000 to 42 000 km^2 whereas the source grid ice concentrations pixels range in size from approximately 485 to 664 km^2.

2.3 Seasonal prediction model data: DEMETER and ENSEMBLES

The seasonal forecast model data from DEMETER and ENSEMBLES used in this study consist of ensembles of 6-months hindcasts from 11 different coupled atmosphere-ocean climate models with nine ensemble members each. These nine ensemble members were generated by slightly altered initial conditions for the coupled model runs (cf. Palmer et al. (2004) and Weisheimer et al. (2009) and references therein for further description). Basically, the methodology consists of two parts: the initialization and the hind-

casts (Fig. 2.1). First, each model's ocean component is forced by radiative, mass, and momentum fluxes from ERA-40 reanalysis (one-way forcing). Forcing the ocean model by the original, a positively perturbed, and a negatively perturbed wind stress field yields three different continuous ocean analyses (represented by just one arrow in Fig. 2.1; see also Palmer et al., 2004, their Fig. 1). Thus, the oceanic state is always consistent with the observed (or, reanalyzed) atmospheric state. The ocean control runs are generated for the entire period covered by the respective model (e.g., from 1959–2001 in Fig. 2.1). The oceanic initial conditions for the hindcasts are taken as the current state of the three ocean analyses at a given start date. Additionally, positive and negative SST perturbations are added to each of the three ocean analyses, yielding a total of nine different initial conditions of the oceanic state. Generally, the atmospheric and land surface initial conditions are taken as the current state in the reanalysis at the start date. Starting from these nine slightly different initial conditions, fully coupled, six months long prediction runs are computed (e.g., August to January or November to April). The next set of hindcasts is generated from the state in the ocean analyses and the atmospheric reanalysis three months later. These hindcasts may be verified against observations or reanalysis data.

Note that the Max Planck Institute (Hamburg) and the Leibniz Institute of Marine Sciences (Kiel) used a slightly different approach. They used a coupled ocean-atmosphere model run restored to observed SST to generate the initial conditions.

Concentrating on winter windstorms, hindcasts starting on 1 November and running to the end of April were used in this study. Within the DEMETER project, three models are available for the 1959–2001 period, and four additional models cover at least the 1980–2001 period (Table 2.1, upper rows). From ENSEMBLES, four models delivered the required data for the period 1960–2001 (Table 2.1, lower rows).

The DEMETER data and model data from ECMF and LFPW were available on a common regular 2.5 degree grid (see Table 2.1 for the models' acronyms used in the following). INGV and IFMK were provided on the original T63 resolution and were interpolated to the common regular 2.5 degree grid using a first-order conservative remapping scheme (Jones, 1999).

Focusing on windstorm occurrence in winter the hindcasts starting on 1 November (running to the end of April) and the hindcasts starting on 1 August (running to the end of January) are evaluated. SST, mean sea level pressure (MSLP) and snow depth data are taken to represent the hemispheric-scale factors. In addition, vertically averaged potential temperature of the uppermost 300 m of the ocean (TAV) has been available for four of the DEMETER models (namely, SCWF, UKMO, SCNR, and CRFC) and is used as a measure of the ocean heat content. Temperature, wind speed and specific humidity on different pressure levels are used to compute the growth factors of cyclones. Surface wind speed is used for the windstorm identification.

The only model providing sea ice data is ECMF. However, it does not use a dynamical sea ice module. Instead, initialized observed sea ice values are relaxed to climatological values in the course of the prediction. Therefore, modeled sea ice has not been considered.

Acronym	Institution	Period covered	Atmospheric component (resolution)	Oceanic component
DEMETER (cf. Palmer et al., 2004, their Table 1)				
SCWF	ECMWF	1959–2001	IFS; T95/L40	HOPE-E; 0.3°-1.4°/L29
CRFC	European Centre for Research and Advanced Training in Scientific Computation, France	1980–2001	ARPEGE; T63/L31	OPA 8.2; 2°/L31
LODY	Laboratoire de l'Océanographie Dynamique et de Climatologie, France	1974–2001	IFS; T95/L40	OPA 8.2; 2.0°/L31
CNRM	Centre National de Recherches Météorologiques, Météo France, France	1959–2001	ARPEGE; T63/L31	OPA 8.0; 182 GP×152 GP/L31
UKMO	UK MetOffice	1959–2001	HadAM3; $2.5° \times 3.75°$/L19	GloSea OGCM, based on HadCM; 1.25°× $0.3° - 1.25°$/L40
SMPI	Max Planck Institute, Germany	1969–2001	ECHAM-5; T42/L19	MPI-OM1; $2.5° \times 0.5° -$ 2.5°/L23
ENSEMBLES (cf. Weisheimer et al., 2009, their Table 1)				
ECMF	ECMWF	1960–2001	IFS CY31R1; T159/L62	HOPE; $0.3° - 1.4°$/L29
LFPW	Météo France	1960–2001	ARPEGE 4.6; T63	OPA8.2; 2°/L31
IFMK	Leibniz Institute of Marine Sciences at Kiel University, Germany	1960–2001	ECHAM5; T63/L31	MPI-OM1; 1.5°/L40
INGV	Euro-Mediterranean Centre for Climate Change, Italy	1960–2001	ECHAM5; T63/L19	OPA8.2; 2°/L31

Table 2.1: Acronyms, institutions, periods covered, atmospheric and ocean components of the seasonal prediction models used for the study. See also Palmer et al. (2004) for further details on the DEMETER models (upper rows) and Weisheimer et al. (2009) for the ENSEMBLES models (lower rows).

2.4 Growth factors of extra-tropical cyclones

Maximum Eady growth rate, equivalent potential temperature, and divergence and wind speeds in the upper-tropospheric have been shown to influence the intensification of cyclones, in both case studies and in climatological analyses (Pinto et al., 2009; Ulbrich et al., 2001). The factors have been computed for both reanalysis and seasonal prediction model data following Pinto et al. (2009). Owing to the availability of pressure level data from the seasonal prediction models, the levels used to calculate the Maximum Eady growth rate have been slightly altered.

The Eady growth rate (denoted as EADY in the following) is a measure of baroclinicity (Hoskins and Valdes, 1990), i.e., it quantifies the large-scale conditions for the potential growth of wave disturbances and extra-tropical cyclones. It is computed as

$$EADY = 0.31(f/N)\left|\frac{\Delta \mathbf{v}}{\Delta z}\right|, \tag{2.1}$$

where f is the Coriolis parameter, N is the static stability, z the vertical pressure coordinate and $\mathbf{v}$ the horizontal wind vector. EADY is calculated between 850–500 hPa. As in Ulbrich et al. (2001) and Pinto et al. (2009), the variable is considered as 3-day running averages.

The equivalent potential temperature (EPT) at 850 hPa is used as a measure of the combined effect of latent and sensible heat which may also contribute to cyclone intensification (e.g., Chang et al., 1984; Gronas, 1995). The quantity is calculated according to Bolton (1980).

Areas of enhanced upper-tropospheric divergence (DIV) at 200 hPa around the jet exit region are well known to induce rapid cyclone growth (e.g., Ulbrich et al., 2001). In the case of the ERA-40 reanalysis DIV is taken from the model output. In the case of the models, it was calculated using finite differences of the zonal and meridional wind speed since divergence is not available as direct model output.

The upper-tropospheric flow has a strong influence on the steering and velocity of cyclone development (e.g., Schultz et al., 1998). Wind speed (JET) at 200 hPa is considered here.

Chapter 3

Definition and identification of windstorms

3.1 Rational

The definition and identification of wintertime windstorms over the North Atlantic and Europe is the starting point of this thesis. Two criteria are important to be met: First, the definition needs to be objective and to be based on meteorological parameters only in order to be applicable to extreme wind events that occurred in reality, e.g., as identified in reanalysis data, but also to potential wind events as reproduced in climate models used for seasonal predictions. Second, the objective definition has to be implemented into an efficient identification scheme. Since probabilistic forecasting is crucial and widely used in state-of-the-art seasonal predictions—mostly through the incorporation of several prediction runs based on slightly disturbed initial conditions (ensemble predictions)—data sets produced by such ensemble prediction approaches are usually very large. Additionally, the identification scheme should be based on as few variables as possible, thereby considerably increasing the efficiency (e.g., the amount of data needed).

Extreme wind events in the North Atlantic and European region are most often related to very deep low pressure systems. Several objective cyclone identification schemes on the basis of, for example, mean sea level pressure (MSLP, Wernli and Schwierz, 2006; Blender et al., 1997), the Laplacian of MSLP (Pinto et al., 2005; Murray and Simmonds, 1991) or vorticity (Hoskins and Hodges, 2002) are in use. Thus, these definitions are based on the physical properties of atmospheric lows. However, a low pressure system is not necessarily accompanied by extreme wind speeds and is therefore not to be taken as a hazardous event *per se*. Focusing on the impacts of such extreme wind events, the wind speed at the surface is the variable of interest.

Yet, the impacts of extreme wind events are not only dependent on the absolute level of wind speed but rather on the wind speed relative to the climatology at a given location (i.e., in risk analysis terms, the vulnerability has to be taken into account). Observational studies have shown a close relation between the wind climatology and reported insured loss (Leckebusch et al., 2007; Klawa and Ulbrich, 2003). They found a good agreement between reported losses and the cube of the relative exceedance of the local 98^{th} percentile of surface wind speeds. Therefore, a percentile approach was used for the definition of windstorms. This approach comes with another advantage. Climate models often exhibit systematic (negative) biases in the reproduction of the absolute level of (extreme) wind speeds, especially over the continents. Through the incorporation of the local model-specific wind climatology, such biases should be reduced. A similar approach was introduced by Della-Marta et al. (2007) to define an "Extreme Wind Index". However, their definition, although being objective, is based on spatially aggregated information, and therefore does not allow to evaluate these events also in their spatial extent.

In contrast to Della-Marta et al. (2007) the identification scheme introduced here identifies windstorms not only in their temporal development, but also in their spatial extent. Therefore, both the time as well as the position of occurrence of an extreme event is known. This extension enables dynamical studies, for instance, on the relation between windstorms to extra-tropical cyclones (e.g., Nissen et al., 2010). Additionally, it allows to define an event-based severity measure of extreme wind events.

In the following, the windstorm definition and identification scheme is illustrated using the example of windstorm "Daria" which hit western Europe in January 1990 (section 3.2.1). The objective Storm Severity Index is introduced in section 3.2.2. Then, the spatial and temporal climatologies of the windstorm events identified by the scheme in the ERA-40 reanalysis data are presented. The sensitivity of the tracking algorithm to the input parameters is analyzed in section 3.4. The use of the identification scheme is illustrated by investigating the relation between growth factors of cyclones and windstorm frequency in the North Atlantic region. Conclusions relevant to the following chapters of the thesis are given at the end.

3.2 Methods

3.2.1 Tracking scheme

In this section, the identification scheme is explained and illustrated by examples. The first step of the identification is the calculation of surface (10 m) wind speed from the zonal and meridional wind components given by the data set considered. Based on these instantaneous 6-hourly data in winter (here defined as November–April, in consistency

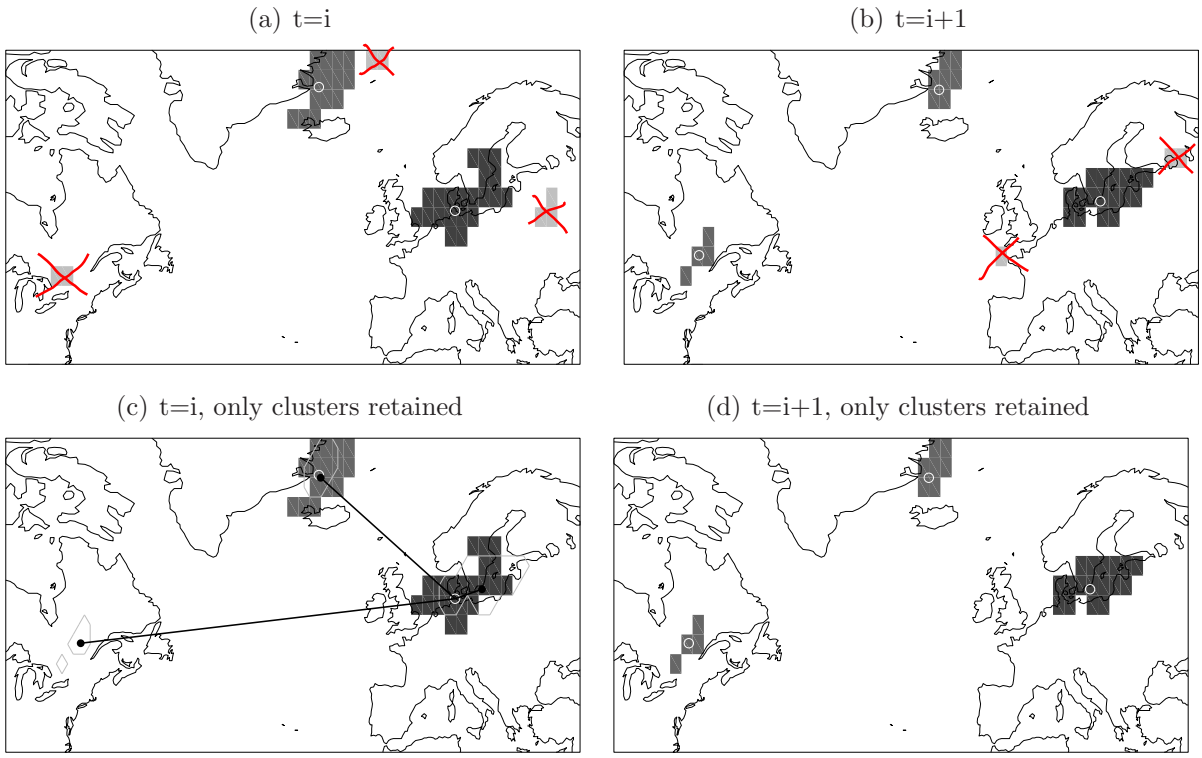

Figure 3.1: Schematic illustration of the tracking algorithm for two timesteps at 26 January 1990, 06 UTC (a, c) and 12 UTC (b, d). Indicated are areas with percentile exceedance smaller than the minimum threshold (light gray shading, crossed out), larger than the minimum threshold (light gray), and areas belonging to windstorm "Daria" (dark gray); centers of clusters at the current timestep (white circles), clusters of next timestep (contours in (c)) and their position (black dots in (c)), and the distance from the current center of "Daria" to all cluster centers of the next timestep (black lines in (c)).

with the temporal extent of the November hindcasts of the DEMETER project), the local 98^{th} percentile is calculated for every grid box. The tracking is then applied to the North Atlantic and European region.

A number of parameters have to be set in order to use the tracking scheme, namely thresholds for minimum area, minimum lifetime and maximum translation velocity. The exact values of these parameters given in the following have been derived by extensive testings during the development stage of the algorithm and should be considered as "best-estimate values" (cf. section 3.4 for the sensitivity analysis).

The tracking scheme is illustrated by two timesteps of windstorm "Daria" (Fig. 3.1). The first step of the tracking algorithm is to identify grid boxes with wind speeds exceeding the local percentile threshold. Then, continuous areas (i.e., adjacent grid boxes) with simultaneous percentile exceedance are identified (so called clusters; light gray shading in Fig. 3.1). Clusters with an area not exceeding a minimum value (approximately 150 000 km^2) are not taken into account in the remainder of the scheme. For clusters exceeding this minimum area threshold, the cluster center (white circles in Fig. 3.1) is calculated

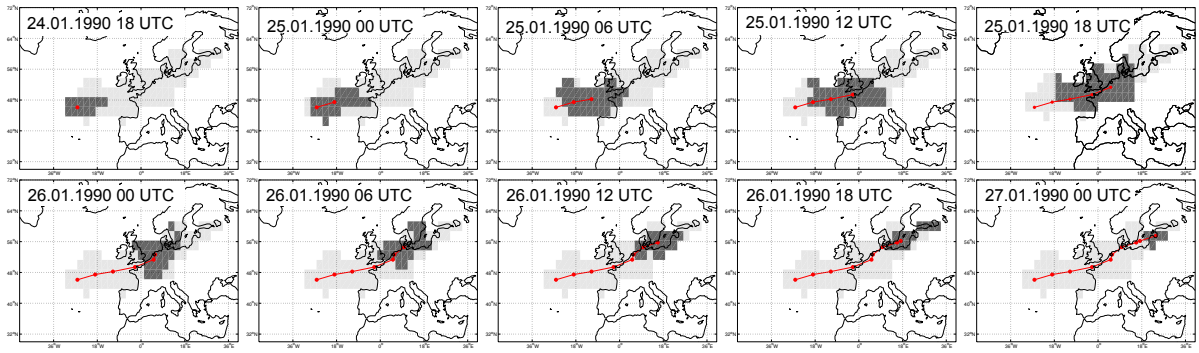

Figure 3.2: The ten timesteps of windstorm "Daria" as identified by the identification scheme in ERA-40 data, with grid boxes exceeding the local 98^{th} percentile of 10 m wind speed at the current timestep (dark gray), grid boxes at least once hit by the windstorm (footprint, light gray), the center of the cluster (red dots) and the track of the windstorm (red solid).

by averaging the longitudes and latitudes the cluster's grid boxes. Then, the clusters are tracked in consecutive timesteps. To this end, the distances are calculated between an individual cluster at a given timestep and all cluster centers at the following timestep (Fig. 3.1, black lines connecting white and black circles). The cluster with the shortest distance is then linked to the current cluster. However, the shortest distance must not exceed 720 km for 6-hourly data, corresponding to a maximum translation velocity of 120 km/h of the extreme wind field. Finally, the tracked events are filtered according to their lifetime. Only events with a minimum lifetime of at least 18 h (equivalent to 4 timesteps) are retained.

The tracking algorithm results in track tables of all identified events, i.e., events consistent with the pre-defined thresholds. The track tables contain properties computed over the entire lifetime (e.g., area of the footprint of the event), and properties computed for each timestep (e.g., geographic location of the storm's center, area, average and maximum wind speed, severity, etc.). For example, windstorm "Daria"—as identified with the tracking algorithm—is represented by ten timesteps in the ERA-40 data (Fig. 3.2). The track of the windstorm agrees with the track of the low pressure system related to those extreme wind speeds (c.f. Leckebusch et al., 2008b, their Fig. 1), but is generally shifted to the south of the cyclone core. This is related to the organization of the frontal structures in extra-tropical cyclones. The highest wind speeds generally occur along the warm and the cold front of a cyclone. Typically, the these fronts are located to the south and east of the cyclone center. A comparison between the location of the windstorm center and the location of the related cyclone generally confirms this assumption (Bierstedt et al., 2010). However, there are differences for windstorms occurring in different areas of the North Atlantic region.

The definition and identification scheme of extreme wind events introduced here has

proofed to be a valuable tool for analyses with respect to windstorm properties in anthropogenic climate change scenarios (Leckebusch et al., 2008b; Nissen et al., 2010). Several other projects at the Institute of Meteorology have used or are currently using the tracking algorithm to investigate, for example, return periods of severe windstorm events (T. Pardowitz), decadal variability of wintertime windstorm climate (T. Kruschke), or to identify windstorms in the data of the ECMWF Ensemble Prediction System (EPS) in order to generate a probabilistic windstorm event set (P. Lorenz, R. Osinski, T. Kruschke).

3.2.2 Storm Severity Index

The discussion whether or not anthropogenic climate change might influence the occurrence of severe winter storms over the Northeast Atlantic affecting Europe often suffers from a lack of an objective measure of the severity of a storm event. Together with the windstorm identification scheme, such an objective storm severity measure was developed. Its definition is based on wind speed only, and therefore more related to the impact of a storm than to its causal development parameters. The so-called ***Storm Severity Index (SSI)*** was introduced by Leckebusch et al. (2008b) and is defined as

$$SSI_{T,K} = \sum_{t}^{T} \sum_{k}^{K} \left[\max \left(0, \frac{v_{k,t}}{v_{perc,k}} - 1 \right)^3 * \frac{A_k}{A_{eq}} \right]. \tag{3.1}$$

The cube of the normalized exceedance of the local 98^{th} percentile is weighted by the area of a given grid box A_k relative to the area of a grid box at the equator A_{eq}, and summed up over all grid boxes K and timesteps T of a given event, but only for grid boxes with surface wind speeds exceeding the local 98^{th} percentile. Slightly altered definitions are also possible, for instance, based on the cube of the scaled exceedance of the percentile (Leckebusch et al., 2008b, their Eq. 2.1), the cube of the absolute percentile exceedance, or the cube of the absolute wind speed, given that the percentile is exceeded. Additionally, other exponents than the cube are possible. However, in consistency with the storm loss model proposed by Klawa and Ulbrich (2003), the SSI as defined by Eq. 3.1 has been used as standard so far. The different properties contributing to the SSI also allow the individual characteristics of a windstorm (i.e., duration, horizontal extent, intensity) to be investigated separately, for example, in terms of their potential changes in a changing climate (Leckebusch et al., 2008b).

3.3 Climatology in reanalysis data

As exemplary shown for windstorm "Daria", the tracking scheme is able to identify historical extreme wind events in reanalysis data. This is also true for the most important

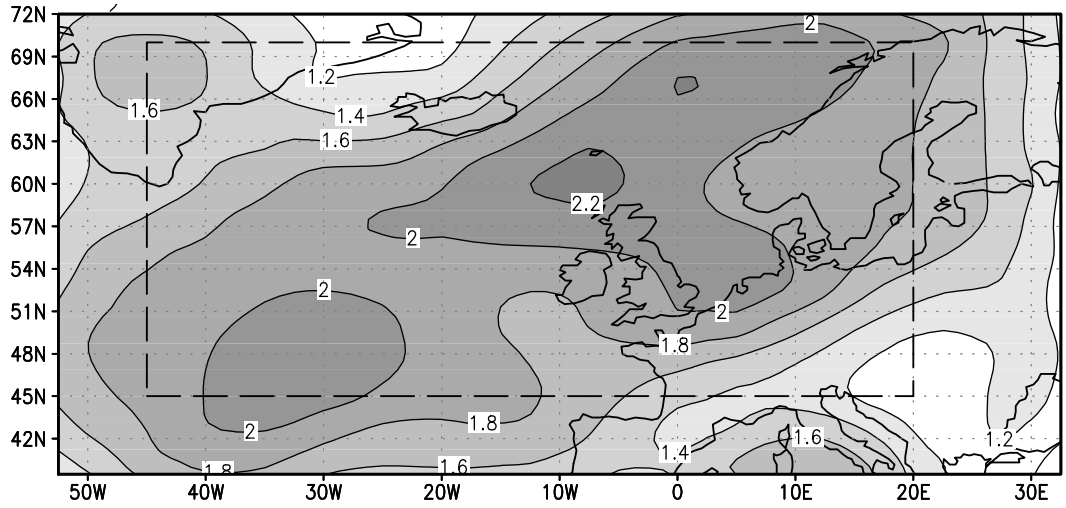

Figure 3.3: Average windstorm track density (Lat^{-2} DJF^{-1}) in ERA-40 1959–2001.

loss-inducing events in the ERA-40 period (e.g., see Leckebusch et al., 2008b, their Table 1 for some other prominent examples). It was shown that about 70% of the events recorded by Munich Re are reasonably identified by the tracking scheme[1]. Furthermore, these events are among the most extremes in terms of severity as measured by the SSI (Leckebusch et al., 2008b, their Table 1). The lack of identification of the missing events is to some degree related to the spatial extent and the representation of these events in reanalysis data. For example, windstorm "Lothar" (26 December 1999) is not very well resolved in reanalysis data, partially owing to its explosive development offshore the west coast of France (Wernli et al., 2002). Some windstorms such as the severe event in Great Britain in October 1987 are related to meso-scale phenomena not well reproduced in reanalysis data ("sting jet", Clark et al., 2005; Browning, 2004). Turning from case studies to climatological considerations, the average spatial, inter-annual and monthly distributions of windstorms as identified by the tracking scheme in the ERA-40 data set are considered in the following.

The average **spatial distribution** of the identified windstorms (in terms of track density computed according to Murray and Simmonds, 1991) in the ERA-40 reanalysis during December–February (DJF) for the 1959–2001 period is shown in Fig. 3.3. The highest values are found over the North Atlantic with a maximum between Iceland and the British Isles. The tracks of the windstorms split over the eastern North Atlantic into two preferred pathways: one leads northeastward into the Norwegian Sea, and the other leads eastward into the North and Baltic Seas. The British Isles and areas adjacent to the North Sea are very exposed regions. A small local maximum is discernible over the

[1]T. Kruschke, 2008: Zusammenhang zwischen verschiedenen meteorologischen Eigenschaften von Winterstürmen und resultierenden Schäden in Europa, BSc Thesis, Institute of Meteorology, Freie Universität Berlin

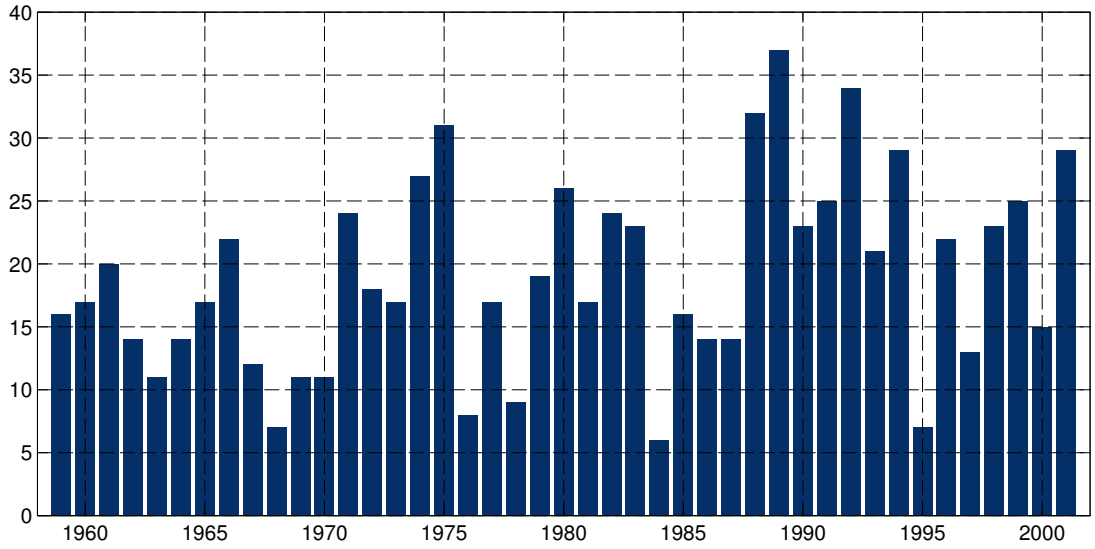

Figure 3.4: Number of windstorm events (windstorm frequency) in the North Atlantic and European region (see dashed box in Fig. 3.3) in ERA-40 during DJF in the 1959–2001 period.

north-western Mediterranean. The track density of cores of cyclones in the North Atlantic region shows a very similar pattern, but is shifted to the north-west (Leckebusch et al., 2008a). This is consistent with the assumption that the highest wind speeds in an extra-tropical low pressure system most frequently occur to the south and east of its center. To derive an **inter-annual time series** of the number of windstorms in the 1959–2001 period, the windstorms affecting the North Atlantic and European region (45°W–20°E, 45°N–70°N; dashed box in Fig. 3.3) during DJF were counted. On average, about 19 windstorms are identified per winter, with considerable inter-annual variability (Fig. 3.4). The winter with the highest windstorm frequency was 1989/1990 with 37 events, including windstorms "Daria", "Vivan" and "Wiebke". This storm season was outstanding also in terms of losses in Germany (Donat et al., 2010b, their Fig. 3). The winter with the lowest windstorm frequency was 1984/1985 with only six events. Generally, the 70s and 90s were decades with rather high windstorm frequencies, whereas during the 60s and 80s storm counts were lower. This is also reflected by a positive trend in the SSI in the ERA-40 period (Leckebusch et al., 2008b). As a third element of the climatological considerations, the **monthly distribution** of windstorm frequency in the North Atlantic and European region between November and April is analyzed (Fig. 3.5). Windstorm frequency increases from November (about 4.0 events) to January (about 7.3 events) and then decreases to about 1.0 event in April. On average, 4.6 events are identified per month. About 70% of windstorms occur during DJF, about 14% during each November and March, and only about 3% during April. This monthly distribution agrees well with those of European loss events and the corresponding socio-economic and insured losses (Münchener Rückversicherungs-Gesellschaft, 2007).

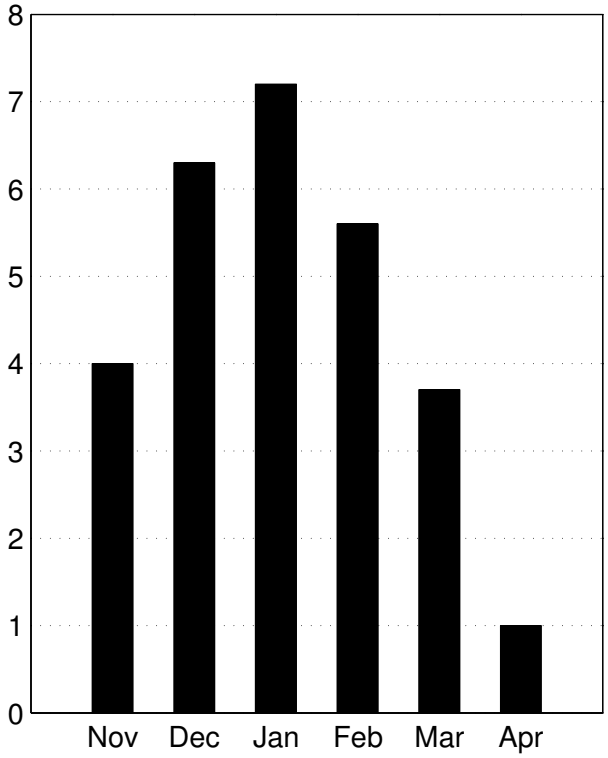

Figure 3.5: Average monthly number of windstorms in the North Atlantic and European region (see dashed box in Fig. 3.3) in ERA-40 for the 1959–2001 period.

3.4 Sensitivity on tracking parameters

Three pre-defined input parameters are necessary for the tracking scheme: the minimum area of adjacent grid boxes with percentile exceedance at each timestep (A), the minimum lifetime of an event (L), and the maximum translation velocity (D). D is computed by the distance between the cluster centers in consecutive timesteps divided by the temporal resolution of the underlying data. For wintertime windstorms in the North Atlantic, the best guess parameter combination was suggested to be $A = 150000$ km^2, $L = 18$ h, and $D = 120$ km h^{-1} (Leckebusch et al., 2008b).

A number of sensitivity experiments have been carried out to test the robustness of these parameter settings. To be consistent with other studies at the Institute of Meteorology using the tracking algorithm, these experiments have been performed on the basis of ERA-interim reanalysis data of the ECMWF for the 1989–2007 period. In general, the climatology of track density (Fig. 3.6) looks similar to the climatology for the entire ERA-40 period (Fig. 3.3). For example, the maximum is located over the North Atlantic, albeit more to the southwest than in ERA-40. The split of the preferred pathway into the Norwegian and Baltic Seas is very nicely resolved as is the secondary maximum over the Mediterranean. However, considerable differences exist. The maximum track density reaches about 3.3 events per winter, i.e., about 50% more than the maximum value in

ERA-40. This might be attributable to the higher resolution of ERA-Interim compared to ERA-40 as well as to the different periods covered by the two data sets. Especially the 1990s was a decade with very high storm activity in the North Atlantic and European region, consequently leading to a higher track density in the ERA-interim data.

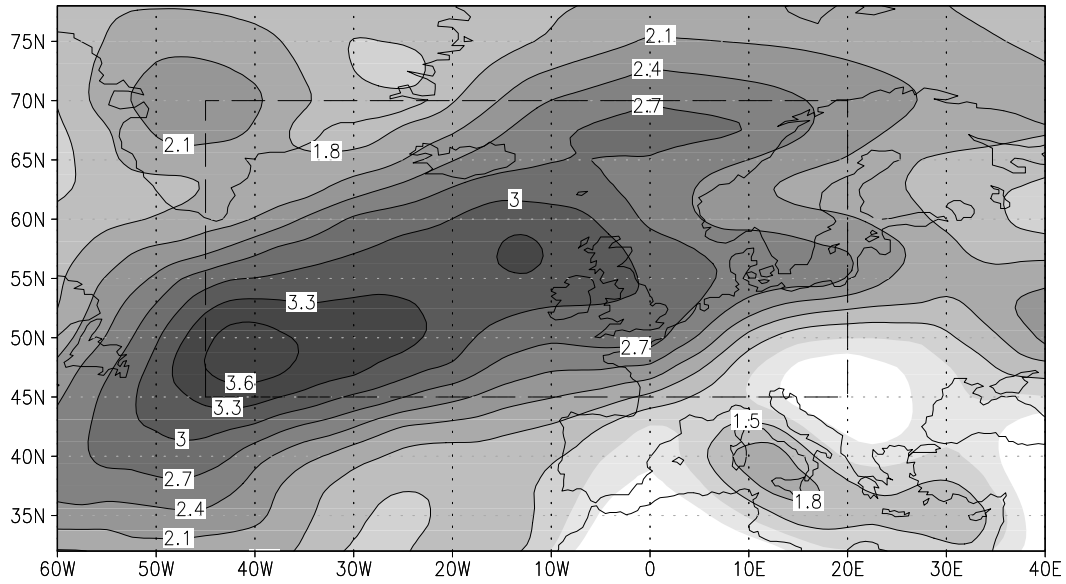

Figure 3.6: As Fig. 3.3, but based on ERA-interim reanalysis data 1989–2007.

For the sensitivity experiments each parameter is changed by −20%, −10%, +10%, and +20%, respectively, while the other two parameters are held fixed. Several properties of the identified windstorms in the different sensitivity experiments are computed (e.g., the mean windstorm frequency during DJF, the accumulated SSI during DJF, etc.). The spread of these quantities between the sensitivity experiments serves as a measure of the sensitivity of the tracking algorithm to the parameter settings.

The inter-annual variability of the windstorm frequency during DJF is consistently reproduced by the ensemble of sensitivity experiments (Fig. 3.7, top), although its spread is substantial. Obviously, changes in the minimum area (A) and minimum lifetime (L) strongly influence the number of identified storms. The sensitivity is much smaller in terms of intensity as measured by the accumulated SSI of all windstorms during DJF (Fig. 3.7, center). In terms of the highest event SSI per winter, the different sensitivity experiments generally agree very well, although there are some years with stronger deviations (Fig. 3.7, bottom). The sensitivity of different windstorm properties on changing parameter settings are summarized in Table 3.1. Windstorm frequency shows the highest sensitivity (standard deviation of 23.9% within the ensemble of sensitivity experiments). The footprint (the total area of all grid boxes affected by a storm) and the lifetime show moderate sensitivity (standard deviation 13.4% and 15.8%, respectively). Obviously, the

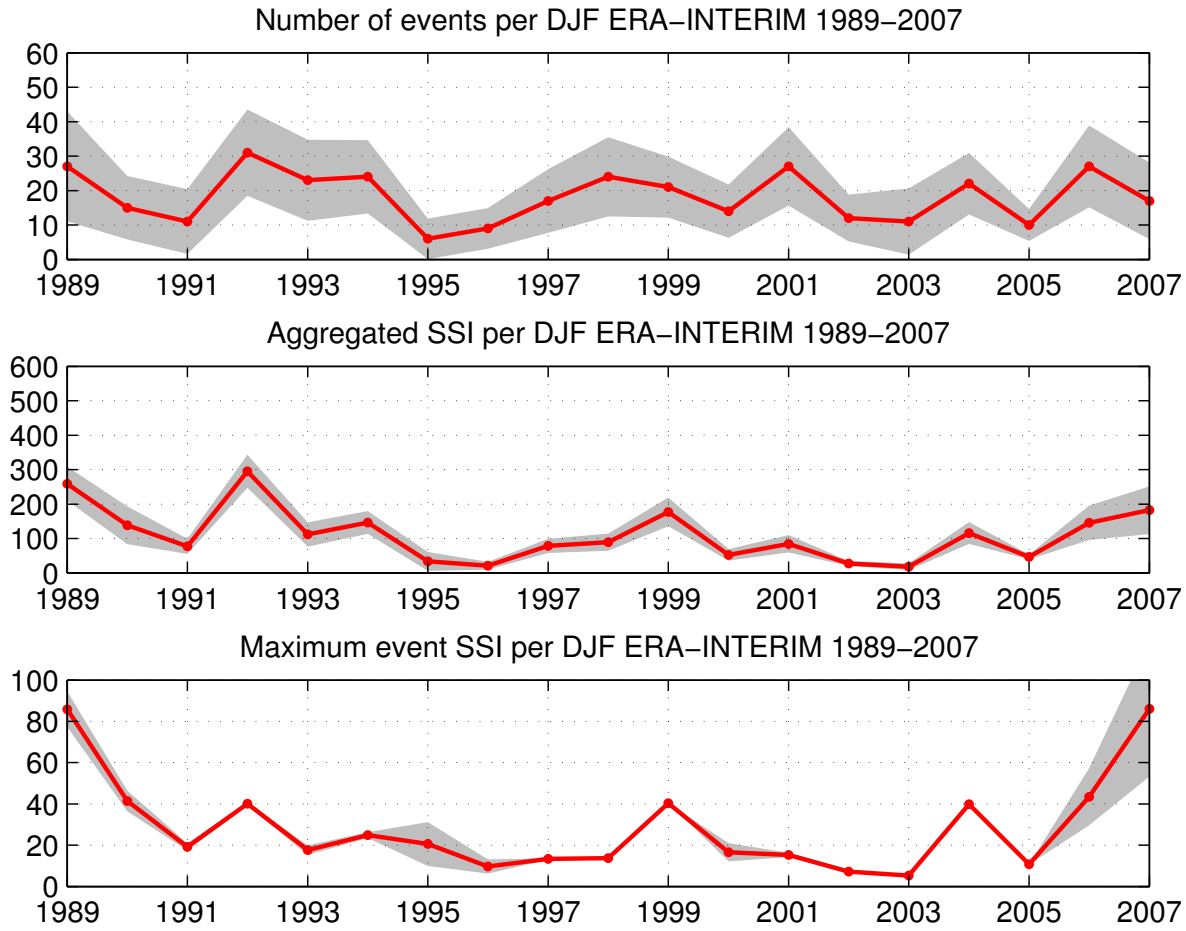

Figure 3.7: Mean (red) and range of standard deviation (gray) of windstorm frequency (top), accumulated SSI (center) and maximum event SSI (bottom) during DJF in tracking sensitivity experiments based on ERA-interim 1989–2007.

lifetime is most sensitive to the choice of L. Most importantly, the SSI as an integrated measure of windstorm properties (wind speed, area, lifetime) shows the lowest sensitivity (standard deviation below 10%). This is especially true for the seasonally accumulated SSI per winter, and the maximum SSI per winter in the 1989–2007 period. The stability of the intensity measures implies that the most important windstorms with respect to their impacts are captured systematically well independent of the exact parameter choice. Furthermore, the correlation between annual time series of the standard parameter settings and the sensitivity experiments (Fig. 3.7) is generally above 0.95. Thus, the inter-annual variability of windstorm climate as identified by the tracking scheme is not sensitive on the parameter setting.

Experiment	Count	r	SSI	r	MSSI	r	ESSI	Footprint	Lifetime
A255-L4-D720	37.8	1.00	200.5	1.00	34.7	1.00	5.3	1.914	6.9
A204-L4-D720	44.2	0.99	216.7	0.99	35.0	1.00	4.9	1.792	7.1
A230-L4-D720	40.2	1.00	206.1	1.00	34.7	1.00	5.1	1.859	7.0
A281-L4-D720	34.7	0.99	195.4	1.00	34.7	1.00	5.6	1.989	7.0
A306-L4-D720	32.6	0.99	188.3	1.00	34.2	1.00	5.8	2.029	6.9
A255-L2-D720	59.9	0.96	216.9	1.00	34.7	1.00	3.6	1.412	5.3
A255-L3-D720	48.0	0.98	211.1	1.00	34.7	1.00	4.4	1.656	6.1
A255-L5-D720	29.6	0.97	184.7	0.99	34.0	0.99	6.2	2.165	7.7
A255-L6-D720	22.4	0.90	162.6	0.97	33.1	0.98	7.2	2.451	8.6
A255-L4-D864	38.8	0.99	215.5	0.99	36.3	0.99	5.6	2.041	7.3
A255-L4-D792	38.5	1.00	208.8	1.00	35.6	0.99	5.4	1.987	7.17
A255-L4-D648	36.1	0.98	185.4	0.99	33.4	0.99	5.1	1.817	6.7
A255-L4-D576	33.7	0.96	159.8	0.96	28.8	0.79	4.7	1.685	6.3
Mean	38.2	–	196.3	–	34.1	–	5.3	1.908	6.9
Std (%)	23.9	–	9.9	–	5.3	–	16.3	13.4	11.6

Table 3.1: Properties of windstorms as identified by the standard parameter setting (first row) and an ensemble of sensitivity experiments with sequentially altered minimum cluster area (A), minimum lifetime (L) and maximum translation velocity (D), the mean and standard deviation (% of mean value) of all experiments during DJF for the 1989–2001 period on the basis of ERA-interim. The properties are the seasonal mean windstorm count, the seasonally accumulated SSI per winter (SSI, dimensionless), and the maximum event SSI per winter (MSSI) in the period 1989–2001; the average event SSI (ESSI), the average event footprint (10^6 km^2), and average event lifetime (timesteps) over the entire period. In addition, the correlations (r) between the seasonally averaged properties obtained by the standard parameter setting and the sensitivity experiments are given.

3.5 Relation to growth factors of cyclones

Wintertime windstorms in the North Atlantic and Europe are most often associated with low pressure systems (however, keep in mind that the tracking scheme works independently of any information of the low pressure system; only wind speed is used for the

detection of storm events). Such low pressure systems usually develop from small initial wave disturbances along the polar front between cold air masses to the north and warm air masses to the south (cf. Wallace and Hobbs, 2006, for an introductory survey). A preferred region of cyclogenesis is the area off the North American east coast. Whether an initial wave disturbance is growing into a organized low pressure systems, and possibly intensifying to ultimately cause severe wind speeds, is closely related to the atmospheric conditions in its surroundings. For example, baroclinicity, latent heat, and upper-tropospheric divergence are important factors supporting the development and intensification of extra-tropical cyclones. Ulbrich et al. (2001) showed that these growth factors have been significantly increased in the (temporal and spatial) vicinity of three strong cyclones related to the severe storms in December 1999. Pinto et al. (2009) analyzed the relation between the growth factors and phases of high and low NAO and found that during high NAO phases growth factors are increased over larger areas in the North Atlantic region than during low NAO phases.

In the following, the relation between windstorms and growth factors of cyclones is investigated focusing on seasonally accumulated measures in contrast to case studies of individual events like in Ulbrich et al. (2001). From the time series of windstorm frequency during DJF (Fig. 3.4) two composites of years with an anomaly of above +1 standard deviation (below −1 standard deviation) with respect to the long-term average are defined. The positive (negative) composite consists of the seven (eight) years with the highest (lowest) storm counts in Fig. 3.4.

Obviously, the difference of windstorm track density between the two composites shows large positive anomalies over the northeastern North Atlantic and western and northern Europe of up to 300% of the local inter-annual standard deviation (Fig. 3.8a). Negative anomalies occur over the Labrador Sea and Greenland, the central North Atlantic, Iberia and the North African coast.

The difference of baroclinicity between the same winters shows a highly organized pattern (Fig. 3.8b). A band of positive anomalies stretches from the east coast of North America towards Iceland and Scandinavia. To the south and north of this region of enhanced baroclinicity, negative anomalies reach from Florida over the central North Atlantic into the Mediterranean, and also prevail around Labrador and Greenland.

Anomalous wind storm activity is related to increased latent heat over northern Europe, i.e., in and downstream of the region of interest (Fig. 3.8c). This is related to the advection of relatively warm and moist air associated with the windstorms. In contrast, negative anomalies occur over the Labrador Sea and Greenland. Interestingly, latent heat is also statistically significantly increased in a region around and north of Florida, i.e., in the entrance region of the climatological storm track over the North Atlantic. These air masses might act as a reservoir of moist air which is transported to the northeast within

(a) Windstorm track density

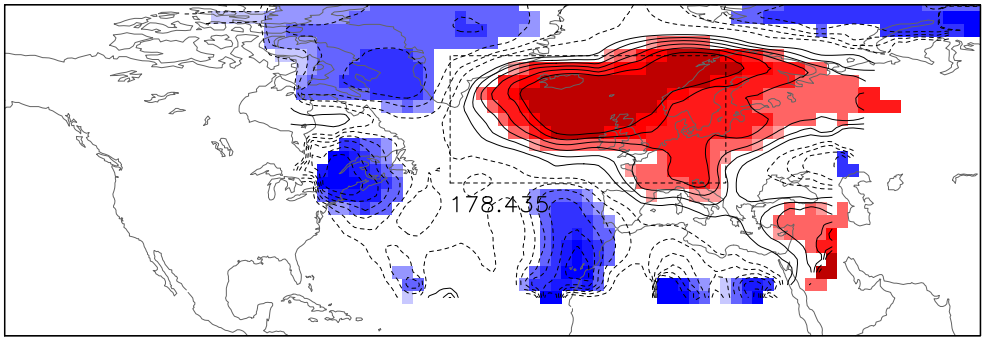

(b) Baroclinicity (EADY)

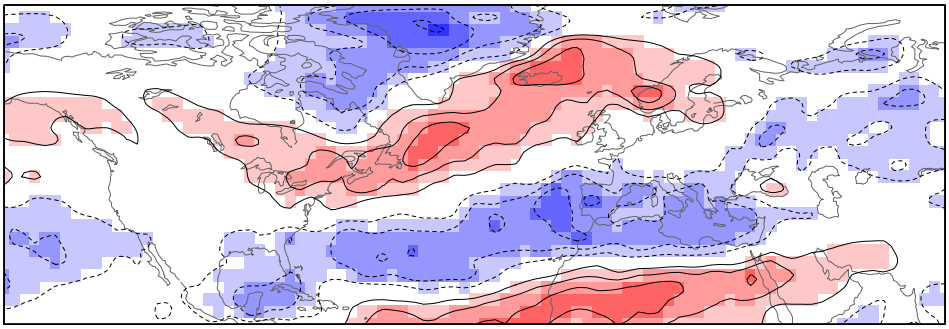

(c) Latent heat (EPT)

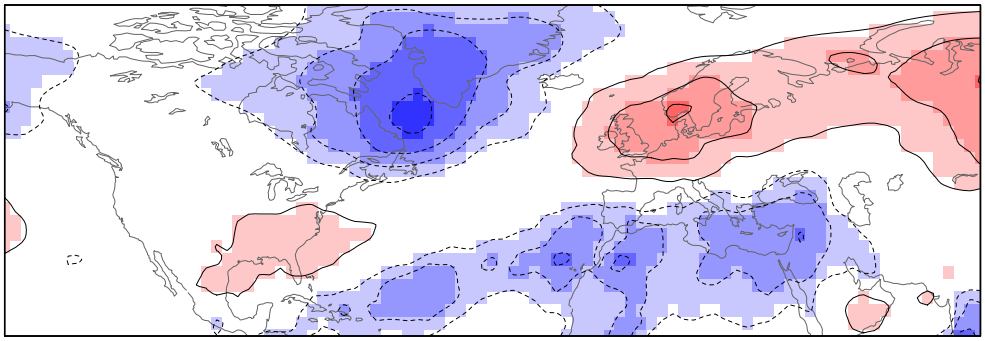

(d) Upper-tropospheric divergence (DIV)

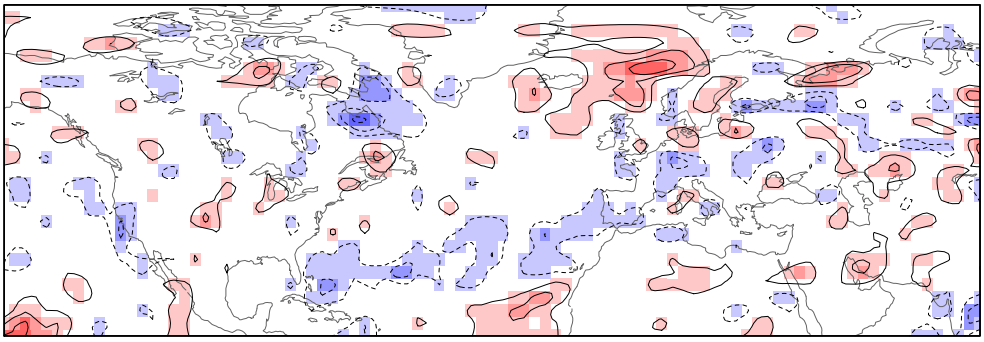

Figure 3.8: Difference in December–February windstorm track density (a), baroclinicity (b), latent heat (c), and upper-tropospheric divergence (d) between composites of high and low windstorm frequency DJF in ERA-40 1959–2001 in % of the local inter-annual standard deviation. The contour interval is 50%, the zero contour is omitted. Significant differences ($p<0.1$) are shaded.

wave disturbances, therefore contributing to the intensification of growing cyclones.

The anomalies of upper-tropospheric divergence (DIV) are rather noisy (Fig. 3.8d). However, a region of predominantly positive anomalies is discernible between Greenland and the Norwegian coast.

In summary, winters with anomalous high windstorm frequency (and, consequently, high windstorm track density) are related to physically consistent anomalies of growth factors of cyclones. With respect to Fig. 3.8 the following scenario is reasonable: Owing to a potential initial wave disturbance off the North American east coast, moist and warm air masses are advected northeastward. Moving northeastward, the disturbance encounters regions of high baroclinicity and intensifies. Latent heat release owing to the condensation of water vapor in ascending air masses contributes to the intensification. The intensification process (especially close to the European continent) is further supported by anomalous upper-tropospheric divergence. Hence, conditions as shown in Fig. 3.8 are indicative of preferred growth conditions for cyclones and, therefore, consistent with the occurrence of a higher number or more intensive windstorms in the North Atlantic region.

3.6 Conclusions

It was shown that the windstorm identification scheme is able to successfully identify individual extreme wind events (e.g., "Daria") in gridded data sets and also yields spatial and temporal climatologies in good agreement with observations. The inter-annual variability as identified in the reanalysis was found to be insensitive to the parameter settings. Thus, the tracking scheme is suitable for the analysis of the inter-annual variability and seasonal predictability of windstorm climate. Furthermore, the tracking scheme has proven valuable for the analysis of climate change scenarios (Leckebusch et al., 2008b; Nissen et al., 2010).

The windstorms identified in ERA-40 reanalysis data form the basis to study the relationships between the wintertime windstorm climate and anomalies of hemispheric-scale factors such as North Atlantic sea surface temperatures or continental snow cover extent. Specific anomalies in growth factors of cyclones in response to anomalous hemispheric-scale factors could explain such relations. Chapter 4 is dealing with these issues.

Additionally, the identification scheme is applied to the seasonal predictions from the DEMETER and ENSEMBLES projects. On one hand, this allows the analysis of predictive skill of state-of-the-art prediction models. On the other, the variability of windstorm climate in the models and its relation to hemispheric-scale factors can be analyzed and compared to observed relationships. These issues will be investigated in the chapters 5 and 6.

Chapter 4

Potential sources of wintertime windstorm predictability over the North Atlantic and Europe on seasonal time scales

4.1 Rational

The occurrence of wintertime windstorms exhibits significant inter-annual variability (e.g., Fig. 3.4). Given the high financial losses involved, the analysis of the inter-annual variability of windstorm occurrence and its predictability on seasonal time scales is not only of scientific but also of economic interest: For example, successful prediction would be beneficial for the risk management industry.

In contrast to the tropics, the influence of anomalous boundary conditions on atmospheric variability at the seasonal time scale is generally weaker in mid-latitudes, but also less understood (e.g., Goddard et al., 2001). Nevertheless, a number of hemispheric-scale factors (HF) evolving on longer time scales than the atmosphere are candidates potentially influencing wintertime windstorm climate —and winter climate in the North Atlantic region in general—on seasonal time scales.

The most prominent of these factors is the North Atlantic SST. Several studies have found robust relations between North Atlantic SST anomalies in summer/autumn and large-scale atmospheric flow in the subsequent winter (Kushnir et al., 2006, 2002; Czaja and Frankignoul, 2002, 1999; Saunders and Qian, 2002; Sutton and Hodson, 2003; Doblas-Reyes et al., 2003; Cassou et al., 2004). For example, a Horseshoe-shaped anomaly pattern of North Atlantic SST in summer and autumn was found to show strong relations to the NAO in subsequent winter (Saunders and Qian, 2002; Czaja and Frankignoul, 2002, 1999).

Such observational evidence was confirmed by studies using coupled ocean-atmosphere models (Cassou et al., 2004; Doblas-Reyes et al., 2003). Continental snow cover can influence the climate owing to its high albedo and thermal properties (Cohen, 1994; Barnett et al., 1989). Additionally, the melting of snow can provide a sink for latent heat. Significant correlations have been found between observed summer and autumn snow cover in the northern hemisphere and the NAO in the following winter (Cohen and Entekhabi, 1999; Saito and Cohen, 2003; Saunders et al., 2003).

Several studies have analyzed the feedback of sea ice anomalies in the North Atlantic region in general atmospheric circulation models (Deser et al., 2007; Kvamstø et al., 2004; Deser et al., 2004; Magnusdottir et al., 2004). They consistently found a negative feedback between anomalous sea ice extent and large-scale flow, reminiscent of the NAO pattern. The existence of a negative feedback in observational data was confirmed by Strong et al. (2009).

Most of the aforementioned studies focus on the North Atlantic climate in general, the large-scale atmospheric flow, or the North Atlantic/Arctic Oscillation. The occurrence and the variability of windstorms in the North Atlantic/European region are related to the large-scale atmospheric flow in this region, as quantified, for example, by the phase and the strength of the NAO. Therefore, it is speculated the aforementioned (hemispheric-scale) factors are also related to the occurrence of wintertime windstorms. For example, Qian and Saunders (2003) developed an empirical approach based on the relation between winter wind climate and preceding summer snow extent to study predictability of high wintertime wind speeds in the North Atlantic region. Palutikof et al. (2002) studied different modes of the North Atlantic large-scale flow and regional modes of global SST regarding their ability to be used as predictors of wintertime wind climate on seasonal time scales. Both studies found potential for an (at least) partial explanation of the inter-annual variability of wintertime windstorm climate in the North Atlantic by the inter-annual variability of specific hemispheric-scale factors.

However, owing to the purely statistical approach in the aforementioned studies, the physical mechanisms behind these relations were not addressed. In order to intensify and finally develop into a severe windstorm, a developing cyclone must encounter specific atmospheric conditions. For example, Ulbrich et al. (2001) showed that growth factors of cyclone development such as baroclinicity, latent head, and upper-tropospheric divergence reached anomalous positive values in the (temporal and spatial) vicinity of three extreme wind events in December 1999, namely the windstorms “Anatol”, “Lothar” and “Martin”. Additionally, (Pinto et al., 2009) investigated the relation between these growth factors with the occurrence of very intense cyclones and the state of the NAO. They found larger areas with conditions favoring cyclone development in positive NAO regimes compared to negative NAO regimes. It is argued that anomalies in the HF may induce

persistent anomalies in these growth factors, with related effects on cyclone development and windstorm occurrence. Thus, cyclone growth factors may constitute an important part of the physical mechanism chain linking hemispheric-scale factors and the occurrence of windstorms on seasonal time scales.

Different reanalysis and observational data are employed in the following. Wind speed to identify windstorms, the data to compute the growths factors of cyclones, SST, and MSLP are taken from ERA-40 reanalysis (see chapter 2). In addition, observations of snow cover, sea ice extent, and a station-based NAO index are employed.

The methods employed in this study are described in section 4.2. Statistical relations on seasonal time scales between the different HF and wintertime windstorm climate are evaluated using Lead-Lag-Correlations in section 4.3. Furthermore, inter-dependencies of different HF are considered. To complement the statistical analysis of the relation between the HF and windstorm occurrence, the link between anomalies in the HF, growth factors of cyclones, and windstorm occurrence is explored in section 4.4 in order to explain the underlying physical processes. Short conclusion relevant to their following chapters are given in section 4.5.

4.2 Methods

4.2.1 Wintertime windstorm climate

In this study, surface (10 m) wind speed data from the ERA-40 reanalysis are used to identify windstorms in winter (November to April) in the North Atlantic/European region in the 1959–2001 period (according the windstorm identification presented in chapter 3). Unless otherwise stated, wintertime windstorm climate is analyzed in terms of the number of windstorm events that occurred from December through February in the North Atlantic region (45°W–20°E, 45°–70°N), termed as wintertime windstorm frequency DJF. Our definition of windstorms and windstorm climate therefore differs markedly from the approaches used by, for example, Qian and Saunders (2003) and Palutikof et al. (2002), which were based on grid point wise defined measures of wind climate.

4.2.2 Lead-Lag-Correlation and partial correlation

The strength of the link on seasonal time scales between the various HF and windstorm climate is quantified using Lead-Lag-Correlations (LLC), with the HF leading wintertime (DJF) windstorm climate by several months. The introduction of a time lag between the two variables excludes the possibility that the lagging variable is the driver of the leading variable.

LLC is expressed as Spearman correlation coefficients. However, LLC based on Pearson correlation coefficients gives very similar and slightly higher coefficients. LLC was performed for different lead times, namely 0–8 months (where a lead time of 0 means the simultaneous correlation between 3-monthly mean DJF of a certain HF and the wintertime windstorm climate DJF; a lead time of eight months means the lagged correlation between the 3-monthly mean HF of the preceding AMJ). In this way, the 3-monthly periods with highest co-variability between HF and storm climate can be identified. The number of years available for LLC depends on the length of the observational record of the respective HF.

However, LLC does not guarantee that the variables are physically linked. Co-variability between different HF or with other, external factors could result in correlation coefficients between windstorm climate and a given HF (even) without a direct effect on windstorm occurrence. Partial correlation analysis allows this effect to be quantified. The partial correlation coefficient measures the residual correlation between the two factors H_1 and W, given their correlation with a third factor H_2. It is defined as

$$r_{HS_1,W|HS_2} = \frac{r_{HS_1,W} - r_{HS_1,HS_2} r_{W,HS_{21}}}{\sqrt{(1 - r^2_{HS_1,HS_2})(1 - r^2_{W,HS_2})}} \tag{4.1}$$

where r is the Spearman correlation coefficient between two variables.

4.2.3 Composites of years with strong HF anomalies

To investigate possible physical mechanisms between HF and storm climate, a composite analysis was employed. For every HF, composites were constructed consisting of years with strong anomalies for specific 3-monthly periods shown to correlate strongly with wintertime windstorm climate by LLC analysis. The positive composite consists of n years with anomalies above 1 standard deviation, the negative composite of m years with anomalies below -1 standard deviation. The difference between the mean of the positive and negative composites is interpreted as the (empirical) response to anomalous HF states. The composites are calculated for selected months and variables. Here, we consider anomalies of ocean heat content (TAV), SST, snow and sea ice cover, EADY, EPT, DIV and JET and windstorm track density.

The statistical significance of the composite anomalies is estimated via a bootstrap method. Composites are constructed by randomly selecting n (m) years for the positive (negative) composite from the considered period. Then, the difference between the mean of the random positive and negative composites is calculated. This is repeated 10 000 times. The significance of the true composite difference is then estimated from the resulting random difference distribution.

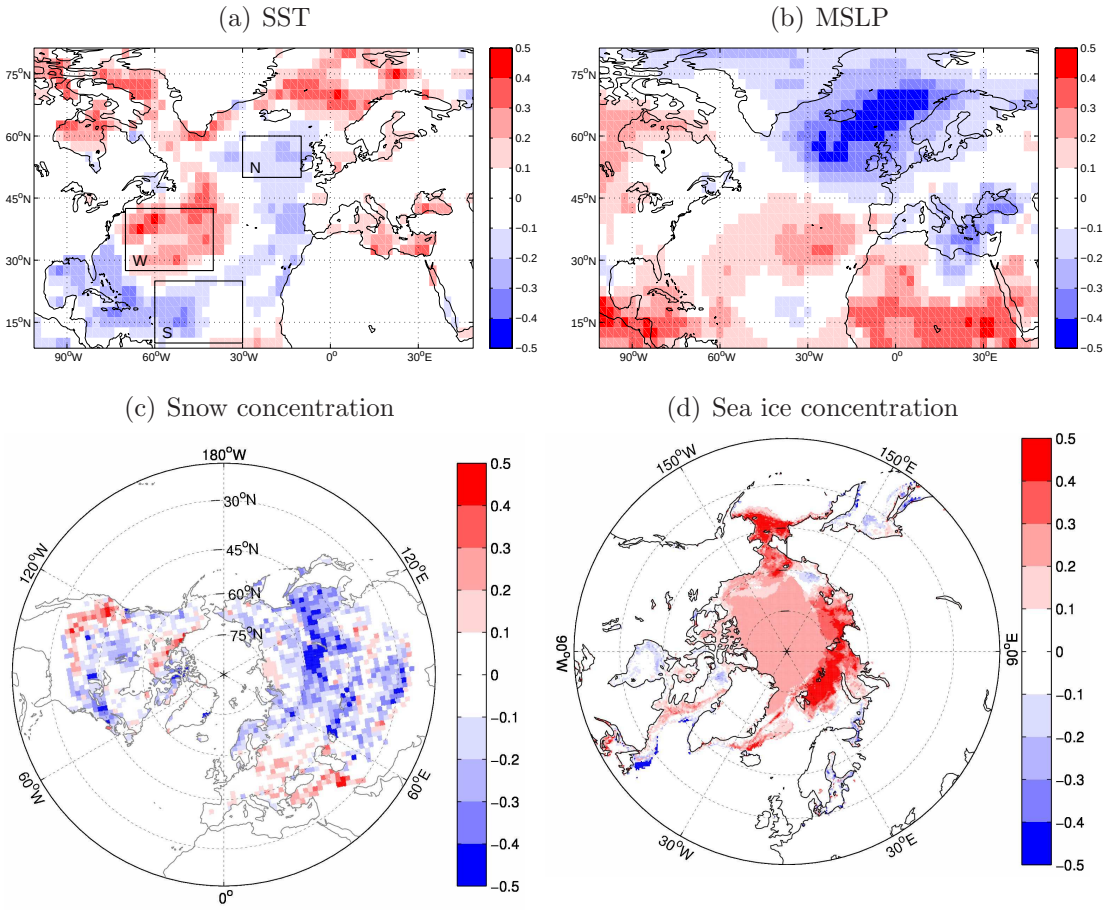

Figure 4.1: Grid point wise Spearman correlation coefficient between windstorm frequency during DJF and SST during preceding ASO 1959–2001 (a), MSLP JJA 1959–2001 (b), snow cover frequency SON 1972–2001 (c) and sea ice cover frequency ASO 1979–2001 (d). The black boxes in (a) indicate the areas used as the basis for calculating the Horseshoe index (see text for further details).

4.3 Relation between HF with different lead times and windstorm climate in winter

4.3.1 Correlation patterns between HF and wintertime windstorm climate

First, the relation between HF and the number of windstorms is illustrated by grid point wise correlations. These correlations were calculated between 3-monthly mean fields of the HF (SST, MSLP, snow cover concentration and sea ice cover concentration) and the storm frequency in winter (DJF), with different lead times for the HF.

A distinct correlation pattern occurs with a lead time of the SST of four months (i.e., 3-monthly mean August-October) consisting of an area with positive correlations in the central North Atlantic that is surrounded by negative correlation to the south, east and

northeast (Fig. 4.1a) and resembling the Horseshoe pattern described, for instance, by Cassou et al. (2004); Wang et al. (2004); Czaja and Frankignoul (2002, 1999). Cassou et al. (2004) and Czaja and Frankignoul (2002, 1999) have shown that such SST anomalies are related to anomalous large-scale atmospheric flow in the following winter. Fig. 4.1a suggests that this Horseshoe-shaped SST anomaly in autumn is also related to the variability of the frequency of extreme windstorms over the North Atlantic and Europe about four months later.

The correlation pattern between MSLP and wintertime windstorm frequency is strongest for the simultaneous correlation (DJF), resembling the positive NAO pattern (not shown). However, for the MSLP in summer, i.e., with a lead time of about six months, a secondary strong pattern emerges over the North Atlantic (Fig. 4.1b). Like the simultaneous correlation, this pattern resembles the positive phase of the NAO.

Snow cover frequency shows negative correlations with the subsequent winter's windstorm frequency in autumn (SON), especially over almost the whole Eurasian continent, but also over large parts of North America (Fig. 4.1c). For sea ice cover (ASO), the most striking feature is an area of positive correlations in the Barents Sea and along the climatological sea ice edge at the east coast of Greenland and in the Arctic Ocean in summer and autumn (Fig. 4.1d).

Hence, the hemispheric-scale factors are linked with the wintertime windstorm frequency for distinct lead times and regions.

4.3.2 LLC between windstorm climate and hemispheric-scale factors

To quantify these relations and their dependence on lead time, LLC between the HF and the wintertime windstorm frequency was employed. As input for LLC, one-dimensional time series for each HF are required. For MSLP, the NAO index was used. For snow and sea ice cover, monthly snow and sea ice extent (in km^2) from NSIDC was used, aggregated over several regions (Eurasian, North American, and the entire northern hemisphere continental snow cover extent; North Atlantic, North Pacific and the entire northern hemisphere sea ice extent). For the SST, the so-called Horseshoe index was defined (HSI, see below).

North Atlantic SST

Based on the correlation pattern between summer and autumn SST in the North Atlantic (Fig. 4.1a) and wintertime windstorm frequency, an index was calculated as the difference between the monthly mean SST in regions related to the subsequent winter's storm climate, defined as

$$HSI = \overline{SST_W} - \frac{1}{2}(\overline{SST_N} + \overline{SST_S}), \tag{4.2}$$

where the horizontal bar represents the area-weighted spatial mean operator; the subscripts denote the areas with positive correlations (W), negative correlations to the north east (N) and to the south (S, Fig. 4.1a). Therefore, the index is a measure of the large-scale SST gradients in the North Atlantic. This approach is similar to that of Wang et al. (2004), although the definition of the boxes is slightly different. The sensitivity of the exact definition was tested and revealed to be of minor importance as long as the areas with maximal correlations are included.

LLC between the HSI and windstorm frequency DJF reveals positive correlations for all lead times considered (Fig. 4.2a, solid red line). Specifically, summer and autumn values are significantly related to the number of windstorms in the subsequent winter, whereas the correlations are weaker for longer and shorter lead times. The maximum correlation of about +0.43 is reached for the 3-monthly mean ASO of the HSI. Thus, this SST anomaly pattern in early autumn explains about 20% of the total variance of the windstorm variability in subsequent DJF. These relations are also valid for the shorter period 1980–2001 (Fig. 4.2a, dashed red line) with correlations of up to +0.60.

North Atlantic Oscillation

LLC was applied to 3-monthly means of different NAO indices, namely an observed station-based index (Hurrell, 1995) and an index based on Principal Component Analysis (PCA, computed from ERA-40 data).

Not surprisingly, the correlation between the number of windstorms and the NAO is positive, and highest (+0.70–0.90) with lead time 0, i.e., the correlation of simultaneous values (Fig. 4.2a, solid blue and black lines). With increasing lead time, the correlation of the NAO indices drops to nearly 0 (for 3-monthly mean SON). However, a secondary maximum is identified with a lead time of four to six months for NAO values (JJA), where the correlation reaches about +0.40. With even longer lead times, the correlation decreases again. Although the two NAO indices exhibit somewhat different evolutions of LLC, the main features (highest correlation simultaneously, but also statistically significant correlations for summer indices) are common to both of them. LLC reveals statistically significant correlations also in the shorter period 1980–2001 for the station-based, but not for the PCA-based index (Fig. 4.2a, dashed blue and black line).

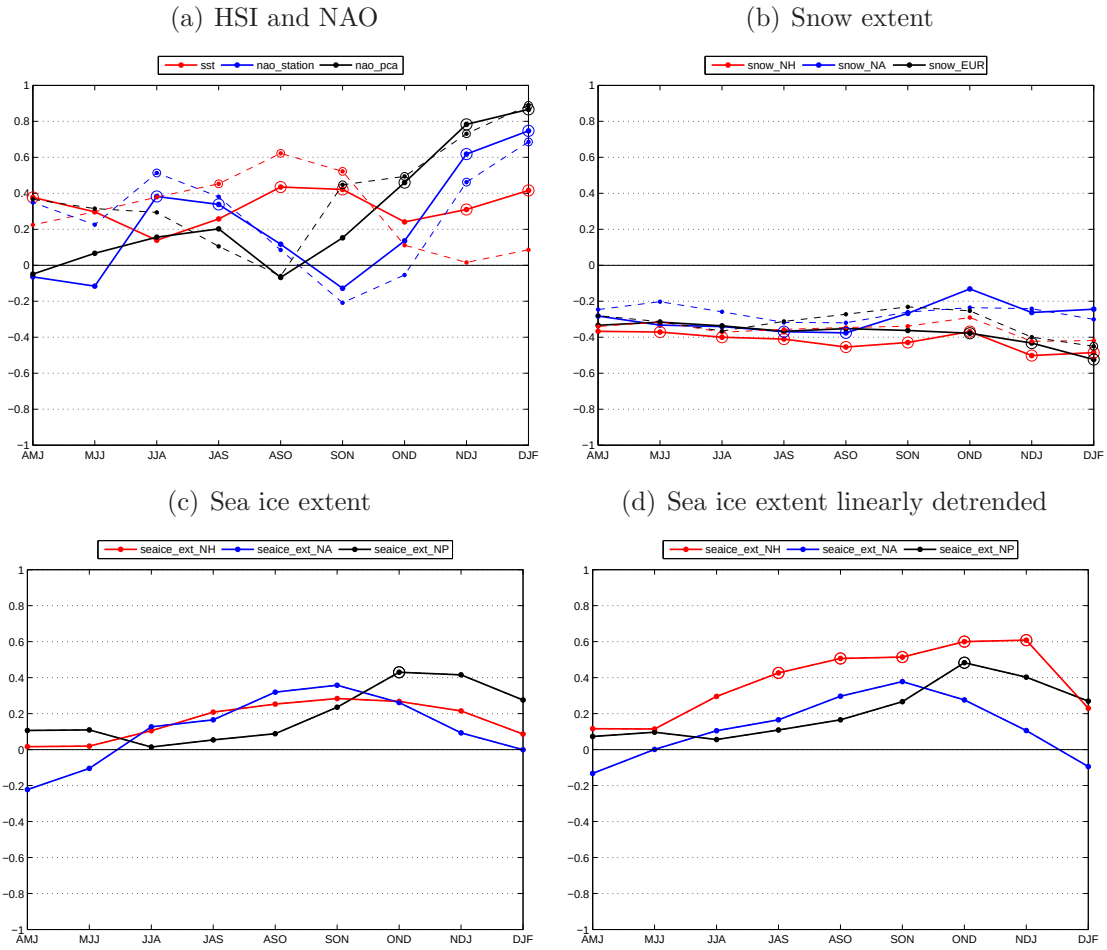

Figure 4.2: Lead-Lag-Correlations (LLC) between windstorm frequency DJF and various hemispheric-scale factors with lead times of 0–9 months; a) Horseshoe index (red), station-based NAO (blue), PCA-based NAO (black) for the 1959–2001 period (solid) and 1980–2001 period (dashed); b) snow cover extent of the entire northern hemisphere (red), North American continent (blue) and Eurasian continent (black) for the 1972–2001 period (solid) and 1980–2001 period (dashed); c) NSIDC sea ice extent for the entire northern hemisphere (red), the North Atlantic region (blue) and the North Pacific region (black) based on undetrended data for the 1980–2001 period; d) same as c), but based on linearly detrended data. The x-axis denotes the accumulating period for the hemispheric-scale factors. The simultaneous correlation between windstorm climate DJF and hemispheric-scale factors DJF, i.e., with lead time 0, is shown on the right. The lead time is increasing to the left up to a lead time of eight months (AMJ). Statistically significant correlations ($p < 0.05$) are marked by a circle.

Continental snow cover extent

LLC between snow cover and storm frequency is generally negative and is quite stable for the lead times considered here (Fig. 4.2b, solid red line). The correlation between northern hemisphere snow cover extent and winter storm frequency is about -0.45 for ASO (lead time four months), but is also significant for lead times between three and eight months. In contrast, the correlation of Eurasian snow cover with wintertime windstorm frequency is highest with lead time 0, but also exhibits significant correlations for lead times of two and six months (OND/JJA; Fig. 4.2b, solid black line). The correlations with North American snow cover extent are strongest in summer, where there are significant correlations, but weaken with lead times below three months (Fig. 4.2b, blue solid line).

However, if LLC is restricted to the 1980–2001 period, no significant correlations are found for lead times on seasonal time scales (Fig. 4.2b, dashed lines). Thus, the continental snow cover–windstorm relation is dependent on the period considered.

Sea ice extent

For sea ice, the data from NSIDC cover an even shorter period than for snow, namely 1978–2001. LLC reveals generally positive correlations between Arctic sea ice extent and wintertime windstorm climate (Fig. 4.2c). However, the correlations are generally not statistically significant. Arctic sea ice extent experienced a large negative trend over the past decades (e.g., Stroeve et al., 2007). In contrast, wintertime windstorm climate in the North Atlantic region exhibits rather positive trends over the past 50 years (Wang et al., 2009; Leckebusch et al., 2008b). Thus, there are opposite trends in the time series. Therefore, LLC was also calculated on the basis of linearly detrended time series. In this case, correlation coefficients become significant for northern hemisphere sea ice extent with lead times of one to five months (i.e., NDJ, OND, SON, ASO, and JAS; Fig. 4.2d, red) culminating in a maximum correlation of above 0.60 (OND), and for sea ice extent in the North Pacific with two months lead time (OND, Fig. 4.2b, blue).

In summary, all HF considered here do show significant correlations with wintertime windstorm frequency, with lead times of about two to six months and correlation coefficients of about 0.30–0.45. That means that up to 20% of the observed inter-annual variability of wintertime windstorm frequency DJF could potentially be explained by these hemispheric-scale factors with lead times on seasonal time scales, the exact value also depending on the inter-dependencies between the different factors.

	HSI ASO	NAO JJA	SC NH ASO	SC NA ASO	SC EU OND	SI NH OND	SI NP OND	SI NA OND
HSI ASO	—	**0.33**	−0.27	−0.26	*−0.34*	0.09	0.14	0.23
NAO JJA	**0.34**	—	**−0.38**	**−0.38**	−0.20	0.19	*0.42*	0.18
SC NH ASO	**0.50**	**0.42**	—	0.01	−0.24	0.31	*0.39*	*0.37*
SC NA ASO	**0.55**	**0.46**	−0.26	—	−0.37	*0.38*	*0.41*	0.39
SC EU OND	**0.58**	**0.41**	*−0.35*	**−0.37**	—	0.19	*0.43*	0.19
SI NH OND	**0.57**	**0.47**	*−0.38*	*−0.42*	−0.17	—	0.36	0.07
SI NP OND	**0.48**	**0.49**	−0.30	−0.30	−0.25	0.08	—	0.16
SI NA OND	**0.59**	**0.52**	−0.43	−0.43	−0.17	0.09	0.38	—

Table 4.1: Partial correlation coefficients of windstorm frequency (DJF) and 3-monthly averages of hemispheric-scale factors (as indicated in the header row), conditional on the correlation of a second hemispheric-scale factor (as indicated in the first column). The partial correlation coefficients are calculated for the longest overlapping period of the respective HF. Statistically significant coefficients ($p< 0.05$/$p< 0.10$) are highlighted (**bold**, *italic*).

4.3.3 Inter-dependencies between hemispheric-scale factors

The HF considered in this study represent different components of the climate system (ocean, atmosphere, land surface) and are obviously not independent of each other. This is illustrated, for example, by the relation between the NAO and HSI for different lags between them (Fig. 4.3). The most prominent feature of the mutual relation is a general lead of the NAO (i.e., the large-scale flow over the North Atlantic region) of about one to two months. This is consistent with the notion of the atmosphere as a driver of anomalies in the ocean, and the ocean considered as integrating an atmospheric forcing over time, resulting in co-variability of the atmosphere–ocean system with a lag of about two months, owing to the longer time scale/large heat capacity of the ocean (e.g., Kushnir et al., 2006, 2002; Christoph et al., 2000). However, a pronounced area of positive correlations is also visible with the autumn HSI leading winter NAO (maximum correlation of about 0.45 between HSI ASO and NAO NDJ). These correlations are consistent with the LLC between HSI and wintertime windstorm shown above.

Therefore, relations between HF and windstorm climate revealed with LLC do not necessarily reflect an independent relationship between a given HF and windstorm climate. Partial correlation allows this effect to be quantified. Partial correlation coefficients (Eq. 4.1) have been computed for every HF for the 3-monthly averages with the highest relation to the windstorm frequency DJF (based on LLC results), conditional on the respective correlations of all other HF (Table 4.1).

Generally, only HSI and NAO retain significant partial correlations in the range of about +0.30–0.60. Additionally, the partial correlations of all HF except NAO lose significance if the correlation between HSI and windstorm climate is accounted for (Table 4.1, first row). Hence, NAO and HSI are regarded as the most important factors influencing

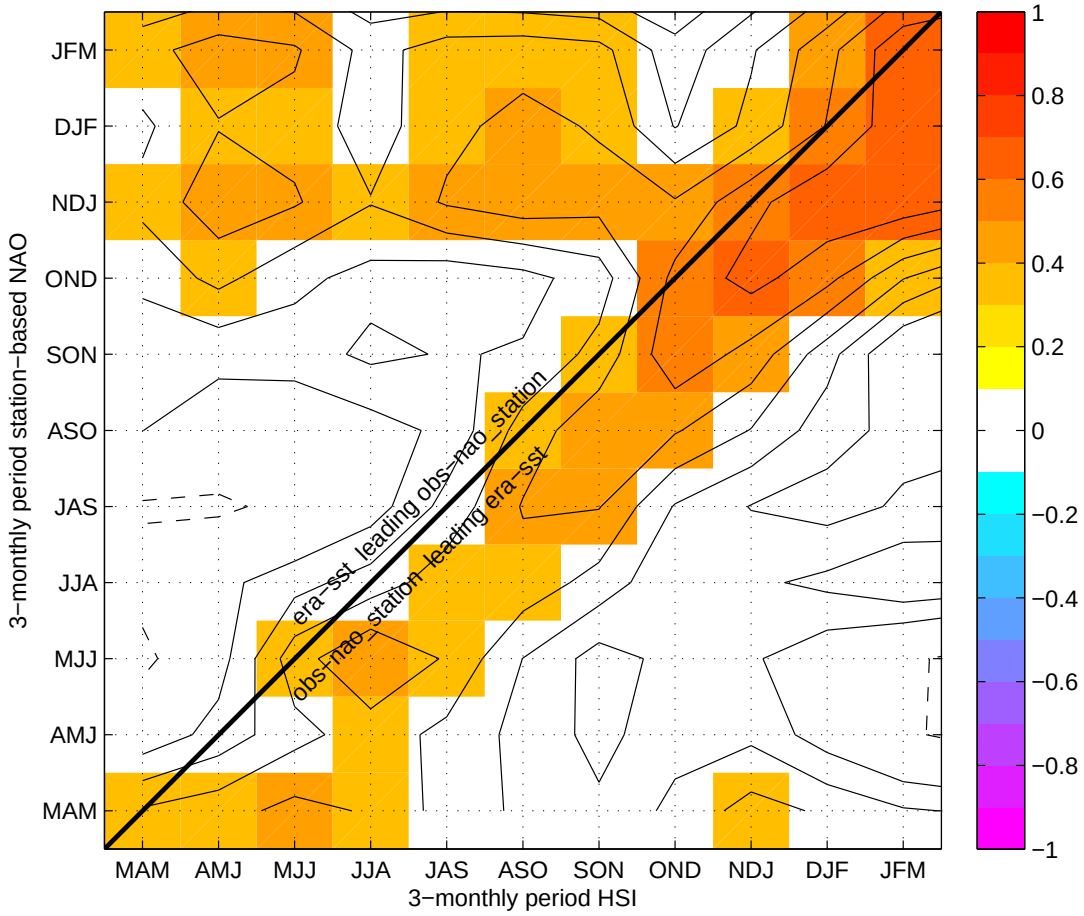

Figure 4.3: Spearman correlation coefficients between HSI and station-based NAO index 1959–2001, for different positive and negative lags. The diagonal indicates simultaneous correlations; below (above) the diagonal NAO leads HSI (HSI leads NAO). Positive (negative) correlations solid (dashed); contour interval is 0.1; the zero line is omitted. Statistically significant correlations ($p < 0.1$) are shaded.

windstorm frequency. This is supported by the consistent, statistically significant LLC irrespective of the period under consideration, correlation coefficient type, or treatment of trends. All other factors generally show insignificant partial correlations with windstorm frequency. These findings also hold if only the 1980–2001 period is considered.

4.4 Possible mechanisms linking HF and windstorm occurrence on seasonal time scales

The statistical relations between HF and windstorm frequency established in the previous section have shown the strongest correlation with wintertime windstorm frequency for Horseshoe-like SST anomalies in the North Atlantic during ASO and the large-scale atmospheric flow (as measured by the NAO index) during JJA. These statistical relations

HF and months	positive composite	negative composite
HSI ASO	1961, 1967, 1974, 1988, 1994	1964, 1966, 1968, 1981, 1995, 1997
station-based NAO JJA	1961, 1972, 1973, 1983, 1988, 1992, 1996	1963, 1968, 1976, 1987, 1995

Table 4.2: Years with HF anomalies above 1 (positive composite) and below −1 (negative composite) standard deviation during the indicated 3-monthly period.

are consistent with the hypothesis that the large-scale atmospheric flow in summer favors the establishment of Horseshoe-like North Atlantic SST anomalies which persist until the onset of the windstorm season. Persistent SST anomalies may influence the overlying atmosphere, mainly through changes in eddy activity, which could in turn feed back to the mean flow, and through linear, thermodynamic interaction (Deser et al., 2010; Peng et al., 2005; Kushnir et al., 2002). Therefore, specific growth factors of cyclones are considered in the following, and their potential relations to anomalous HF states are evaluated. To this end, the temporal and spatial evolution of anomalies of SST, MSLP, growth factors of cyclones and windstorm track density are evaluated in composites of years with strong HF anomalies.

The relation of continental snow cover and sea ice extent to wintertime windstorm frequency is generally weaker and less robust. Therefore, less emphasis is laid on these HF.

4.4.1 The contribution of NAO anomalies to the onset of the North Atlantic Horseshoe

LLC revealed a significant correlation between NAO in summer and windstorm activity in the subsequent winter. The lead time of maximum correlation was shown to be six months (JJA) for the station-based NAO index, and five months (JAS) for the PCA-based NAO index. However, the latter's correlation (about 0.30) is considerably lower than the former's (about 0.45). Cassou et al. (2004) showed that the large-scale flow over the North Atlantic in summer may be regarded as one potential source of the Horseshoe anomaly pattern in North Atlantic SST in the subsequent autumn. The mutual and partial correlations of NAO and HSI are also consistent with this assumption (Table 4.1 and Fig. 4.3). Consistently, the composite difference between years with high and low summer NAO indexes (Table 4.2) shows the emergence of a Horseshoe-like signal in the SST of the North Atlantic (Fig. 4.4a).

Both the warm and northeastern cold anomalies are persistent through autumn. Hence, we hypothesize that in the context of their influence on wintertime windstorm

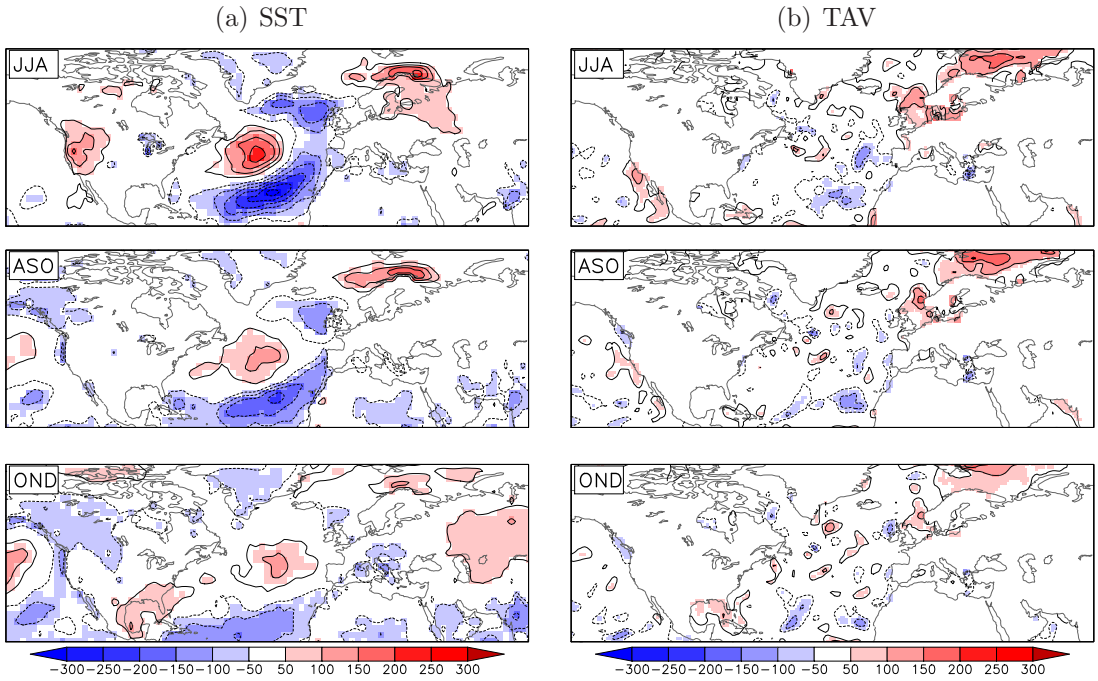

Figure 4.4: Difference of 3-monthly averaged surface temperature (SST over oceans, uppermost soil level temperature over continents; a) and TAV (b) between composites of years with strongly positive and negative station-based NAO during JJA . For comparability, the anomalies are expressed in % of the local inter-annual standard deviation of the respective variable. Solid (dashed) contours show positive (negative) values. The zero line is omitted. Statistically significant anomalies ($p < 0.10$) are shaded.

activity, the NAO and the Horseshoe pattern should be seen as closely related. It seems that the summer large-scale flow over the North Atlantic is driving SST anomalies which are persistent from late summer through early winter, as described in the previous section. As will be shown below, the anomalies in ocean heat content are weaker and less well structured than in the HSI composites (compare Fig. 4.4b with Fig. 4.5b). Thus, summer NAO is hardly the only source of the late summer/early autumn Horseshoe pattern. (In this case, the partial correlation of HSI and windstorm frequency should be weak, given the NAO-windstorm relation in Table 4.1). Instead, oceanic processes could also play a role, e.g., the advection of subsurface anomalies with ocean currents and feedback on the SST (Seager et al., 2000), or re-emergence of previous winter-spring anomalies retained below the shallow summertime mixed-layer in autumn (Timlin et al., 2002; Seager et al., 2000).

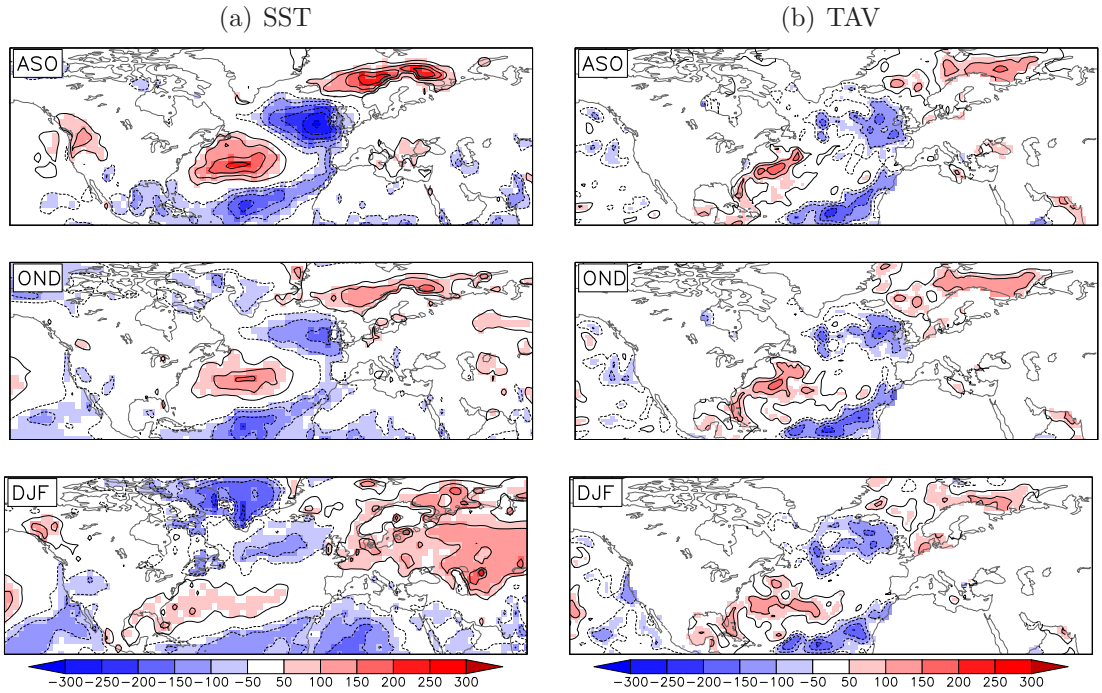

Figure 4.5: Difference of 3-monthly averaged surface temperature (SST over oceans, uppermost soil level temperature over continents; a) and TAV (b) between composites of years with strongly positive and negative HSI during ASO. For comparability, the anomalies are expressed in % of the local inter-annual standard deviation of the respective variable. Solid (dashed) contours show positive (negative) values. The zero line is omitted. Statistically significant anomalies ($p < 0.10$) are shaded.

4.4.2 The role of the North Atlantic Horseshoe pattern in modulating windstorm frequency

As shown in Fig. 4.2a, the HSI attains the highest correlation with wintertime windstorm frequency DJF in summer/autumn, namely for the 3-monthly mean ASO. Therefore, the composites in the following analysis are based on years with anomalous states of HSI in ASO. The resulting positive (negative) composite consists of five (six) years (Table 4.2). In the following, we consider the temporal evolution of the difference between the means of the positive and the negative composites from summer (August) to winter (January).

Considering years with very strong anomalies of the HSI, we start our consideration with composites of surface temperature (Fig. 4.5a). By definition of the composite according the HSI ASO, strong anomalies related to the positive phase of the Horseshoe pattern are visible in August–October, which are, as expected, similar to the correlation pattern in Fig. 4.1a. Significant differences between the positive and negative composites occur over large parts of the North Atlantic attaining levels of up to +300% of the local standard deviation. Although the anomalies weaken slightly, significant differences are persistent through November. Note that differences above 100% standard deviation persist especially in the northern region of cold anomalies. The anomalies also persist through the subsequent months. During December–February, the SST pattern is more similar to the Tripole pattern (Rodwell et al., 1999) associated with the oceanic forcing of a positive NAO anomaly. This is consistent with a winter of high storm activity (and a positive NAO regime) according to the LLC between HSI and windstorm frequency shown above. SST anomalies may be regarded as the surface expression of changes in the heat content of a well-mixed upper-ocean layer (Kushnir et al., 2002). Indeed, the Horseshoe-like signal is not only a surface feature. It is also visible in the ocean heat content of the upper 300 m (Fig. 4.5b). Here, the anomalies are more or less constant from August to February and also attain an amplitude of above 150% standard deviation, both in the warm and the two cold anomaly regions. Both the SST and TAV anomalies suggest advection of the warm anomaly from the east coast of North America towards the northeast. The deviation patterns of TAV become more similar to the SST anomalies during DJF than for the preceding months. This might be an effect of more intensive mixing in the winter months compared to the autumn. SST (TAV) anomalies consistently leading TAV (SST) anomalies would indicate an atmospheric (oceanic) origin of the SST-TAV anomalies. However, we found no clear evidence of significant lags between anomalies in TAV and SST. This is consistent with (Seager et al., 2000) who reported anomalous ocean heat transports to be just as important as surface fluxes in generating SST anomalies in the far North Atlantic (i.e., north of about 30° N).

Persistent oceanic anomalies from summer to winter may influence the atmosphere by

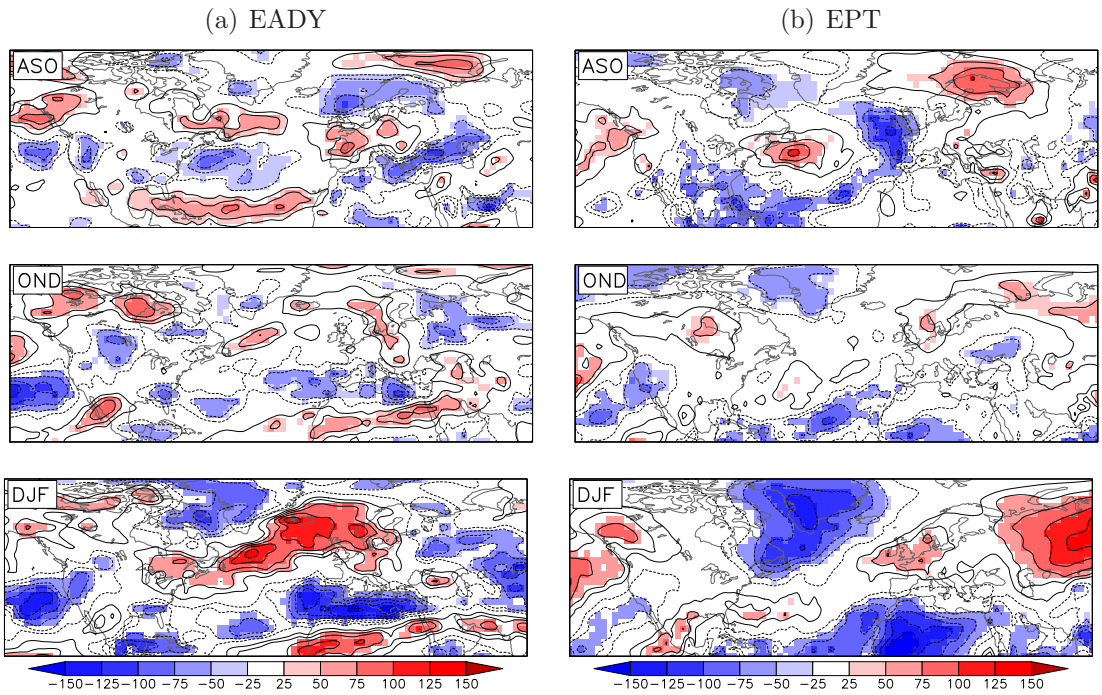

Figure 4.6: Difference of 3-monthly averaged EADY (a) and EPT (b) between composites of years with strongly positive and negative HSI during ASO. For comparability, the anomalies are expressed in % of the local inter-annual standard deviation of the respective variable. Solid (dashed) contours show positive (negative) values. The zero line is omitted. Statistically significant anomalies ($p < 0.10$) are shaded.

anomalous latent and sensible heat fluxes (Shukla and Kinter III, 2006). Indeed, the baroclinicity in terms of EADY is increased (decreased) in regions with increased (decreased) zonal SST gradients (Fig. 4.6a), e.g., between the warm and the northern cold anomalies related to the Horseshoe pattern. These anomalies in baroclinicity are very strong and basin-widely significant during ASO, becoming weaker in the subsequent months. However, throughout the period under consideration, positive anomalies of EADY are visible between Newfoundland and Northern Europe. Thus, the Horseshoe pattern seems to be accompanied by enhanced baroclinicity over the northern parts of the North Atlantic from summer to early winter. From December to February, baroclinicity again shows very high anomalies, but these values are rather an imprint of an active storm season as indicated by LLC analysis. Like baroclinicity, the anomalies of the equivalent potential temperature (EPT) are generally in good agreement with the underlying SST anomalies (Fig. 4.6b). Positive anomalies of EPT occur over positive SST anomalies (e.g., over the warm SST anomaly related to the Horseshoe pattern in August). The positive anomalies in EPT over the central North Atlantic persist throughout the period considered. Consistent with EADY, wind speed on 200 hPa (JET) does reveal persistent positive anomalies over the North Atlantic between Newfoundland and Northern Europe (Fig. 4.7a). The pattern of anomalies of upper-tropospheric divergence (DIV) is rather noisy (Fig. 4.7b). However, mostly divergent conditions prevail over northwestern Europe.

In conclusion, specific anomalies in the North Atlantic (SST and TAV) are persistent from summer to early winter. These anomalies are accompanied by physically consistent anomalies of growth factors of cyclones: enhanced baroclinicity and upper-tropospheric wind speeds between Newfoundland and Western Europe, a reservoir of moist air over the central North Atlantic (the entrance of the climatological storm track), and upper-tropospheric divergence over Northern Europe close to the continent. Note the general agreement between the anomaly patterns related to strong HSI anomalies in autumn and those related to anomalous windstorm frequency during DJF (Fig. 3.8). These factors might contribute to better growth conditions for cyclones and lead to more intense cyclones ultimately related to severe windstorm events. Indeed, respective anomalies in track density can be found in the difference composite (Fig. 4.8). In line with the Horseshoe pattern in the North Atlantic and the growth conditions shown before, we find enhanced track densities of windstorms over Western Europe through December to February.

4.5 Conclusions

Summer and autumn anomalies of all hemispheric-scale factors considered are statistically significantly correlated with the number of windstorms in the North Atlantic and European region in the subsequent winter, i.e., with lead times between two to six months.

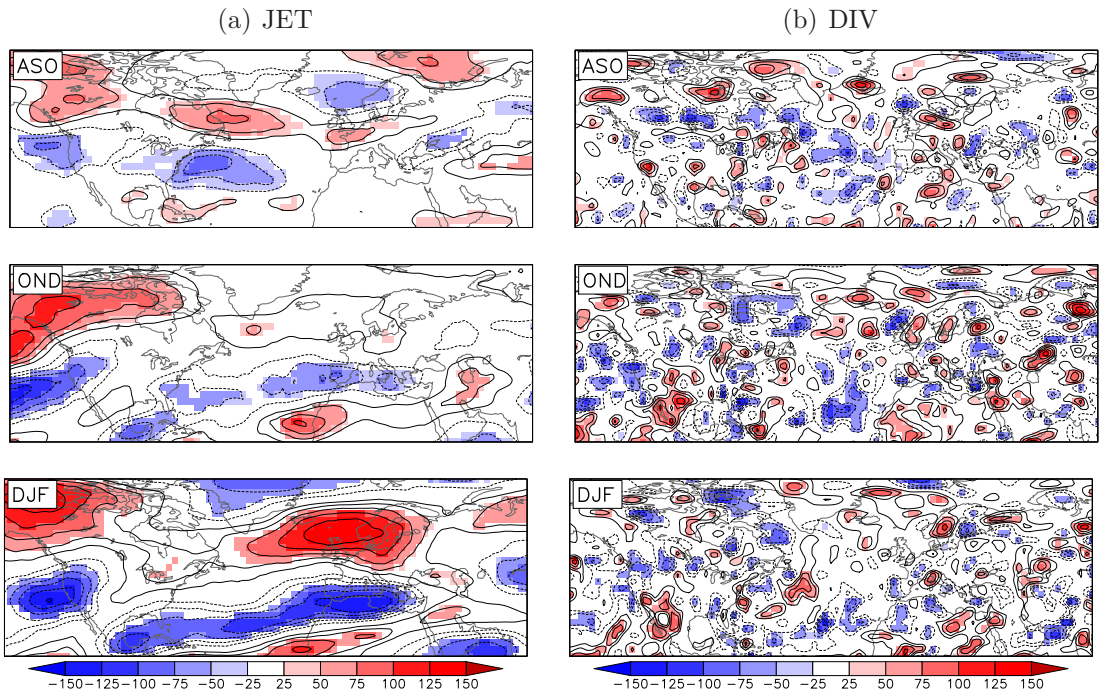

Figure 4.7: Difference of 3-monthly averaged JET (a) and DIV (b) between composites of years with strongly positive and negative HSI during ASO. For comparability, the anomalies are expressed in % of the local inter-annual standard deviation of the respective variable. Solid (dashed) contours show positive (negative) values. The zero line is omitted. Statistically significant anomalies ($p < 0.10$) are shaded.

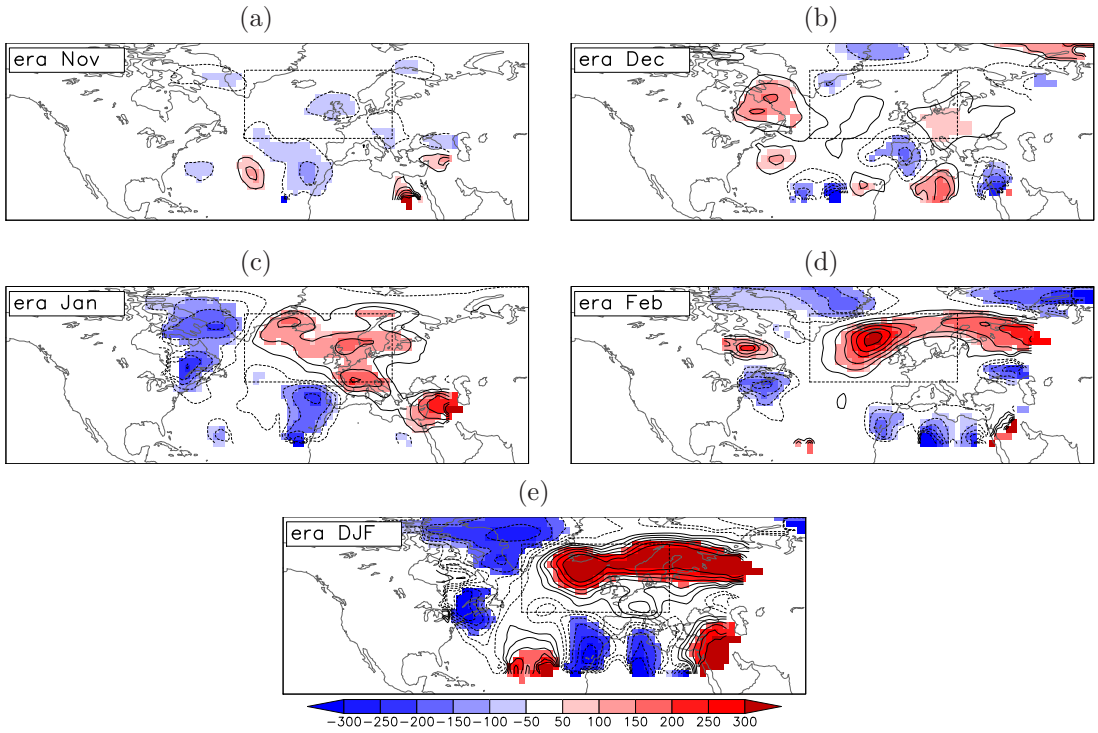

Figure 4.8: Difference in windstorm track density during November (a), December (b), January (c), February (d), and DJF (e) between composites of years with strongly positive and negative HSI during ASO. For comparability, the anomalies are expressed in % of the local inter-annual standard deviation of the respective variable. Solid (dashed) contours show positive (negative) values. The zero line is omitted. Statistically significant anomalies ($p < 0.10$) are shaded.

They attain correlation coefficients of up to +0.43, which corresponds to an explained variance of the inter-annual windstorm variability of about 20%. Robust correlations have been found for summer NAO and the Horseshoe pattern of North Atlantic SST anomalies in autumn. In contrast, the correlations between snow cover and windstorms are strong in the 1972–2001 period, but not statistically significant for the shorter 1980–2001 period. The correlations between sea ice and windstorms depend on the treatment of trends in the time series. Furthermore, the link of snow cover and sea ice to windstorm occurrence is markedly reduced if the HSI–windstorm or NAO–windstorm relation is accounted for. Such inter-dependencies have not been analyzed in prior studies with respect to the relation between hemispheric-scale factors and North Atlantic wind climate.

The composite analysis revealed evidence of a physically consistent relationship between (high) summer NAO indices, a (positive) Horseshoe SST pattern in the subsequent autumn, related to better growth conditions for cyclones through winter, and consequently a higher number of windstorms in the North Atlantic and European region. Although composites of years with strong snow cover anomalies have been analyzed as well, they have not helped to increase the understanding of the physical mechanisms involved (not shown).

In conclusion, summer NAO and autumn HSI are robust precursors of wintertime North Atlantic wind climate. Such relations imply the potential of seasonal predictability of wintertime windstorms. Skillful seasonal predictions would be possible if state-of-the-art prediction models are able to reproduce the underlying observed physical mechanisms. The skill of such models to forecast wintertime windstorm frequency in the North Atlantic and European region is therefore evaluated in the next chapter.

Chapter 5

Predictive skill in seasonal ensemble prediction systems to forecast wintertime wind storm climate

5.1 Rational

Seasonal predictability is generally assumed to be much lower in the mid-latitudes than in the tropics and to stem from the oceans, especially the North Atlantic (e.g., Kushnir et al., 2006; Czaja and Frankignoul, 2002; Rodwell and Folland, 2002), or from sea-ice variability. Other possible sources include variations of land surface properties such as the extent of continental snow cover (Fletcher et al., 2009; Orsolini and Kvamstø, 2009) or soil moisture (Conil et al., 2009; Fischer et al., 2007), stratospheric variability (e.g., Douville, 2009), or the remote influence of tropical variability, e.g., ENSO (Ineson and Scaife, 2009). However, the amount of skill in the North Atlantic region arising from ENSO variability is still strongly under debate (Van Oldenborgh, 2005; Mathieu et al., 2004). Physically motivated links between such hemispheric-scale factors and wintertime windstorm occurrence on the seasonal time scale have been described in chapter 4 and could serve as sources of predictability in seasonal forecast models.

Predictions on time scales of months to seasons, thus beyond the medium-range weather forecasts, are of major scientific and economic interest. Skillful longer-term predictions of frequency and intensity of extreme meteorological events with enormous loss potential could help to improve foresightful risk management. Windstorms in the North Atlantic/European region are of particular interest as they cause about two thirds of overall and insured loss due to natural hazards in this region (Münchener Rückversicherungs-Gesellschaft, 2007). Consequently, there is a need for skillful forecasts of such events with different lead times (Murnane et al., 2002; Murnane, 2004). Whereas short-term

forecasts of extremes have been considerably improved in recent decades (Buizza and Hollingsworth, 2002), little is known about the longer-term predictability of windstorms on seasonal time scales.

Research on seasonal predictions has greatly advanced in the last two decades (Troccoli et al., 2008; Schwierz et al., 2006; Harrison, 2005; Goddard et al., 2001). Seasonal predictability has been extensively studied for many variables, e.g., surface temperature, precipitation, mean sea level pressure, or sea surface temperatures (SST)—including indices of the El Niño-Southern Oscillation (ENSO)—and tropical cyclones (e.g., Weisheimer et al., 2009; Jin et al., 2008; Wang et al., 2008; Vitart et al., 2007; Shongwe et al., 2007; Rodwell and Doblas-Reyes, 2006; Vitart, 2006; Palmer et al., 2004). Today, seasonal predictions for most of these variables are operationally issued by several institutions such as the International Research Institute of Climate and Society, UK MetOffice, or the European Centre for Medium-Range Weather Forecasts (ECMWF).

Studies of predictive skill for the extra-tropics focusing on variables other than surface temperature and precipitation are rare. Müller et al. (2005) and Johansson (2007) demonstrated that there is significant skill in dynamical predictions for the mean winter (December–February) North Atlantic Oscillation (NAO) in a multi-model ensemble of seasonal hindcasts with a lead time of 1–4 months. Our analysis of seasonal predictability of windstorms was motivated by the general relation between the NAO and windstorm climate over the North Atlantic (Donat et al., 2010a; Pinto et al., 2009). It must be noted, however, that this relation is not as simple as a linear rise of storm number with the value of the NAO index. A mean negative or neutral phase of NAO in a given winter does not necessarily mean that there are no severe windstorm events because about 30–40% of gale days in Europe occur during negative or neutral NAO phases (Donat et al., 2010a).

A number of empirical studies explored the potential of seasonal wind climate predictability (Qian and Saunders, 2003; Palutikof et al., 2002). For example, Qian and Saunders (2003) found correlation coefficients of about 0.60 between the mean number of gale days in winter and the extent of July-August snow cover in the northern hemisphere during the preceding summer. Using dynamical climate model runs with prescribed SST anomalies, Compo and Sardeshmukh (2004) found few prospects for the potential predictability of storm tracks (2–7-day bandpass-filtered variance of 500 hPa vertical velocity) on seasonal and decadal time scales for the North Atlantic region. In a study on the estimation of return periods of windstorms, no significant predictive skill was found for a monthly averaged measure of intensity of windstorms (Extreme Wind Index, EWI) in seasonal forecast data of the ECMWF except in the first month (Della-Marta et al., 2010). In contrast to these studies, a different, event-based definition of wintertime windstorm climate is used in this study, and predictive skill is analyzed not only in one but also in ensembles of several dynamical seasonal prediction models.

In Europe, seasonal predictability was investigated particularly within two EU-funded projects, namely, DEMETER (Palmer et al., 2004) and, more recently, ENSEMBLES (Weisheimer et al., 2009). Both projects used coupled ocean-atmosphere climate models to generate retrospective seasonal forecasts (so-called hindcasts) for about the last 40 years. In this study, data from both projects are used to analyze the predictive skill of wintertime windstorm frequency in the North Atlantic and European region (45°W–20°E, 45°–70°N) within hindcasts of different (multi-) model ensembles, periods and target months, and, additionally, in different versions of the same models. Furthermore, the dependence of the variability of predictive skill on the windstorm frequency in a given winter is analyzed. Thus, a systematic skill assessment in dynamical seasonal predictions is carried out.

Descriptions of the model data and the reanalysis data used for verification have been given in section 2.3. The definition and identification of winter windstorms in coupled climate model and reanalysis data is based on the identification scheme presented in chapter 3. Some further details relevant to this chapter are given in section 5.2.1. The probabilistic verification measures and windstorm frequency classes are defined in sections 5.2.2 and 5.2.3. The representation of windstorms in the hindcast data, predictive skill, and aspects of the variability of skill are shown in sections 5.3 to 5.5. Conclusions and implications for the remainder of the thesis are given in section 5.6.

5.2 Methods

5.2.1 Definition and identification of wintertime windstorm

So far, studies on the seasonal predictability of wind climate in the North Atlantic and European region have mostly used approaches involving grid point wise measures, e.g., the number of days with wind speeds above a certain (absolute or relative) threshold (Qian and Saunders, 2003; Palutikof et al., 2002) or measures spatially aggregated over a pre-defined domain (Della-Marta et al., 2010). In contrast, this study is based on the identification of individual windstorm events as entities extending over both space and time (see chapter 3). Individual windstorm events (in contrast to the individual model or re-analysis grid points) are used to define seasonally averaged properties of the windstorm climate and then analyze the hindcasts accordingly. The potential influence of differences in the local (model-specific) wind climatologies (e.g., systematic model biases in wind speeds over the continents or different boundary-layer parameterizations) is reduced by the use of the local 98^{th} percentile of a given data set. Generally, 6-hourly surface (10 m) wind speed data were used, except for the ECMWF model in the ENSEMBLES database (labeled ECMF in the following, cf. Table 2.1 for acronyms of the other models). A numerical problem in this model led to an unrealistic intensification of extreme surface

wind speeds[1]. Therefore, ECMWF recommends using wind speed on the 925 hPa level instead. However, pressure level wind data are only available in 12-hourly resolution. Hence, the windstorm identification for ECMF had to be performed with a lower temporal resolution compared to the other models. Therefore, the original threshold of minimum lifetime of 18 hours (i.e., four timesteps for 6-hourly data) was set to 12 hours for ECMF (i.e., two timesteps for 12-hourly data). This weaker constraint leads to a systematic positive bias in the number of identified windstorms (cf. Table 5.1 and Fig. 5.2), but this bias is successfully accounted for by the simple correction scheme applied in this study (cf. Table 5.2).

The identification scheme is applied to both reanalysis and model data. The windstorm frequency for each month is defined as the number of identified storms occurring in the considered region (45°W–20°E/45°–70°N) in the respective months and extracted from the reanalysis data and the model ensembles.

5.2.2 Measures of predictive skill

In this study, the predictive skill of the windstorm frequency during December–February (DJF) and January–April (JFMA) is analyzed in hindcasts starting on 1 November (i.e., with lead times of 1–4 and 2–6 months, respectively) in the 11 single-model ensembles, in the multi-model ensembles of DEMETER and ENSEMBLES, and in the combined DEMETER-ENSEMBLES multi-model ensemble. Owing to the availability of the data, two different periods are verified, namely, 1960–2001 and 1980–2001.

Both the Relative Operating Characteristic (ROC) and the Ranked Probability Skill Score (RPSS) are used for forecast verification. The ROC measures the ability of a set of forecasts to discriminate between occurrence and non-occurrence of specific events, namely, the occurrence of a certain observed windstorm frequency class in the case of this study. These classes are defined by tercile thresholds ("high","medium" and "low" windstorm frequency). The predicted probabilities are defined as the fraction of ensemble members below the first tercile (low frequency), between the first and the second tercile (medium frequency), and above the second tercile (high frequency). The tercile thresholds are defined for each model separately. The observed probabilities are defined as 1 for the occurred class, and 0 for the two other classes. Calculation of the ROC requires dichotomous events and is therefore performed for each windstorm frequency class separately. Assuming that a set of n forecast–observations pairs is divided into n_1 occurrences of the

[1]http://www.ecmwf.int/products/forecasts/seasonal/documentation/system3/knownissues.html

event, and n_2 non-occurrences, the ROC score is defined as

$$A = 1 - \frac{1}{n_1 n_2} \sum_{\substack{n_1 \le i \le n_1 \\ n_2 \le j \le n_2}} I(P_i < P_j) - \frac{1}{2 n_1 n_2} \sum_{\substack{n_1 \le i \le n_1 \\ n_2 \le j \le n_2}} I(P_i < P_j), \tag{5.1}$$

where P_i (P_j) is the forecast probability issued prior to the occurrence (non-occurrence) of a given frequency class, and I is set to 1 if the condition in parentheses holds, and 0 otherwise (Shongwe et al., 2007; Mason and Graham, 2002). A is equivalent to the area under the ROC curve, i.e., the line spanned by the hit rate and false-alarm rate for different warning thresholds. The ROC Skill Score (ROCSS), defined as

$$ROCSS = 2A - 1, \tag{5.2}$$

(Wilks, 2006; Mason and Graham, 1999), is 1 for a perfect forecast, and below 0 for a forecast worse than a random forecast. The critical levels of statistical significant ROCSS are estimated from 10 000 random forecasts. For $p<0.05$ ($p<0.10$) they are 0.44 (0.35) for the 1980–2001 period (in consistency with Shongwe et al., 2007) and 0.26 (0.20) for the 1960–2001 period. In contrast to the ROCSS, the Ranked Probability Skill Score (RPSS) measures the quality of a multiple-class forecast with respect to a reference forecast. Generally, the Ranked Probability Score of a given forecast-observation pair (RPS_{fc}) is defined as

$$RPS = \sum_{k=1}^{K} (P_k - Ok)^2. \tag{5.3}$$

P_k and O_k denote the predicted and observed cumulative probabilities for the k^{th} class, and K is the number of classes (Toth et al., 2003, K=3 in this study). The reference forecast is a simple climatological forecast with a constant probability of 1/3 for each of the three frequency classes. Similar to the RPS_{fc}, the RPS of the climatological forecast (RPS_{clm}) is defined as the sum of the squared differences between the cumulative climatological probabilities and the cumulative observed probabilities. The RPSS is defined as

$$RPSS = 1 - \frac{\overline{RPS_{fc}}}{\overline{RPS_{clm}}}. \tag{5.4}$$

The horizontal bars denote the average of scores for a given period. Thus, a perfect forecast would have an RPSS of 1. A positive (negative) RPSS means that the model forecast is better (worse) than a climatological forecast, i.e., it contains additional (no additional) information compared to a forecast based only on climatological knowledge. To account for the ensemble size, the debiased version of the RPSS is used (Weigel et al., 2007). The statistical significance of the RPSS is calculated by a bootstrap method

(Weigel et al., 2008). The hindcasts are re-sampled in such a way that a certain year could occur several times, whereas another is not included at all. The skill score is re-calculated for this modified sample. The re-sampling is repeated 10 000 times. If the 5^{th} percentile of the resulting distribution is greater than 0, the respective skill score is assumed to be significantly positive.

5.2.3 Relation between predictive skill and windstorm frequency

An interesting question is whether all winters are equally well predicted, or whether there is a systematic relation to the windstorm frequency of a given winter. From a scientific point of view, such a relation may allow processes contributing to predictive skill to be identified and evaluated. From a user perspective, it would be desirable to know whether, for example, winters with high storm frequency are better predicted than average winters. Since the ROCSS is evaluated for different windstorm frequency classes, it will be possible to draw some conclusions from this evaluation. In a complementary approach, the relation between skill and windstorm frequency is also analyzed for the RPSS. To this end the storm frequency class for every winter in a given period is calculated from ERA-40 as described in section 5.2.2. Additionally, it is possible to calculate a measure of skill for every winter in the same period for a given forecast ensemble as

$$RPSS_t = 1 - \frac{RPS_{fc,t}}{RPS_{clm,t}}. \tag{5.5}$$

Note that Equation 5.5 is very similar to Equation 5.4 except that the quotient is not evaluated for the average, but for every winter t of a given period. Based on RPSS_t two sub-samples are computed, the first containing winters with good skill (RPSS_t above the median) and the second, winters with low skill (RPSS_t below the median). The proportion of each frequency class is then calculated in both sub-samples. A disproportional representation of any frequency class in the sub-samples is indicative of dependence of skill on storm frequency. For example, the extreme case with all medium-frequency winters in the well-predicted sample and none in the poorly predicted sample would indicate that medium-frequency winters are generally better predicted than high- and low-frequency winters. The statistical significance is estimated by a bootstrap method where the winters of a given period are randomly sampled into two sub-samples and the proportion for every frequency class is calculated. This is repeated 10 000 times. In the case of 22 winters (i.e., the 1980–2001 period) and 3 storm frequency classes, it was found that a given storm frequency class is significantly underrepresented (overrepresented, $p<0.05$) if it attains at most 9% (at least 55%). Focusing on the applicability of the seasonal forecast systems, a measure of confidence is introduced by a slight modification of the

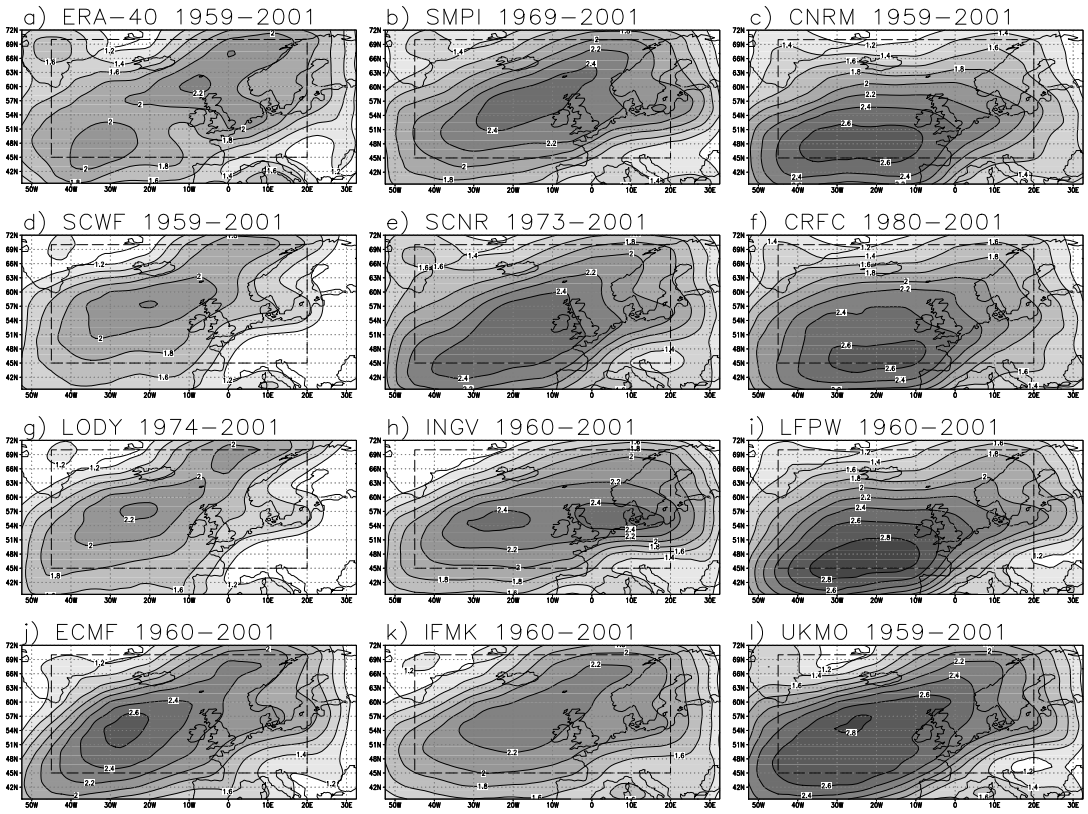

Figure 5.1: Climatological track density (tracks DJF^{-1} Lat^{-2}) of ERA-40 reanalysis (a), DEMETER and ENSEMBLES models (b–l) in the North Atlantic/European region for the period covered by the respective data set (cf. Table 2.1). Isoline interval is 0.2 starting at 1.2.

aforementioned approach. Instead of the windstorm frequency class being calculated on the basis of ERA-40 (observed frequency class), the storm frequency is calculated as the mean storm frequency of the forecast ensemble (predicted frequency class). A relation between the level of skill and the predicted storm frequency would help a potential user to estimate the confidence in a forecast for a given winter before it is actually verified.

5.3 Representation of windstorms in reanalysis and seasonal hindcast data

In a first step, the representation of windstorms according to the definition used in this study is evaluated in the reanalysis and seasonal hindcast data. The average spatial distributions of the identified windstorms (in terms of track density) in the reanalysis and model data during DJF are shown in Fig. 5.1. In the reanalysis data, the highest values are found over the North Atlantic with a maximum between Iceland and the British Isles (Fig. 5.1a). The tracks of the windstorms split into two preferred pathways over the eastern North Atlantic: one leads northeastward into the Norwegian Sea, and the other

	Nov	Dec	Jan	Feb	Mar	Apr	DJF	JFMA	NDJFMA
ERA	4.0	6.3	7.2	5.6	3.7	1.0	19.0	17.4	27.6
SCWF	–14.6	***–12.3***	–8.6	–8.7	–22.8	***–30.7***	–9.8	–12.9	***–13.0***
UKMO	***+30.8***	***+22.6***	***+25.1***	***+44.9***	***+23.6***	+29.2	***+30.1***	***+31.4***	***+29.3***
CNRM	***+31.9***	***+38.4***	***+22.3***	***+13.6***	–11.9	+1.3	***+25.0***	***11.1***	***+20.3***
SMPI	***+39.8***	***+22.8***	+16.7	***+30.1***	+9.1	+31.0	***22.6***	***+20.3***	***+23.6***
SCNR	***+58.7***	***+25.4***	+13.2	***+31.1***	+7.4	+32.3	***+22.3***	***+18.7***	***+25.6***
LODY	–4.6	–7.9	***–19.5***	***–22.4***	***–35.9***	***–37.6***	***–16.7***	***–24.9***	***–18.5***
CRFC	+7.2	***+19.7***	+0.5	+15.6	–10.4	–11.5	+10.8	+2.4	+6.7
ECMF	***+32.9***	***+44.8***	***+56.5***	***+76.6***	***+56.7***	***+107.0***	***+58.7***	***+65.8***	***+56.4***
INGV	***+32.9***	***+14.8***	***+13.8***	***+26.8***	***+18.4***	***+43.4***	***+18.0***	***+20.6***	***+21.1***
IFMK	***+38.8***	***+24.7***	***+13.6***	***+24.1***	***+13.2***	***+61.5***	***+20.3***	***+19.6***	***+23.4***
LFPW	***–17.9***	+8.8	***+19.2***	***+41.9***	***+15.2***	+14.4	***+22.5***	***+25.4***	***+15.5***

Table 5.1: Monthly distribution of windstorm frequency expressed as the mean number of identified windstorms per month and during DJF, JFMA, and NDJFMA, respectively, in ERA-40 (upper row) and deviations from ERA-40 of the seven DEMETER models (central rows, in %) and the three ENSEMBLES models (lower rows, in %) for the periods covered by the respective models (cf. Table 2.1). Significant deviations ($p<10\%$, two-sided rank sum test) are denoted in bold italics. The systematic overestimation in ECMF is due to a weaker threshold concerning the duration of windstorm events related to the different temporal resolution of the data (see section 2.3 for details.

leads eastward into the North and Baltic Seas. The British Isles and areas adjacent to the North Sea are very exposed regions. A small local maximum is discernible over the north-western Mediterranean. The track density of cores of cyclones in the North Atlantic region shows a very similar pattern but is shifted to the north-west (Leckebusch et al., 2008a). This is consistent with the assumption that the highest wind speeds in an extra-tropical low pressure system most frequently occur to the south and east of its center. Owing to the large ensemble size of nine members per model, the track density patterns are smoother in the seasonal forecast model data than in the reanalysis (Fig. 5.1b–l). The models are generally able to capture the main features of the observed track density. For example, all models consistently show the maximum track density over the North Atlantic. However, most models overestimate the track density and reproduce the center of the storm track shifted to the south-west compared with the reanalysis. This is most prominent in the models using ARPEGE (CNRM, CRFC and LFPW, cf. Table 2.1), which show the maximum track density between 45° and 54°N (Fig. 5.1c, f, i), and less obvious for models using ECHAM (SMPI, SCNR, INGV, IFMK; Fig. 5.1b, e, h, k). Furthermore, models using the Integrated Forecast System (IFS) of ECMWF as their atmospheric component underestimate the track density especially over Scandinavia and central Europe (SCWF, LODY; ECMF to a smaller degree; Fig. 5.1d, g, j). The splitting into two preferred pathways revealed in the reanalysis data is discernible in several of the climate models (namely, in SMPI, SCWF, SCNR, LODY, ECMF and UKMO).

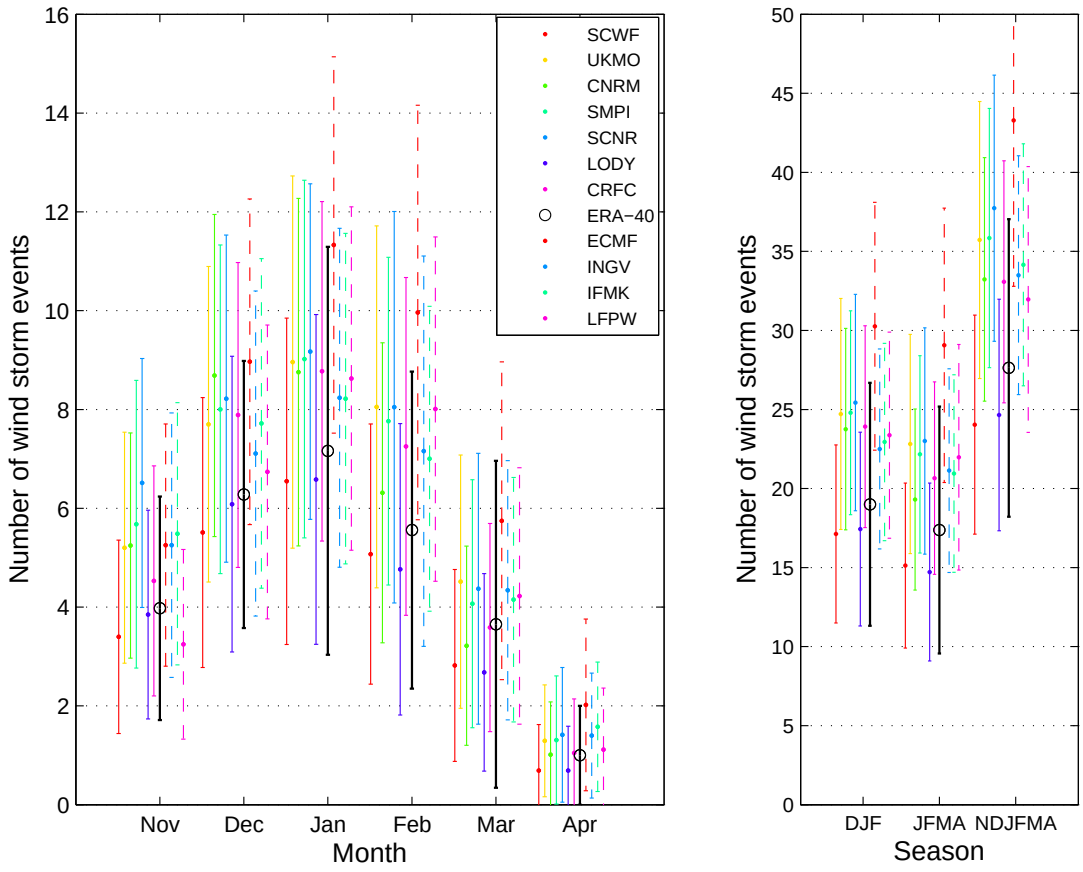

Figure 5.2: Monthly distribution of windstorm frequency as represented by the absolute mean monthly number of windstorms per month (left) and during DJF and JFMA, respectively (right) for ERA-40 (black), DEMETER (solid) and ENSEMBLES models (dashed) with standard deviations for the periods covered by the respective models (cf. Table 2.1) and over the region of interest (dashed boxes in Fig. 5.1).

The intra-seasonal distribution of the identified windstorms is expressed as the monthly number of windstorms (i.e., the monthly windstorm frequency) affecting the North Atlantic and European region (dashed boxes in Fig. 5.1). In ERA-40, the monthly distribution of windstorm frequency peaks in January (about seven events on average) with a subsequent decrease to below one event in April (Fig. 5.2 and Table 5.1). In the region of interest, 27.7 storms are identified on average from November to April (i.e., about 4.6 storms per month), with considerable inter-annual variability (Fig. 5.2, black whiskers). An average number of 19 windstorms is counted during DJF (Table 5.1).

In general, the seasonal forecast models reproduce the monthly distribution well, e.g., the peak in January (Fig. 5.2). However, significant biases exist for certain models and months (Table 5.1). The biases of storm frequency during DJF range from -9.8% (SCWF) to +30.1% (UKMO, Table 5.1) and are model-specific. For example, the two models with IFS (namely, SCWF and LODY) underestimate the absolute windstorm frequency, which is consistent with the aforementioned underestimation of track density (Fig. 5.1). These

	Nov	Dec	Jan	Feb	Mar	Apr	DJF	JFMA	NDJFMA
ERA	0.88	1.37	1.60	1.25	0.74	0.16	4.22	3.75	6.00
SCWF	–1.8	+0.8	+5.1	+4.9	–11.3	–20.4	+3.6	+0.1	0.0
UKMO	+1.2	–5.2	–3.2	**+12.0**	–4.4	–0.1	+0.6	+1.6	0.0
CNRM	+9.7	**+15.0**	+1.6	–5.6	–26.7	**−15.8**	+3.9	–7.6	0.0
SMPI	+13.1	–0.6	–5.6	+5.2	–11.7	+6.0	–0.8	–2.7	0.0
SCNR	**+26.3**	–0.2	–9.9	+4.3	–14.5	+5.3	–2.6	–5.5	0.0
LODY	+17.0	+13.0	–1.2	–4.8	–21.3	–23.5	+2.2	–7.9	0.0
CRFC	+0.4	+12.2	–5.8	+8.4	–16.0	**−17.1**	+3.8	–4.1	0.0
ECMF	–15.0	–7.4	+0.1	**+12.9**	+0.2	**+32.4**	+6.3	–0.4	0.0
INGV	+9.8	–5.2	–6.0	+4.8	–2.2	+18.4	–2.6	–0.4	0.0
IFMK	+12.4	+1.0	–8.0	+0.5	–8.3	+30.8	–2.6	–3.2	0.0
LFPW	**−28.9**	–5.8	+3.2	**+22.9**	–0.2	–1.0	+6.1	+8.6	0.0

Table 5.2: As Table 5.1, but scaled for every model with its multi-year monthly mean frequency including all months (November to April), i.e., corrected for systematic errors.

biases are accounted for by scaling the monthly storm frequency with the multi-year monthly mean frequency including all months (November to April, e.g., 4.6 storms per month for ERA-40) and for each model separately. For the seasonal forecast models, the scaling factor is calculated as the average over all ensemble members. Thus, in the following, the storm frequency is expressed as an anomaly with respect to the models' climatologies. The bias-corrected windstorm frequencies of the models during DJF and JFMA (the focus of the remainder of the study) are not significantly different from ERA-40 (Table 5.2). Hence, the climatology of North Atlantic/European windstorms is reproduced sufficiently well in the hindcast data to conduct studies of the skill of windstorm frequency predictions on seasonal time scales.

5.4 Predictive skill

One major outcome of the study is that there is significant predictive skill, both in terms of ROCSS and RPSS, particularly in the multi-model ensembles. The skill reveals a dependence on the period considered. Furthermore, the level of the ROCSS indicates a dependence on the observed windstorm frequency. Concentrating on winters with an anomalous high or low number of windstorms, ROCSSs have been computed for windstorm frequency in the lower tercile ("low windstorm frequency") and upper tercile ("high windstorm frequency"), therefore avoiding known negative biases for the middle tercile class (Kharin and Zwiers, 2003). Figure 5.3 shows the corresponding ROC curves for windstorm frequency during DJF in the 1980–2001 period. For most of the ensembles, the upper tercile ROC curve deviates from the diagonal, indicating successful discrimination of the high windstorm frequency winters. For example, LFPW exhibit an almost perfect ROC curve (Fig. 5.3a). In contrast, the ROC curve of the lower-tercile category is above the diagonal for fewer ensembles (LFPW, GRAND, CRFC, DEM, SCWF, CNRM),

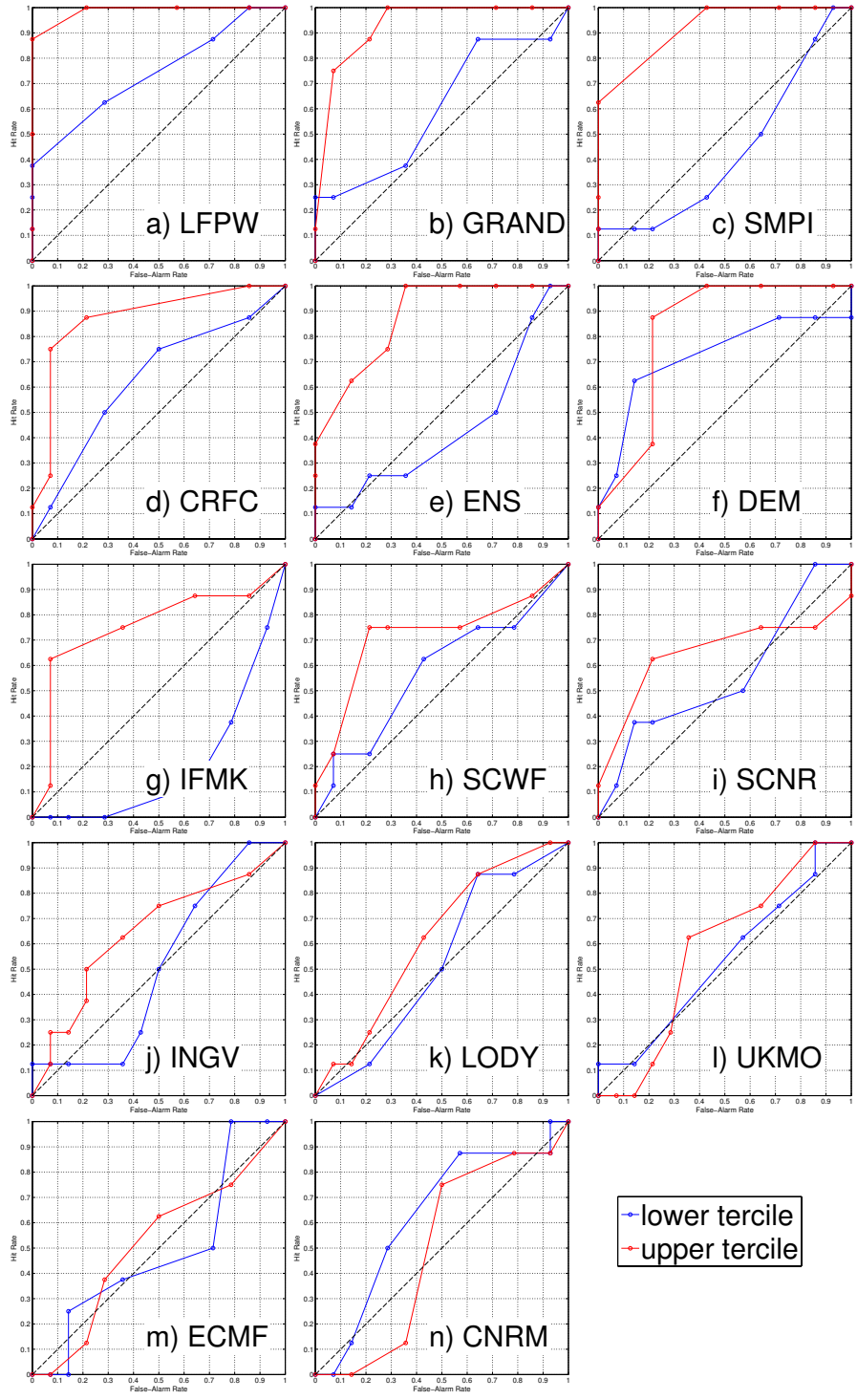

Figure 5.3: ROC curves for windstorm frequency in the lower tercile (blue), and upper tercile (red) during DJF for the 1980–2001 period for different single and multi-model ensembles, decreasingly sorted according to the ROCSS of the upper-tercile forecast. The curves show the hit rate (vertical) and false alarm rate (horizontal) for different warning threshold probabilities.

	1980–2001				1960–2001			
	a) DJF		b) JFMA		c) DJF		d) JFMA	
	$< 33\%$	$> 66\%$	$< 33\%$	$> 66\%$	$< 33\%$	$> 66\%$	$< 33\%$	$> 66\%$
GRAND	0.17	**0.90**	*0.40*	0.23	0.02	*0.25*	*0.26*	*0.26*
ENS	–0.13	**0.72**	*0.41*	0.02	0.13	**0.34**	**0.44**	**0.32**
DEM	**0.52**	**0.62**	0.21	0.21	–0.03	0.07	–0.13	0.07
LFPW	**0.48**	**0.97**	0.28	**0.64**	*0.26*	*0.32*	0.10	0.19
ECMF	–0.02	0.04	0.28	–0.20	*0.24*	0.15	0.17	–0.03
IFMK	–0.60	**0.51**	–0.11	0.14	0.13	0.05	*0.32*	–0.14
INGV	0.01	0.29	**0.48**	–0.29	–0.11	0.16	**0.38**	**0.44**
SCWF	0.15	*0.44*	0.35	0.28	0.00	0.07	0.05	0.18
CNRM	0.26	0.00	–0.10	0.09	–0.04	–0.01	–0.02	0.16
UKMO	0.07	0.15	–0.18	–0.28	–0.21	0.04	–0.34	–0.11
SMPI	–0.13	**0.84**	0.15	0.28				
SCNR	0.13	0.30	–0.04	*0.38*				
LODY	0.05	0.24	0.26	0.00				
CRFC	0.26	**0.75**	–0.26	–0.26				

Table 5.3: ROCSS of windstorm frequency hindcasts during DJF (a) and JFMA (b) 1980–2001, and during DJF (c) and JFMA (d) 1960–2001 in the combined DEMETER-ENSEMBLES multi-model ensemble (GRAND), the ENSEMBLES multi-model ensemble (ENS), the DEMETER multi-model ensemble (DEM, top rows); the ENSEMBLES single-model ensembles (central rows); and the DEMETER single-model ensembles (bottom rows) for the events as indicated in the header ($< 33\%$: lower tercile;$> 66\%$: upper tercile). Statistically significant scores ($p < 0.05/p < 0.10$) are denoted in bold/italic.

and close or even below otherwise. As expected from Figure 5.3, all models attain positive ROCSSs for the upper tercile, the majority significantly (p<0.05, Table 5.3a).

Although generally lower, the skill for the upper tercile remains positive in the longer period 1960–2001, except in CNRM (Table 5.3c). In contrast, the ROCSSs of the lower tercile are only significant in two ensembles (DEM, LFPW) in the 1980–2001 period (Table 5.3a). Generally, the scores of the upper-tercile category are higher than of the lower-tercile category. Compared to DJF, the ROCSS is generally smaller for windstorm frequency during JFMA, as expected from the longer lead times (Table 5.3b and 5.3). Only INGV has consistently significant scores for both the lower and upper terciles, which is also reflected in significant skill for the GRAND and ENSEMBLES multi-model ensembles. Especially successful are the the hindcasts of the LFPW and SCWF single-model and the GRAND multi-model ensembles. They attain positive skill scores in all cases shown in Table 5.3. The ROCSSs for an additional above-median category agree well with the upper-tercile category (not shown). The performance of the dynamical prediction models to forecast the probability of three windstorm frequency classes with respect to a climatological reference forecast is quantified in terms of RPSS (Fig. 5.4). For

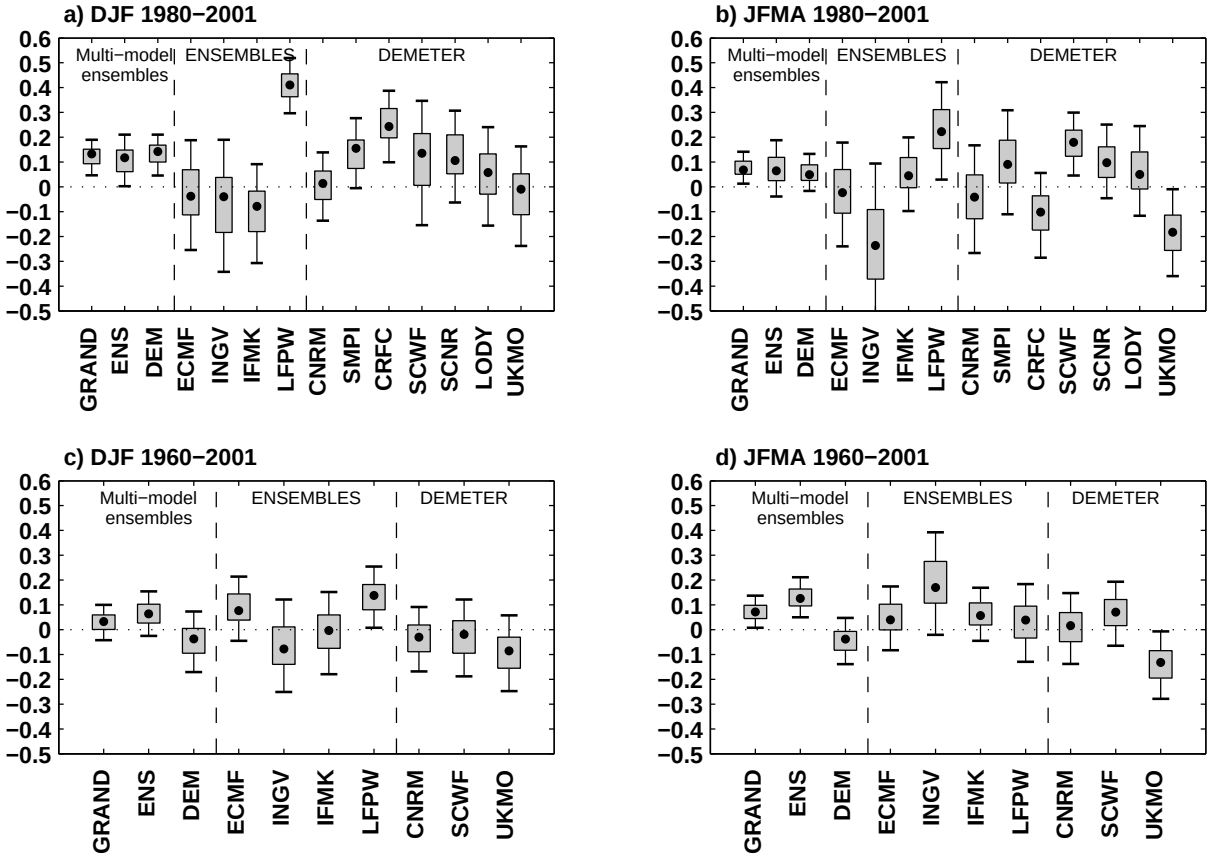

Figure 5.4: Predictive skill (RPSS) of a) windstorm frequency during DJF (i.e., lead time of 1–4 months) and b) JFMA (2–6 months) for the 1980–2001 period; c) windstorm frequency during DJF and d) JFMA for the 1960–2001 period in the single-model ensembles of DEMETER (right), ENSEMBLES (center), the respective multi-model ensemble (left, DEM and ENS) and the multi-model ensemble combining all 11 models (left, GRAND). The box (whiskers) indicates the 50% (90%) confidence interval based on a bootstrap method.

the period 1980–2001, 7 of the 11 single-model ensembles exhibit positive skill scores for the windstorm frequency during DJF (Fig. 5.4a). In particular, the models from Météo France (CRFC and LFPW) attain statistically significant skill scores of 0.24 and 0.41, respectively. Additionally, SMPI has a skill of 0.16, but with a significance marginally above 0.05 (p=0.058 estimated from the distribution of the random sample as described in section 5.2.2). All considered multi-model combinations consistently exhibit significant positive skill, but on a lower level (about 0.15). For the hindcasts of the windstorm frequency during JFMA the skill scores are generally lower (Fig. 5.4b). Still, LFPW and SCWF have significant skill (0.22 and 0.18, respectively), as has the combined GRAND multi-model ensemble (0.07). For the longer period 1960–2001, skill is generally lower than for the shorter period (e.g., compare the different skill scores of the LFPW model in Fig. 5.4). The three DEMETER single-model as well as the DEMETER multi-model hindcasts of windstorm frequency during DJF show negative skill (Fig. 5.4c). In contrast, the ENSEMBLES multi-model ensemble and two of its single-model ensembles (ECMF, LFPW) attain positive skill (0.06–0.14), the latter even significantly (Fig. 5.4c). For the longer period 1960–2001, the skill scores differ less for JFMA than for DJF (Fig. 5.4d). Interestingly, although none of the ENSEMBLES single-model ensembles has significant skill, both its multi-model ensemble and the GRAND multi-model ensemble have significant RPSS of 0.07. This demonstrates that information in multi-model seasonal forecasts of windstorm frequency with a lead time beyond three months outperforms a climatological forecast. It also illustrates the value of large (multi-model) ensembles in climate predictions (Hagedorn et al., 2005). Owing to the large ensemble size, the confidence intervals are smaller for the multi-model ensemble than for the single-model ensembles. Thus, it is possible to conclude that even a relatively low skill score is significantly different from a random sample. This is more difficult for smaller ensembles with the same level of skill. Furthermore, the use of the multi-model is motivated by the fact that it is almost impossible to know which model performs best before the prediction is verified by observations.

Note that the significant skill scores of the multi-model ensembles generally remain significant even if the LFPW model is removed from the ensembles. The only exception is the ENSEMBLE multi-model prediction of windstorm frequency during DJF for the 1980–2001 period (Fig. 5.4a). Please note that the results from the ROCSS and RPSS analysis agree very well. Forecast ensembles with high ROCSS tend to have high RPSS.

The single-model ensembles show considerable differences in predictive skill. However, there are no obvious relations between skill and the resolution of the models (Table 2.1) or their systematic biases (Table 5.1 and 3). In addition to the standard climatological reference forecast, the RPSS was also calculated using three different reference forecasts based on persistence. The first reference forecast equals the observation of the preceding

year ("inter-annual persistence"); the second considers the preceding four years (weighted by the auto-correlation function of the observed windstorm frequency; "multi-year persistence"); the third equals the observed windstorm frequency during November, the initial month of the dynamical hindcasts ("November persistence"). The RPSS of the dynamical models with respect to the different persistence reference all become positive and in most cases statistically significant (not shown). Thus, the persistence reference forecast is a weaker benchmark for the dynamical predictions than its climatological counterpart (i.e., the RPS_{clim} in Eq. 2 is generally higher for the persistence than for the climatological reference), in consistency with Qian and Saunders (2003). Note that these results do not exclude the possibility that an optimal combination of persistence and climatological reference forecasts could yield a stronger benchmark. The results shown so far are based on windstorm frequency. Additionally, predictive skill was analyzed in terms of the intensity of winter windstorms as measured by the Storm Severity Index (SSI, Leckebusch et al., 2008b) and three storm intensity classes defined according to the accumulated SSI values of the storms in a given winter. No significant skill was found for this particular measure of storm intensity (not shown).

5.5 Some aspects of the variability of skill

It has been noted that considering only average skill may mask potentially important skill variations (Compo and Sardeshmukh, 2004). Therefore, some aspects of the variability of skill are addressed in the following, namely, differences in skill between the 1980–2001 and 1960–2001 period, and the relation between skill and windstorm frequency.

Predictive skill 1980–2001 versus 1960–2001

Both skill measures tend to score more highly in the 1980–2001 than the 1960–2001 period (compare Fig. 5.4a and b or Table 5.3a and c). One possible reason could simply be the higher quality of the initial conditions due to improved observational data for the later period, especially with the introduction of satellite data, also related to more accurate storm identification in the reanalysis data. The analysis of the impact of better observations would ultimately depend on very specialized hindcast runs, e.g., by withholding new observations or observation types to mimic the state of the observation system in the earlier periods. Such hindcasts do not exist up to now. To test whether sampling issues explain these findings, a bootstrap test is employed by randomly choosing 22 years (the same number as in the period 1980–2001) for each of the 10 single and multi-model ensembles available for the entire 1960–2001 period and computing the corresponding RPSS. This is repeated 10 000 times. From the resulting distribution, the fraction of random peri-

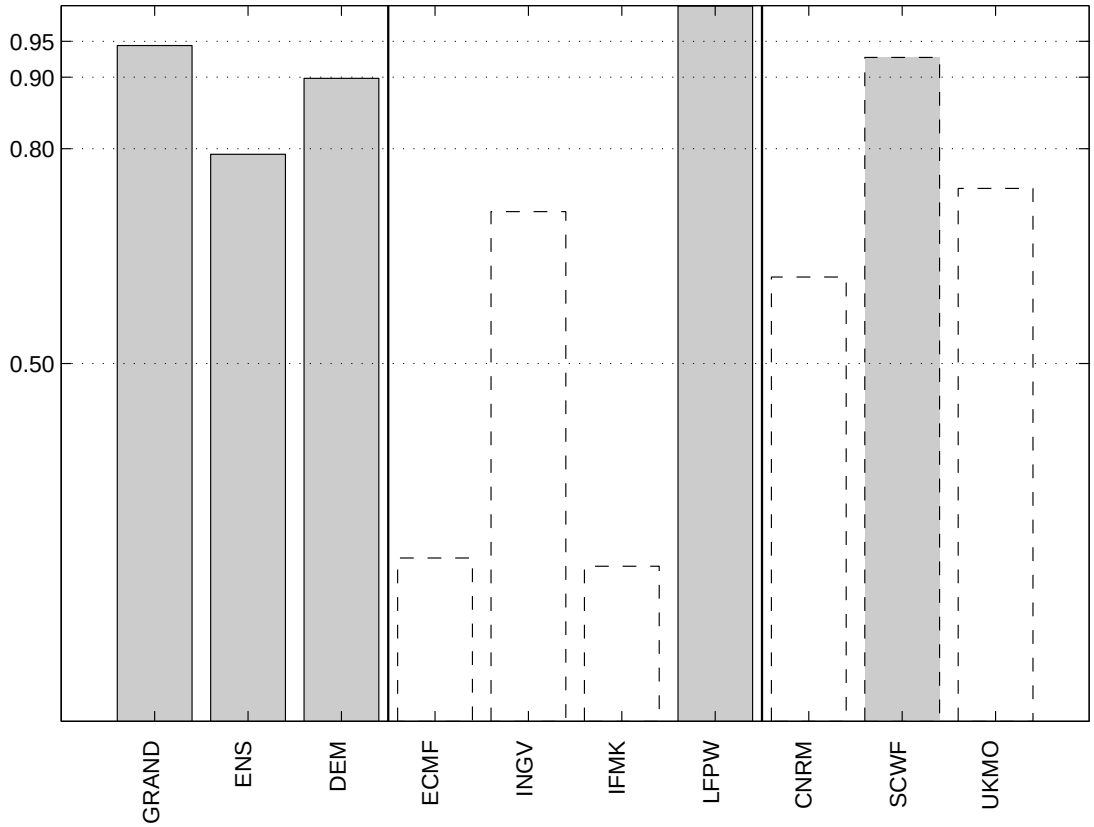

Figure 5.5: Fraction of times the skill in the 1980–2001 period outperforms the skill of 10 000 random samples of the entire 1960–2001 period with the same number of years for model ensembles available for the entire period (solid edged/shaded bars for ensembles with significant skill $p<0.05$/$p<0.20$).

ods outperformed by the regular 1980–2001 period (in terms of RPSS) is computed. If this fraction is above 0.50, the regular 1980–2001 period is interpreted as being better predicted. This is indeed the case for eight of the ten model ensembles (Fig. 5.5). Only two models, IFMK and ECMF, show fractions of about 0.20. The performance of these models is doubtful, however, since none of them shows significant skill. In contrast, the LFPW model ensemble, which provides statistically significant skill scores for both the long and the short period, attains a fraction of above 0.99, i.e., only 1% of the randomly chosen 22 forecast-observation pairs have skill of at least the value found for the regular 1980–2001 period. Additionally, the other models with significant skill in the 1980–2001 period show fractions of 0.80 or above. Therefore, we argue that sampling effects do not explain the better predictability of the 1980–2001 period. Physical reasons may play a role as well. However, the long-term trend of sea level pressure in the North Atlantic region (reflected by a positive trend of the wintertime NAO in the 1960–2001 period) is not confirmed as a possible explanation. First, the forecast models do not reproduce the trend of the winter mean NAO. Second, the long-term trend accounts for only about 10% of

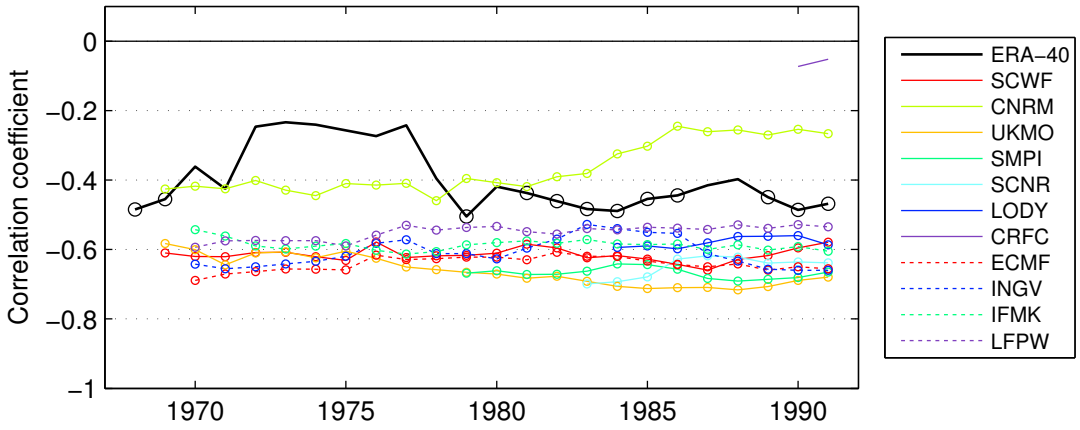

Figure 5.6: 21yr-running correlation between PNA and NAO indices in ERA-40 (black), DEMETER (solid lines) and ENSEMBLES single-model ensembles (dashed lines). The x-axis denotes the central year of the running correlation. Significant correlation coefficients ($p<0.05$) are marked.

the total inter-annual variability. One possibility could be the temporally varying relation between the Pacific North American pattern (PNA) and the NAO. It was suggested that there are phases of strong and weak relations, both in data from coupled climate models and reanalyses (Pinto et al., 2011; Luksch et al., 2005). During phases of strong relations, predictive skill from the ENSO region could be propagating into the North Atlantic, potentially leading to higher skill on the seasonal time scale. To evaluate the PNA-NAO link in the seasonal prediction models, PNA and NAO indices were computed in both hindcast and reanalysis data. The indices are defined as the leading Principal Components in the North Pacific (140°E–30°W, 20°N–87.5°N) and North Atlantic (110°W–60°E, 20°N–87.5°N) region, respectively, based on the pooled monthly anomalies of geopotential height on the 500 hPa level from November–March. Then, the 21-year running correlations between PNA and NAO were computed for both the reanalysis and hindcast data. The observed link between PNA and NAO is weak in the 1970s but relatively strong in the 1980s (Fig. 5.6), in consistency with Pinto et al. (2011). The same figure reveals that the seasonal prediction models generally overestimate the strength of the PNA-NAO link. The two exceptions are CNRM and CRFC. However, the latter is only available for 22 years, and therefore is represented by only two points in Fig. 5.6. Specifically, the models do not reproduce the decadal-scale variability found in the observations. Thus, the link produced in the models fits the observed link in the 1980s and 1990s, but not in the 1970s. Compared to observations, the model climate in the North Atlantic might be too strongly influenced by the Pacific region in the earlier period.

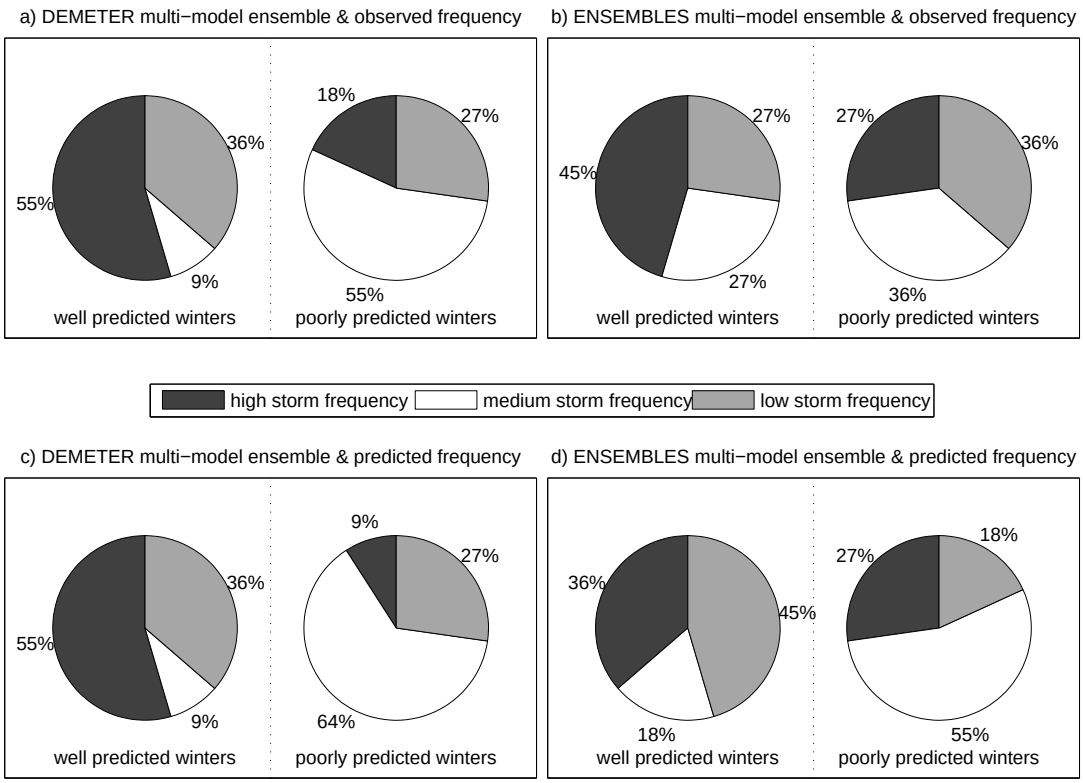

Figure 5.7: Proportions of winters (DJF) with high (dark gray), medium (white) and low windstorm frequency (light gray) in a sub-sample of winters with skill above (left) and below (right) the median for the 1980–2001 period based on a) hindcasts of the DEMETER multi-model ensemble and observed storm frequency, b) hindcasts of the ENSEMBLES multi-model ensemble and observed storm frequency, c) hindcasts of the DEMETER multi-model ensemble and predicted storm frequency, d) hindcasts of the ENSEMBLES multi-model ensemble and predicted storm frequency.

Relation between predictive skill and windstorm frequency

The results of ROCSS analysis indicate differences between the skill for high and low windstorm frequency winters. In the following it is tested whether such dependence is also found for the RPSS by analyzing the fractioning of the three windstorm frequency classes in well and poorly predicted years (as described in section 5.2.3). In the sub-sample of well-predicted winters (skill above median) based on the DEMETER multi-model ensemble during the 1980–2001 period, the high, medium and low storm frequency classes attain proportions of 55%, 9%, and 36%, respectively (Fig. 5.7a). Thus, the high-frequency class is significantly overrepresented in well-predicted years. In contrast, the sub-sample of poorly predicted winters (skill below median) consists of 18% high-frequency, 55% medium-frequency, and 27% low-frequency winters. Hence, the medium frequency class is significantly underrepresented in well-predicted winters, but significantly overrepresented in poorly predicted winters (cf. section 5.2.3). This tendency is also found in the ENSEMBLES multi-model (Fig. 5.7b). High- (medium-) frequency winters are more

(less) frequent in the well-predicted than in the poorly predicted sub-samples. In contrast to the DEMETER multi-model ensemble, low-frequency winters are less frequent in well-predicted years (27%) than in poorly predicted winters (36%). However, the proportions based on the ENSEMBLES multi-model skill are not statistically significant. Thus, there is a tendency towards higher (lower) RPSSs in winters with high (medium) observed windstorm frequency, in consistency with high ROCSSs for the upper-tercile category (cf. Table 5.3). However, this result is derived from information that would not be available at the time the forecast is issued (namely, the observed storm frequency). Therefore, a question immediately arising is whether similar relation of skill is manifested also with respect to the windstorm frequency predicted by the multi-model ensemble. In the following, the storm frequency class for a given winter is defined as the ensemble average of the windstorm frequency during DJF of the respective multi-model ensemble, i.e., the predicted storm frequency. Thus, only information available at the time the forecast was issued is used. For the DEMETER multi-model ensemble, the proportions of the three predicted frequency classes in the well-predicted sub-sample (Fig. 5.7c, left) are the same as for the observed frequency classes (Fig. 5.7a, left). However, the fractioning in the sub-sample of poorly predicted winters is more pronounced. The high-, medium-, and low-frequency classes attain proportions of 9%, 64%, and 27%, respectively (Fig. 5.7c, right). Thus, the fractioning of both the high- and medium-frequency classes is statistically different to a random distribution for both the well- and poorly predicted years. A tendency to more pronounced fractioning is also visible in the hindcasts of the ENSEMBLES multi-model ensemble. The well-predicted sub-sample consists of 36% high-frequency, 45% low-frequency, but only 18% medium-frequency winters. In contrast, the poorly predicted years consist of 27% high- and 18% low-frequency winters, but the medium-frequency winters are significantly overrepresented with a proportion of 55%. Hence, the tendency towards higher (lower) predictive skill of high- (medium-) frequency winters is also discernible in the predictions themselves. These tendencies are also manifested in the multi-model ensembles for the period 1960–2001, but not significantly (not shown). The single-model ensembles generally agree but exhibit more variability.

5.6 Conclusions

In conclusion, the study provides a systematic assessment of the reproduction of wintertime windstorms over the North Atlantic and Europe in several single-model ensembles and their ability to predict wintertime windstorm frequency over the North Atlantic and Europe. Statistically significant skill has been found for the multi-model ensembles and specific single-model ensembles. The two skill measures employed (RPSS and ROCSS) agree very well. The best single-model (LFPW) attains skill scores of up to 0.41 in terms

of the RPSS for the 1980–2001 period. The level of skill of the multi-model ensembles is about 0.10–0.15. Generally, the skill in the 1960–1980 period is worse than in the 1980–2001 period. Additionally, winters with a high windstorm frequency are better predicted than winters with an average number of windstorms.

This study serves as a starting point in two ways: Firstly, even if the skill might seem low, such predictions might be valuable for specialized users (Garcia-Morales and Dubus, 2007; Hurrell et al., 2006; Kushnir et al., 2006; Murnane, 2004). However, it shows the necessity of developing foresightful procedures for risk management practices—such as better preparation of liquidity for indemnity payout—that rely on seasonal forecasts. Secondly, it shows that seasonal forecast ensembles exhibit significant predictive skill, encouraging further development of model diagnostics (especially with respect to extreme events) and improvements of seasonal forecast models. In particular, the sources of skill should be analyzed in the hindcast data and compared to observations. This would enhance the understanding of differences in model performance with possible implications for further model improvements. These issues are analyzed in the following chapter.

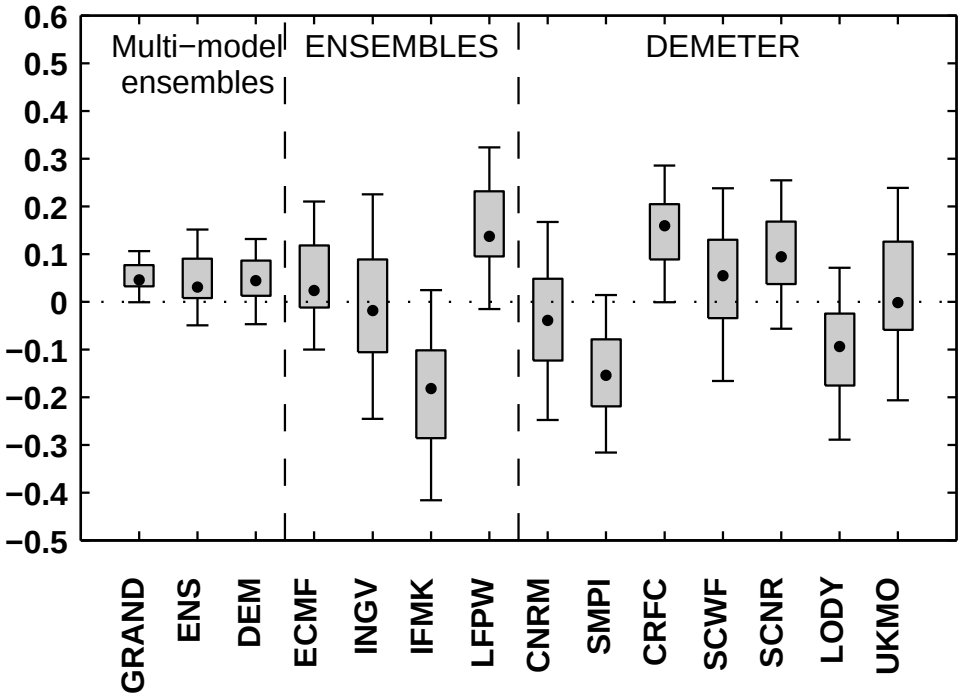

Figure 5.8: Predictive skill (RPSS) of the Storm Severity Index accumulated over DJF (i.e., lead time of 1–4 months) for the 1980–2001 period in the single-model ensembles of DEMETER (right), ENSEMBLES (center), the respective multi-model ensemble (left, DEM and ENS) and the multi-model ensemble combining all 11 models (left, GRAND). The box (whiskers) indicates the 50% (90%) confidence interval based on a bootstrap method.

5.7 Appendix

In order to complete the results shown before additional material is shortly presented in the following. First, the skill scores of windstorm intensity predictions (in contrast to windstorm frequency) are shown for both the ENSEMBLES and DEMETER models and their multi-model ensembles. Second, the skill scores of the August hindcasts have been quantified for the DEMETER models.

Similar to windstorm frequency, the skill to forecast the intensity was quantified in terms of the RPSS of three equiprobable classes of the accumulated SSI of all events occurring during December–February. The skill is found to be lower than for windstorm frequency (Fig. 5.8), and neither the single-models nor the multi-model ensembles attain statistically significant skill. However, LFPW and CRFC attain comparatively high scores that are marginally significant. Both models have been shown to successfully predict windstorm frequency. Obviously, the prediction of accumulated intensity is related to the prediction of the storm counts in the same period. Nevertheless, skill scores is considerably lower for windstorm frequency (0.13 compared to 0.41 for LFPW; 0.16 compared to 0.23 for CRFC). The intensity (in terms of SSI) is related to the local 98^{th} percentile of surface wind speeds (cf. Eq. 3.1). The spatial pattern of the local percentile shows strong land-sea-

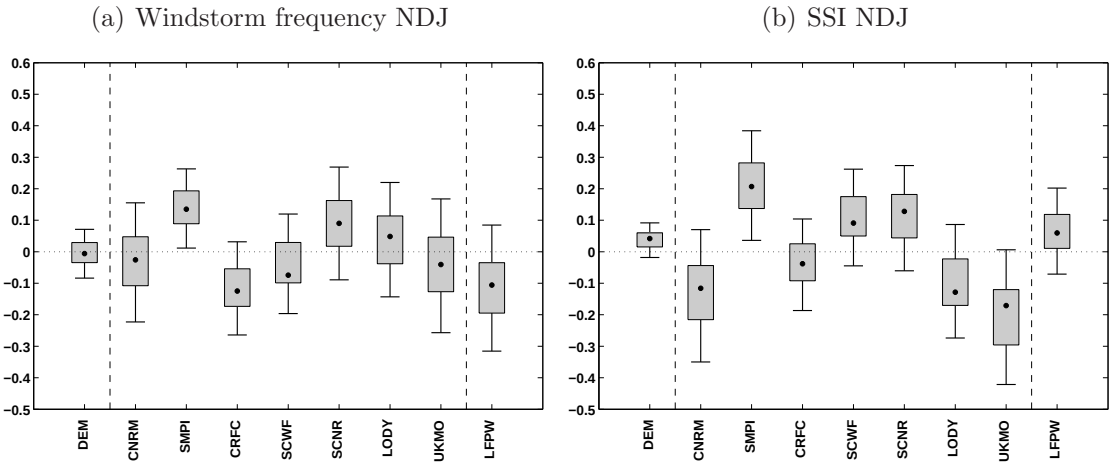

Figure 5.9: Predictive skill (RPSS) of the windstorm frequency DJF (a) and the accumulated Storm Severity Index NDJ (i.e., lead time of 3–6 months) for the 1980–2001 period in the LFPW single-model ensemble (right), the DEMETER single-model ensembles (center), and the DEMETER multi-model ensemble (left). The box (whiskers) indicates the 50% (90%) confidence interval based on a bootstrap method.

contrasts. Therefore, the SSI of an individual windstorm event is to some extent dependent on the particular track of the event. For example, SSI values are considerably increased if a windstorm hits land, since the local percentile is generally lower over land than over oceans. Thus, the successful prediction of intensity includes not only that of the existence of an event, but also its track. This seems to be beyond the capability of the seasonal prediction models. Whereas such an event definition might seem disadvantageous in terms of seasonal predictability, it is very reasonable from a risk management perspective. Still, the geographical dependance of the Storm Severity Index is a topic which should be further investigated but was beyond the scope of this thesis.

Similar to the November hindcasts, the August hindcast have been evaluated in terms of windstorm predictability. Successful predictions running from August to January would allow to forecast the upcoming windstorm season with up to five months forecast time. It has been shown in chapter 4 that various hemispheric-scale factors in summer and autumn are related to wintertime windstorm climate. Although these relations constitute potential predictability even on relatively long time scales, the skill scores are relatively low and generally not significant for both windstorm frequency and intensities (Fig. 5.9). This might be expected from the longer forecast time. Existing drifts of the prediction models towards their internal equilibrium are one reason for skill deterioration with increasing forecast times. However, the SMPI model attains statistically significant skill scores for both quantities (RPSS=13.5% for frequency, 20.7% for intensity). It will be shown in the next chapter that this might be related to the strong persistence of anomalies in the North Atlantic Ocean in this model.

Chapter 6

Sources of skill in seasonal prediction models forecasting North Atlantic and European wintertime windstorms

6.1 Rational

In the previous chapter, ensembles of seasonal hindcasts have been analyzed in terms of predictive skill to forecast the number of wintertime windstorms in the North Atlantic and European region (see also Renggli et al., 2011). Winter windstorm frequency (December–February and January–April) was shown to be successfully predicted in the November hindcasts of the multi-model and several single-model ensembles during the 1980–2001 period. However, the sources of skill in such prediction models, i.e., the factors modulating windstorm climate on seasonal time scales, and the related physical processes are not well understood. It is argued that inter-model differences in the reproduction of these processes explain the considerable performance differences of the individual models.

The inter-annual variability of wintertime windstorm occurrence in the North Atlantic region is argued to be modulated, and therefore (at least partially) explained, by the inter-annual variability of certain hemispheric-scale factors. Hence, possible sources of predictive skill to forecast windstorm in winter on the seasonal time scale could include anomalies of such factors in the summer and autumn. In chapter 4, statistically significant relations between such anomalies and windstorm occurrence over the North Atlantic and Europe in the subsequent winter have been found in observational and reanalysis data. It has been suggested that NAO-like atmospheric circulation in summer (JJA) favors the development of distinct anomalies in the North Atlantic SST (the so-called Horseshoe

pattern Cassou et al., 2004; Wang et al., 2004; Czaja and Frankignoul, 2002) in subsequent autumn (ASO, see upper part of Fig. 6.1). These anomalies have been shown to persist for several months and correspond to distinct anomalies of growth conditions of cyclones, for example, increased baroclinicity between Newfoundland and Europe, and moister air over the central North Atlantic, supporting the intensification of extra-tropical cyclones (Pinto et al., 2009). Since strong cyclones are regarded as the major source of severe windstorm events, such relations explain the physically motivated link between the hemispheric-scale factors in summer and autumn and windstorm occurrence in subsequent winter.

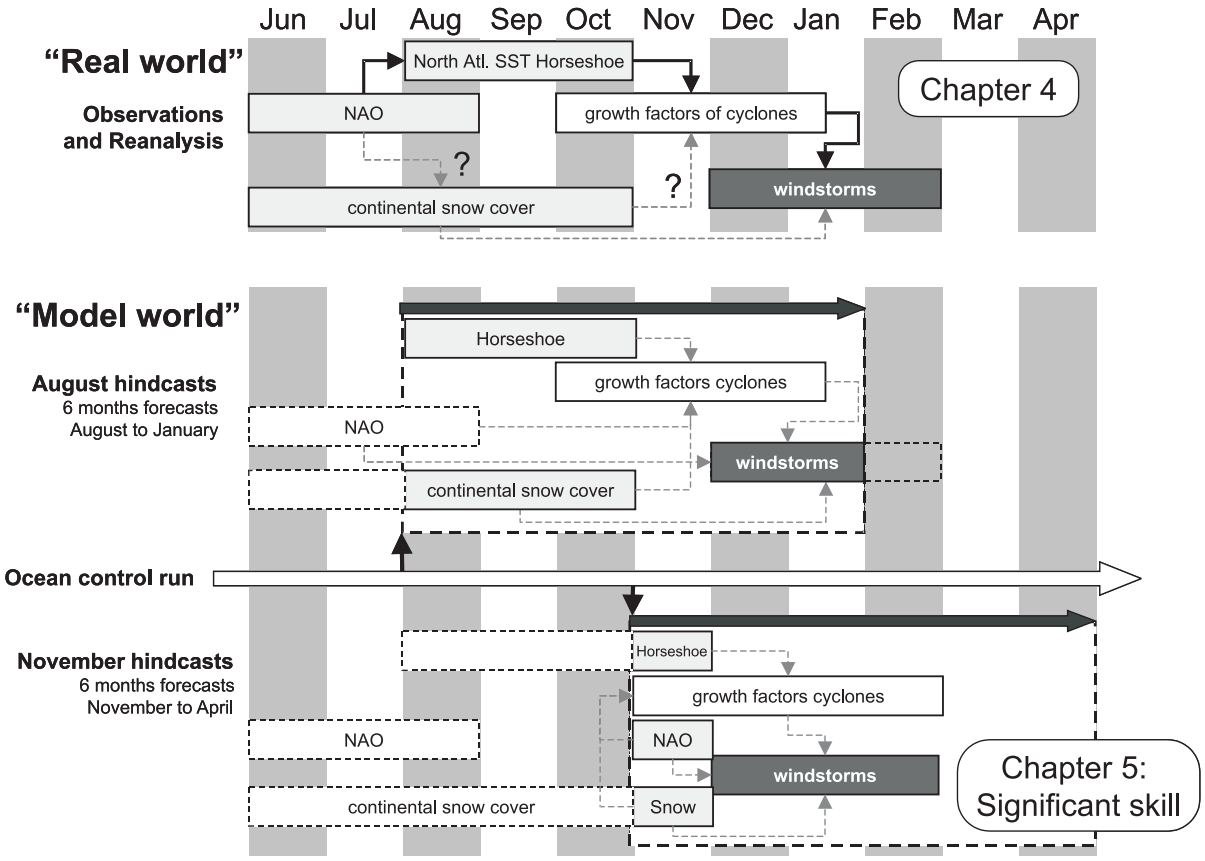

Figure 6.1: Illustration of the relations between hemispheric-scale factors (light gray boxes), growth factors of cyclones (white), and the occurrence of windstorms (dark gray) on seasonal timescales as revealed in observational and reanalysis data (top), and possible analogue relations in 6-months hindcasts of seasonal prediction models started on 1 August and on 1 November, respectively (see text for details).

Relationships like these become sources of skill if the corresponding physical mechanisms are accurately reproduced by dynamical prediction models. The reproduction in the models depends on the existence of anomalies of the hemispheric-scale factors in the initialization or their development in the course of the prediction run, and the feedback of the anomalies on the atmosphere. Differences in the reproduction between the models might help to explain differences in performance of the models as reported by Renggli

et al. (2011). For example, Shongwe et al. (2007) investigated the extent and persistence of snow cover in hindcasts of three different seasonal prediction models and their link to the predictability of spring temperatures in Europe. They found that models with better agreement between their snow predictions and observations show higher skill in predicting cold spring seasons. No study addressing similar mechanisms for winter storms was found in the published literature. Therefore, this study evaluates the relation between

- hemispheric-scale factors (namely, North Atlantic SST, NAO, and continental snow cover),
- growth factors of cyclones, and
- the occurrence of windstorms,

within *hindcasts of seasonal prediction model ensembles* of the DEMETER and ENSEMBLES projects. The employment of hindcasts allows to test whether the observed relations and mechanisms described in chapter 4 are also found in the prediction models, and to characterize differences between the individual models. However, the hindcast outline of the DEMETER and ENSEMBLES projects prevents the exact replication of the chapter 4 study. For example, the link of June–August NAO and snow cover to the windstorm climate in subsequent December–February cannot be analyzed completely similar in the August hindcasts (running from August to January central part of Fig. 6.1, dashed boxes). Therefore, the analysis of the August hindcasts focuses on the role of North Atlantic SST anomalies. Obviously, the impact of summer anomalies in hemispheric-scale factors cannot be analyzed in the November hindcasts (covering November to April), unless a signal is transported from summer to the November prediction within the ocean control run of the prediction models (Fig. 6.1, white arrow). Therefore, oceanic anomalies in the first month of the November hindcasts and their possible influence on windstorm occurrence during December–February are analyzed, together with anomalous states of the NAO and continental snow cover extent (Fig. 6.1, lower part).

Owing to the shortest period covered by the CRFC model in DEMETER (cf. Table 2.1), the analysis is restricted to the period 1980–2001. Furthermore, statistically significant skill has been found for this period. In addition to the seven DEMETER models, the ENSEMBLES contribution of Météo France (LFPW) is used in this study. This model was included since it has been shown to exhibit especially high predictive skill of the windstorm frequency in the North Atlantic and European region (Renggli et al., 2011).

This study tackles essentially four questions: Are the *modeled* hemispheric-scale factors related to the *modeled* occurrence of windstorms in seasonal predictions? Which role do growth factors of cyclones play in these relations? How do these relations compare to

reanalysis/observations and between the individual models? Are inter-model differences related to the skill of seasonal windstorm predictions?

This chapter is outlined as follows. The methods used in the study are described in sections 6.2. The relations between hemispheric-scale factors and windstorm occurrence in the August hindcasts are analyzed in section 6.3. The persistence of an oceanic signal from summer to the November hindcasts, the possible role of the NAO and snow cover and its link to predictability are discussed in section 6.4. Conclusions are presented in section 6.5.

In line with Renggli et al. (2011) and chapter 4, wintertime windstorm climate is analyzed in the following in terms of the number of windstorms occurring in the North Atlantic region (45°W–20°E, 45°–70°N) during a certain period (e.g., December–February) and termed windstorm frequency (e.g., DJF).

6.2 Methods

6.2.1 Hemispheric-scale factors

As in chapter 4, SST is used to calculate the so-called *North Atlantic Horseshoe index* (HSI), defined according Equation 4.2 in section 4.3.2, in each of the seasonal prediction models considered. The HSI computed from ERA-40 is used for validation. MSLP is used to compute the *NAO index* measuring the large-scale atmospheric circulation in the North Atlantic region, using an equivalent to the station-based NAO index (nearest grid points to Reykjavik and Azores) for the prediction models. The observed station-based NAO index (Hurrell, 1995) is used for comparison. To obtain an index of *snow cover extent* and for comparison with observational data, the gridded information of snow depth in the prediction models has to be converted into a scalar value of snow cover extent. Shongwe et al. (2007) used a simple threshold approach to calculate snow coverage for each grid for ERA-40 data. They defined a grid to be snow-covered on a given day if snow water equivalent is at least 3 mm, and 0 otherwise. This procedure resulted in encouraging agreement between observed and reanalyzed snow extent. Despite ERA-40 assimilates some snow observations (Uppala et al., 2005) it relies heavily on modeled snow precipitation and melt parameterizations. Therefore, the procedure proposed by Shongwe et al. (2007) was applied to the seasonal prediction model output. Snow coverage was set to 1 if the snow water equivalent on a given day was at least 3 mm, and 0 otherwise. Then, monthly snow concentration was computed by averaging daily snow coverage. Snow cover extent was computed by summing the grids of a continent, weighted by the monthly snow concentration and the area of a given grid. Modeled monthly mean values of snow cover extent (in km^2) defined by this procedure are shown together with corresponding

observations from the Rutgers University Global Snow Lab in Figure 6.2. In general, all models reproduce the sharp increase in observed snow cover extent from September to December and the slower decrease from February onwards. However, the models differ in the absolute numbers of snow-covered area. Most prominent is the overestimation of snow-covered area in March and April in the models of Météo France using ARPEGE as their atmospheric component (CNRM, CRFC, LFPW) and the two models using ECHAM5 as their atmospheric component (SMPI, SCNR). The root mean square error between observations and models range between 5.9% (LFPW) and 15.4% (UKMO) in the August hindcasts (solid lines in Fig. 6.2) and between 5.3% (LODY) and 16.6% (CNRM) in the November hindcasts (dashed lines in Fig. 6.2). The dependence of the inter-annual variability of continental snow cover extent on the threshold value used is very weak (not shown). In consistency with Shongwe et al. (2007) a threshold value of 3 mm was finally chosen for this study.

6.2.2 Composite analysis

To investigate possible physical mechanisms between HF and storm climate, a composite analysis is employed. For every HF, composites are constructed consisting of ensemble runs with strong anomalies during August–October. The positive composite consists of hindcast runs with anomalies above 1 standard deviation, the negative composite of hindcast runs with anomalies below -1 standard deviation. The difference between the mean of the positive and negative composite is interpreted as the (empirical) response for anomalous HF states. The composites are calculated for all available months and selected variables. Gridded anomalies of ocean heat content (TAV, where available), SST, EADY, EPT, and wintertime windstorm track density are considered. Besides the gridded anomalies, spatially aggregated anomalies are computed for both windstorm frequency (i.e., the number of windstorms occurring in the North Atlantic region) and the gridded variables (the averaged absolute anomaly in the North Atlantic region).

The statistical significance of the composite anomalies is estimated via a bootstrap method. Instead of selecting n (m) ensemble runs for the positive (negative) composite according the specific HF anomaly in these runs, the n (m) ensemble runs are randomly selected from the considered period. Then, the difference between the mean of the random positive and negative composite is calculated. This is repeated 1000 times. The significance of the true composite difference is then estimated from the resulting random difference distribution.

(a) Northern hemisphere

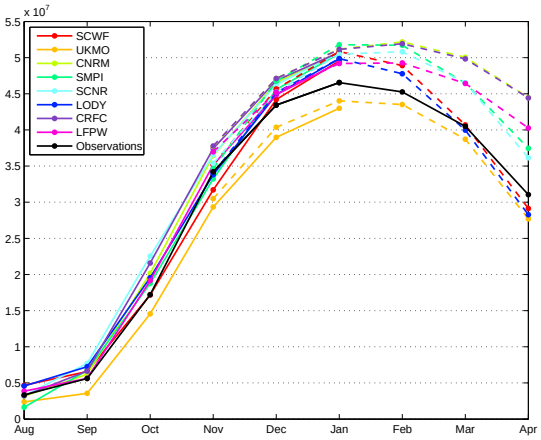

(b) Eurasia

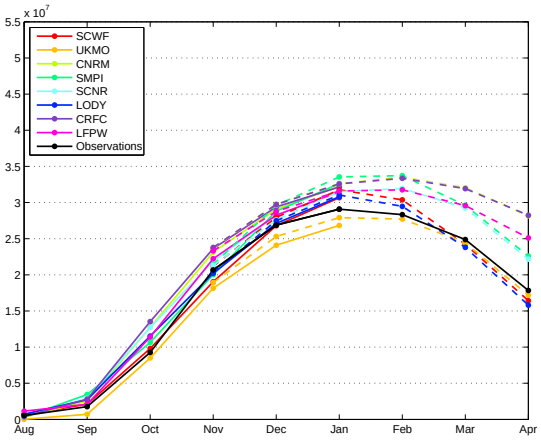

(c) North America

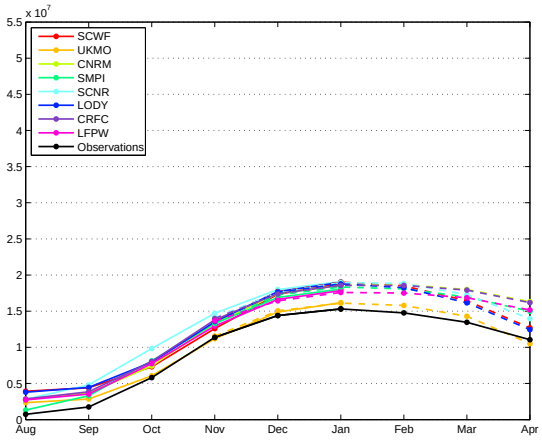

Figure 6.2: Averaged monthly snow cover extent over the entire northern hemisphere (a), Eurasian (b), and North American continent (c) in the August hindcasts (solid) and November hindcasts (dashed) in the eight seasonal prediction models; observed values (NSIDC) for comparison (black solid).

6.3 The relation of anomalous hemispheric-scale factors in summer to subsequent winter's windstorm occurrence

In observations and reanalysis data, statistically significant correlations have been found between between the state of certain hemispheric-scale factors and subsequent winter's windstorm occurrence. In particular, a physical consistent link between anomalous North Atlantic SST, growth factors of cyclones, and windstorm occurrence has been detected. In the following, these links are analyzed on the basis of the August hindcasts of the seasonal prediction models, covering the months from August to January. In addition to North Atlantic SST anomalies, the impacts of continental snow cover are briefly discussed.

6.3.1 North Atlantic SST Horseshoe

Analogously to chapter 4, Lead-Lag-Correlations (LLC) are considered between the Horseshoe-Index with different lead times and windstorm frequency during DJ. For clarity, correlations based on 3-monthly averages of HSI are shown. LLC based on monthly HSI are somewhat noisier but agree well with 3-monthly averages. In ERA-40, statistically significant correlations of about 0.45 have been found between the HSI during ASO and windstorm frequency during subsequent DJF. In contrast, the correlation coefficients in the seasonal prediction models are generally weak and attain significant values only for lead times shorter than two months (Fig. 6.3). The correlations are positive without a lag (i.e., the simultaneous correlation between HSI NDJ and windstorm frequency DJ) and statistically significant for six of the eight models. The weakening of correlations with longer lead times is in clear contrast to the relations between HSI and windstorms in winter as shown in ERA-40 (black line in Fig. 6.3). Thus, the relation between summer HSI and winter's storm occurrence is much weaker in the prediction models than in the reanalysis.

In order to quantify the sensitivity of European windstorm frequency on anomalous states of the North Atlantic SST in summer, composites of hindcast runs with anomalously high HSI (above 1 standard deviation) and anomalously low (below -1 standard deviation) HSI during ASO have been generated for each model. Then, the difference in windstorm frequency during DJ between high and low HSI composites was computed. In ERA-40, this difference in windstorm frequency (normalized by the inter-annual standard deviation) is +243.4% (Table 6.1, first row). Thus, the number of windstorms in the high HSI composite is more than two standard deviations higher than in the low HSI composite. In contrast, the sensitivity of windstorm climate on anomalous North Atlantic SST is weak in the prediction models. The composite difference is generally small and

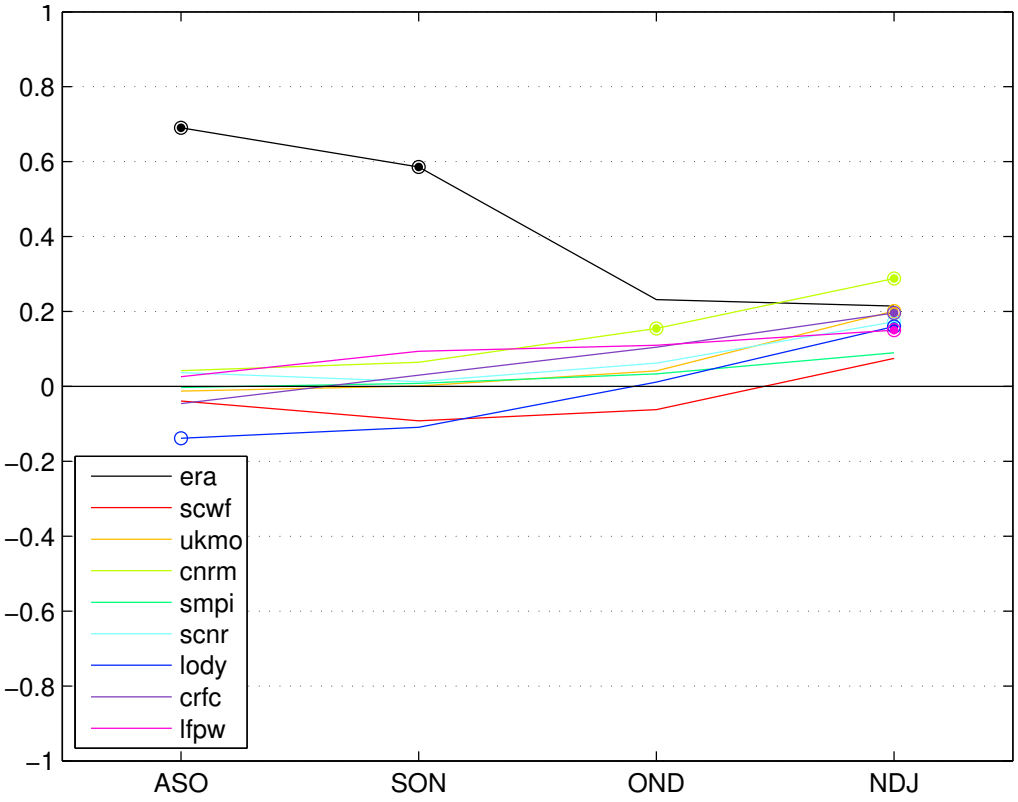

Figure 6.3: Spearman Lead-Lag-Correlation of 3-monthly averages of the North Atlantic SST Horseshoe- Index (HSI) with windstorm frequency during subsequent DJ for the 1980–2001 period in the August hindcasts of the seasonal prediction models (colored) and reanalysis for comparison (black). Dotted (circled) correlation coefficient are statistically significant with p< 0.10 (0.20).

	OBS	SCWF	UKMO	CNRM	SMPI	SCNR	LODY	CRFC	LFPW
HSI	**243.4**	–12.3	–22.1	8.4	–2.0	13.0	*–30.4*	–15.4	37.5
SCNH	–112.1	–9.1	**53.9**	**–38.9**	–9.2	24.4	*–30.0*	26.4	8.8
SCNA	–117.4	–9.4	–23.5	–20.7	13.3	**53.5**	**–44.8**	5.5	27.2
SCEU	18.4	22.3	**68.9**	15.2	0.7	–8.1	13.3	17.3	–24.3

Table 6.1: Difference of windstorm frequency DJ between composites of **August** hindcasts with strong positive and negative ASO anomalies in the North Atlantic Horseshoe pattern (HSI), and northern hemisphere (SCNH), North American (SCNA) and Eurasian (SCEU) continental snow cover extent (in % of inter-annual standard deviation) in the 1980–2001 period for the models, in the 1959–2001 period for ERA-40 HSI, and in the 1972–2001 period for observed snow cover. Significant differences (p< 0.1/p< 0.2) are highlighted (**bold**/*italic*).

not statistically significant (Table 6.1, first row). In the case of LODY, the difference is marginally significant ($p<0.2$), but with reversed sign compared to ERA-40. These findings are similar if based on the 3-monthly windstorm period NDJ.

The models' difficulties to reproduce the observed link between summer SST anomalies and windstorms in winter might be related to the tendency of seasonal prediction models to drift towards their own climatological mean state with increasing forecast time (e.g., Weisheimer et al., 2009; Hoskins and Schopf, 2008; Wallace and Hobbs, 2006). Therefore, the evolution of SST anomalies, growth factors of cyclones and resulting windstorms are analyzed in more detail. The same high and low composites are employed to analyze the temporal and spatial evolution of anomalies in SST, growth factors of cyclones and resulting windstorms occurrence. For brevity, the evolution of these anomalies is shown for the most extreme models only. An overview of the characteristics of all models is given later.

As a starting point, the evolution of the HSI in the positive and negative composite is exemplarily shown for three models (Fig. 6.4). Per definition, the HSI values are well separated between the positive and the negative composite during August–October. A tendency towards the climatological mean state (i.e., model drift) is visible after October in all models, although to a different degree. In SCNR, the average HSI values in the positive composites (thick red line in Fig. 6.4a) remain always one standard deviation above the mean state. At the end of the hindcast runs, the average HSI values of the two composites in SCNR and CRFC are still separated by about one standard deviation. In contrast, the mean anomaly of the negative HSI composite in UKMO has vanished almost completely (i.e., a mean anomaly of 0; Fig. 6.4c, thick blue line).

Hence, the seasonal prediction models differ in the persistence of the North Atlantic Horseshoe from summer through winter. This has potential impacts on the SST anomaly patterns, and anomalies of growth factors of cyclones related to these SST anomalies. Therefore, the temporal evolution of the spatial difference pattern between high and low HSI composites are analyzed for SST, ocean heat content, baroclinicity, latent heat, and windstorm track density. For comparability, the anomalies have been normalized with the local inter-annual standard deviation of a given variable. For brevity, results are presented for the two most extreme models in respect of the persistence of HSI, namely SCNR and UKMO (Fig. 6.4a and c).

In reanalysis data the North Atlantic Horseshoe pattern in SST has been shown to be persistent from summer to early winter. The Horseshoe is not only a surface feature, but also manifested in the ocean heat content (vertically averaged potential temperature in the topmost 300 m). Furthermore, the SST anomalies are related to corresponding anomalies in baroclinicity (e.g., in regions where SST anomalies increase the meridional temperature gradient) or latent heat (e.g., over warm SST anomalies). These anomalies

(a) SCNR

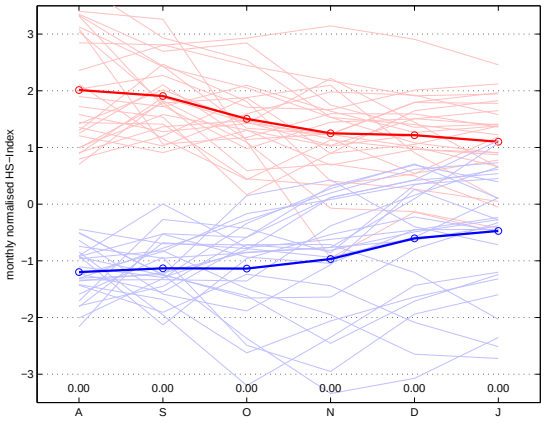

(b) CRFC

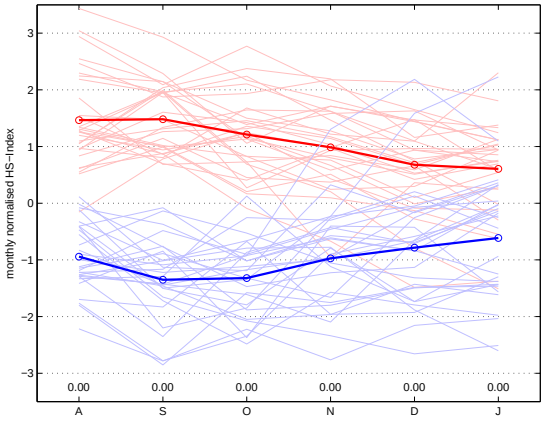

(c) UKMO

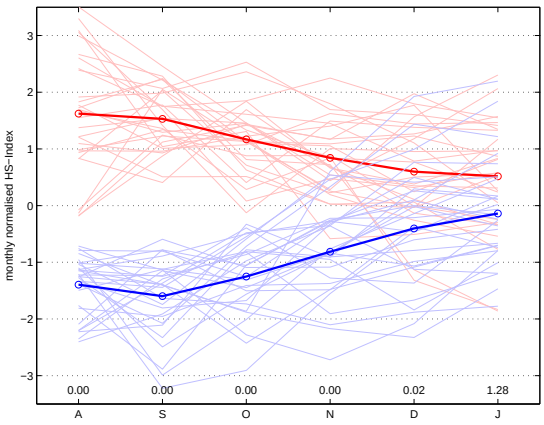

Figure 6.4: Evolution of the Horseshoe-Index (HSI) in composites of ensemble runs with strong positive (red) and negative (blue) anomalies during ASO in the August in SCNR (a), CRFC (b), and UKMO (c).

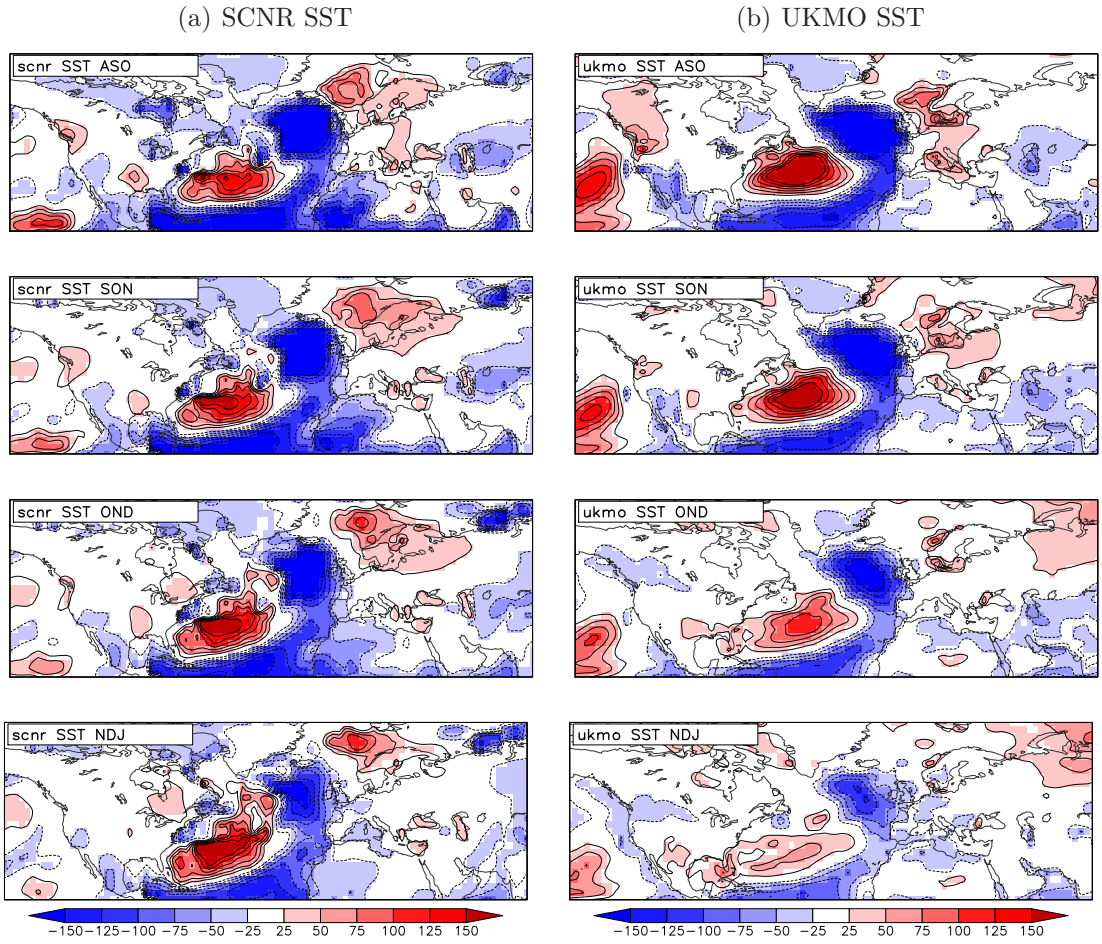

Figure 6.5: Difference of SST between composites with high and low HS-Index during ASO in the August hindcasts for 3-monthly means during ASO (first row), SON (second row), OND (third row), and NDJ (fourth row) in the SCNR (left) and UKMO model (right) in % of the local inter-annual standard deviation; statistically significant differences ($p < 0.10$) are shaded.

are consistent with better growth conditions for cyclones, and therefore with a potentially higher number of severe windstorms in the North Atlantic and European region.

Owing to the composite definition, the composite differences of SST during ASO in both considered prediction models show anomalies clearly resembling a Horseshoe pattern in the North Atlantic (Fig. 6.5), in consistency with Fig. 6.4. The anomalies exceed values of +150% in certain regions. The patterns in the models are reasonably consistent with the pattern derived from anomalous years in reanalysis data. For example, the spatial correlation coefficient in the North Atlantic region between the UKMO pattern during ASO (Fig. 6.5, top right) and ERA-40 is 0.82, and 0.75 for SCNR (Fig. 6.5, top left). However, a striking feature of the evolution of the SST anomaly pattern is its persistence. Whereas in SCNR the cold anomalies weaken only slightly from summer to winter and the warm anomaly even slightly strengthens (Fig. 6.5, left), the corresponding anomalies in UKMO strongly weaken after October. The anomalies in winter (NDJ) in

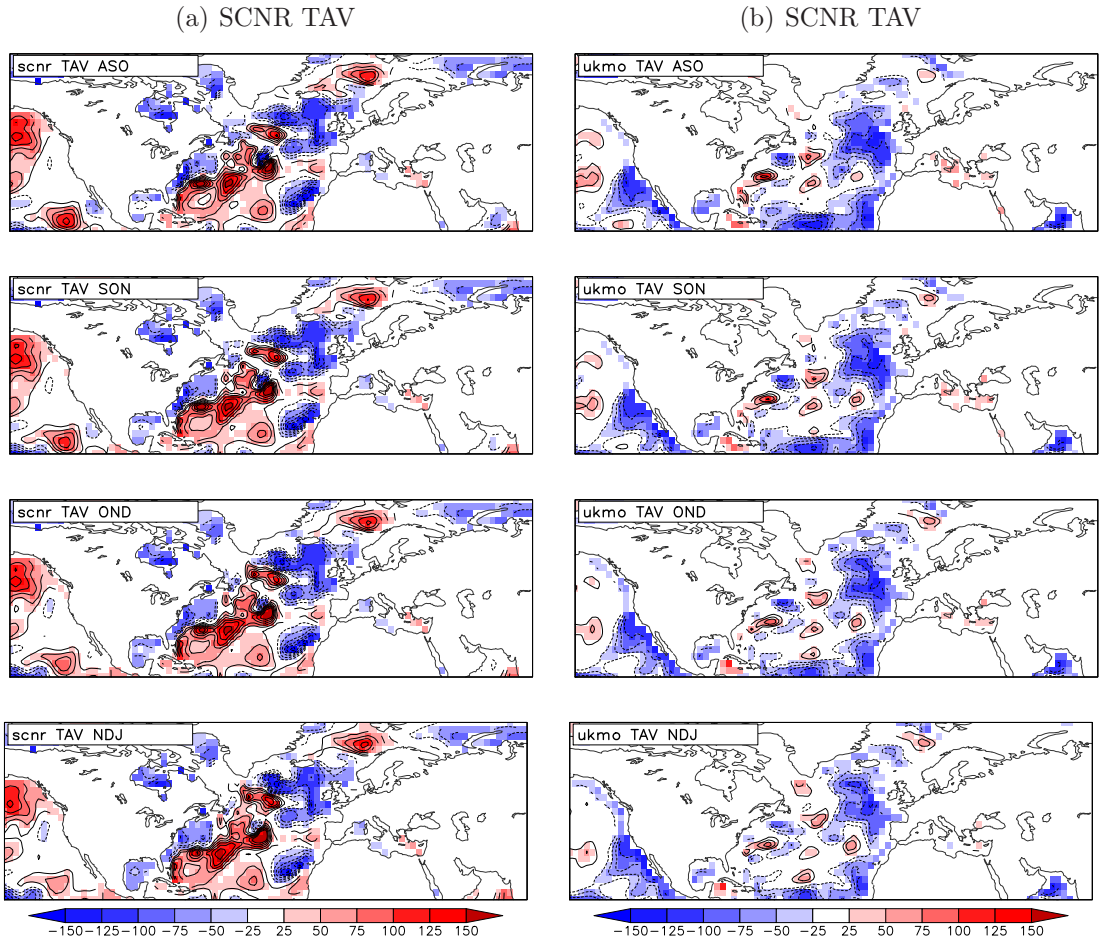

Figure 6.6: Difference of TAV between composites with high and low HS-Index during ASO in the August hindcasts for 3-monthly means during ASO (first row), SON (second row), OND (third row), and NDJ (fourth row) in the SCNR (left) and UKMO model (right) in % of the local inter-annual standard deviation; statistically significant differences ($p < 0.10$) are shaded.

SCNR still attain magnitudes of above 150%. In UKMO, especially the warm anomaly is substantially weakened (maximum anomalies about 50%). These differences in persistence points to dynamical differences between the models and might have severe impacts on the persistence of a potential signal leading to predictability in the forecast run.

Anomalies related to strong HSI anomalies are not only manifested at the ocean surface. Generally, the anomalies in vertically averaged ocean heat content in the uppermost 300 m (TAV, Fig. 6.6) agree well with the SST anomalies (Fig. 6.5). Most prominently, the northeastern cold SST anomaly corresponds to negative anomalies in TAV. The warm SST anomaly in the central North Atlantic is consistent with a warmer ocean, although more pronounced in SCNR than in UKMO. In contrast, the southern cold SST anomaly in UKMO is consistent with corresponding anomalies in TAV, and less obvious in SCNR. The magnitude of the anomalies is generally higher in SCNR than in UKMO.

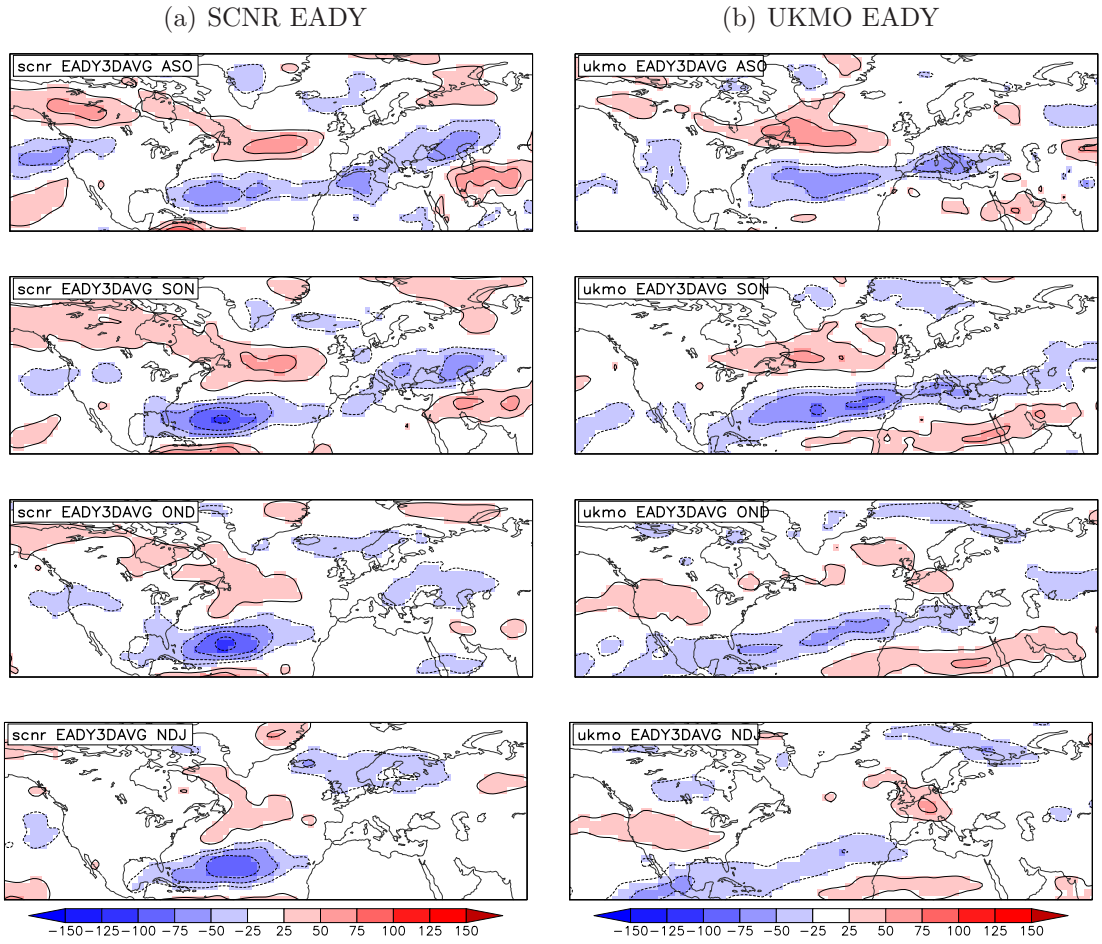

Figure 6.7: Difference of EADY between composites with high and low HS-Index during ASO in the August hindcasts for 3-monthly means during ASO (first row), SON (second row), OND (third row), and NDJ (fourth row) in the SCNR (left) and UKMO model (right) in % of the local inter-annual standard deviation; statistically significant differences ($p < 0.10$) are shaded.

The corresponding composite difference patterns of baroclinicity (Fig. 6.7) show a clear tendency towards positive anomalies in areas where the zonal SST gradient is increased (i.e., warm anomalies to the south, cold anomalies to the north), especially if the underlying SST anomalies are strong. Thus, the models support the findings from reanalysis data (compare with 4.4.2) and model studies (Cassou et al., 2004) showing baroclinicity to be related to SST anomalies. Whereas SCNR (the model with persistent SST anomalies) shows enhanced baroclinicity over the central North Atlantic between Newfoundland and Western Europe from late summer to winter, these anomalies fade earlier in UKMO. This is consistent with the weakening SST anomalies (cf. Fig. 6.5). Similarly, positive (negative) anomalies of latent heat (EPT) prevail over regions of warm (cold) SST anomalies (Fig. 6.8). Again, these anomalies are more persistent in SCNR. In UKMO, especially the northern cold anomaly and the warm anomaly over the Central North Atlantic almost vanish.

(a) SCNR EPT (b) UKMO EPT

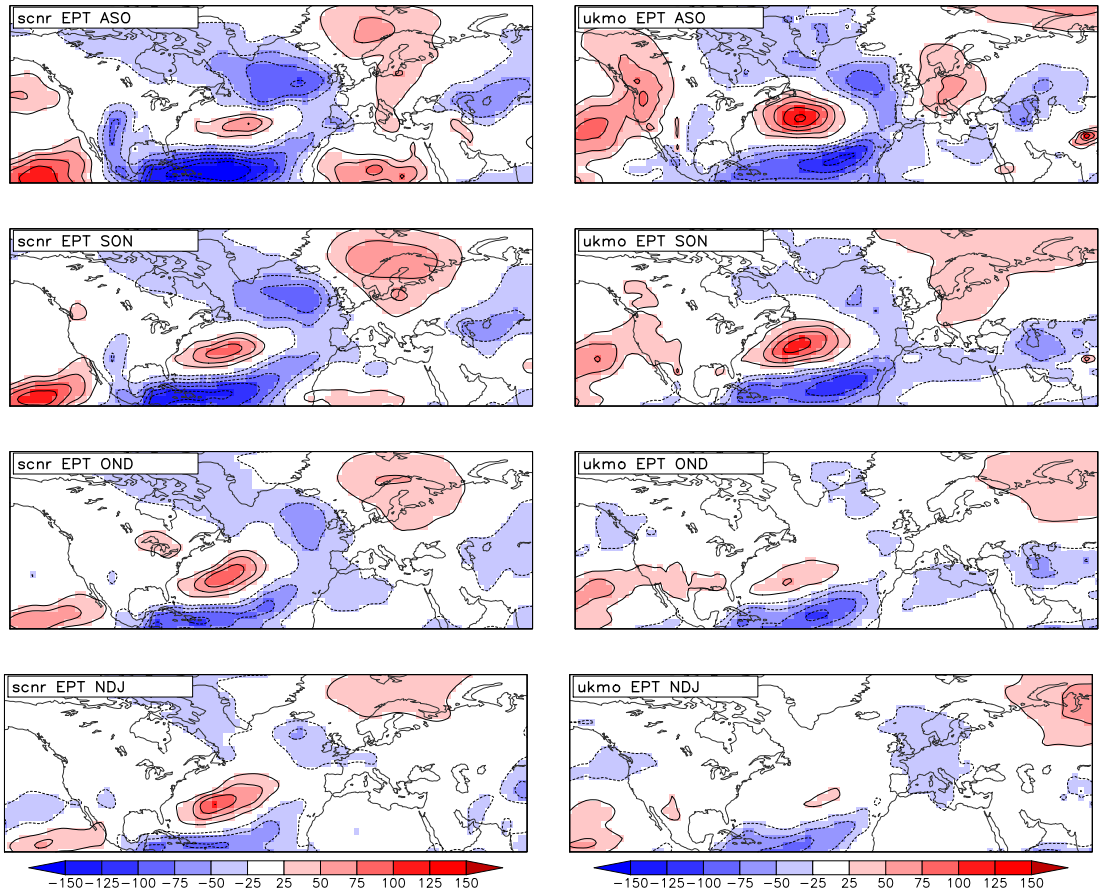

Figure 6.8: Difference of EPT between composites with high and low HS-Index during ASO in the August hindcasts for 3-monthly means during ASO (first row), SON (second row), OND (third row), and NDJ (fourth row) in the SCNR (left) and UKMO model (right) in % of the local inter-annual standard deviation; statistically significant differences ($p < 0.10$) are shaded.

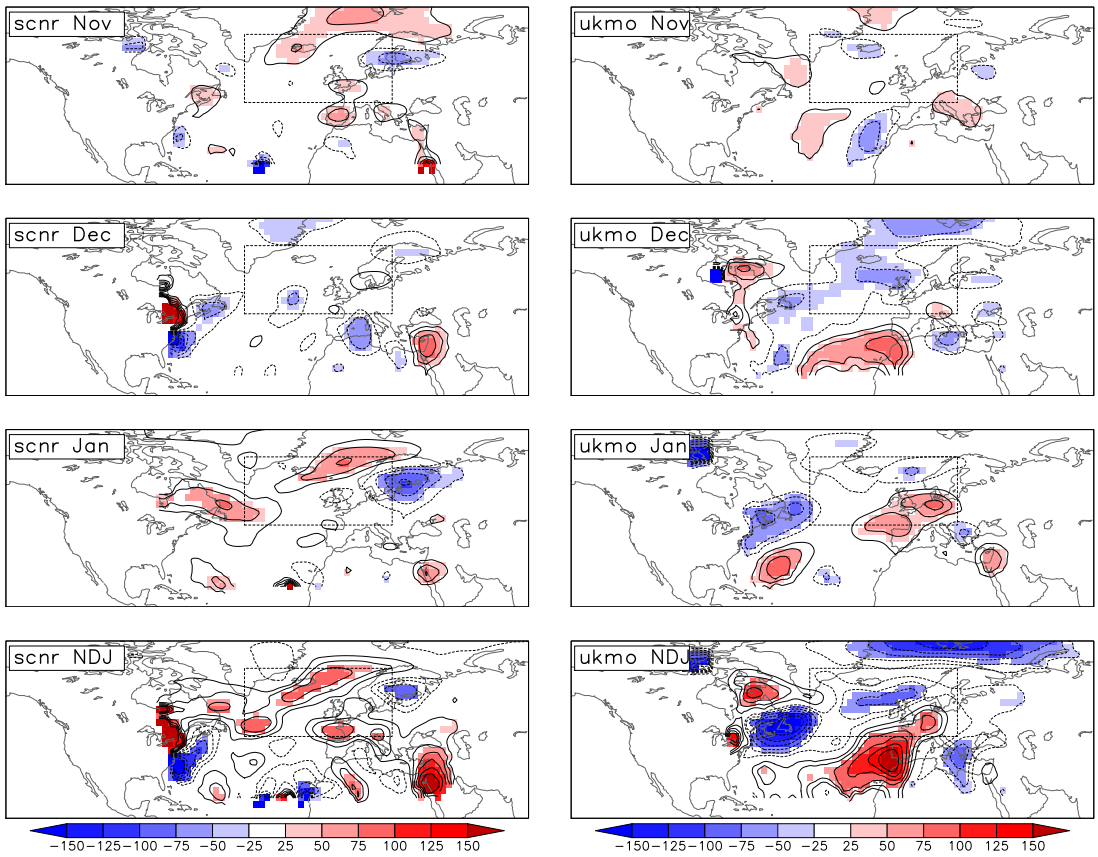

Figure 6.9: Difference of windstorm track density between composites with high and low HS-Index during ASO in the August hindcasts for 3-monthly means during ASO (first row), SON (second row), OND (third row), and NDJ (fourth row) in the SCNR (left) and UKMO model (right) in % of the local inter-annual standard deviation; statistically significant differences ($p < 0.10$) are shaded.

Consequently, there is a tendency towards more wintertime windstorms in August hindcasts of SCNR with a strong positive Horseshoe pattern during ASO than in ensemble runs with a negative Horseshoe pattern. The track density is locally enhanced over the northern North Atlantic and Western Europe (Fig. 6.9, left). Note the consistence with a higher number of wintertime windstorms in the North Atlantic region (cf. Table 6.1, first row). In contrast, the corresponding track density anomaly pattern in UKMO shows negative anomalies spanning the North Atlantic from Newfoundland to Scandinavia, and strong positive anomalies especially around Iberia (consistent with a lower windstorm frequency in ensemble runs with strong positive HSI; Table 6.1, first row).

To summarize the characteristics of all prediction models, the spatially averaged absolute anomaly over all grid points in the North Atlantic and European region (90°W–40°E, 15°N–80°N) was computed for every month of the August hindcasts (Fig. 6.10). For comparison, the same numbers have been computed for the reanalysis. The more the composites differ from the mean climate state in the model (i.e., the stronger the shad-

(a) SST

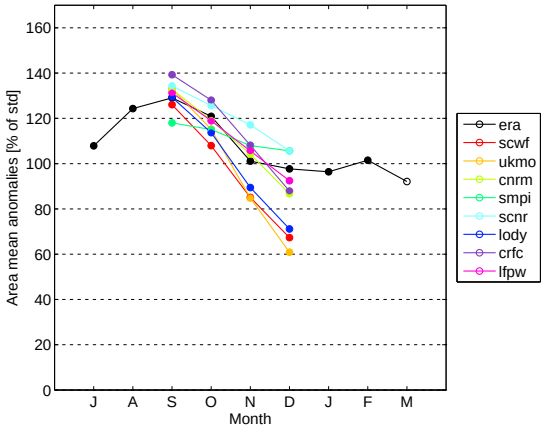

(b) EADY

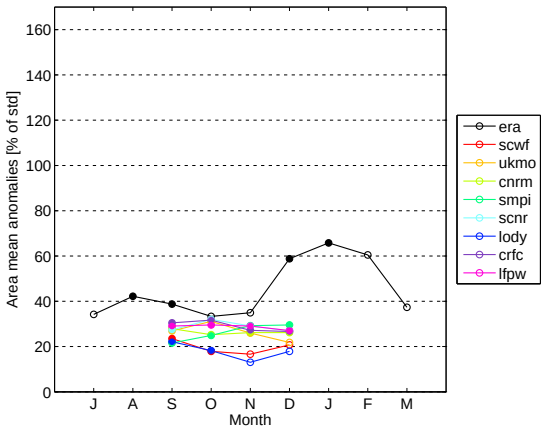

(c) TAV

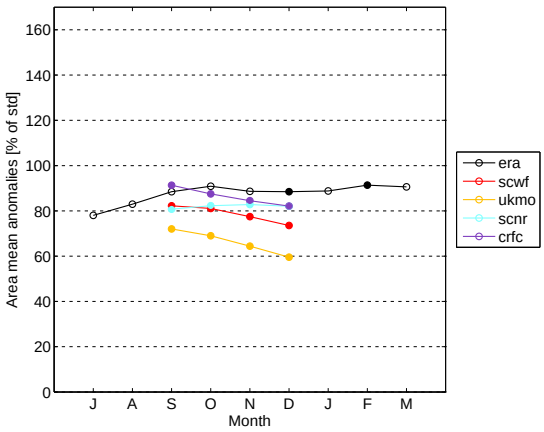

Figure 6.10: Averaged absolute anomalies (3-monthly means and averaged over the North Atlantic region) between HSI ASO composites in August hindcasts of the seasonal prediction models (colored) for SST (a), EADY (b), and TAV (c), with ERA-40 for comparison (black). Dotted magnitudes are significantly ($p < 0.10$) different from the 1000 random samples.

ings in Figs. 6.5 to 6.9) the higher the averaged absolute anomaly. In contrast, low values of the averaged absolute anomaly indicate low deviations from the mean climate state.

Per definition, the averaged absolute anomalies for SST are strongest during ASO and agree generally well between the models and reanalysis (Fig. 6.10a): The values of the models spread around the value of the reanalysis (130%) in a range between 120 and 140% (of the inter-annual standard variability). Note the spatial correlation of the anomaly patterns in the reanalysis and the models range between 0.70 and 0.85 (not shown). Thus, Horseshoe-like SST anomalies in autumn are present in all models. With increasing forecast time the averaged anomalies weaken. For example, the magnitude is weakening by about 15% in SMPI, 27% in SCNR, but 70% in UKMO, consistent with Figure 6.5. The spatially averaged anomalies of EADY in the models (roughly 20–30%) do not reach the levels of ERA-40 (about 30–60%; Fig. 6.10b). This fact indicates an underestimation of the ocean-atmosphere coupling in the models. However, models with relatively strong SST anomalies during NDJ (SCNR, SMPI, LFPW, CRFC, CNRM) tend to have stronger anomalies in EADY in the same period than the other models (SCWF, LODY, UKMO). The anomalies of TAV weaken only slowly (Fig. 6.10c), and are in general agreement with the SST anomaly magnitudes. Whereas CRFC retains anomalies in the range of the ORA reanalysis, UKMO has consistently weaker anomalies throughout the August hindcast.

In conclusion, we have shown that the evolution of the ocean and atmosphere in ensemble runs of anomalous SST conditions in summer can be linked with distinct anomalies in growth factors of windstorms. First of all, anomaly patterns in SST are accompanied by corresponding anomalies in baroclinicity and latent heat (and, to some degree, also to anomalies in windstorm frequency and track density; Fig. 6.9, Table 6.1, first row). Second, there are differences particularly in the persistence of SST anomalies. Models with high persistence tend to retain stronger anomalies also in the atmosphere. The persistence of SST anomalies is possibly linked to that of the ocean heat content. Note that the SMPI model shows the strongest persistence of the Horseshoe anomalies within the August hindcasts (Fig. 6.9). It has been shown in section 5.7 that this model also attains statistically significant skill scores in predicting windstorm frequency and intensity within the August hindcasts. It has not been further analyzed whether this particular high persistence is related to the different initialization method used for the SMPI model.

6.3.2 Continental snow cover extent

In addition to anomalies in North Atlantic SST, continental snow cover extent was considered as another potential source of windstorm predictability (Fig. 6.1). Basically, the same metrics applied for North Atlantic Horseshoe anomalies have been used for compos-

ites of hindcast runs with anomalous high and low snow cover on the continents of the northern hemisphere. These are briefly discussed in the following.

With respect to differences in the number of European windstorms there are significant differences between composites of ensemble runs with strong snow cover anomalies. However, there are both models with statistically significant positive and significant negative signals. Hence, the models do not agree on the polarity of the snow signal (Table 6.1).

For example, CNRM windstorm frequency shows significant negative sensitivity to northern hemisphere snow cover (i.e., low snow cover corresponds to high windstorm frequency). This is in agreement with the observed relations. On the contrary, the same relation is reversed in UKMO. Furthermore, SCNR and LODY show significant windstorm sensitivity to North American snow cover, but with opposite sign. This might be related to subtle difference in the climatology of snow coverage in the different models. Composites of strong anomalies in North American snow cover reveal that these anomalies occur predominantly over the eastern (western) parts of the continent in SCNR (LODY, not shown). Negative snow cover anomalies along the east coast of North America lead to positive anomalies in surface temperature and EPT, i.e., the temperature contrast to the warmer ocean is reduced. This is than related to lower baroclinicity over the region, and hence a lower potential for wave disturbances to grow in the entrance region of the North Atlantic storm track in SCNR. In contrast, snow cover anomalies reveal a dipole of strong negative anomalies on the west coast of the North American continent, but (weaker) positive anomalies along the eastern coast in LODY. In analogy to the aforementioned, this leads to an increased temperature contrast between continent and ocean, increased baroclinicity, better growth conditions and subsequently more frequent storms in the North Atlantic and European region.

6.4 Sources of predictive skill in forecasting winter-time windstorm occurrence

Three of the seasonal prediction models considered in this study were shown to attain statistically significant levels of skill in predicting mean winter windstorm frequency (DJF) in the November hindcasts (chapter 5, and Renggli et al., 2011). Anomalies in the North Atlantic ocean constitute one possible source of predictability for the November predictions. Such anomalies could be generated in summer and preserved in the ocean control run through November, and influence the windstorm occurrence in the subsequent winter. Additionally, the state of the large-scale atmospheric flow (i.e., the NAO) and continental snow cover at the initialization could serve as sources of predictability of windstorm occurrence in the prediction models. Therefore, the persistence of the Horseshoe pattern from

August to November hindcasts is analyzed in the following. In order to explain predictive skill in the seasonal forecast models, the state of the NAO and continental snow cover extent in the initialization months of the November hindcasts are taken into account as potential sources of predictive skill of windstorm occurrence.

6.4.1 Persistence of North Atlantic Horseshoe anomalies from summer to winter

The persistence of a North Atlantic Horseshoe anomaly in the August hindcasts was shown to differ considerably between the different models (Fig. 6.10). A crucial question with respect to predictive skill in the November hindcasts is whether these hindcasts also differ in the persistence of an oceanic anomaly from summer to November? Therefore, composites of the November hindcast are generated on the basis of the runs in the August composite. In other words, if a given hindcast run had an anomalous Horseshoe anomaly in the August hindcast, it is also part of the respective composites of the November hindcasts. In this way it can be analyzed to what extent the Horseshoe anomaly is still present in the subsequent November hindcast.

The initial state of the Horseshoe-Index and its evolution in the November hindcast shows considerable differences between the models (Fig. 6.11). The two composites are well separated in SCNR from November to January. From February to April, the composites do not differ significantly from each other anymore (Fig. 6.11a). The separation into the two composites is most stable in CRFC. The separation between the two composites remains statistically highly significant ($p<0.01$) over the entire November hindcast (Fig. 6.11b). In contrast, the two composites are nearly indistinguishable from each other in the UKMO model ($p>0.13$) in the November hindcasts (Fig. 6.11c). Thus, whereas the Horseshoe anomaly is preserved to some extent in the November hindcast of CRFC and SCNR, this information is completely lost in the UKMO model. These differences are further analyzed in terms of the temporal evolution of the spatial anomaly patterns in the following. Interestingly, HSI values of the positive composite are increasing from November to December (most clearly visible in SCNR, to a lesser degree also in the two other models in Fig. 6.11).

As expected from the previous findings, an SST pattern similar to the Horseshoe is retained in CRFC during November, and persistent until February (Fig. 6.12, center). The anomaly pattern in SCNR still has some similarity with the Horseshoe pattern, especially the cold anomaly regions in the northeastern and southern North Atlantic, respectively (Fig. 6.12, top). In UKMO, the anomalies are generally weaker, and the warm anomaly region is shifted to the east and cut off from another warm anomaly over southern US and the Gulf of Mexico. In contrast to the other two models, the anomalies

(a) SCNR

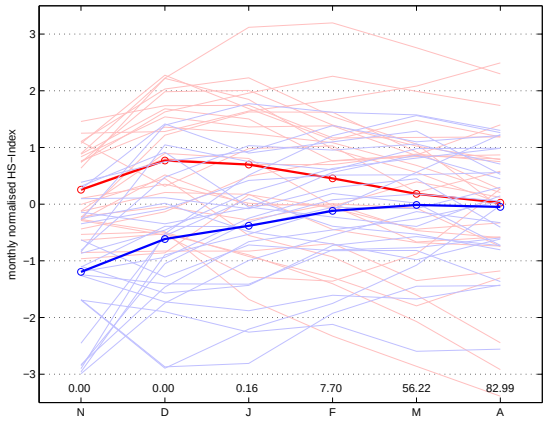

(b) CRFC

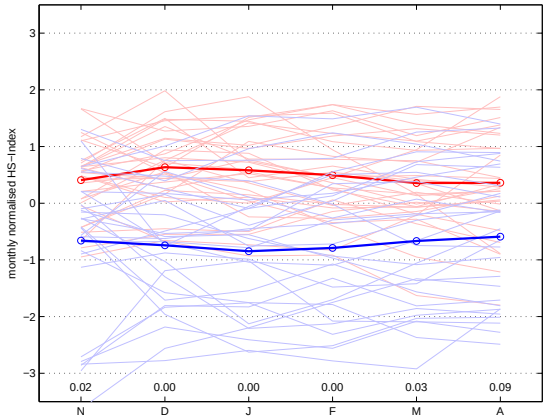

(c) UKMO

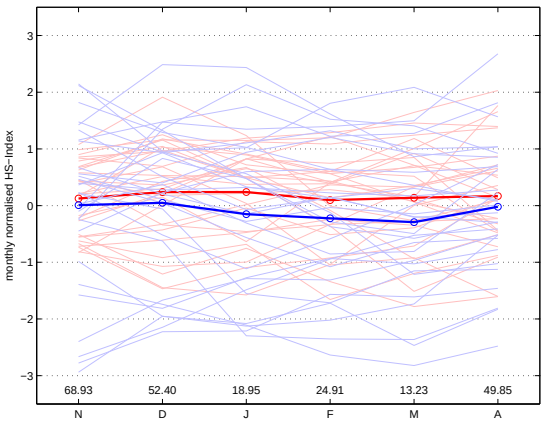

Figure 6.11: Evolution of the Horseshoe-Index in composites of ensemble runs in the November hindcasts with strong positive (red) and negative (blue) anomalies during ASO in the previous August hindcasts in SCNR (top), CRFC (center), and UKMO (bottom).

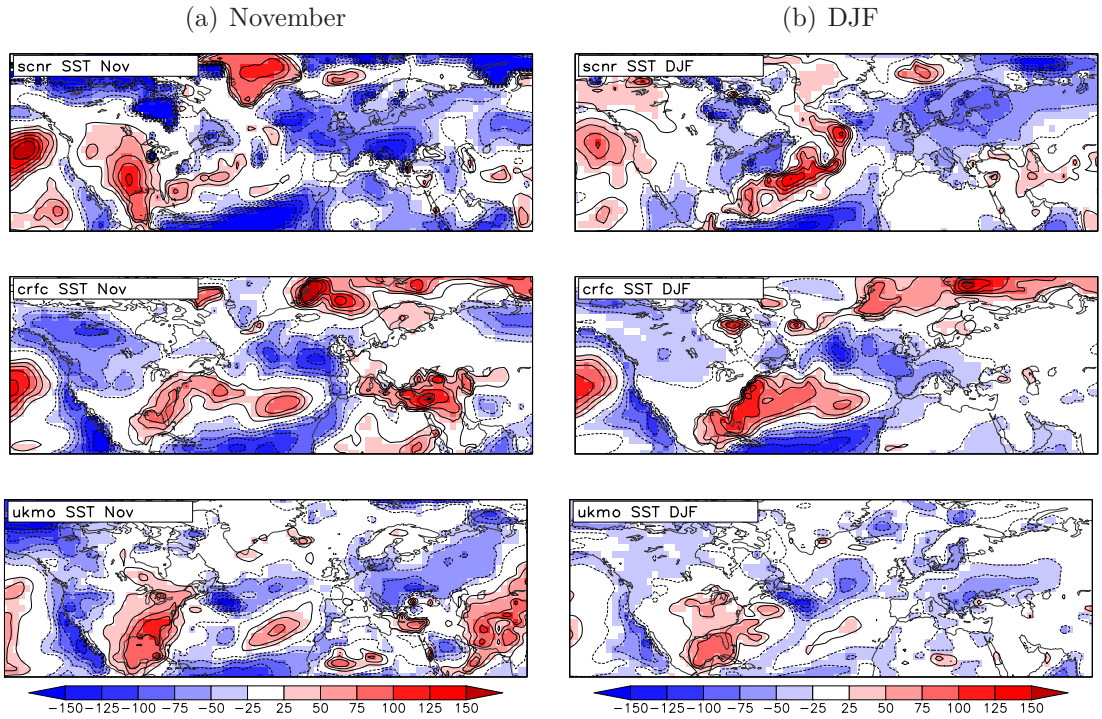

Figure 6.12: Difference of SST in November hindcast data between composites with high and low HS-Index during ASO in the previous August hindcasts for November (a) and DJF (b) in SCNR (top), CRFC (center), and UKMO (bottom) in % of the local inter-annual standard deviation; statistically significant differences ($p < 0.10$) are shaded.

weaken until February (Fig. 6.12, bottom). Again, the anomalies in TAV agree with the SST anomalies (Fig. 6.13). Additionally, the EADY anomaly patterns are consistent with the SST anomalies (Figs. 6.14). In UKMO, the baroclinicity is decreased between Newfoundland and Europe during November whereas these anomalies are very weak in SCNR. In contrast, increased baroclinicity (local anomalies above 75%) prevail over the Central North Atlantic in CRFC. These conditions change during December–February. Whereas baroclinic conditions prevail over Newfoundland and (weaker) over the North Atlantic in CRFC, the region of enhanced baroclinicity is shifted southward in SCNR (in agreement with the strengthening of the warm SST anomaly, cf. Fig. 6.12). As noted before, the anomalies are generally weaker in UKMO, but positive anomalies occur over the northeast coast of North America and Western Europe. Additionally, the EPT anomalies correspond well to the underlying SST anomalies (Fig. 6.15). In all three models, positive anomalies prevail over the Gulf of Mexico. In SCNR and CRFC, these anomalies are elongated to the northeast.

Corresponding anomalies are also found for windstorm track density (Fig. 6.16). Track density is increased in all models (consistent with Table 6.3, first row) even if the anomaly patterns differ between the models.

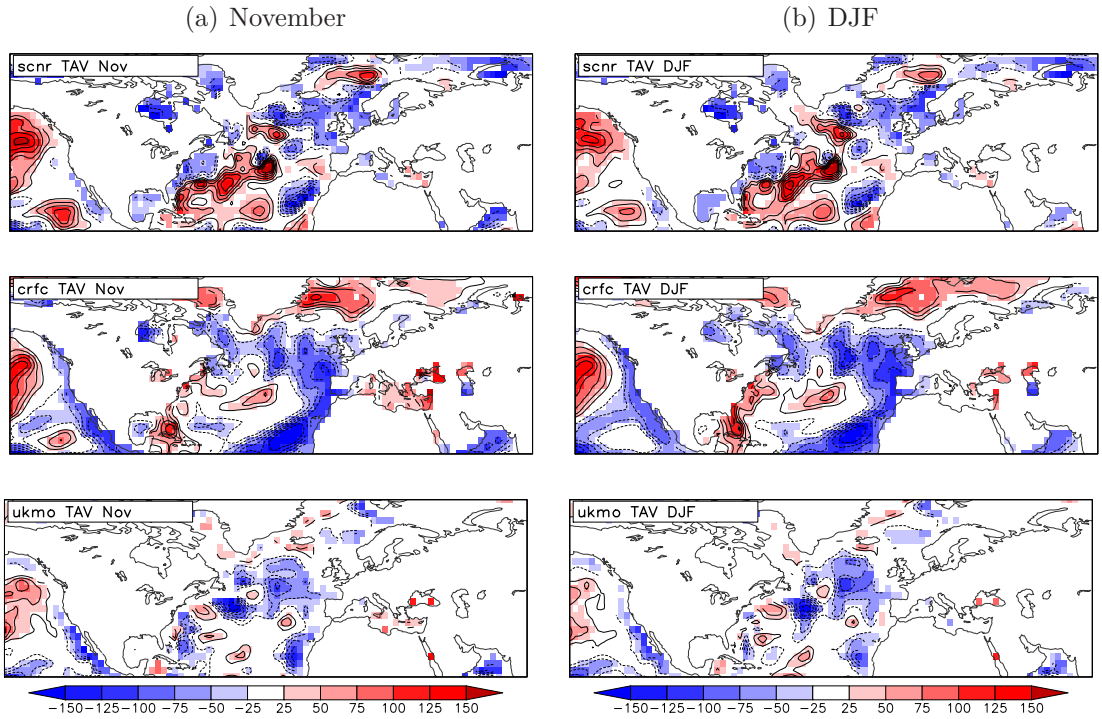

Figure 6.13: Difference of TAV in November hindcast data between composites with high and low HS-Index during ASO in the previous August hindcasts for November (a) and DJF (b) in SCNR (top), CRFC (center), and UKMO (bottom) in % of the local inter-annual standard deviation; statistically significant differences ($p < 0.10$) are shaded.

Analogously to the August hindcasts, the averaged absolute anomaly was also computed for the November hindcasts in order to summarize and compare the characteristics the prediction models (Fig. 6.17). As expected from Figures 6.5 and 6.12, both CRFC and SCNR show high magnitudes in SST during NDJ of the November hindcasts (together with LFPW) compared to the other models (Fig. 6.17a). In contrast, the anomalis are very low in UKMO. This is also reflected in low anomaly magnitudes for EADY (Fig. 6.17b). Strikingly, none of the models is able to reproduce the sharp increase in EADY anomalies found in the reanalysis (reminiscent of winters with anomalous windstorm frequency following anomalous HSI during ASO). Most notably, the average absolute anomaly of TAV in the four models with data of the ocean sub-surface differ considerably (Fig. 6.17c). Whereas the magnitude of the ocean heat content anomalies in CRFC is close to that in ORA, UKMO is about 40% lower. In consistency with Figures 6.6 and 6.13, the signal of an anomalous summer ocean state is much more preserved in the CRFC model than in UKMO.

The differences in windstorm frequency during DJF in the two composites are especially revealing: All models consistently show a positive signal of windstorm frequency in ensemble runs of anomalous HSI in the previous summer, in agreement with the relation found in reanalysis data (Table 6.2, third row). This signal is statistically significant for

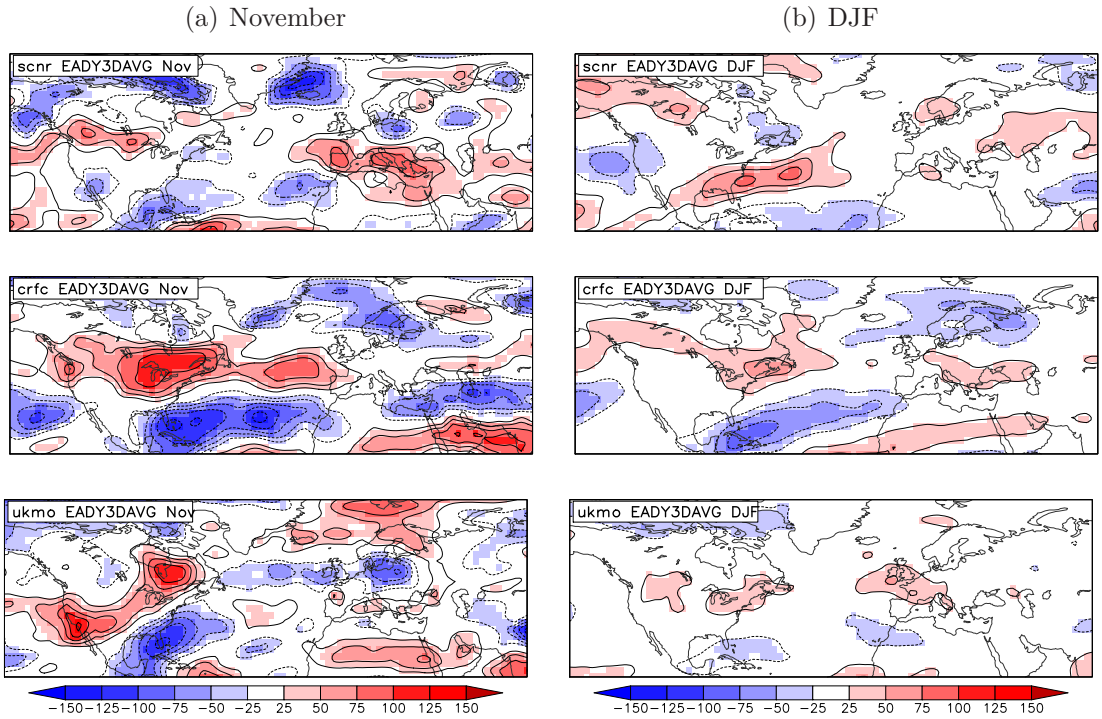

Figure 6.14: Difference of EADY in November hindcast data between composites with high and low HS-Index during ASO in the previous August hindcasts for November (a) and DJF (b) in SCNR (top), CRFC (center), and UKMO (bottom) in % of the local inter-annual standard deviation; statistically significant differences ($p < 0.10$) are shaded.

	ERA	SCWF	UKMO	CNRM	SMPI	SCNR	LODY	CRFC	LFPW
HSI	**236.5**	**47.4**	*37.3*	11.8	**52.6**	15.5	29.8	**50**.9	**58.7**

Table 6.2: Difference of windstorm frequency DJF between composites of **November** hindcasts with strong positive and negative ASO anomalies in the North Atlantic Horseshoe pattern in the preceding **August** hindcasts (in % of inter-annual standard deviation) in the 1980–2001 period for the models, and in the 1959–2001 period for ERA-40 HSI. Significant differences ($p < 0.1$/$p < 0.2$) are highlighted (**bold**/*italic*).

five of the eight models, and largest in the LFPW, CRFC and SCWF models. These findings are also consistent with the windstorm track density anomalies in Figure 6.16.

The signal in the number of windstorms is generally similar if composites of anomalous Horseshoe-Index values during November are considered (i.e., the initialization months of the November hindcasts): it is positive in all models except CNRM, and statistically significant for four of the eight models (SCNR, LODY, CRFC, LFPW; cf. Table 6.3).

Thus, differences in the persistence of oceanic anomalies are also found in the November hindcasts following summers with anomalous Horseshoe indices. The higher the preserved anomalies in the ocean are, the higher the potential influence on growth conditions of cyclones, and therefore the occurrence of severe windstorms. Consequences on predictability are further discussed in section 6.4.3.

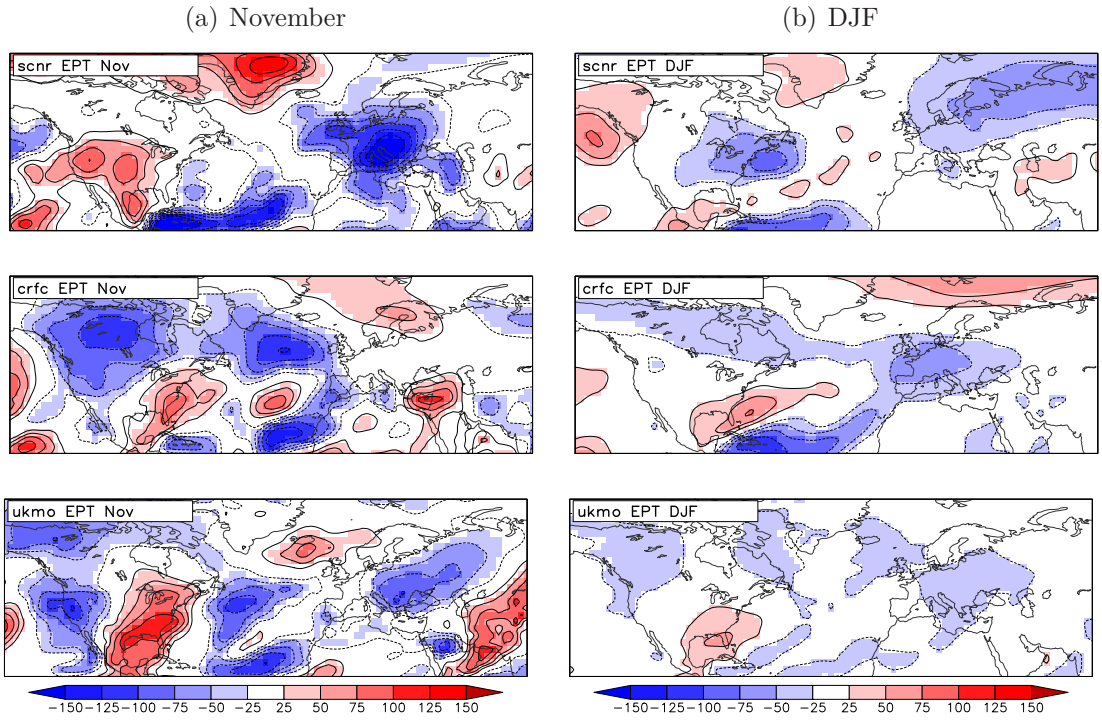

Figure 6.15: Difference of EPT in November hindcast data between composites with high and low HS-Index during ASO in the previous August hindcasts for November (a) and DJF (b) in SCNR (top), CRFC (center), and UKMO (bottom) in % of the local inter-annual standard deviation; statistically significant differences ($p < 0.10$) are shaded.

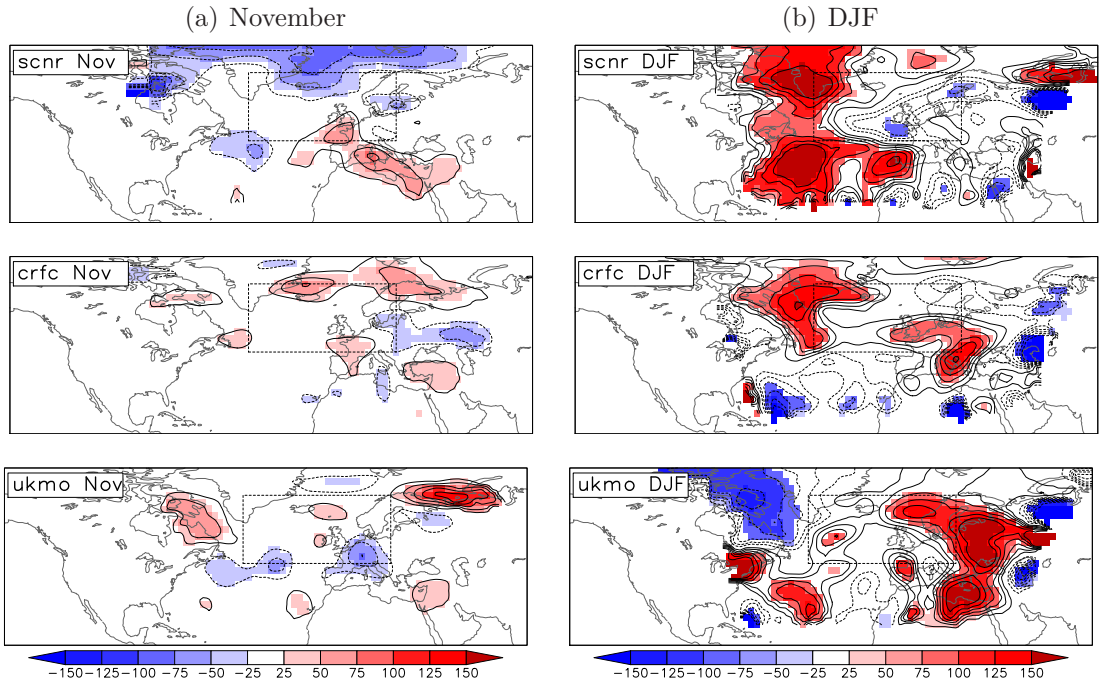

Figure 6.16: Difference of windstorm track density in November hindcast data between composites with high and low HS-Index during ASO in the previous August hindcasts for November (a) and DJF (b) in SCNR (top), CRFC (center), and UKMO (bottom) in % of the local inter-annual standard deviation; statistically significant differences ($p < 0.10$) are shaded.

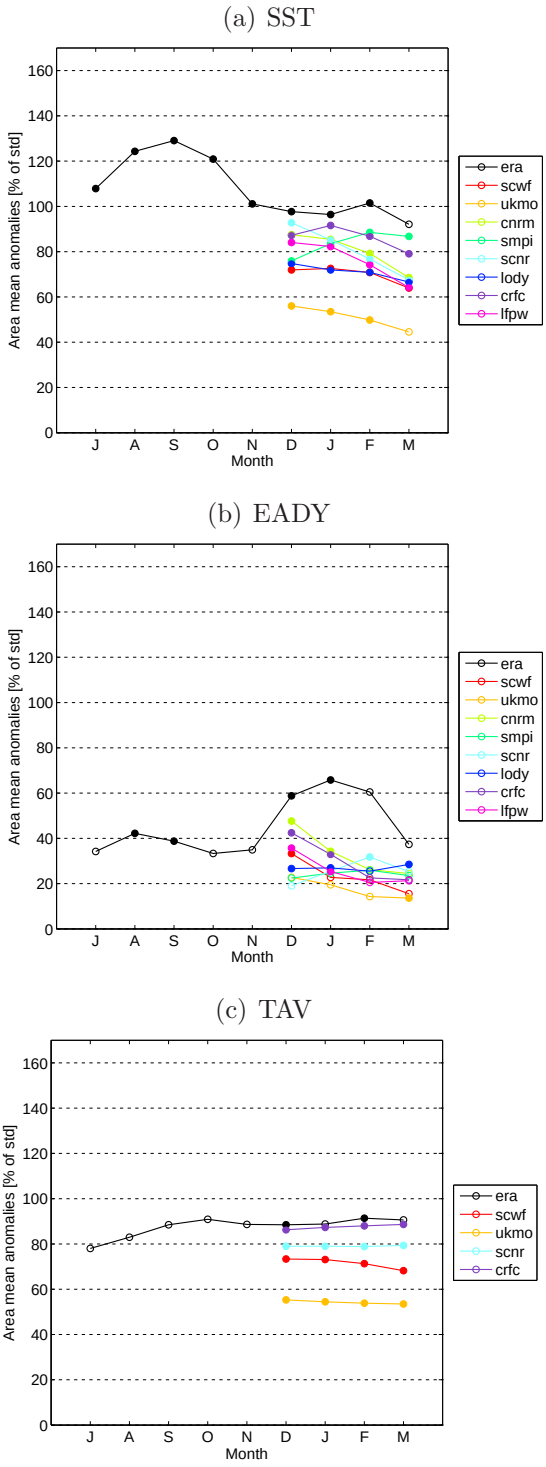

Figure 6.17: Averaged absolute anomalies (3-monthly means and averaged over the North Atlantic region) in composites of November hindcast following an August hindcasts with high and low HSI ASO of the seasonal prediction models (colored) for SST (top), EADY (center), and TAV (bottom), with ERA-40 for comparison (black). Dotted magnitudes are statistically significant ($p < 0.10$).

	ERA	SCWF	UKMO	CNRM	SMPI	SCNR	LODY	CRFC	LFPW
HSI	103.7	16.4	33.5	−15.5	20.9	*33.4*	*40.3*	*29.9*	**45.9**
NAO	–7.2	**63.9**	12.9	−9.7	−9.6	−6.1	**79.0**	24.6	**51.8**
SC NH	–91.1	**41.6**	17.7	5.4	–17.3	12.6	2.3	4.1	9.8
SC NA	–93.3	**44.3**	**37.6**	*33.7*	21.9	2.4	28.5	*45.2*	*43.5*
SC EU	–44.5	24.5	4.1	–7.9	1.4	–24.9	–16.4	*–35.3*	*–34.9*

Table 6.3: Difference of windstorm frequency DJF between composites of **November** hindcast runs with strong positive and negative November anomalies in the North Atlantic Horseshoe pattern (HSI), station-based NAO index (NAO), northern hemisphere (SCNH), North American (SCNA), and Eurasian (SCEU) continental snow cover extent (in % of inter-annual standard deviation) in the 1980–2001 period for the models, in the 1959–2001 period for ERA-40 HSI and observed NAO, and in the 1972–2001 period for observed snow cover. Significant differences ($p< 0.1$/$p< 0.2$) are highlighted (**bold**/*italic*).

6.4.2 NAO and continental snow cover as additional sources of skill?

As potential sources of predictability, anomalies of the NAO and continental snow cover during November (i.e., the initialization month of the November hindcasts) and the sensitivity of windstorm frequency to these anomalies have been analyzed in the different prediction models. Both Lead-Lag-Correlation (LLC) and composites based on anomalous states of the NAO and snow cover extent during November are employed and briefly discussed in the following.

As expected, Lead-Lag-Correlation (LLC) between monthly NAO values and the number of windstorms during DJF is positive with maximum correlation coefficients of about 0.5 during January and February (Fig. 6.18a). Three models (LFPW, LODY, SCWF) also exhibit significant correlations of about 0.20 with the NAO index during November. In these prediction models, the NAO of the initial month is thus statistically significantly related to the winter windstorm frequency. In consistency with generally positive correlations between NAO and windstorm occurrence, most models produce more windstorms in the composite of anomalous high NAO index values during November than in the low NAO composite (Table 6.3). In particular, the difference is statistically significant in the models with significant correlations to November NAO, namely LFPW, SCWF, and LODY, with values between +51.8 and +79.0% of the inter-annual standard deviation of windstorm frequency. This could be related to a tendency of persistence of the NAO in the models on time scales above one month. A positive feedback with the underlying ocean might contribute to this persistence. Corresponding composite anomaly patterns indicate that the large-scale flow pattern related to anomalous NAO in November supports the persistence and/or generation of SST anomalies similar to the Horseshoe pattern, which in turn could influence growth factors of cyclones. However, note that the corresponding

(a) NAO

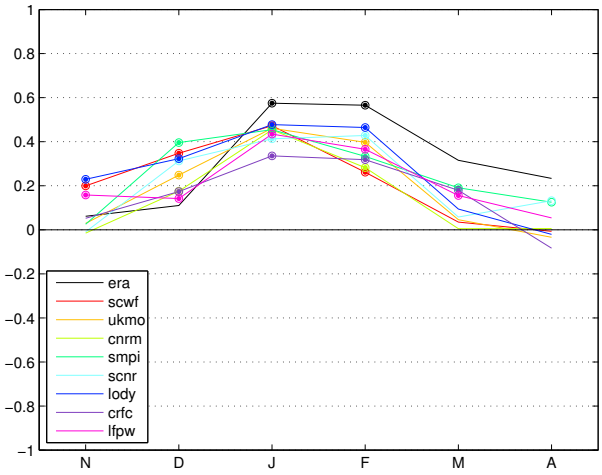

(b) Eurasian snow cover

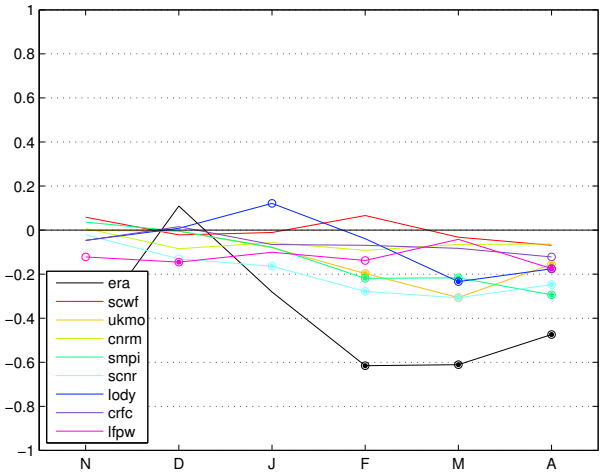

(c) North American snow cover

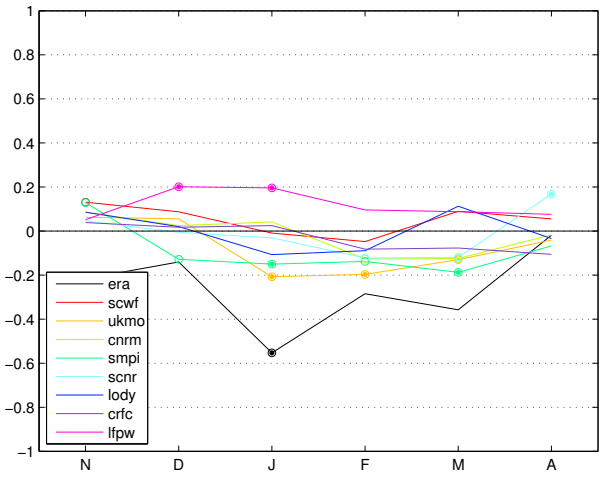

Figure 6.18: Spearman Lead-Lag-Correlation of monthly averages of the NAO (a), Eurasian (b) and North American (c) snow cover extent with windstorm frequency during DJF for the 1980–2001 period in the November hindcasts of the seasonal prediction models (colored) and reanalysis/observations for comparison (black). Dotted (circled) correlation coefficient are statistically significant with $p < 0.10$ (0.20).

value from observations is about −7.2%, or almost zero. Thus, these models produce a stronger early winter NAO–windstorm frequency relation than found in observations. This persistence of NAO-like conditions from the initial months of the November hindcast could deteriorate predictive skill of DJF windstorm frequency forecasts.

Observed continental snow cover extent during summer and autumn has been shown to be related to the climate in the North Atlantic region in subsequent winter. Low snow cover extent is linked to positive NAO regimes and a higher number of windstorms (chapter 4, or Orsolini and Kvamstø, 2009; Fletcher and Saunders, 2006; Qian and Saunders, 2003; Saunders et al., 2003). LLC between monthly snow cover extent and windstorm frequency during DJF is generally negative for observations (Fig. 6.18b and c, black). The majority of the models reproduce a negative relation between snow and windstorm frequency, but only from January to April. In contrast, the correlations between snow cover in November and windstorm frequency in subsequent DJF are very weak and mostly insignificant. However, the models generally agree on a positive relationship between North American snow cover in November and winter storm occurrence (Fig. 6.18). The respective composite difference in windstorm frequency is positive for all models (Table 6.3), and statistically significant in five of the eight models. This sensitivity is opposite to that found from observational data. Hence, the sensitivity of windstorm frequency to November North American snow cover extent might deteriorate predictive skill.

The models show less agreement on the response to Eurasian snow anomalies during November. However, Eurasian snow cover in November and December is statistically significantly correlated with windstorm frequency during DJF in the LFPW model. In terms of difference of windstorm frequency in composites with high and low Eurasian snow cover, both CRFC and LFPW show a statistically significant response ($p< 0.20$) consistent with the observations. This might also contribute to predictive skill. None of the other prediction models show such characteristics.

6.4.3 The link to predictive skill

Some of the model ensembles considered here indeed show significant predictive skill forecasting windstorm frequency during DJF for the 1980–2001 period (chapter 5, Renggli et al., 2011, Table 6.4 shows the respective skill scores and p-values). The skill scores range from 0.41 to −0.01, and are highly significant ($p< 0.01$) for the two Météo France models LFPW and CRFC, significant ($p< 0.10$) for SMPI, and marginally significant ($p< 0.20$) for SCNR. These models show stronger averaged absolute SST anomalies than the other models in the November hindcasts following strong North Atlantic SST anomalies in summer (Fig. 6.17a). Comparing Table 6.4 with Figure 6.17c reveals a one-to-one correspondence between the ranking of the p-values and the average absolute anomalies

	LFPW	CRFC	SMPI	SCNR	SCWF	LODY	CNRM	UKMO
RPSS	0.41	0.24	0.16	0.11	0.14	0.06	0.01	−0.01
p	0.00	0.01	0.06	0.12	0.24	0.33	0.48	0.60

Table 6.4: Ranked Probability Skill Score (RPSS) of predictions of three equiprobable windstorm frequency classes during December–February for the 1980–2001 with lead times of 1–3 months (i.e., started on 1 November) with corresponding p-values (estimated with a bootstrap method), ranked according to the p-values (descending to the right). See chapter 5 and Renggli et al. (2011) for further details.

of ocean heat content for the given models. CRFC retains anomalies from the previous summer/autumn in accordance with reanalysis, and shows modest, but highly significant skill in predicting wintertime windstorm frequency. In contrast, the anomaly is weak in UKMO (Fig. 6.17c), and, additionally, not very well related to the reanalysis (compare Fig. 6.12 to Fig. 4.5). The other models rank in-between. Therefore, it is argued that ocean heat content plays a crucial role in transporting a predictable signal from late summer and early autumn into the winter predictions.

The state of the NAO and continental snow cover in the initialization of the November hindcasts have also been considered as potential sources of predictability. Some models indeed reveal sensitivity on the initialized state of these variables. In particular, the French LFPW model does not only have a high persistence of the oceanic signal, but also reproduces the relation between Eurasian snow cover extent consistent with those found from observational data. Thus, these relations might further improve predictive skill. As a consequence, LFPW attains an RPSS of 0.41, by far the highest skill score of all models. However, note that this model also reproduces an relation between the November NAO and windstorm occurrence in DJF that is not found in observations.

6.5 Conclusions

Hindcasts of seasonal prediction models from the DEMETER and ENSEMBLES project have been analyzed in terms of the relation between hemispheric-scale factors (North Atlantic SST, continental snow cover, NAO) to growth factors of cyclones and the occurrence of windstorms on seasonal time scales. These relations have been investigated in both August and November hindcasts. It has been shown that there are significant inter-model differences in the reproduction of the observed relationships. Most importantly, the persistence of summer anomalies in the North Atlantic ocean is generally underestimated compared to observations and varies considerably between the individual models. On the one hand, differences are found in the persistence of the models' anomalies within the August hindcast. This fact points to weaknesses in the coupling between the ocean and atmosphere components of the coupled model. On the other hand, the models differ in

the persistence of oceanic anomalies from summer until the initialization of the subsequent November hindcast, i.e., anomalies present in summer are not equally preserved in the ocean control run used for the hindcast initialization. Generally, models with a higher persistence show stronger anomalies in growth factor of cyclones and windstorm occurrence, and attain higher levels of predictive skill.

Thus, it is argued that North Atlantic SST indeed serves as one source of predictive skill for seasonal prediction of European windstorm occurrence. The predictive skill is closely related to the reproduction of the observed anomalies in SST, their persistence, and their feedback on the atmosphere. This implies that improvements in the coupling between ocean (and, also, land surfaces) and the atmosphere in the seasonal prediction models could lead to further improvements in terms of skill.

Chapter 7

Synthesis

7.1 Summary

European wintertime windstorms are the natural hazard with the highest loss potential to society and economy in the mid-latitudes. Skilful predictions of storm risk on seasonal time scales could help to improve risk management practices. Although it was noted that at least some parts of the atmospheric variability in the North Atlantic region is predictable on seasonal time scales, the seasonal predictability of windstorm occurrence has not yet been extensively studied. Therefore, this thesis has addressed different aspects of the seasonal predictability of wintertime windstorms in the North Atlantic and European region. Four topics have been extensively studied, namely the development of an objective windstorm identification scheme focused on the impacts of these events, the potential sources of seasonal predictability, the predictive skill in ensembles of different dynamical seasonal prediction models, and the sources of skill in these seasonal prediction models.

First, an impact-related definition of windstorms has been developed. Basically, a windstorm is defined as a region of extreme wind speeds (above the local 98th percentile threshold) with a minimum area which can be tracked for at least 18 hours. An identification scheme based on this definition has been implemented and applied to reanalysis and seasonal prediction model data. The identification scheme successfully identifies historical windstorm events, but also yields reasonable climatological distributions. It has been used, e.g., for studying the impact of anthropogenic climate change on the properties and occurrence of windstorms (Nissen et al., 2010; Leckebusch et al., 2008b).

On the basis of observational and reanalysis data it has been shown that anomalies in hemispheric-scale factors—such as sea surface temperatures and sea ice extent in the North Atlantic, continental snow cover extent, and the North Atlantic Oscillation—in late summer and autumn are statistically significantly linked with anomalous windstorm

activity in the North Atlantic and European region in subsequent winter (i.e. with lead times of four to six months), explaining about 20% of the inter-annual variability of windstorm climate. Thus, they may be considered as potential sources of seasonal windstorm predictability. Possible physical mechanisms responsible for these relationships include the relation of hemispheric-scale factors to anomalies in growth factors of cyclones. In particular, specific anomalies of North Atlantic SST during late summer and autumn (resembling the so-called Horseshoe pattern) are persistent to winter and related to better growth conditions for cyclones (e.g., higher baroclinicity between Newfoundland and the British Isles), potentially leading to more intense or a higher number of windstorms. It was also shown that the development of the North Atlantic Horseshoe pattern is favored by anomalous NAO indices in summer. Potential physical processes related to anomalies of continental snow cover and sea ice extent are less clear.

Then, the predictive skill in ensembles of different dynamical seasonal prediction models of the DEMETER and ENSEMBLES projects to forecast the windstorm frequency has been assessed in terms of the Ranked Probability Skill Score (RPSS) and the Relative Operative Characteristic Skill Score (ROCSS). It has been shown that there are multi- and single-model ensembles with statistically significant skill, ranging from about 0.15 to 0.40 in terms of RPSS. One specific model suite used at Météo France (CRFC/LFPW) shows consistently high skill scores. High windstorm frequency winters generally attain better scores than low frequency winters. Furthermore, the 1980–2001 period is generally better predicted than the 1960–2001 period. It is speculated that the variable link between the PNA and NAO might contribute to this decadal-scale variability in predictability.

The sources of skill in the seasonal prediction models have been evaluated. Both August and November hindcasts have been considered. Focusing on the North Atlantic SST–windstorm relationship, it has been shown that SST anomalies are accompanied by physically consistent anomalies in growth factors of cyclones, in good agreement with observations. However, the persistence of the SST anomalies from summer to winter differs significantly between different models, and is generally weaker than in observations. The ability to retain the anomalous oceanic conditions from summer through winter in the models' ocean control run used to initialize the hindcasts was shown to be crucial. Some models preserve anomalies, e.g., in ocean heat content, until winter and develop specific anomalies in SST, growth conditions of cyclones, and windstorm frequency. In other models, this information is lost in the model ocean control run from August to November. Generally, models with the ability to preserve North Atlantic anomalies show higher skill. This is an indication that the state of the North Atlantic in summer and autumn is indeed a source of seasonal windstorm predictability, and that improvements of the ocean–atmosphere coupling could increase predictive skill of windstorm occurrence on seasonal time scales. The response to anomalous continental snow cover was shown

to be very different between the individual models. Thus, the land surface–atmosphere coupling is another promising candidate for potential improvements.

7.2 Discussion and Conclusions

The results of the previous chapters are discussed in the following in terms of the objectives of the thesis as outlined in section 1.3.3.

Development of an impact-orientated definition of windstorms and objective identification scheme, appropriate for application to large (multi-) model ensembles

A powerful scheme for the identification of windstorms has been developed on the basis of an event definition focused on the impacts of such extreme wind events. The feasibility of such an approach was demonstrated by the successful identification of individual windstorm events as well as in temporal and spatial climatologies of the identified windstorms in good agreement with observations. Although absolutely sufficient for the purpose of this thesis, several technical issues could potentially be improved.

As described in section 3.2.1 the tracking algorithm to identify windstorms uses a nearest-neighbor approach. This simple method of linking spatial entities in consecutive timesteps was shown to provide reasonable results. However, the current version of the tracking algorithm could certainly be extended by more sophisticated tracking methods, for instance, by introducing an estimation of the location of cluster of extreme wind speeds in the next timestep, and search the nearest neighboring cluster in the vicinity of the estimated future location. This estimation could be based on the previous translation velocity and direction of the cluster or on the direction and velocity of upper-level wind speeds. The latter approach is used by Murray and Simmonds (1991) in their cyclone tracking scheme. However, the relation between the location of (locally!) extreme wind speeds and the upper-level flow is not assumed to be as straightforward as the relation between the center of a low pressure system and the upper-level flow. Furthermore, additional data on the upper-level conditions had to be included. Since the algorithm was developed to analyze particularly large multi-model ensembles of seasonal predictions, the emphasis was on reducing the necessary data amount to a minimum. Therefore, such more complex tracking methods have not been developed up to now.

Furthermore, the use of a nearest-neighbor approach comes with some constraint on the temporal resolution of the underlying data. Tests with 12-hourly data (e.g., the timesteps at 0 and 12 UTC of the ERA-40 data) showed the climatological properties of the identified windstorms still agree well with the original 6-hourly data. With 24-hourly data only, the identification scheme fails to produce reasonable results.

Despite the fact that the tracking scheme was developed and mainly used on the basis of surface wind speed, it is also applicable to pressure level wind speeds. Sensitivity tests confirmed that the windstorm climatologies differ not very much between windstorms defined by surface and low-level wind speeds. The use of surface wind speed is mainly motivated by its relevance for impact studies.

One major advantage of the tracking scheme is the possibility to compute statistics for individual windstorm events which are defined as both temporally and spatially extended entities. Previous studies have most often used either grid-point wise measures (e.g., Qian and Saunders, 2003; Palutikof et al., 2002) or spatially aggregated measures (Della-Marta et al., 2009; Smits et al., 2005). The new approach presented in this thesis thus offers a wide range of possible applications. Indeed, the windstorm identification tool is used in several recent and ongoing research projects.

Application of the windstorm identification scheme to reanalysis and seasonal prediction model

The windstorm identification scheme was successfully used to characterize the variability wintertime windstorm climate in the North Atlantic and European region in different data. Both the spatial and the temporal variability of European windstorms identified in ERA-40 agree well with observations. For example, the average pattern of windstorm track density is shifted to the south-east compared to cyclone track density, in line with the relation between low pressure systems and extreme wind fields (Leckebusch et al., 2008b). Keep in mind, however, that the identification scheme is not restricted to cyclonic windstorms, but identifies the coherent occurrence of locally extreme wind speeds independent of their physical origin. The monthly distributions of windstorm frequency agrees with the frequency of loss events reported by reinsurance companies. Furthermore, the properties of windstorms identified in hindcast data from seasonal prediction models are in good agreement with reanalysis if systematic biases in the number of identified storms are accounted for (Renggli et al., 2011). This allowed the relations between hemispheric-scale factors, growth factors of cyclones and the occurrence of windstorms to be investigated as well as the predictive skill of seasonal predictions to be quantified.

The windstorm identification scheme has not only been used to analyze seasonal predictability of windstorms: several other projects have used the windstorm tracking as well. For example, specific properties of windstorms such as area, mean and maximum wind speeds, lifetime, etc. have been studied climate change scenarios by Leckebusch et al. (2008b). They concluded that future windstorms may become more severe, mainly owing to the occurrence of higher wind speeds, and to larger areas affected by the storms. Especially fruitful proved the introduction of the *Storm Severity Index* as an objective

impact-related measure for storm severity for individual windstorm events (Leckebusch et al., 2008b). For example, the event-based SSI has been used to calculated the climate change signal in return periods of severe windstorm events (Pardowitz et al., 2010) or to identify impact-relevant extreme wind events in the large data set of the Ensemble Prediction System of the ECMWF (Lorenz et al., 2010). These studies also attract the attention of stakeholders in the risk management industry (Burghoff et al., 2010; Kuhnel, 2010).

The identification scheme was originally developed with a spatial focus on the North Atlantic region. With appropriate adjustment of the parameter settings, the identification can also be applied to detect extreme windstorms over the Mediterranean (Nissen et al., 2010). Preliminary tests to identify meso-cyclones in polar regions (polar lows), and, if data of sufficient spatial resolution are available, tropical cyclones were promising. Hence, the approach might finally develop into a unified objective definition and identification tool of extreme wind events of different temporal and spatial scales and in different regions of the world.

Are hemispheric-scale factors related to windstorm occurrence on seasonal time scales

Several hemispheric-scale factors in summer and autumn are statistically significantly correlated with the number of windstorms in the North Atlantic and European region in the subsequent winter, i.e., with lead times of up to six months and correlations coefficients of up to 0.43 (equivalent to an explained variance of about 20%). Robust correlations were found for summer NAO and the Horseshoe pattern of North Atlantic SST anomalies in autumn. In contrast, the relations of continental snow cover and sea ice extent to windstorm occurrence are not temporally robust and depend on the treatment of trends in the time series, respectively. Furthermore, partial correlation analysis showed that the link of snow cover and sea ice to windstorm occurrence is markedly reduced if the HSI–windstorm or NAO–windstorm relation is accounted for. Therefore, summer NAO and autumn HSI are robust precursors of wintertime North Atlantic wind climate, and snow cover and sea ice are not. These findings go beyond results of prior studies on the relation between hemispheric-scale factors and North Atlantic wind climate.

These findings are consistent with previous studies. Significant relations have been found between the North Atlantic ocean in summer and autumn with the large-scale atmospheric flow in the subsequent winter, both in observational and model data (Losada et al., 2007; Wang et al., 2004; Cassou et al., 2004; Saunders and Qian, 2002; Czaja and Frankignoul, 2002, 1999; Sutton et al., 2001; Rodwell et al., 1999) , mainly associated with anomalies projecting on the NAO. We extend these results, showing that similar anomalies are related to the number of severe windstorm events with potentially strong impacts on society.

The mutual correlation between summer NAO and the North Atlantic Horseshoe in the subsequent autumn, on the one hand, and the composites of years with strong NAO anomalies in summer, on the other, indicate that anomalous atmospheric flow is a possible source of such SST anomalies. Cassou et al. (2004) also investigated possible origins of the Horseshoe pattern and argued that NAO-like flow patterns in summer could serve as one potential source of the Horseshoe pattern. They link these NAO-like anomalies to anomalous convection in the tropics in spring and related Rossby waves traveling into the extra-tropics, e.g., to the North Atlantic region. Such a pathway provides a possibility of how tropical variability can influence the North Atlantic region (e.g., Wu et al., 2007; Peng et al., 2005), but has not been further analyzed in this thesis. Furthermore, Cassou et al. (2007) also state that the reemergence effect of ocean anomalies could play a role in the establishment of the Horseshoe pattern in autumn. Significant correlations between spring HSI and subsequent winter's windstorm frequency (Fig. 4.2a) are consistent with such a mechanism. Furthermore, Seager et al. (2000) argue that both atmospheric and ocean dynamics contribute to (sub-) surface ocean anomalies, especially in the far North Atlantic.

In contrast to HSI and NAO, the relationship of continental snow cover and sea ice extent to windstorm occurrence is less robust, probably related to the relatively short observational data record. For snow cover, significant correlations emerge only if the longer period 1972–2001 is considered, but not for the shorter period 1980–2001. For sea ice, LLC results are dependent on the treatment of trends. Only if the time series are linearly detrended does sea ice cover extent exhibit significant correlations with wintertime windstorm climate. We argue that this behavior is related to the influence of the strong negative trends in the observational data of snow cover and sea ice (Stroeve et al., 2007). For example, our results with respect to sea ice are generally consistent with a recent study about the relation between sea ice in the North Atlantic region and the NAO (Strong et al., 2009). They showed in observational data that anomalously high sea ice extent in the Barents Sea is related to a tendency to positive NAO anomalies. Our results imply that this relation is not only valid for the NAO, but also for a measure of storm activity related to the impacts of such events. However, Strong et al. (2009) used linearly detrended data, but have not commented on the effect of detrending on their results.

Which physical processes explain such relationships? Are hemispheric-scale factors related to growth conditions of extra-tropical cyclones?

A composite analyses of years with strong anomalies of the NAO and the North Atlantic Horseshoe pattern reveal physically consistent relationships between (high) summer NAO, a (positive) Horseshoe SST pattern, (better) growth conditions for cyclones and, conse-

quently, (a higher number of) windstorms in the North Atlantic and European region have been found. Such relations imply the potential of seasonal predictability of wintertime windstorms.

Specifically, the Horseshoe pattern consists of warm anomalies in the central North Atlantic, surrounded by cold anomalies to the south and the north-east. It is argued that the anomalous large-scale atmospheric flow related to a positive NAO regime during summer contributes to the development of the Horseshoe pattern in autumn. These SST anomalies are persistent until early winter and related to better growth conditions (e.g., increased values of baroclinicity and latent heat) over the North Atlantic. Better growth conditions of cyclones in turn lead to a higher number of windstorms. Such a pathway is generally consistent with the findings of Cassou et al. (2004). They investigated the impact of prescribed summer Horseshoe SST anomalies on subsequent winter large-scale atmospheric flow in the North Atlantic region in the ARPEGE atmospheric general circulation model and also found regions of increased baroclinicity in early winter which could give rise to more active storm tracks.

Although composites of years with strong snow cover anomalies have been analyzed, they have not helped to increase the understanding of the physical mechanisms involved (not shown). Several studies have shown that the snow–atmosphere interaction involves changes in the vertical wave flux into the stratosphere (e.g., Allen and Zender, 2010; Fletcher et al., 2007; Gong et al., 2002). Wave flux anomalies could induce stratospheric circulation anomalies which are propagated downwards into the troposphere leading to large-scale flow anomalies (e.g., as quantified by the Arctic Oscillation). Thus, such a pathway is not expected to affect growth factors in the first place, and growth factors are not ideal measures to understand the relation between anomalous snow cover and the occurrence of windstorms. Targeted climate model runs with prescribed boundary conditions would be necessary to further evaluate the physical pathways from anomalous hemispheric-scale factors to wintertime windstorms.

Our results show that the boundary conditions can indeed influence wintertime windstorm climate on seasonal time scales. This implies that a better representation of the boundary conditions and the coupling between atmosphere and its boundaries could enhance the skill of dynamical seasonal predictions, both in the North Atlantic region and for variables such as wintertime windstorms. Indeed, Orsolini and Kvamstø (2009) showed that prescribing both observed SST and snow cover extent markedly improves the reproduction of the observed winter NAO compared to model runs with only prescribed observed SST. In a similar study, Douville (2009) showed that the reproduction of the NAO is highly improved with prescribed stratosphere from observations. Thus, a more realistic reproduction of the atmosphere's boundary conditions and their impact in seasonal forecast models could potentially improve predictive skill in the mid-latitudes.

How skillful are forecasts of state-of-the-art dynamical seasonal prediction models?

The seasonal forecast systems of the DEMETER and ENSEMBLES projects have been investigated in terms of their ability to produce reliable forecasts of windstorm climate over the North Atlantic and Europe. The Ranked Probability Skill Score of the multi-model ensembles predicting the number of windstorms during December–February in the November hindcasts (i.e., with a lead time of 1–3 months) attains statistically significant levels of about 0.10–0.15% in the 1980–2001 period. Specific single-model ensembles exhibit skill scores of up to 0.41. Thus, there is potential for successful windstorm predictions on seasonal time scales. However, the skill is dependent on the models used for the prediction, on the period (only the LFPW model and the ENSEMBLES multi-model attain significant skill score in the 1960–2001 period), and on the windstorm frequency. Previous studies demonstrated small (about 0.15 in terms of RPSS) but statistically significant skill in the DEMETER seasonal prediction ensembles in forecasting the mean winter NAO when started on 1 November (Johansson, 2007; Müller et al., 2005). The statistically significant skill of windstorm frequency of the same magnitude (about 0.15 for the multi-model ensembles) is comparatively high and even suggests an economic usability of the predictions, for example in the insurance industry.

Several limitations of the ability of the numerical systems to predict North Atlantic and European windstorms on a seasonal time scale were identified. First of all, significant skill is only found for windstorm frequency, but not for intensity. Thus, the skill of seasonal predictions of windstorm climate in this region depends on the predictand used. For example, Della-Marta et al. (2010) found no significant skill for the monthly mean intensity of wintertime wind events in the 1958-2001 period (except in the first month of the predictions) in various seasonal prediction systems of the ECMWF. Owing to the different lead times, different predictand and models, and a different validation period, a direct comparison of the results is not possible; our results are, however, consistent with those reported by Della-Marta et al. (2010) with respect to generally lower skill for the 1960-2001 period and no significant skill when using a seasonally accumulated intensity measure (SSI, cf. section 5.4).

As expected, it was found that the predictive skill depends on the single models used or on the composition of the multi-model ensemble. Previous studies have found a negative relation between systematic biases in seasonal prediction models and skill, i.e., the smaller the bias, the higher the skill (e.g., Lee et al., 2010; DelSole and Shukla, 2010). Our study supports those findings to some extent. The correlation between the systematic biases in the number of windstorms during DJF (Table 5.1) with predictive skill (Fig. 5.4a) is negative, although not statistically significant. On the other hand, the most

successful models (CRFC and LFPW) both have a strong systematic bias in terms of the location of the wind storms. It is thus not clear which attempts to correct the systematic biases in the representation of the climatological state are most likely to result in significantly improved seasonal predictions. This statement is also consistent with the finding that the ENSEMBLES hindcasts do not generally show better skill compared with the DEMETER models (Figs. 5.3 and 5.4, Table 5.3), despite improvements in the horizontal and vertical resolution of the models, for example (cf. Table 2.1, Weisheimer et al., 2009; Palmer et al., 2004). In contrast, some improvements of skill have been achieved in tropical regions (Weisheimer et al., 2009). However, Weisheimer et al. (2009) also mention that there are regions on the globe where systematic errors (with respect to SST) have not been improved, but that it is hardly possible to attribute certain improvements or deteriorations to specific changes in the models without targeted model runs. The one exception with considerable improvements in predictive skill is the ENSEMBLES contribution from Météo France (LFPW). This model's components correspond to the ones used in CRFC of DEMETER. Hence, improvements in LFPW compared with CRFC (e.g., a newer version of the atmospheric component, GELATO sea ice model, slightly different initialization) result in an increased skill of 0.17 (0.32) for the windstorm frequency DJF (JFMA). The fact that the LFPW-CRFC models provide robust skillful predictions for wintertime windstorm frequency-both in DEMETER and ENSEMBLES and for the entire hindcast period-lends even more credibility to the forecast ability of this particular model suite.

What are the characteristics of the variability of skill?

Predictive skill of the forecast of windstorm frequency depends on the forecasted frequency itself as well on the frequency eventually observed. A tendency towards higher (lower) skill in observed high-frequency (medium-frequency) winters is found for both skill scores (RPSS and ROCSS) used in the study. This finding is consistent with a tendency towards higher skill scores in NAO predictions in winters of extreme mean NAO index values (Müller et al., 2005). Possible mechanisms leading to higher skill in extreme winters could be related to anomalous North Atlantic SSTs or continental snow cover anomalies in summer/autumn. They have been related to anomalies in the atmospheric conditions in the following winter (Fletcher et al., 2009; Cassou et al., 2004; Wang et al., 2004; Qian and Saunders, 2003; Czaja and Frankignoul, 2002). Thus, more extreme observed anomalies, if appropriately initialized, should increase the likelihood that the forecast model will produce a response in accordance with the observation. In contrast, if the anomalies are small or counteracting, a model response is less strongly triggered.

Furthermore, the predictive skill is dependent on the period considered. The 1980–2001 period is generally better predicted than the 1960–1980 period. A possible explanation include the variability of global teleconnections. For example, the influence of ENSO variability on Central Europe is temporally varying (e.g., Knippertz et al., 2003). Such variations could affect Central Europe through the strong ENSO–PNA link and a variable PNA–NAO link, which is found both in observations and in coupled atmosphere–ocean GCMs. The seasonal prediction models generally overestimate the observed strength of the link between PNA and NAO (see Fig. 5.6), possibly related to the exaggerated zonality of the models (e.g., Ulbrich et al., 2009). While the observed link varies with time, the seasonal prediction models produce a constantly strong link, without such variations on decadal scales. The better agreement between the strength of the link in the 1980s and 1990s compared to the 1960s and 1970s could therefore lead to the better predictability in the 1980–2001 period. In-depth analyses of these topics would be very useful but are beyond the scope of this thesis.

Are the modeled hemispheric-scale factors related to the modeled occurrence of windstorms in seasonal prediction models?

The relation of hemispheric-scales factors to the occurrence of windstorms is generally weak on seasonal time scales, and dependent on the prediction model. For example, Lead-Lag-Correlations with the hemispheric-scale factors leading windstorms are generally not significant beyond lead times of one month. Thus, the modeled relations are generally weaker than in reanalysis data. Possible reasons include a) a general underestimation of the impacts of hemispheric-scale factors on the atmosphere in the prediction models, which could explain the relatively low skill of the models in predicting windstorm occurrence; b) an overestimation of the relations in the reanalysis data, e.g., owing to the relatively short period covered by the reanalysis/observational data; or c) the influence of other factors in the models not considered in this study. For example, the general overestimation of the link between the PNA and the NAO in the models compared to reanalysis data (Pinto et al., 2011) could perturb or override a possible weaker influence of the hemispheric-scale factors considered in this study. Fully controlled experiments with specific prescribed boundary conditions and longer lead times would be necessary for further analyses of the physical mechanisms (e.g., as in Rodwell et al., 2004).

However, composites of model ensemble runs with strong anomalies in the hemispheric-scale factors (where the signal-to-noise ratio is increased) revealed a consistent response of windstorm occurrence in the November hindcasts. In all models, windstorm frequency is increased in hindcasts following strong North Atlantic SST Horseshoe anomalies in previous summer (Table 6.3, first row). Additionally, all models agree on a positive

response to anomalies of North American snow cover extent (Table 6.3, fourth row). For the other hemispheric-scale factors, the sensitivity is generally not statistically significant. The exception is the LFPW model. Its windstorms frequency during DJF is also sensitive to November anomalies of both NAO and Eurasian snow cover.

Which role do growth factors of cyclones play in these relations?

It was shown that SST anomalies persisting from summer until winter are linked to specific anomalies in growth factors. For example, regions with increased meridional SST gradients correspond to regions of enhanced baroclinicity. Generally, positive (negative) anomalies of equivalent potential temperature are found above positive (negative) SST anomalies. Windstorm track density is generally increased (decreased) close to regions with favorable (unfavorable) growth conditions for cyclones. Furthermore, models with stronger SST anomalies do also develop stronger anomalies in growth factors of cyclones. These findings corroborate the results with respect to the observed relationships (chapter 4) and are in line with previous studies on the influence of summer/autumn oceanic conditions in the North Atlantic and the atmospheric circulation in the subsequent winter (Cassou et al., 2004; Rodwell and Folland, 2003; Kushnir et al., 2002; Rodwell et al., 1999). These results suggest that anomalous growth conditions for cyclones are indeed a physical link between North Atlantic SST and wintertime windstorm climate.

How do these relations compare to reanalysis/observations and between the models?

The relation between North Atlantic SST anomalies and wintertime windstorm occurrence is in agreement with those found in observations (chapter 4), albeit the link is weaker, consistent with (Rodwell and Folland, 2003). Current coupled GCM tend to overestimate the atmosphere–ocean forcing, and underestimate the ocean–atmosphere forcing in the North Atlantic region (Rodwell and Folland, 2003, 2002; Kushnir et al., 2002). For example, the averaged absolute anomaly of baroclinicity has been shown to be always weaker in the prediction models than in reanalysis, although the underlying SST anomalies are of similar magnitude (Figs. 6.10 and 6.17).

The second relation where all models agree is a positive response to North American snow cover anomalies. The response is related to an increased temperature gradient between an anomalously snow covered North American continent and the adjacent North Atlantic Ocean leading to increased baroclinicity at the entrance of the North Atlantic storm track. However, this is opposite to the negative response found in the observational data (Table 6.3, fourth row). Such disagreement between models and observations could lead to deterioration of predictive skill.

As noted before (e.g., Lin and Derome, 2003; Kushnir et al., 2002), there are considerable model differences in the atmosphere–ocean interaction. The results presented here revealed considerable inter-model difference in the persistence of oceanic anomalies, both within the August hindcasts and from anomalies in summer to the onset of the November hindcasts. Whereas in some models the persistence is in good agreement with reanalysis (e.g., CRFC) it is much lower in others. Particularly in UKMO, a signal present in the summer ocean is lost at the onset of the November hindcasts. Rodwell and Folland (2002) have found that this specific coupled model fails to reproduce the observed link between North Atlantic SST and the atmospheric circulation. They argue that the model's extratropical response to SST anomalies is too weak. The results of this thesis suggest that the weak persistence of oceanic anomalies contribute these characteristics. These two reasons may also be related to each other. Furthermore, it would be interesting to analyze a possible role of re-emergence of oceanic spring anomalies in subsequent autumn and model differences in its reproduction. However, this is not possible with the 6-monthly hindcast data used in this study. Prediction runs running from spring to subsequent winter would be necessary to investigate these issues.

The general disagreement between the models on the role of northern hemisphere and Eurasian snow cover fails to support findings from observational data. Only the LFPW model reproduces a (negative) response in consistency with observations. This fact points to shortcomings of the coupling between the land surface and the atmosphere in the models . For example, the quality of land surface initialization is still in its infancy. Furthermore, it was suggested that snow–atmosphere interactions on seasonal time scales in the North Atlantic region incorporates the stratosphere (Fletcher et al., 2007; Saito and Cohen, 2003). Since the stratosphere is not especially well resolved in the seasonal prediction models considered in this study, it is questionable how reliable the models reproduce stratospheric processes. The gains of including a well-resolved stratosphere in terms of predictive skill was illustrated by Orsolini et al. (2011). The skill of seasonal winter (JFM) NAO forecasts increased by about 30% compared to the same model with an ordinary stratospheric resolution.

Are inter-model differences related to the skill of seasonal windstorm predictions?

Given the proposed physical causal links from North Atlantic SST to growth factors of cyclones and windstorm occurrence, differences in the persistence of North Atlantic anomalies could affect predictability on seasonal time scales. If a potential signal is lost in the course of the seasonal prediction, no significant skill is to be expected. This is particularly true for anomalies in the ocean heat content in the ocean control run used

for the initialization of the prediction every three months. The level of agreement in the persistence of anomalies between a model and observations determines, at least to some degree, its ability to forecast wintertime windstorm frequency. Models retaining the ocean signal (e.g., CRFC, SCNR) are shown to produce significantly more windstorms in case of strong North Atlantic Horseshoe SST anomalies (Table 6.3, first row), in accordance with observations, and therefore attain better skill scores than models with lower persistence. Thus, inter-model differences in the reproduction of observed physical mechanisms are related to the predictive skill of the models. The sensitivity of skill to the persistence of oceanic anomalies suggests that anomalies in the North Atlantic in summer and autumn serve as one source of seasonal predictability of wintertime windstorms over Europe. Furthermore, the response of windstorm frequency in the LFPW model to anomalies of the NAO and Eurasian snow cover in November is consistent with the observed response. This might further contribute to the high skill score of this particular model.

Hence, improvements with respect to hemispheric-scale factors could finally lead to improved seasonal predictions. Most promising approaches include better assimilation and initialization techniques, improvements of the coupling between different components of the climate system, and model improvements. Better assimilation and initialization may be especially important for the ocean–atmosphere system (e.g., Balmaseda et al., 2010). For example, observations of the ocean state can be incorporated by nudging (e.g., Baehr et al., 2010), or coupled initialization (see Balmaseda and Anderson, 2009, for an review of different initialization strategies for seasonal forecasting). The importance of coupling between the atmosphere and climate components other than the oceans have been shown to be of particular importance for the North Atlantic region (e.g., Balmaseda et al. (2010) on the importance of sea ice, or Ni-Meister (2008) for review of soil moisture assimilation). Seasonal hindcasts of North Atlantic and European climate have been considerably improved through prescribing snow cover properties (Douville, 2010; Orsolini and Kvamstø, 2009), soil moisture (Douville, 2010), or stratospheric variability (Douville, 2009). However, soil moisture might be of more importance for summer months than for winter. Finally, model improvements may be achieved by increasing resolution (e.g., Balmaseda et al., 2010) or better parameterizations. However, despite constant model improvements, model errors are assumed to remain a critical problem of seasonal forecasts in the future (EUROSIP online documentation[1]).

7.3 Potential applicability of the results

Because our windstorm-event definition is based on the level of surface wind speed relevant to the local occurrence of losses, our study suggests potential applicability of seasonal forecasts to Europe-wide risk management. With respect to the loss potential of windstorms

(Leckebusch et al., 2007), the prospect of significant skill of any quantity being related to wintertime windstorms is relevant from a risk management perspective, even if the skills derived in this study seem low. Nonetheless, a fairly low skill may potentially be exploited by users with a wide spatial and temporal scope as long as the seasonal predictions outperform simple forecasts based on climatology or persistence (Garcia-Morales and Dubus, 2007; Hurrell et al., 2006; Murnane, 2004). Additionally, the tendency towards higher skill in high storm frequency winters is interesting, since from a risk perspective winters with extreme (high or low) frequency might be more relevant than winters with medium frequency. The same tendency is also noted in the predictions themselves, i.e., in the predicted storm frequency. Thus, this information can be used as a measure of confidence in a given prediction.

The tools and diagnostics developed in this study form the scientific basis for the use of operational predictions. In an operational framework, windstorm climate, systematic biases etc. would be analyzed for operational data. The hindcasts used in this study stem from research projects which have not produced operational seasonal forecasts. However, several institutions issue operational dynamical seasonal prediction (e.g., ECMWF or the International Research Institute at the Columbia University, New York). With respect to a potential applicability of the tools and methods elaborated in this thesis, the operational multi-model ensemble at the ECMWF (EUROSIP[1], Vitart et al., 2007) might be of particular interest. This multi-model ensemble consists of three independent coupled systems, namely those of the ECMWF, the UK Met Office, and Météo France. Note that the EUROSIP models are newer versions of the models used by the respective institution in the DEMETER and ENSEMBLES projects. It is noteworthy that the model from Météo France contributes to the multi-model ensemble since this model has been shown to be especially successful in predicting North Atlantic windstorm occurrences (e.g., see Figs. 5.3 and 5.4). The EUROSIP model ensemble has produced forecasts since 2005. The output data of the prediction models is archived at ECMWF and available under the terms of the EUROSIP data policy. The forecasts are produced once a month and run for at least six months, depending on the model. All data become available on the 15th of each month. Thus, it would be possible to issue a forecast of the windstorm frequency during DJF on the 15th of November, for example.

To find ways how such a forecast product could be used in operational risk management is beyond the scope of this study. Clearly, close cooperation between potential forecast users and forecast providers is necessary. Because this study showed that there is indeed predictive skill it may serve as a starting point for further analysis more focused on the application of these results.

[1]See http://www.ecmwf.int/products/forecasts/seasonal/documentation/eurosip/ch1.html for an online documentation

It has been noted, however, that the time scale of seasonal forecasts does not match the operational cycles in risk management industries (Murnane, 2004). For example, (re-) insurance contracts are mostly written for an entire calendar year, from January through December. Although it has been shown in section 5.4 that it may be possible to successfully anticipate anomalous windstorm frequency during January–April from predictions issued at mid of November, the time to react may be too short. Therefore, potential users might be more interested in predictions on longer time scales, e.g., decadal predictions (e.g., Hurrell et al., 2009). Although efforts on decadal predictions are still in their infancy, some recent studies have shown the potential of predictions on these time scales (e.g., Smith et al., 2007; Lee et al., 2006; Keenlyside et al., 2008; Latif et al., 2006). Potential decadal predictability was found to be substantial for the European region (Keenlyside et al., 2008). One section of the upcoming 5th Assessment Report (AR5) of the Intergovernmental Panel on Climate Change (IPCC) will be devoted in particular to climate variability and predictability on decadal time scales[2]. In Germany, the co-ordinated research program MIKLIP focusing on decadal predictability will start in summer 2011 and run until 2014. For research purposes, multi-model decadal hindcasts have already been produced for about the last 50 years in the ENSEMBLES project. Clearly, problems of few forecast-observation pairs available for evaluation (e.g., for skill assessment) on the seasonal time scale become even more pronounced with decadal hindcasts. However, the methods developed and employed in this thesis to study seasonal predictability could also be applied to investigate potential physical processes responsible for decadal predictability.

[2]See outlines of the AR5, http://www.ipcc.ch/pdf/ar5/ar5-outline-compilation.pdf

Bibliography

Alexander, M., C. Deser, and M. Timlin, 1999: The reemergence of SST anomalies in the North Pacific Ocean. *J. Climate*, **12 (8)**, 2419–2433.

Alexander, M. A., I. Blade, M. Newman, J. R. Lanzante, N. C. Lau, and J. D. Scott, 2002: The atmospheric bridge: The influence of ENSO teleconnections on air-sea interaction over the global oceans. *J. Climate*, **15 (16)**, 2205–2231.

Alexander, M. A. and C. Deser, 1995: A Mechanism for the Recurrence of Wintertime Midlatitude SST Anomalies. *J. Phys. Oceanogr.*, **25 (1)**, 122–137.

Allen, R. J. and C. S. Zender, 2010: Effects of continental-scale snow albedo anomalies on the wintertime Arctic oscillation. *J. Geophys. Res.*, **115**, D23 105, doi:10.1029/2010JD014490.

Anandaraja, N., T. Rathakrishnan, M. Ramasubramanian, P. Saravanan, and N. S. Suganthi, 2008: Indigenous weather and forecast practices of Coimbatore district farmers of Tamil Nadu. *Indian Journal of Traditional Knowledge*, **7 (4)**, 630–633.

Anderson, D. L. T., 2008: Overview of Seasonal Forecasting. *Seasonal Climate: Forecasting and Managing Risk*, A. Troccoli, M. Harrison, D. L. T. Anderson, and S. J. Mason, Eds., Springer Academic Publishers, Series IV: Earth and Environmental Sciences, Vol. 82, chap. 3, 45–65.

Armstrong, R. L. and M. J. Brodzik, 2005 (updated 2007): Northern Hemisphere EASE-Grid weekly snow cover and sea ice extent version 3. Boulder, Colorado, USA: National Snow and Ice Data Center. Digital Media. Online documentation: http://nsidc.org/data/docs/daac/nsidc0046_nh_ease_snow_seaice.gd.html.

Baehr, J., W. Müller, R. Piontek, L. Kornblueh, D. Matei, M. Botzet, and H. Haak, 2010: Initialisierung von saisonalen Klimavorhersagen mit ECHAM5/MPI-OM. *Kurzfassungen der Meteorologentagung DACH*, Bonn, Deutschland, 20.–24. September 2010.

Baldwin, M. P. and T. J. Dunkerton, 2001: Stratospheric harbingers of anomalous weather regimes. *Science*, **294 (5542)**, 581–584.

Baldwin, M. P., D. B. Stephenson, D. W. J. Thompson, T. J. Dunkerton, A. J. Charlton, and A. O'Neill, 2003: Stratospheric memory and skill of extended-range weather forecasts. *Science*, **301 (5633)**, 636–640.

Balmaseda, M. and D. Anderson, 2009: Impact of initialization strategies and observations on seasonal forecast skill. *Geophys. Res. Let.*, **36 (1)**, L01 701.

Balmaseda, M. A., L. Ferranti, F. Molteni, and T. N. Palmer, 2010: Impact of 2007 and 2008 Arctic ice anomalies on the atmospheric circulation: Implications for long-range predictions. *Quart. J. Roy. Meteor. Soc*, **136 (652)**, 1655–1664.

Balmaseda, M. A., A. Vidard, and D. L. T. Anderson, 2008: The ECMWF ocean analysis system: ORA-S3. *Mon. Wea. Rev.*, **9 (4)**, 3018–3034.

Barnett, T. P., L. Dümenil, U. Schlese, E. Roeckner, and M. Latif, 1989: The Effect of Eurasian Snow Cover on Regional and Global Climate Variations. *J. Atmos. Sci*, **46 (5)**, 661–685.

Beltrán-Przekurat, A., C. H. Marshal, and R. A. Pielke, 2008: Ensemble reforecasts of recent warm-season weather: Impacts of a dynamic vegetation parameterization. *J. Geophys. Res.*, **113**, D24 116, doi:10.1029/2007JD009480.

Berrisford, P., D. Dee, K. Fielding, M. Fuentes, P. Kållberg, S. Kobayashi, and S. Uppala, 2009: The ERA-Interim archive. ERA Report Series 1, European Centre for Medium Range Weather Forecasts, Reading, UK.

Berz, G., 2008: Versicherungsrisiko "Klimawandel". *promet*, **34 (1–2)**, 3–9.

Bierstedt, S., K. M. Nissen, G. C. Leckebusch, D. Renggli, and U. Ulbrich, 2010: Raum-zeitliche Beziehung zwischen extremen Windfeldern und Zyklonen. *Kurzfassungen der Meteorologentagung DACH*, DACH2010-261.

Blade, I., 1997: The influence of midlatitude ocean-atmosphere coupling on the low-frequency variability of a GCM. Part 1: No tropical forcing. *J. Climate*, **10 (8)**, 2087–2106.

Blender, R., K. Fraedrich, and F. Lunkeit, 1997: Identification of cyclone-track regimes in the North Atlantic. *Quart. J. Roy. Meteor. Soc*, **123 (539)**, 727–741.

Bolton, D., 1980: The Computation of Equivalent Potential Temperature. *Mon. Wea. Rev.*, **108 (7)**, 1046–1053.

Brankovic, C. and T. N. Palmer, 2000: Seasonal skill and predictability of ECMWF PROVOST ensembles. *Quart. J. Roy. Meteor. Soc*, **126 (567)**, 2035–2067.

Bretherton, C. S. and D. S. Battisti, 2000: An interpretation of the results from atmospheric general circulation models forced by the time history of the observed sea surface temperature distribution. *Geophys. Res. Let.*, **27 (6)**, 767–770.

Browning, K. A., 2004: The sting at the end of the tail: Damaging winds associated with extratropical cyclones. *Quart. J. Roy. Meteor. Soc*, **130 (597)**, 375–399, doi: 10.1256/qj.02.143.

Budikova, D., 2009: Role of Arctic sea ice in global atmospheric circulation: A review. *Global and Planetary Change*, **68 (3)**, 149–163, doi:10.1016/j.gloplacha.2009.04.001.

Buizza, R. and A. Hollingsworth, 2002: Storm prediction over Europe using the ECMWF ensemble prediction system. *Meteor. Applic.*, **9 (3)**, 289–305.

Buizza, R. and T. N. Palmer, 1995: The Singular-Vector Structur of the Atmospheric Global Circulation. *J. Atmos. Sci*, **52 (9)**, 1434–1456.

Burghoff, O., O. Hauner, and A. Kubik, 2010: Weather-driven natural hazards - Approaches of risk management in the German insurance industry. *Geophysical Research Abstracts*, Vol. 12, EGU2010–15 081.

Cantelaube, P. and J. M. Terres, 2005: Seasonal weather forecasts for crop yield modelling in Europe. *Tellus A*, **57 (3)**, 476–487.

Cassou, C., C. Deser, and M. A. Alexander, 2007: Investigating the impact of reemerging sea surface temperature anomalies on the winter atmospheric circulation over the North Atlantic. *J. Climate*, **20 (14)**, 3510–3526.

Cassou, C., C. Deser, L. Terray, J. W. Hurrell, and M. Drevillon, 2004: Summer sea surface temperature conditions in the North Atlantic and their impact upon the atmospheric circulation in early winter. *J. Climate*, **17 (17)**, 3349–3363.

Chang, C. B., D. J. Perkey, and C. W. Kreitzberg, 1984: Latent-Heat Induced Energy Transformation during Cyclogenesis. *Mon. Wea. Rev.*, **112 (2)**, 357–367.

Charney, J. G., R. Fjortoft, and J. von Neumann, 1950: Numerical Integration of the Barotropic Vorticity Equation. *Tellus*, **2 (4)**, 237–254.

Charney, J. G. and J. Shukla, 1981: Predictability of monsoons. *Monsoon Dynamics*, J. Lighthill, Ed., Cambridge University Press, 99–109.

Christoph, M., U. Ulbrich, J. M. Oberhuber, and E. Roeckner, 2000: The role of ocean dynamics for low-frequency fluctuations of the NAO in a coupled ocean-atmosphere GCM. *J. Climate*, **13 (14)**, 2536–2549.

Clark, P. A., K. A. Browning, and C. Wang, 2005: The sting at the end of the tail: Model diagnostics of fine-scale three-dimensional structure of the cloud head. *Quart. J. Roy. Meteor. Soc*, **131 (610)**, 2263–2292, doi:10.1256/qj.04.36.

Cohen, J., 1994: Snow cover and climate. *Weather*, **49**, 150–156.

Cohen, J. and D. Entekhabi, 1999: Eurasian snow cover variability and Northern Hemisphere climate predictability. *Geophys. Res. Let.*, **26 (3)**, 345–348.

Collins, M., 2007: Ensembles and probabilities: a new era in the prediction of climate change. *Philos. Transac. Roy. Soc. A*, **365 (1857)**, 1957–1970.

Compo, G. P. and P. D. Sardeshmukh, 2004: Storm track predictability on seasonal and decadal scales. *J. Climate*, **17 (19)**, 3701–3720.

Conil, S., H. Douville, and S. Tyteca, 2009: Contribution of realistic soil moisture initial conditions to boreal summer climate predictability. *Climate Dyn.*, **32 (1)**, 75–93.

Cornford, S. G., 2002: Human and economic impacts of weather events in 2001. *WMO Bulletin*, **51**, 257–277.

Czaja, A. and C. Frankignoul, 1999: Influence of the North Atlantic SST on the atmospheric circulation. *Geophys. Res. Let.*, **26 (19)**, 2969–2972.

Czaja, A. and C. Frankignoul, 2002: Observed impact of Atlantic SST anomalies on the North Atlantic oscillation. *J. Climate*, **15 (6)**, 606–623.

de Coetlogon, G. and C. Frankignoul, 2003: The persistence of winter sea surface temperature in the North Atlantic. *J. Climate*, **16 (9)**, 1364–1377.

Della-Marta, P. M., M. A. Liniger, C. Appenzeller, D. N. Bresch, P. Koellner-Heck, and V. Muccione, 2010: Improved estimates of the European winter wind storm climate and the risk of reinsurance loss using climate model data. *J. Appl. Meteor. Climatol.*, **49 (10)**, 2092–2120.

Della-Marta, P. M., J. Luterbacher, H. von Weissenfluh, E. Xoplaki, M. Brunet, and H. Wanner, 2007: Summer heat waves over western Europe 1880–2003, their relationship to large-scale forcings and predictability. *Climate Dyn.*, **29 (2–3)**, 251–275, doi:10.1007/s00382-007-0233-1.

Della-Marta, P. M., H. Mathis, C. Frei, M. A. Liniger, J. Kleinn, and C. Appenzeller, 2009: The return period of wind storms over Europe. *Int. J. Clim.*, **29 (3, Sp. Iss. SI)**, 437–459, doi:10.1002/joc.1794.

DelSole, T. and J. Shukla, 2010: Model Fidelity versus Skill in Seasonal Forecasting. *J. Climate*, **23 (28)**, 4794–4806, doi:10.1175/2010JCLI3164.1.

Deser, C., M. A. Alexander, S. P. Xie, and A. S. Phillips, 2010: Sea Surface Temperature Variability: Patterns and Mechanisms. *Annual Review of Marine Science*, **2**, 115–143.

Deser, C., G. Magnusdottir, R. Saravanan, and A. Phillips, 2004: The effects of North Atlantic SST and sea ice anomalies on the winter circulation in CCM3. Part II: Direct and indirect components of the response. *J. Climate*, **17 (5)**, 877–889.

Deser, C. and M. S. Timlin, 1997: Atmosphere-ocean interaction on weekly timescales in the North Atlantic and Pacific. *J. Climate*, **10 (3)**, 393–408.

Deser, C., R. A. Tomas, and S. Peng, 2007: The transient atmospheric circulation response to North Atlantic SST and sea ice anomalies. *J. Climate*, **20 (18)**, 4751–4767, doi: 10.1175/JCLI4278.1.

di Lernia, S., 2006: Building monuments, creating identiy: Cattle cult as a social response to rapid environmental changes in the Holocene Sahara. *Quaternary International*, **151**, 50–62.

Diamond, J., 1998: *Guns, germs, and steel: The fates of human societies*. Norton, New York, 480 pp.

Diaz, H. F., M. P. Hoerling, and J. K. Eischeid, 2001: ENSO variability, teleconnections and climate change. *Int. J. Clim.*, **21 (15)**, 1845–1862.

Dickson, R. R., et al., 2000: The Arctic Ocean response to the North Atlantic Oscillation. *J. Climate*, **13 (15)**, 2671–2696.

Dilley, M., 2002: The use of climate information and seasonal prediction to prevent disasters. *WMO Bulletin*, **51 (1)**, 42–48.

Doblas-Reyes, F. J., R. Hagedorn, and T. N. Palmer, 2005: The rationale behind the success of multi-model ensembles in seasonal forecasting - II. Calibration and combination. *Tellus A*, **57 (3)**, 234–252.

Doblas-Reyes, F. J., V. Pavan, and D. B. Stephenson, 2003: The skill of multi-model seasonal forecasts of the wintertime North Atlantic Oscillation. *Climate Dyn.*, **21 (5–6)**, 501–514.

Donat, M. G., G. C. Leckebusch, J. G. Pinto, and U. Ulbrich, 2010a: Examination of wind storms over Central Europe with respect to circulation weather types and NAO phases. *Int. J. Clim.*, **30 (9)**, 1289–1300, doi:10.1002/joc.1982.

Donat, M. G., G. C. Leckebusch, S. Wild, and U. Ulbrich, 2010b: Benefits and limitations of regional multi-model ensembles for storm loss estimations. *Clim. Res.*, **44 (2–3)**, 211–225.

Douville, H., 2004: Relevance of soil moisture for seasonal atmospheric predictions: is it an initial value problem? *Climate Dyn.*, **22 (4)**, 429–446.

Douville, H., 2009: Stratospheric polar vortex influence on Northern Hemispheric winter climate variability. *Geophys. Res. Let.*, **36**, L19 703, doi:10.1029/2009GL039334.

Douville, H., 2010: Relative contribution of soil moisture and snow mass to seasonal climate predictability: a pilot study. *Climate Dyn.*, **34 (6)**, 797–818.

Douville, H. and F. Chauvin, 2000: Relevance of soil moisture for seasonal climate predictions: a preliminary study. *Climate Dyn.*, **16 (10-11)**, 719–736.

Eakin, H., 1999: Seasonal climate forecasting and the relevance of local knowledge. *Physical Geography*, **20 (6)**, 447–460.

Engelstaedter, S. and R. Washington, 2007: Atmospheric controls on the annual cycle of North African dust. *J. Geophys. Res.*, **112 (D3)**, D03 103.

Fang, Z. F. and J. M. Wallace, 1994: Arctic sea-ice variability on a timescale of 10 weeks and its relation to atmospheric forcing. *J. Climate*, **7 (12)**, 1897–1914.

Ferranti, L. and P. Viterbo, 2006: The European summer of 2003: Sensitivity to soil water initial conditions. *J. Climate*, **19 (15)**, 3659–3680.

Fil, C. and L. Dubus, 2005: Winter climate regimes over the North Atlantic and European region in ERA40 reanalysis and DEMETER seasonal hindcasts. *Tellus A*, **57 (3)**, 290–307.

Fink, A. H., T. Brücher, V. Ermert, A. Krüger, and J. G. Pinto, 2009: The European storm Kyrill in January 2007: synoptic evolution, meteorological impacts and some considerations with respect to climate change. *Nat. Hazard Earth Syst. Sci.*, **9 (2)**, 405–423.

Fischer, E. M., S. I. Seneviratne, P. L. Vidale, D. Luethi, and C. Schaer, 2007: Soil Moisture-Atmosphere Interactions during the 2003 European Summer Heat Wave. *J. Climate*, **20**, 5081–5099, doi:10.1175/JCLI4288.1.

Fletcher, C. G., S. C. Hardiman, P. J. Kushner, and J. Cohen, 2009: The Dynamical Response to Snow Cover Perturbations in a Large Ensemble of Atmospheric GCM Integrations. *J. Climate*, **22 (5)**, 1208–1222, doi:10.1175/2008JCLI2505.1.

Fletcher, C. G., P. J. Kushner, and J. Cohen, 2007: Stratospheric control of the extratropical circulation response to surface forcing. *Geophys. Res. Let.*, **34 (21)**, L21 802, doi:10.1029/2007GL031626.

Fletcher, C. G. and M. A. Saunders, 2006: Winter North Atlantic Oscillation hindcast skill: 1900-2001. *J. Climate*, **19 (22)**, 5762–5776.

Frankignoul, C., 1985: Sea surface temperature anomalies, planetary waves and air-sea feedback in the middle latitudes. *Rev. Geophys.*, **23**, 357–390.

Frias, M. D., S. Herrera, A. S. Cofino, and J. M. Gutierrez, 2010: Assessing the Skill of Precipitation and Temperature Seasonal Forecasts in Spain: Windows of Opportunity Related to ENSO Events. *J. Climate*, **23 (2)**, 209–220.

Garcia-Morales, M. B. and L. Dubus, 2007: Forecasting precipitation for hydroelectric power management: how to exploit GCM's seasonal ensemble forecasts. *Int. J. Clim.*, **27**, 1691–1705.

Gerber, E. P., C. Orbe, and L. M. Polvani, 2009: Stratospheric influence on the tropospheric circulation revealed by idealized ensemble forecasts. *Geophys. Res. Let.*, **36**, L24 801.

Goddard, L., S. J. Mason, S. E. Zebiak, C. F. Ropelewski, R. Basher, and M. A. Cane, 2001: Current approaches to seasonal-to-interannual climate predictions. *Int. J. Clim.*, **21 (9)**, 1111–1152.

Gong, G., D. Entekhabi, and J. Cohen, 2002: A large-ensemble model study of the wintertime AO-NAO and the role of interannual snow perturbations. *J. Climate*, **15 (23)**, 3488–3499.

Gong, G., D. Entekhabi, and J. Cohen, 2003a: Modeled Northern Hemisphere winter climate response to realistic Siberian snow anomalies. *J. Climate*, **16 (23)**, 3917–3931.

Gong, G., D. Entekhabi, and J. Cohen, 2003b: Relative impacts of Siberian and north American snow anomalies on the winter Arctic Oscillation. *Geophys. Res. Let.*, **30 (16)**, 1848, doi:10.1029/2003GL017749.

Gong, G., D. Entekhabi, and J. Cohen, 2004a: Orographic constraints on a modeled Siberian snow-tropospheric-stratospheric teleconnection pathway. *J. Climate*, **17 (6)**, 1176–1189.

Gong, G., D. Entekhabi, J. Cohen, and D. Robinson, 2004b: Sensitivity of atmospheric response to modeled snow anomaly characteristics. *J. Geophys. Res.*, **109 (D6)**, D06 107.

Graham, R. J., M. Gordon, P. J. Mclean, S. Ineson, M. R. Huddleston, M. K. Davey, A. Brookshaw, and R. T. H. Barnes, 2005: A performance comparison of coupled and uncoupled versions of the Met Office seasonal prediction general circulation model. *Tellus A*, **57 (3)**, 320–339.

Green, D., J. Billy, and A. Tapim, 2010: Indigenous Australians' knowledge of weather and climate. *Climatic Change*, **100 (2)**, 337–354.

Gronas, S., 1995: THE SECLUSION INTENSIFICATION OF THE NEW-YEARS-DAY STORM 1992. *Tellus A*, **47 (5)**, 733–746.

Guérémy, J. F., M. Déqué, A. Braun, and J. P. Piedlièvre, 2005: Actual and potential skill of seasonal predictions using the CNRM contribution to DEMETER: coupled versus uncoupled model. *Tellus A*, **57 (3)**, 308–319.

Hagedorn, R., F. J. Doblas-Reyes, and T. N. Palmer, 2005: The rationale behind the success of multi-model ensembles in seasonal forecasting - I. Basic concept. *Tellus A*, **57 (3)**, 219–233.

Harrison, M., 2005: The development of seasonal and inter-annual climate forecasting. *Climatic Change*, **70 (1-2)**, 201–220.

Harrison, M., A. Troccoli, D. L. T. Anderson, and S. J. Mason, 2008: Introduction. *Seasonal Climate: Forecasting and Managing Risk*, A. Troccoli, M. Harrison, D. L. T. Anderson, and S. J. Mason, Eds., Springer Academic Publishers, Series IV: Earth and Environmental Sciences, Vol. 82, chap. 1, 3–11.

Holland, M. M., 2003: The North Atlantic Oscillation-Arctic Oscillation in the CCSM2 and its influence on Arctic climate variability. *J. Climate*, **16 (16)**, 2767–2781.

Hoskins, B. and P. S. Schopf, 2008: Ocean-Atmosphere Basis for Seasonal Climate Forecasting. *Seasonal Climate: Forecasting and Managing Risk*, A. Troccoli, M. Harrison, D. L. T. Anderson, and S. J. Mason, Eds., Springer Academic Publishers, Series IV: Earth and Environmental Sciences, Vol. 82, chap. 4, 67–89.

Hoskins, B. J. and K. I. Hodges, 2002: New perspectives on the northern hemisphere winter storm tracks. *J. Atmos. Sci*, **59 (6)**, 1041–1061.

Hoskins, B. J. and P. J. Valdes, 1990: On the existence of storm-tracks. *J. Atmos. Sci*, **47 (15)**, 1854–1864.

Houtekamer, P. L. and H. L. Mitchell, 2005: Ensemble Kalman filtering. *Quart. J. Roy. Meteor. Soc*, **131**, 3269–3289.

Hurrell, J. W., 1995: Decadal trends in the North-Atlantic Oscillation - regional temperatures and precipitation. *Science*, **269 (5224)**, 676–679.

Hurrell, J. W., Y. Kushnir, G. Ottersen, and M. Visbeck, 2003: An Overview of the North Atlantic Oscillation. *The North Atlantic Oscillation: Climatic Significance and Environmental Impact*, J. W. Hurrell, Y. Kushnir, G. Ottersen, and M. Visbeck, Eds., American Geophysical Union, Geophysical Monograph, Vol. 134, 1–35.

Hurrell, J. W., et al., 2006: Atlantic climate variability and predictability: A CLIVAR perspective. *J. Climate*, **19 (20)**, 5100–5121.

Hurrell, J. W., et al., 2009: DECADAL CLIMATE PREDICTION: OPPORTUNITIES AND CHALLENGES. *Ocean Obs'09 White Paper*.

Ineson, S. and A. A. Scaife, 2009: The role of the stratosphere in the European climate response to El Niño. *Nature Geosci.*, **2 (1)**, 32–36.

Jin, E. K., et al., 2008: Current status of ENSO prediction skill in coupled ocean-atmosphere models. *Climate Dyn.*, **31 (6)**, 647–664, doi:10.1007/s00382-008-0397-3.

Johansson, A., 2007: Prediction Skill of the NAO and PNA from Daily to Seasonal Time Scales. *J. Climate*, **20 (10)**, 1957–1975, doi:10.1175/JCLI4072.1.

Jones, P. W., 1999: First- and second-order conservative remapping schemes for grids in spherical coordinates. *Mon. Wea. Rev.*, **127 (9)**, 2204–2210.

Keenlyside, N., M. Latif, J. Jungclaus, L. Kornblueh, and E. Roeckner, 2008: Advancing decadal-scale climate prediction in the North Atlantic sector. *Nature*, **435 (7191)**, 84–88, doi:10.1038/nature06921.

Kharin, V. V. and F. W. Zwiers, 2003: On the ROC Score of Probability Forecasts. *J. Climate*, **16 (24)**, 4145–4150.

King, D. N. T., A. Skipper, and W. B. Tawhai, 2008: Mauori environmental knowledge of local weather and climate change in Aotearoa - New Zealand. *Climatic Change*, **100 (2)**, 385–409.

Klawa, M. and U. Ulbrich, 2003: A model for the estimation of storm losses and the identification of severe winter storms in Germany. *Nat. Hazard Earth Syst. Sci.*, **3 (6)**, 725–732.

Klinker, E., F. Rabier, G. Kelly, and J. F. Mahfouf, 2000: The ECMWF operational implementation of four-dimensional variational assimilation. III: Experimental results and diagnostics with operational configuration. *Quart. J. Roy. Meteor. Soc*, **126 (564)**, 1191–1215.

Knippertz, P., U. Ulbrich, F. Marques, and J. Corte-Real, 2003: Decadal changes in the link between El Nino and springtime North Atlantic oscillation and European-North African rainfall. *Int. J. Clim.*, **23 (22)**, 1293–1311.

Koster, R. D., P. A. Dirmeyer, and Z. C. e. a. Guo, 2004: Regions of strong coupling between soil moisture and precipitation. *Science*, **305 (5687)**, 1138–1140.

Kuhnel, I., 2010: Applicability of AOGCM simulations to insurance loss-oriented modeling of extra-tropical windstorms. *Geophysical Research Abstracts*, Vol. 12, EGU2010–12 890.

Kuper, R. and S. Kropelin, 2006: Climate-controlled Holocene occupation in the Sahara: Motor of Africa's evolution. *Science*, **313 (5788)**, 803–807, doi:10.1126/science.1130989.

Kushnir, Y., W. A. Robinson, I. Blade, N. M. J. Hall, S. Peng, and R. Sutton, 2002: Atmospheric GCM response to extratropical SST anomalies: Synthesis and evaluation. *J. Climate*, **15 (16)**, 2233–2256.

Kushnir, Y., W. A. Robinson, P. Chang, and A. W. Robertson, 2006: The Physical Basis for Predicting Atlantic Sector Seasonal-to-Interannual Climate Variability. *J. Climate*, **19 (23)**, 5949–5970.

Kvamstø, N. G., P. Skeie, and D. B. Stephenson, 2004: Impact of Labrador sea-ice extent on the North Atlantic Oscillation. *Int. J. Clim.*, **24 (5)**, 603–612.

Latif, M., M. Collins, H. Pohlmann, and N. Keenlyside, 2006: A Review of Predictability Studies of Atlantic Sector Climate on Decadal Time Scale. *J. Climate*, **19 (23)**, 5971–5987.

Leckebusch, G. C., M. Donat, U. Ulbrich, and J. G. Pinto, 2008a: Mid-latitude Cyclones and Storms in an Ensemble of European AOGCMs under ACC. *CLIVAR Exchanges*, **13 (3)**, 3–5.

Leckebusch, G. C., D. Renggli, and U. Ulbrich, 2008b: Development and application of an objective storm severity measure for the Northeast Atlantic region. *Meteorol. Z.*, **17 (5)**, 575–587, doi:10.1127/0941-2948/2008/0323.

Leckebusch, G. C. and U. Ulbrich, 2004: On the relationship between cyclones and extreme windstorm events over Europe under climate change. *Global and Planetary Change*, **44 (1-4)**, 181–193.

Leckebusch, G. C., U. Ulbrich, L. Fröhlich, and J. G. Pinto, 2007: Property loss potentials for European midlatitude storms in a changing climate. *Geophys. Res. Let.*, **34**, L05 703, doi:10.1029/2006GL027663.

Leckebusch, G. C., A. Weimer, J. G. Pinto, M. Reyers, and P. Speth, 2008c: Extreme wind storms over Europe in present and future climate: a cluster analysis approach. *Meteorol. Z.*, **17 (1)**, 67–82.

Lee, J.-Y., et al., 2010: How are seasonal prediction skills related to models' performance on mean state and annual cycle? *Climate Dyn.*, **35 (2–3)**, 267–283, doi:10.1007/s00382-010-0857-4.

Lee, T. C. K., F. W. Zwiers, X. Zhang, and M. Tsao, 2006: Evidence of decadal climate prediction skill resulting from changes in anthropogenic forcing. *J. Climate*, **19 (20)**, 5305–5318.

Lefale, P. F., 2010: *Ua 'afa le Aso* Stormy weather today: traditional ecological knowledge of weather and climate. The Samoa experience. *Climatic Change*, **100 (2)**, 317–335.

Lewis, J. M., 2005: Roots of Ensemble Forecasting. *Mon. Wea. Rev.*, **133 (7)**, 1865–1885.

Lin, H. and J. Derome, 2003: The atmospheric response to North Atlantic SST anomalies in seasonal prediction experiments. *Tellus A*, **55 (3)**, 193–207.

Lloyd-Hughes, B. and M. A. Saunders, 2002: Seasonal prediction of European spring precipitation from El Nino-Southern Oscillation and local sea-surface temperatures. *Int. J. Clim.*, **22 (1)**, 1–14.

Lorenz, E. N., 1963: Deterministic Nonperiodic Flow. *J. Atmos. Sci*, **20 (2)**, 130–141.

Lorenz, E. N., 1965: A study of the predictability of a 28-variable model. *Tellus*, **17**, 321–333.

Lorenz, E. N., 1969a: Atmospheric predictability as revealed by naturally occurring analogues. *J. Atmos. Sci*, **26**, 636–646.

Lorenz, E. N., 1969b: The predictability of a flow which possess many scales of motion. *Tellus*, **21**, 289–307.

Lorenz, E. N., 1979: Forced and Free Variations of Weather and Climate. *J. Atmos. Sci*, **36 (8)**, 1367–1376.

Lorenz, E. N., 1982: Atmospheric predictability experiments with a large numerical model. *Tellus A*, **34 (6)**, 505–513, doi:10.1111/j.2153-3490.1982.tb01839.x.

Lorenz, P., et al., 2010: Extreme European winter storms - a new event set approach. *Geophysical Research Abstracts*, Vol. 12, EGU2010–10 005.

Losada, T., B. Rodríguez-Fonseca, C. R. Mechoso, and H.-Y. Ma, 2007: Impacts of SST anomalies on the North Atlantic atmospheric circulation: a case study for the northern winter 1995/1996. *Climate Dyn.*, **29 (7–8)**, 807–819.

Lu, J. and R. J. Greatbatch, 2002: The changing relationship between the NAO and northern hemisphere climate variability. *Geophys. Res. Let.*, **29 (7)**, 1148.

Luksch, U., C. C. Raible, R. Blender, and K. Fraedrich, 2005: Decadal cyclone variability in the North Atlantic. *Meteorol. Z.*, **14 (6)**, 747–753.

Magnusdottir, G., C. Deser, and R. Saravanan, 2004: The effects of North Atlantic SST and sea ice anomalies on the winter circulation in CCM3. Part I: Main features and storm track characteristics of the response. *J. Climate*, **17 (5)**, 857–87.

Mahfouf, J. F. and F. Rabier, 2000: The ECMWF operational implementation of four-dimensional variational assimilation. II: Experimental results with improved physics. *Quart. J. Roy. Meteor. Soc*, **126 (564)**, 1171–1190.

Malmquist, D. L., (Ed.) , 1999: *European Windstorms and the North Atlantic Oscillation: Impacts, Characteristics, and Predictability*, RPI Series, Vol. 2. Risk Prediction Initiative/Bermuda Biological Station for Research, Hamilton, Bermuda, 21 pp.

Marletto, V., et al., 2005: Evaluation of downscaled DEMETER multi-model ensemble seasonal hindcasts in a northern Italy location by means of a model of wheat growth and soil water balance. *Tellus A*, **57 (3)**, 488–497.

Marshall, J., et al., 2001: North Atlantic climate variability: Phenomena, impacts and mechanisms. *Int. J. Clim.*, **21 (15)**, 1863–1898.

Mason, S. J. and N. E. Graham, 1999: Conditional probabilities, relative operating characteristics, and relative operating levels. *Wea. Forecasting*, **14 (5)**, 713–725.

Mason, S. J. and N. E. Graham, 2002: Areas beneath the relative operating characteristics (ROC) and relative operating levels (ROL) curves: Statistical significance and interpretation. *Quart. J. Roy. Meteor. Soc*, **128 (584)**, 2145–2166.

Mathieu, P.-P., R. T. Sutton, B. Dong, and M. Collins, 2004: Predictability of Winter Climate over the North Atlantic European Region during ENSO Events. *J. Climate*, **17 (10)**, 1953–1974.

McPhaden, M. J., et al., 1998: The tropical ocean global atmosphere observing system: A decade of progress. *J. Geophys. Res.*, **103 (C7)**, 14 169–14 240.

Minobe, S., A. Kuwano-Yoshida, N. Komori, S. P. Xie, and R. J. Small, 2008: Influence of the Gulf Stream on the troposphere. *Nature*, **452 (7184)**, 206–210, doi:10.1038/nature06690.

Müller, W. A., C. Appenzeller, and C. Schär, 2005: Probabilistic seasonal prediction of the winter North Atlantic Oscillation and its impact on near surface temperature. *Climate Dyn.*, **24 (2-3)**, 213–226.

Münchener Rückversicherungs-Gesellschaft, (Ed.) , 1999: *Naturkatastrophen in Deutschland. Schadenerfahrungen und Schadenpotentiale*. Bestellnummer 2798-E-d, Veröffentlichung der Münchener Rückversicherungs-Gesellschaft.

Münchener Rückversicherungs-Gesellschaft, (Ed.) , 2007: *Zwischen Hoch und Tief. Wetterrisiken in Mitteleuropa*. Edition Wissen, Veröffentlichung der Münchener Rückversicherungs-Gesellschaft.

Murnane, R. J., 2004: Climate research and reinsurance. *Bull. Amer. Meteor. Soc.*, **85 (5)**, 697–707.

Murnane, R. J., M. Crowe, A. Eustis, S. Howard, J. Koepsell, R. Leffler, and R. Livezey, 2002: The weather risk management industry's climate forecast and data needs. *Bull. Amer. Meteor. Soc.*, **83 (8)**, 1193–1198.

Murphy, J. M., B. B. B. Booth, M. Collins, G. R. Harris, D. M. H. Sexton, and M. J. Webb, 2007: A methodology for probabilistic predictions of regional climate change from perturbed physics ensembles. *Philos. Transac. Roy. Soc. A*, **365**, 1993–2028.

Murphy, J. M. and T. N. Palmer, 1986: Experimental monthly long-range forecasts for the United Kingdom. Part II. A real-time long-range forecast by an ensemble of numerical integrations. *Meteor. Magazine*, **115 (1372)**, 337–349.

Murray, R. J. and I. Simmonds, 1991: A numerical scheme for tracking cyclone centres from digital data - Part I: development and operation of the scheme. *Austr. Met. Mag.*, **39**, 155–166.

Ni-Meister, W., 2008: Recent advances on soil moisture data assimilation. *Physical Geography*, **29 (1)**, 19–37.

Nicholls, N., 1999: Cognitive illusions, heuristics, and climate prediction. *Bull. Amer. Meteor. Soc.*, **80 (7)**, 1385–1397.

Nissen, K. M., G. C. Leckebusch, J. G. Pinto, D. Renggli, S. Ulbrich, and U. Ulbrich, 2010: Cyclones causing wind storms in the Mediterranean: characteristics, trends and links to large-scale patterns. *Nat. Hazard Earth Syst. Sci.*, **1 (7)**, 1379–1391, doi:10.5194/nhess-10-1-2010.

Orlove, B., C. Roncoli, M. Kabugo, and A. Majugu, 2010: Indigenous climate knowledge in southern Uganda: the multiple components of a dynamic reginal system. *Climatic Change*, **100 (2)**, 243–265.

Orlove, B. S., J. C. H. Chiang, and M. A. Cane, 2000: Forecasting Andean rainfall and crop yield from the influence of El Nino on Pleiades visibility. *Nature*, **40 (6765)**, 68–71.

Orsolini, Y. J., I. T. Kindem, and N. G. Kvamstø, 2011: On the potential impact of the stratosphere upon seasonal dynamical hindcasts of the North Atlantic Oscillation: a pilot study. *Climate Dyn.*, **36 (3–4)**, 579–588.

Orsolini, Y. J. and N. G. Kvamstø, 2009: The role of the Eurasian snow cover upon the wintertime circulation: decadal simulations forced with satellite observations. *J. Geophys. Res.*, **114**, D19 108.

Palmer, T. N., A. Alessandri, U. Andersen, P. Cantelaube, and M. Davey, 2004: Development of a European multimodel ensemble system for seasonal-to-interannual prediction (DEMETER). *Bull. Amer. Meteor. Soc.*, **85 (6)**, 853–872.

Palmer, T. N., C. Brankovic, and D. S. Richardson, 2000: A probability and decision-model analysis of PROVOST seasonal multi-model ensemble integrations. *Quart. J. Roy. Meteor. Soc*, **126 (567)**, 2013–2033.

Palmer, T. N. and J. Shukla, 2000: Editorial to DSP/PROVOST special issue. *Quart. J. Roy. Meteor. Soc*, **126 (567)**, 1989–1990, doi:10.1002/qj.49712656701.

Palmer, T. N., G. Shutts, R. Hagedorn, F. Doblas-Reyes, T. Jung, and M. Leutbecher, 2005: Representing model uncertainty in weather and climate prediction. *Ann. Rev. Earth Planet Sci.*, **33**, 163–193.

Palutikof, J. P., T. Holt, and T. J. Osborn, 2002: Seasonal forecasting of strong winds over Europe. *16th Conference on Probability and Statistics in the Atmospheric Sciences, 13th Symposium on Global Change and Climate Variations*.

Pardowitz, T., M. Donat, T. Kruschke, D. Renggli, G. Leckebusch, and U. Ulbrich, 2010: Severe European Wind Storms in RCM ensemble simulations. *Geophysical Research Abstracts*, Vol. 12, EGU2010–14 558.

Peng, S. L., W. A. Robinson, S. L. Li, and M. P. Hoerling, 2005: Tropical Atlantic SST forcing of coupled north Atlantic seasonal responses. *J. Climate*, **18 (3)**, 480–496.

Pinto, J. G., M. Reyers, and U. Ulbrich, 2011: The variable link between PNA and NAO in observations and in multi-century CGCM simulations. *Climate Dyn.*, **36 (1–2)**, 337–354, doi:10.1007/s00382-010-0770-x.

Pinto, J. G., T. Spangehl, U. Ulbrich, and P. Speth, 2005: Sensitivities of a cyclone detection and tracking algorithm: individual tracks and climatology. *Meteorol. Z.*, **14 (6)**, 823–838.

Pinto, J. G., S. Zacharias, A. H. Fink, G. C. Leckebusch, and U. Ulbrich, 2009: Factors contributing to the development of extreme North Atlantic cyclones and their relationship with the NAO. *Climate Dyn.*, **32 (5)**, 711–737, doi:10.1007/s00382-008-0396-4.

Qian, B. D. and M. A. Saunders, 2003: Seasonal predictability of wintertime storminess over the North Atlantic. *Geophys. Res. Let.*, **30 (13)**, 1698, doi:10.1029/2003GL017401.

Rabier, F., H. Jarvinen, E. Klinker, J. F. Mahfouf, and A. Simmons, 2000: The ECMWF operational implementation of four-dimensional variational assimilation. I: Experimental results with simplified physics. *Quart. J. Roy. Meteor. Soc*, **126 (564)**, 1143–1170.

Rauch, E., 2005: *Wetterkatastrophen und Klimawandel – Sind wir noch zu retten?*, chap. Sturm und Unwetter, 132–143. Münchener Rückversicherungs-Gesellschaft.

Renggli, D., G. C. Leckebusch, S. N. Gleixner, U. Ulbrich, and E. Faust, 2011: The skill of seasonal ensemble prediction systems to forecast wintertime windstorm frequency over the North Atlantic and Europe. *Mon. Wea. Rev.*, accepted, doi:10.1175/2011MWR3518.1.

Rimbu, N., C. Boroneant, C. Buta, and M. Dima, 2002: Decadal variability of the Danube river flow in the lower basin and its relation with the North Atlantic Oscillation. *Int. J. Clim.*, **22 (10)**, 1169–1179.

Robinson, D. A., K. F. Dewey, and R. R. Heim, 1993: Global Snow Cover Monitoring - An Update. *Bull. Amer. Meteor. Soc.*, **74 (9)**, 1689–1696.

Rodwell, M. and C. K. Folland, 2003: Atlantic air-sea interaction and model validation. *Annals of Geophysics*, **46 (1)**, 47–56.

Rodwell, M. J. and F. J. Doblas-Reyes, 2006: Medium-range, monthly, and seasonal prediction for Europe and the use of forecast information. *J. Climate*, **19 (23)**, 6025–6046.

Rodwell, M. J., M. Drevillon, C. Frankignoul, J. W. Hurrell, H. Pohlmann, M. Stendel, and R. T. Sutton, 2004: North Atlantic forcing of climate and its uncertainty from a multi-model experiment. *Quart. J. Roy. Meteor. Soc*, **130 (601)**, 2013–2032.

Rodwell, M. J. and C. K. Folland, 2002: Atlantic air-sea interaction and seasonal predictability. *Quart. J. Roy. Meteor. Soc*, **128 (583)**, 1413–1443.

Rodwell, M. J., D. P. Rowell, and C. K. Folland, 1999: Oceanic forcing of the wintertime North Atlantic Oscillation and European climate. *Nature*, **398 (6725)**, 320–323.

Roncoli, C., K. Ingram, and P. Kirshen, 2002: Reading the rains: Local knowledge and rainfall forecasting in Burkina Faso. *Society and Natural Resources*, **15 (5)**, 409–427.

Saito, K. and J. Cohen, 2003: The potential role of snow cover in forcing interannual variability of the major Northern Hemisphere mode. *Geophys. Res. Let.*, **30 (6)**, 1302.

Saunders, M. A. and B. D. Qian, 2002: Seasonal predictability of the winter NAO from north Atlantic sea surface temperatures. *Geophys. Res. Let.*, **29 (22)**, 2049, doi:10.1029/2002GL014952.

Saunders, M. A., B. D. Qian, and B. Lloyd-Hughes, 2003: Summer snow extent heralding of the winter North Atlantic Oscillation. *Geophys. Res. Let.*, **30 (7)**, 1378.

Schott, F. A., S. P. Xie, and J. P. McCreary, 2009: INDIAN OCEAN CIRCULATION AND CLIMATE VARIABILITY. *Rev. Geophys.*, **47**, RG1002.

Schultz, D. M., D. Keyser, and L. F. Bosart, 1998: The effect of large-scale flow on low-level frontal structure and evolution in midlatitude cyclones . *Mon. Wea. Rev.*, **126 (7)**, 1767–1791.

Schwierz, C., C. Appenzeller, H. C. Davies, M. A. Liniger, W. Müller, T. F. Stocker, and M. Yoshimori, 2006: Challenges posed by and approaches to the study of seasonal-to-decadal climate variability. *Climatic Change*, **79 (1-2)**, 31–63.

Schwierz, C., P. Koellner-Heck, E. Zenklusen Mutter, D. N. Bresch, P.-L. Vidale, M. Wild, and C. Schär, 2009: Modelling European winter wind storm losses in current and future climate. *Climatic Change*, doi:10.1007/s10584-009-9712-1.

Seager, R., Y. Kushnir, M. Visbeck, N. Naik, J. Miller, G. Krahmann, and H. Cullen, 2000: Causes of Atlantic Ocean Climate Variability between 1958 and 1998. *J. Climate*, **13 (16)**, 2845–2862.

Seierstad, I. A., D. B. Stephenson, and N. G. Kvamstø, 2007: How useful are teleconnection patterns for explaining variability in extratropical storminess ? *Tellus A*, **59 (2)**, 170–181.

Semple, A. T., 2003: A review and unification of conceptual models of cyclogenesis. *Meteor. Applic.*, **10 (1)**, 39–59.

Shongwe, M. E., C. A. T. Ferro, C. A. S. Coelho, and G. J. Van Oldenborgh, 2007: Predictability of cold spring seasons in Europe. *Mon. Wea. Rev.*, **135 (12)**, 4185–4201.

Shukla, J., 1998: Predictability in the midst of chaos: A scientific basis for climate forecasting. *Science*, **282 (5389)**, 728–731.

Shukla, J. and J. L. Kinter III, 2006: Predictability of seasonal climate variations: a pedagoical review. *Predictability of Weather and Climate*, T. Palmer and R. Hagedorn, Eds., Cambridge University Press, chap. 12, 306–341.

Smith, D. M., S. Cusack, A. W. Colman, C. K. Folland, G. R. Harris, and J. M. Murphy, 2007: Improved surface temperature prediction for the coming decade from a global climate model. *Science*, **317 (5839)**, 796–799.

Smits, A., A. M. G. K. Tank, and G. P. Konnen, 2005: Trends in storminess over the netherlands, 1962-2002. *Int. J. Clim.*, **25 (10)**, 1331–1344.

Speranza, C. I., B. Kiteme, P. Ambenje, U. Wiesmann, and S. Makali, 2010: Indigenous knowledge related to climate variability and change: insights from droughts in semi-arid areas of former Makueni District, Kenya. *Climatic Change*, **100 (2)**, 295–315.

Stroeve, J., M. M. Holland, W. Meier, T. Scambos, and M. C. Serreze, 2007: Arctic sea ice decline: Faster than forecast. *Geophys. Res. Let.*, **34 (9)**, L09 501.

Strong, C., G. Magnusdottir, and H. Stern, 2009: Observed Feedback between Winter Sea Ice and the North Atlantic Oscillation. *J. Climate*, **22 (22)**, 6021–6032.

Sutton, R. T. and D. L. R. Hodson, 2003: Influence of the Ocean on North Atlantic Climate Variability 1871-1999. *J. Climate*, **20 (10)**, 2251–2272.

Sutton, R. T. and D. L. R. Hodson, 2005: Atlantic Ocean Forcing of North American and European Summer Climate. *Science*, **209 (115)**, 115–118, doi:10.1126/science.1109496.

Sutton, R. T., W. A. Norton, and S. P. Jewson, 2001: The North Atlantic Oscillation—what role for the Ocean? *Atm. Sci. Let.*, **1 (2)**, 89–100.

Thompson, D. W. J., M. P. Baldwin, and J. M. Wallace, 2002: Stratospheric connection to Northern Hemisphere wintertime weather: Implications for prediction. *J. Climate*, **15 (12)**, 1421–1428.

Timlin, M. S., M. A. Alexander, and C. Deser, 2002: On the reemergence of north atlantic sst anomalies. *J. Climate*, **15 (18)**, 2707–2712.

Toth, Z. and E. Kalnay, 1997: Ensemble Forecasting at NCEP and the breeding method. *Mon. Wea. Rev.*, **125**, 3297–3319.

Toth, Z., O. Talagrand, G. Candille, and Y. Zhu, 2003: Probability and Ensemble Forecasts. *Forecast Verification: A Practitioner's Guide in Atmospheric Science*, I. T. Jolliffe and D. B. Stephenson, Eds., John Wiley & Sons, Ltd, New York, chap. 7, 137–163.

Troccoli, A., 2010: Seasonal climate forecasting. *Meteor. Applic.*, **17 (3)**, 251–268, doi:10.1002/met.184.

Troccoli, A., M. Harrison, D. L. T. Anderson, and S. J. Mason, (Eds.) , 2008: *Seasonal Climate: Forecasting and Managing Risk*. Springer Academic Publishers.

Ulbrich, U., A. H. Fink, M. Klawa, and J. G. Pinto, 2001: Three extreme storms over Europe in December 1999. *Weather*, **56 (3)**, 70–80.

Ulbrich, U., G. C. Leckebusch, and J. G. Pinto, 2009: Extra-tropical cyclones in the present and future climate: a review. *Theor. Appl. Climatol.*, **96 (1-2)**, 117–131.

Ulbrich, U., J. G. Pinto, H. Kupfer, G. C. Leckebusch, T. Spangehl, and M. Reyers, 2008: Changing northern hemisphere storm tracks in an ensemble of IPCC climate change simulations. *J. Climate*, **21 (8)**, 1669–1679, doi:10.1175/2007JCLI1992.1.

Uppala, S. M., et al., 2005: The ERA-40 re-analysis. *Quart. J. Roy. Meteor. Soc*, **131 (612)**, 2961–3012.

Van Oldenborgh, G. J., 2005: Predictability of Winter Climate over the North Atlantic European Region during ENSO Events. *J. Climate*, **18 (14)**, 2770–2772.

Van Oldenborgh, G. J., G. Burgers, and A. K. Tank, 2000: On the El Nino teleconnection to spring precipitation in Europe. *Int. J. Clim.*, **20 (5)**, 565–574.

Vitart, F., 2006: Seasonal forecasting of tropical storm frequency using a multi-model ensemble. *Quart. J. Roy. Meteor. Soc*, **132 (615)**, 647–666.

Vitart, F., et al., 2007: Dynamically-based seasonal forecasts of Atlantic tropical storm activity issued in June by EUROSIP. *Geophys. Res. Let.*, **34 (16)**, L16 815.

Walker, G. T., 1924: Correlations in seasonal variations of weather. *IX. Mem. Ind. Meteorol. Dept.*, **24**, 275–332.

Wallace, J. M. and P. V. Hobbs, 2006: *Atmospheric Science. An Introductory Survey*, International Geophysics Series, Vol. 92. Elsevier.

Wang, B., et al., 2008: Advance and prospectus of seasonal prediction: assessment of the APCC/CliPAS 14-model ensemble retrospective seasonal prediction (1980-2004). *Climate Dyn.*, **33 (1)**, 93–117, doi:10.1007/s00382-008-0460-0.

Wang, W., B. T. Anderson, R. K. Kaufmann, and R. B. Myneni, 2004: The Relation between the North Atlantic Oscillation and SSTs in the North Atlantic Basin. *J. Climate*, **17 (24)**, 4752–4759.

Wang, X. L. L., F. W. Zwiers, V. R. Swail, and Y. Feng, 2009: Trends and variability of storminess in the Northeast Atlantic region, 1874-2007. *Climate Dyn.*, **33 (7–8)**, 1179–1195, doi:10.1007/s00382-008-0504-5.

Weigel, A. P., D. Baggenstos, M. A. Liniger, F. Vitart, and C. Appenzeller, 2008: Probabilistic verification of monthly temperature forecasts. *Mon. Wea. Rev.*, **136 (12)**, 5162 –5182, doi:10.1175/2008MWR2551.1.

Weigel, A. P., M. A. Liniger, and C. Appenzeller, 2007: The discrete brier and ranked probability skill scores. *Mon. Wea. Rev.*, **135 (1)**, 118–124.

Weisheimer, A., et al., 2009: ENSEMBLES: A new multi-model ensemble for seasonal-to-annual predictions - Skill and progress beyond DEMETER in forecasting tropical Pacific SST. *Geophys. Res. Let.*, **36**, L21 711, doi:10.1029/2009GL0408096.

Wernli, H., S. Dirren, M. A. Liniger, and M. Zillig, 2002: Dynamical aspects of the life cycle of the winter storm 'Lothar' (24-26 December 1999). *Quart. J. Roy. Meteor. Soc*, **128 (580)**, 405–429.

Wernli, H. and C. Schwierz, 2006: Surface cyclones in the ERA-40 dataset (1958-2001). Part I: Novel identification method and global climatology. *J. Atmos. Sci*, **63 (10)**, 2486–2507.

Wilks, D., 2006: *Statistical Methods in the Atmospheric Sciences: An Introduction*, International Geophysics Series, Vol. 91. 2d ed., Elsevier, 627 pp.

Wu, L., F. He, Z. Liu, and C. Li, 2007: Atmospheric Teleconnections of Tropical Atlantic Variability: Interhemispheric, Tropical-Extratropical, and Cross-Basin Interactions. *J. Climate*, **20 (5)**, 856–870.

Zebiak, S. E. and M. A. Cane, 1987: A MODEL EL-NINO SOUTHERN OSCILLATION. *Mon. Wea. Rev.*, **115 (10)**, 2262–2278.

Acknowledgments

First of all, I would like to thank Uwe Ulbrich and Gregor Leckebusch for giving me the opportunity to work on this project, for their support, advice and guidance. I have learned so much during the collaboration with you! It has been a pleasure to work together with Eberhard Faust of Munich Re. His constructive comments from a user's perspective helped me very much. I thank all the colleagues at the Institute of Meteorology, particularly the members of the AG Clidia, for the friendly and productive working atmosphere. Tim Kruschke, Simon Wild and Daniel Befort, the Squash Team, and the guys of Torpedo Taupunkt have accompanied me also outside of our offices. Thank you very much for that! Finally, I am very grateful to my parents, my family, and especially to Lilian, for being there for me whenever I need it.